

Xuy You Lin

Ph.D.

6 July 92

The University of Sydney

Copyright in relation to this thesis*

Under the Copyright Act 1968 (several provisions of which are referred to below), this thesis must be used only under the normal conditions of scholarly fair dealing for the purposes of research, criticism or review. In particular no results or conclusions should be extracted from it, nor should it be copied or closely paraphrased in whole or in part without the written consent of the author. Proper written acknowledgement should be made for any assistance obtained from this thesis.

Under Section 35(2) of the Copyright Act 1968 'the author of a literary, dramatic, musical or artistic work is the owner of any copyright subsisting in the work'. By virtue of Section 32(1) copyright 'subsists in an original literary, dramatic, musical or artistic work that is unpublished' and of which the author was an Australian citizen, an Australian protected person or a person resident in Australia.

The Act, by Section 36(1) provides: 'Subject to this Act, the copyright in a literary, dramatic, musical or artistic work is infringed by a person who, not being the owner of the copyright and without the licence of the owner of the copyright, does in Australia, or authorises the doing in Australia of, any act comprised in the copyright'.

Section 31(1)(a)(i) provides that copyright includes the exclusive right to 'reproduce the work in a material form'. Thus, copyright is infringed by a person who, not being the owner of the copyright and without the licence of the owner of the copyright, reproduces or authorises the reproduction of a work, or of more than a reasonable part of the work, in a material form, unless the reproduction is a 'fair dealing' with the work 'for the purpose of research or study' as further defined in Sections 40 and 41 of the Act.

Section 51(2) provides that 'Where a manuscript, or a copy, of a thesis or other similar literary work that has not been published is kept in a library of a university or other similar institution or in an archives, the copyright in the thesis or other work is not infringed by the making of a copy of the thesis or other work by or on behalf of the officer in charge of the library or archives if the copy is supplied to a person who satisfies an authorized officer of the library or archives that he requires the copy for the purpose of research or study'.

Keith Jennings
Registrar and Deputy Principal

*'Thesis' includes 'treatise', 'dissertation' and other similar productions.

This thesis has been
accepted for the award
of the degree in the
Faculty of Engineering

**VIBRATION CONTROL
OF WIND-EXCITED
TALL/SLENDER
STRUCTURES**

by

You Lin Xu
Dip.Mech.Eng., M.Eng.Sc.

A thesis presented
for the degree of Doctor of Philosophy

*School of Civil and Mining Engineering
University of Sydney*

November, 1991

VIBRATION CONTROL OF WIND-EXCITED TALL/SLENDER STRUCTURES

Y.L. Xu

SUMMARY

The results of a theoretical and experimental investigation of the vibration control of wind-excited tall/slender structures are presented in this thesis. The investigation was divided into two parts. The first part was based on aeroelastic model tests of tall buildings in the wind tunnel. It included experiments and analyses of alongwind and crosswind vibration control of tall buildings by passive mass dampers (TMDs); torsional vibration of tall buildings and its control by TMDs; a semi-analytical method of performing parametric study of TMDs; alongwind, crosswind and torsional mode shape correction factors; and a prediction procedure for assessment of the effectiveness of an active mass damper control system. The second part was a theoretical study of vibration control of wind-excited slender structures by using computation techniques. It included the possible application of tuned liquid column dampers in reducing the response of wind-sensitive structures; and soil-structure-mass damper interaction under wind loading.

The aeroelastic test of alongwind and crosswind vibration control was carried out on a CAARC model in a suburban boundary layer wind model, by using a conventional aeroelastic test rig which simulated two fundamental sway modes. The torsional vibration control experiments were performed on a rectangular tall building model in an open country boundary layer wind model, by using an aeroelastic test rig designed for torsional vibration only. The results obtained from the aeroelastic test programs demonstrated the effectiveness of the TMD systems in suppressing the wind-induced dynamic responses of the tall buildings. The TMD system reduced the vibration caused by alongwind turbulence excitation, crosswind wake excitation or

torsional excitation by 20%–45% provided that the parameters of the TMDs were properly selected. The TMD system was found to be even more effective in reducing the vibration caused by lock-in excitation by a factor of 2 or more.

A series of wind tunnel model tests were also conducted to investigate the mechanism of torsional excitation and torsional response of tall buildings, and the sensitivity of the torsional response to eccentricity between centres of twist and building geometry. With the angle of wind incidence normal to the wide face of the building, vortex shedding is the dominant mechanism of torsional excitation. With the angle of wind incidence normal to the narrow face, the incident turbulence and the shear layer re-attachment intermittencies are two important excitation mechanisms. At a reduced wind velocity of 8, the maximum dynamic torque for the eccentric model increased by 30% and the maximum mean torque increased by a factor of 2.8, compared with the values of the basic model.

Based on direct measurements in the wind tunnel of wind-induced response or excitation spectra of the plain building without TMDs, a semi-analytical method of performing parametric study of the TMD was proposed. The results obtained by this method were in good agreement with the corresponding experimental results. In contrast, the conventional parametric study method, which is based on a white noise excitation model, usually overestimates the effectiveness of TMDs for most real situations. The effectiveness of the TMD was also found to be dependent on the type of external wind excitation.

The semi-analytical method was also used to investigate the feasibility of a suboptimal active mass damper vibration control system. Analytical results showed that the effectiveness of passive tuned mass dampers can be considerably enhanced by the inclusion of the suboptimal active control system. The analytical procedure provides a method of selecting the most beneficial control parameters which result in a larger reduction of the building and damper responses by using a small control force or moment.

Sources of error in the aeroelastic modelling technique, caused by the

discrepancy between the building model and prototype mode shapes, were discussed. Three mode shape correction factors, for alongwind, crosswind and torsional responses respectively, were suggested to adjust the experimental response results to the corresponding prototype values. The results obtained by the proposed expressions were in reasonable agreement with the available experimental results.

In the theoretical study of vibration control of wind-excited slender structures, the structure was modelled as a n -degree-of-freedom lumped mass system taking into account both bending and shear. The soil behaviour, including footing embedment effect, was characterised by a known frequency-dependent compliant matrix. A transfer matrix formulation for non-periodic structures was developed to analyse the effects of liquid dampers and soil compliancy on wind-induced response of slender structures. The numerical computer accuracy of direct matrix multiplication was investigated and the results indicated that the accuracy of the computed results can be guaranteed. Numerical examples showed that tuned liquid column damper systems, which have significant practical advantages, can achieve the same level of motion reduction as passive mass dampers. The numerical examples also showed that soil compliancy can significantly affect the structural responses and the effectiveness of the dampers, depending on the properties of the soil, the properties of the structure, the nature of the excitation and the type of structural response.

PREFACE

This thesis is submitted to the University of Sydney, Australia, for the degree of Doctor of Philosophy. The work described in this thesis commenced in April 1989 and was completed in November 1991 at the School of Civil and Mining Engineering, the University of Sydney, under the supervision of Associate Professor K.C.S. Kwok.

To the best of the candidate's knowledge and belief, the thesis contains no material previously published or written by another person, except when due reference is made in the text. No part of the work described in this thesis has been presented for the award of any other degree or diploma in any university.

The thesis is supported by seven papers:-

1. Xu, Y.L., Samali, B. and Kwok, K.C.S., Control of along-wind response of structures by mass and liquid dampers, to be published in *Journal of Engineering Mechanics*, ASCE, Vol. 118, No.1, January, 1992.
2. Xu, Y.L., Kwok, K.C.S. and Samali, B., Control of wind-induced tall building response by tuned mass dampers, manuscript accepted for publication by *Journal of Wind Engineering and Industrial Aerodynamics*.
3. Xu, Y.L., Kwok, K.C.S. and Samali, B., The effect of tuned mass dampers and liquid dampers on cross-wind response of tall/slender structures, manuscript accepted for publication by *Journal of Wind Engineering and Industrial Aerodynamics*.
4. Xu, Y.L., Kwok, K.C.S. and Samali, B., Torsional response and vibration suppression of wind-excited buildings, manuscript accepted for publication by *Journal of Wind Engineering and Industrial Aerodynamics*.
5. Xu, Y.L. and Kwok, K.C.S., Wind-induced response of soil-structure-mass damper systems, manuscript submitted to *Journal of Wind Engineering and Industrial Aerodynamics*.
6. Xu, Y.L., Kwok, K.C.S. and Samali, B., Tuned mass dampers to suppress wind-induced torsional vibration of tall buildings, to be presented at *Asia-Pacific Vibration Conference*, Melbourne, Australia, November, 1991.

7. Xu, Y.L., Samali, B. and Kwok, K.C.S., Dynamic analysis of structures using transfer matrices --- an assessment of the numerical accuracy, to be presented at *Asia-Pacific Conference on Computational Mechanics*, Hong Kong, December, 1991.

Papers 1 to 5 were first published in the following conference proceedings:

1. Xu, Y.L., Samali, B. and Kwok, K.C.S. (1990). The effect of passive damping devices on wind-induced response of tall buildings, *Tall Buildings: 2000 and Beyond*, Fourth World Congress, Council on Tall Buildings and Urban Habitat, Hong Kong, November, pp. 751-766.

2. Xu, Y.L., Kwok, K.C.S. and Samali, B. (1990). Wind-induced vibration of tall buildings and its control by tuned mass dampers, *Proceedings of Vibration and Noise Conference*, the Institution of Engineers Australia, Melbourne, Australia, September, pp.73-80.

3. Xu, Y.L., Samali, B. and Kwok, K.C.S. (1990). The effect of passive damping devices on the response of wind-sensitive structures, *Proceedings of Second Structural Engineering Conference*, the Institution of Engineers Australia, Adelaide, Australia, October, pp. 38-44.

4. Xu, Y.L., Kwok, K.C.S. and Samali, B. (1991). Torsional response and vibration suppression of wind-excited buildings, *Proceedings of the 8th International Conference on Wind Engineering*, London, Canada, July, Summary Paper No. 1-13.

5. Xu, Y.L. and Kwok, K.C.S. (1991). Wind-induced response of soil-structure-mass damper system, *Proceedings of the 8th International Conference on Wind Engineering*, London, Canada, July, Summary Paper No. 8-16.

ACKNOWLEDGEMENTS

The research project described herein was supported by an Australian Development Training Award from the Australian International Development Assistance Bureau, and the Wind Tunnel Investigation Fund from the School of Civil and Mining Engineering, the University of Sydney, to which I am grateful.

I am greatly indebted to my supervisor, Associate Professor K.C.S. Kwok, for his continuous encouragement, support and guidance in all aspect of my research activities and even my personal problems. I also wish to thank Dr. B. Samali, Senior Lecturer at the University of Technology, Sydney, and co-investigator of the project, for his unfailing confidence in my ability and valuable suggestions. The contribution of Dr. R.D. Watkins in developing the wind tunnel and the co-operation of Dr. L.W. Apperley with regard to the data acquisition system are also acknowledged.

Thanks also to Mr. D.H. Kim and Mr. K. Barry for developing the wind tunnel, and Mr. D. Cockram for developing the aeroelastic test rig for pure torsion vibration. I am thankful for the assistance of Mr. R. Brew and Ms. K. Pham in plotting graphs and for the friendship of all staff and students of the Fluids Laboratory during the work.

Finally I would like to express my heartfelt thanks to my wife and my daughter for their tolerance, love and encouragement throughout the course of this work.

CONTENTS

	Page
SUMMARY	i
PREFACE	iv
ACKNOWLEDGEMENTS	vi
CONTENTS	vii

Chapter 1. INTRODUCTION

1.1 Aims and Limitations of the Research Project	1
1.2 Layout of the Presentation	3

Chapter 2. BACKGROUND

2.1 Wind-Induced Vibration of Tall/Slender Structures	6
2.1.1 Alongwind vibration	8
2.1.2 Crosswind vibration	8
2.1.3 Torsional vibration	9
2.1.4 Coupled translational-torsional vibration	9
2.2 Significance and Method of Vibration Control	10
2.2.1 Significance	10
2.2.2 Method	11
2.3 Literature Survey	14
2.3.1 Passive control	14
2.3.1.1 Impact dampers	14
2.3.1.2 Viscoelastic dampers	16
2.3.1.3 Tuned mass dampers	18
2.3.1.4 Liquid dampers	23
2.3.2 Active control	26

**Chapter 3. PASSIVE CONTROL OF WIND-INDUCED
TRANSLATIONAL VIBRATION OF TALL
BUILDINGS BY TUNED MASS DAMPERS**

3.1	Introduction	30
3.2	Aeroelastic Model Requirements	31
3.3	Modelling of Natural Wind	32
3.3.1	Wind tunnel	32
3.3.2	Mean wind speed profile	35
3.3.3	Longitudinal turbulent intensity profile	38
3.3.4	Integral length scale of longitudinal turbulence	38
3.4	Aeroelastic Modelling of Buildings and Dampers	41
3.4.1	General discription	41
3.4.2	Derivation of scaling ratios	43
3.4.3	Model building and tuned mass dampers	45
3.5	Experimental Arrangements	47
3.6	Experimental Results and Analysis	50
3.6.1	Alongwind responses	50
3.6.2	Crosswind responses	50
3.6.3	Wake spectra	53
3.6.4	Probability distributions of peaks	56
3.6.5	Normalised displacement response spectra	56
3.6.6	Effect of angle of wind incidence	58
3.7	Conclusions	58

**Chapter 4. WIND-INDUCED TORSIONAL VIBRATION
OF TALL BUILDINGS AND ITS PASSIVE
CONTROL BY TUNED MASS DAMPERS**

4.1	Introduction	62
4.2	Experimental Techniques	64
4.2.1	Modelling of turbulent boundary layer wind	64
4.2.2	Model building and tuned mass damper	65
4.2.3	Test rig and data acquisition	70
4.2.4	Experimental program	73

4.3 Basic Model Tests	73
4.3.1 Torsional response	73
4.3.2 Response and excitation spectra	79
4.3.3 Probability distributions of peaks	81
4.3.4 Aerodynamic damping	85
4.4 Eccentric Model Tests	90
4.4.1 Effect of eccentricity on torsional excitation	90
4.4.2 Effect of eccentricity on torsional response	92
4.5 Eccentric Model with Tuned Mass Damper	95
4.5.1 Comparison of torsional responses	95
4.5.2 Comparison of response spectra	98
4.6 Conclusions	98

**Chapter 5. A SEMI-ANALYTICAL METHOD OF
PERFORMING PARAMETRIC STUDY
OF TUNED MASS DAMPERS**

5.1 Introduction	105
5.2 Basic Theory	108
5.2.1 Translational vibration	109
5.2.2 Torsional vibration	112
5.3 Experimental Verification of the Method	113
5.3.1 Alongwind vibration	114
5.3.2 Crosswind vibration	114
5.3.3 Torsional vibration	114
5.4 TMD Parametric Studies with Semi-Analytical Method	118
5.4.1 Estimate of TMD parameters	118
5.4.2 Selection of optimum TMD parameters	125
5.5 Results Based on White Noise Excitation	130
5.5.1 Comparison with experimental results	130
5.5.2 Comparison with semi-analytical results	130
5.5.3 Displacement and acceleration responses	131
5.6 Discussions	134
5.7 Conclusions	135

**Chapter 6. MODE SHAPE CORRECTION FOR WIND
TUNNEL TESTS OF TALL BUILDINGS**

6.1 Introduction	137
6.2 Identification of Sources of Error	139
6.3 Two Limits to Mode Shape Correction Factor	141
6.3.1 Assumption of co-spectrum	141
6.3.2 Low correlation level	143
6.3.3 High correlation level	144
6.4 Characteristics of Mode Shape Correction Factor	144
6.4.1 Alongwind correction factor	144
6.4.2 Crosswind correction factor	146
6.4.3 Torsional correction factor	146
6.5 Comparison and Discussion	146
6.6 Conclusions	151

**Chapter 7. ANALYSIS OF AN ACTIVE CONTROL
SYSTEM BASED ON AEROELASTIC
TEST TECHNIQUES**

7.1 Introduction	152
7.2 Basic Theory	155
7.3 Effectiveness of Active Mass Damper	160
7.3.1 Comparison of responses	160
7.3.2 Comparison of response spectra	162
7.3.3 Comparison of frequency response functions	164
7.4 Parametric Studies of Active Mass Damper	164
7.4.1 Effect of parameters K_t and ϵ	166
7.4.2 Effect of parameters ϵ and τ	166
7.4.3 Effect of wind excitations	172
7.5 Conclusions	175

**Chapter 8. VIBRATION CONTROL OF SLENDER
STRUCTURES BY TUNED LIQUID
COLUMN DAMPERS**

8.1	Introduction	177
8.2	Formulation of the Problem	181
8.2.1	Transfer matrix	181
8.2.2	Tuned mass damper	183
8.2.3	Tuned liquid column damper	188
8.2.4	Tuned liquid column/mass damper	191
8.2.5	Spectral relationships and system responses	193
8.3	Wind Load Spectra	196
8.3.1	Alongwind turbulence spectrum	196
8.3.2	Crosswind wake spectrum	197
8.4	Numerical Examples	198
8.4.1	TV tower	198
8.4.2	Office tower	210
8.5	Conclusions	218

**Chapter 9. SOIL-STRUCTURE-MASS DAMPER
INTERACTION**

9.1	Introduction	228
9.2	Basic Equations	229
9.2.1	Superstructure	231
9.2.2	Footing and soil	232
9.2.3	Mass damper	234
9.3	Frequency Response Function of System	235
9.4	System Response	244
9.5	Numerical Examples	246
9.5.1	Office tower	246
9.5.2	TV tower	260
9.6	Conclusions	275

**Chapter 10. GENERAL CONCLUSIONS AND
RECOMMENDATIONS**

10.1	Conclusions	278
10.1.1	Control of alongwind and crosswind vibrations by TMDs	278

10.1.2 Torsional vibration and control by TMDs	278
10.1.3 Parametric study of TMDs	279
10.1.4 Mode shape corrections	280
10.1.5 Active mass dampers	280
10.1.6 Tuned liquid column dampers	281
10.1.7 Soil-structure-mass damper interaction	281
10.2 Recommendations for further research	282
NOTATION	285
REFERENCES	292
APPENDIX A - FREE DECAY VIBRATIONS OF A TWO-FREEDOM-OF- DEGREE SYSTEM	307
APPENDIX B - ACCURACY OF NUMERICAL COMPUTATION FOR NON- PERIODIC STRUCTURES BY THE TRANSFER MATRIX APPROACH	311

Chapter 1

INTRODUCTION

1.1 Aims and Limitations of the Research Project

The use of high strength materials and the development of new building techniques have reduced the cost of modern structures to a great extent, but at the same time caused modern structures to be more flexible and lightly damped than in the past. The multi-function requirements of modern structures also make structural shapes and systems more complex. Such structures are inherently sensitive to alongwind, crosswind or torsional excitation. Consequently, wind-induced oscillations of structures may cause human discomfort, cracked partitions, broken glass, damaged sensitive equipments and even catastrophic failure of some bridges and towers.

To ensure functional performance of structures it is important to reduce undesirable structural vibrations under wind loading. Various possibilities exist to achieve this goal, which include structural modification, aerodynamic modification and use of control technology. The use of passive or active control technology, however, is gaining wide acceptance in the building industry as evidenced by recent implementation of control devices on tall buildings and other flexible structures. In fact, we are entering a new era, leaving behind the days in which buildings and structures only offered space or a single function, to an era of providing an environment of comfort, multi-function services, high-level communication network systems and highly efficient productivity. 'Super-tall' buildings with up to 500 storeys are being considered as possibilities in the near future. Hence, control systems, either active or passive, will become an integral part of structural systems. It has also been predicted that the realization of control technology in civil engineering may cause a revolution in this field.

The broad aim of the research project described in this thesis was to investigate, by experimental and theoretical studies, the effectiveness of tuned mass dampers (TMDs) and liquid column dampers (TLCDs) in suppressing wind-induced structural vibrations. More special goals were as follows:

(a) To evaluate, by using aeroelastic model tests in wind tunnel, the effectiveness of passive TMDs in suppressing tall building vibrations induced by alongwind turbulence excitation, crosswind wake excitation, lock-in excitation and torsional excitation.

(b) To provide, by combining experimental results with theoretical analysis, a reliable and economical method of determining optimum design parameters of passive TMDs for wind-excited tall buildings.

(c) To perform parametric studies of a suboptimal active mass damper control system and to estimate its effectiveness in reducing wind-induced building vibration compared with passive TMDs.

(d) To address a new approach which facilitates the mitigation of wind-induced motions of slender structures by utilising tuned liquid column dampers.

(e) To assess the effect of soil compliancy under the footing of slender structures on the effectiveness of TMDs designed for the slender structures.

Information about the mechanism of wind-induced torsional excitation on tall buildings is not plentiful. Therefore, an aeroelastic model for torsional vibration was designed and built, and some basic characteristics of wind-induced torsional vibration of tall buildings were investigated before the suppression experiment of wind-induced torsional vibration of tall buildings was performed. Furthermore, some error will arise when the mode shapes of building models depart significantly from the prototype fundamental mode shapes. The mode shape corrections, for alongwind, crosswind and torsional vibration, were discussed. However, it is not intended to examine in wind tunnel the effect of TMDs on coupled

translational-torsional vibration of wind-excited tall buildings. The experimental verification of the proposed semi-analytical method to predict the effectiveness of active mass dampers in suppressing wind-induced vibrations of tall buildings is also not included in this thesis.

With limitations in experimental equipment and technique, a theoretical study was adopted to investigate the possible application of TLCDs in reducing the wind-induced response of slender structures, and the soil-structure-damper interaction under wind loading. The theoretical expressions for wind excitations, tuned liquid column damper and soil behaviours were mostly derived from the relevant experiments by other researchers. However, the use of more complicated structural models in the theoretical study presented in this thesis made it possible to estimate the effect of dampers and soil compliancy on wind-induced vibrations of higher modes.

1.2 Layout of the Presentation

As a general introduction to the thesis, this chapter indicates the background of the research project, outlines the aims of the research project and points out the approach undertaken and the limitations of the proposed project.

Chapter 2 describes in detail the background of the research project. It begins with an introduction to wind-induced vibrations of tall/slender structures, which is followed by an description of the significance and method of wind-induced vibration control. The last section is a literature review of vibration control, with particular reference to passive and active control technology in civil engineering and wind engineering.

Chapters 3 to 6 give an overall description of the effectiveness of passive TMDs in suppressing various wind-induced vibrations of tall buildings and the parametric design of the passive TMD.

After discussing the scaling requirements of the natural wind simulation

and aeroelastic modelling of building in wind tunnel, the experimental results of wind-induced translational vibration control of tall buildings by passive TMDs are presented and analysed in Chapter 3. The wind-induced translational vibrations considered here are due to alongwind turbulence, crosswind wake excitation and lock-in excitation.

In Chapter 4, an aeroelastic test rig for pure torsional vibration is first described. The wind-excited torsional response of tall building is presented and the mechanism of the wind-induced torsional excitation is discussed in terms of torsional excitation spectra, probability distributions of peaks and aerodynamic damping. This is followed by an examination of the sensitivity of the torsional response to eccentricity between centres of twist and building geometry. This Chapter ends with a section on the effect of a passive TMD on the torsional response of the tall building.

Chapter 5 presents a reliable and economical method of performing parametric studies of TMDs, by using measured response or excitation spectra of a tall building in wind tunnel. The semi-analytical results obtained by this method are compared with the corresponding experimental results and the conventional theoretical results obtained by using ideal white noise excitation. The application of this technique to optimum parametric design of TMDs is also discussed.

Chapter 6 deals with the mode shape corrections for wind tunnel tests of tall buildings. The results of this study are presented in terms of mode shape correction factors. These factors can be used to adjust the wind tunnel experimental results to the corresponding prototype values.

Chapter 7 performs parametric studies of a suboptimal active control system by using the semi-analytical method. The effectiveness of this active control system in reducing building vibrations is also assessed in comparison with passive TMDs. It is expected that the results of this study can lay the foundation for the corresponding experimental verification in wind tunnel of the effectiveness of active control system.

In Chapter 8, a theoretical investigation is made of the possible

application of tuned liquid column dampers and tuned liquid column/mass dampers in reducing wind-induced response of slender structures in comparison with the tuned mass dampers. The effectiveness of the damping device is measured in terms of the reduced motion of the structures.

In Chapter 9, the effect of soil compliancy on wind-induced structural responses and the effectiveness of TMDs is theoretically investigated. The discussion of numerical examples is based on the properties of the soil, the properties of the structure, the nature of the excitation and the type of the structural response. A random vibration analysis of a multi-degree-of-freedom lumped mass structural system, by utilising transfer matrix formulation, is carried out in both Chapter 8 and Chapter 9.

General conclusions and recommendations for the further research are presented in Chapter 10. These are followed by Notation and a list of references used in this thesis. The appendices which follow contain relevant supporting materials.

Chapter 2

BACKGROUND

2.1 Wind-Induced Vibration of Tall/Slender Structures

The wind, in common with all meteorological phenomena, derives its energy from the sun. The immediate causes of atmospheric motion are pressure differences in the atmosphere set up by variations in air temperature due to differential heating of the earth's surface by the sun.

Closer to the ground, i.e., in the boundary layer of the atmosphere which is the location of most engineering structures, the airflow is slowed down by the shear action of surface roughness and the eddies or turbulence arise due to the basic instability of shear flows. Fig. 2.1 shows a record of wind speed in the boundary layer of the atmosphere from a tall mast in open country near East Sale, Australia (Deacon, 1955). It is clear that, from Fig. 2.1, natural winds are neither steady nor uniform. The fluctuations in wind speed and the further distorted flow by wind-structure interaction cause aerodynamic force and moment acting on structures.

The resultant aerodynamic force is usually resolved into two components, one parallel and the other normal to the direction of the mean speed in the undisturbed wind flow. These are referred to as the alongwind force and crosswind force, respectively. The aerodynamic moment (torque) with respect to elastic centre of a structure is equal to the product of the aerodynamic force by its moment arm with respect to that centre. It is the aerodynamic force and moment that cause the corresponding alongwind, crosswind and torsional vibrations and responses of tall buildings and structures.

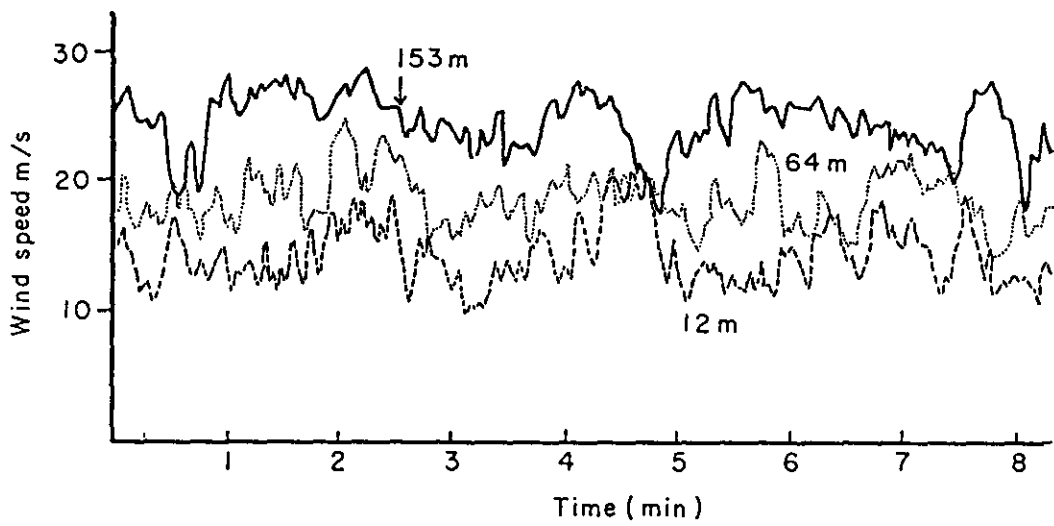


**FIG. 2.1 RECORD OF WIND SPEED AT THREE HEIGHTS
ON A 500 FT MAST IN OPEN TERRAIN
(AFTER DEACON, 1955)**

2.1.1 Alongwind vibration

It can be concluded from the work mainly by Davenport and Vickery in the 1960's that the alongwind vibration of most slender structures is due primarily to the buffeting of the longitudinal component of turbulence in the natural wind. Although alternating alongwind forces due to vortex shedding are detectable, in practice, they are very small and seldom encountered. The analytical methods for the prediction of the alongwind vibration of tall/slender structures have been reported by Davenport (1962, 1967), Vickery (1966, 1971), and later by Simiu (1980), Yang and Lin (1981), Solari (1982) and others.

2.1.2 Crosswind vibration

Satisfying attempts have been made by Melbourne (1975) to identify the crosswind excitation mechanisms which can be divided into three categories as associated with:

- (a) the incident turbulence,
- (b) the wake,
- (c) the crosswind displacement.

The significance of incident turbulence in causing crosswind vibration depends on the ability of the incident turbulence to generate a crosswind force on the structure as a function of longitudinal wind velocity and angle of incidence of the mean wind. The wake-induced vibration of structures is associated with shed vortices which have a dominant periodicity defined by the Strouhal number. If the shedding frequency of the vortices is close to the natural frequency of the structure, large amplitude crosswind vibration of the structure will occur. The crosswind displacement of the structure then causes an increase in wake energy which in turn increases the crosswind response of the structure. This aeroelastic instability phenomenon is usually called lock-in. Another crosswind displacement dependent vibration is galloping, which depends on the sectional aerodynamic force characteristics and on the rate of crosswind displacement to produce a force in phase with the displacement.

In practice, wake excitation, and occasionally lock-in, seems to be dominant for a majority of tall/slender structures in crosswind direction. It is only when the afterbody of the structure becomes long enough to cause significant flow reattachment that the incident turbulence excitation becomes dominant. At very high reduced wind velocities, galloping then becomes significant for some structures with particular sectional shapes. The detailed description of the crosswind vibration of tall/slender structures in simulated natural wind can be found from the work of Vickery and Clark (1972), Saunders (1974), Kwok (1977), ESDU (1978), Kareem (1982), Vickery and Basu (1983), and others.

2.1.3 Torsional vibration

Wind-induced torsional vibration of modern tall buildings occurs because the elastic centre of the building does not coincide with the instantaneous point of application of the resultant aerodynamic force. The magnitude of eccentricity between the elastic centre and the aerodynamic centre depends on instantaneous wind pressure distribution on the building surface. In comparison with alongwind or crosswind vibration, information on torsional vibration of tall buildings is not plentiful. A literature review of torsional and coupled translational-torsional vibrations is given in Chapter 4 of the thesis.

2.1.4 Coupled translational-torsional vibration

When the mass centre of a tall building also does not coincide with the elastic centre, translational vibration (including alongwind vibration and crosswind vibration) and torsional vibration of the building are coupled inertially. This inertial coupling usually increases the building response, especially when the torsional and translational fundamental vibration periods are close. With increasing reduced wind velocity and building displacement, the coupled translational-torsional vibration may become unstable. This aeroelastic instability is referred to as flutter. Discussions on the significance of flutter of modern buildings can be found in Parkinson (1971), Durgin and Tong (1972).

No matter what kind of wind-induced vibration is generated, an aeroelastic force which depends on the structural motion may be developed. This force is usually referred to as the aerodynamic damping force and is quantified by aerodynamic damping. Aerodynamic dampings of prismatic bodies in the alongwind and crosswind directions have been discussed by Davenport (1979) and Kareem (1982), although the relevant data are still not plentiful. Torsional aerodynamic damping of a prism was investigated in this research project.

2.2 Significance and Method of Vibration Control

2.2.1 Significance

Tall/slender structures, with low natural frequencies and dampings, have always been susceptible to a dynamic mode of failure due to wind. The most spectacular and catastrophic demonstrations of the ability of the wind to cause violent oscillations were the vibrations and subsequent collapses of the Tacoma Narrow Bridge in Washington, U.S.A. in 1940, and the three 113m high cooling towers at Ferrybridge Power Station, U.K. in 1965. Slender chimneys and towers are also ideal generators of regular patterns of vortices and this type of structure has also a history of vibrational problems and collapses.

Although complete collapse of tall buildings under wind action has no recorded case, at least two major buildings, namely the Meyer-Kaiser Building in the Miami Hurricane in 1926 and the Great Plains Life Building during the Lubbock Tornado in 1970, have suffered permanent structural damage and exhibited marked permanent deformations in torsion. There have also been many reported cases in which, due to movement of buildings induced by wind, interior walls were cracked, windows were dislodged, valuable and sensitive equipments housed in buildings were damaged and occupants suffered from dizziness, headache or nausea.

The importance of vibration control is to ensure structural safety and structural performance by using various means to limit the undesirable

motion levels. The realisation of advanced control technology in structural engineering will make the dream of constructing 'super-tall' buildings up to 500 storeys high come true, and will elevate structural design concepts from a static and passive level to one of dynamicism and adaptability.

2.2.2 Method

Various possibilities exist to control wind-induced vibration of structures. A well known summary was made by Walshe and Wootton in 1970 for preventing the instability of circular section structures due to strong wind. Control methods for wind-induced structural vibration can be divided into three categories:

- (a) structural modification,
- (b) aerodynamic modification,
- (c) passive or active control technology.

Structural modification can be applied to the three important dynamic properties of structures, i.e., stiffness, damping and mass through the change of building materials or the rearrangement of the structural systems. Aerodynamic modification alters the flow pattern around a structure directly to reduce aerodynamic force or moment acting on the structure by an appropriate choice of structural shape or the addition of some aerodynamic devices, e.g., spoilers, vanes and openings. The installation of passive absorbers in structures, e.g., tuned mass dampers, tuned liquid dampers and viscoelastic dampers provides an extra energy dissipation device which increases the overall effective damping of the main structure and accordingly reduces the wind-induced structural vibration. Active control technology is a logical extension of passive control technology. Active control relies on the supply of external energy and the input of control information to provide active control forces which modify the overall structural characteristics leading to a reduction of structural vibration. An active control system usually consists of (a) sensors installed at suitable locations of the structure to measure either the external excitations or the structural response quantities or both, (b) devices to process the measured information and to compute the necessary control forces based on a given control algorithm, and (c)

actuators, usually powered by external energy sources, to produce the required force. The basic configuration of an active structural control system is shown schematically in Fig. 2.2.

Vickery, Isyumov and Davenport (1983) examined how stiffness, damping and mass influenced the dynamic behaviour of a structure subject to alongwind turbulence, aerodynamic damping force, crosswind wake excitation associated with the vortex shedding process and crosswind incident turbulence. Their conclusion is that an increase in the damping capacity is always beneficial. The role of mass and stiffness is not clear, although, with exception of vortex shedding, an increase in stiffness is advantageous. Based on the damping measurements obtained from one hundred and sixty five buildings, Davenport and Hill-Carroll (1986) found that taller concrete buildings tend to have roughly 30% more damping than steel buildings. Kareem (1983) also pointed out that composite steel-concrete buildings have considerably higher values of damping compared to those of steel buildings. The adjustment of structural stiffness can be achieved through a change of structural system and materials, e.g., from a rigid frame to a braced frame by using prestressed cables or rods connecting across the diagonal of frames.

One of the earlier accounts of suppressing vibration of slender structures due to vortex shedding by aerodynamic modification of the structure belongs to Scruton and Walshe (1957). Helical strakes were added to the surface of a lightly-damped chimney stack to disrupt the vortex shedding process. A detailed review and classification of various aerodynamic and hydrodynamic means for suppressing vortex shedding, with particular reference to slender structures with a circular cross-section, can be found in Zdravkovich (1981). For prismatic structures, Devonport (1971), Cermak (1972), Naudascher et al (1981), Kwok and Bailey (1987), Kwok (1988), Hayashida and Iwasa (1990), and others individually investigated the effect of structural shape and some aerodynamic devices on structural vibrations due to alongwind turbulence, crosswind incident turbulence, crosswind wake excitation associated with vortex shedding process, lock-in and galloping.

Although wind-induced structural vibrations can be controlled to some extent by structural or aerodynamic modification, the construction cost, the

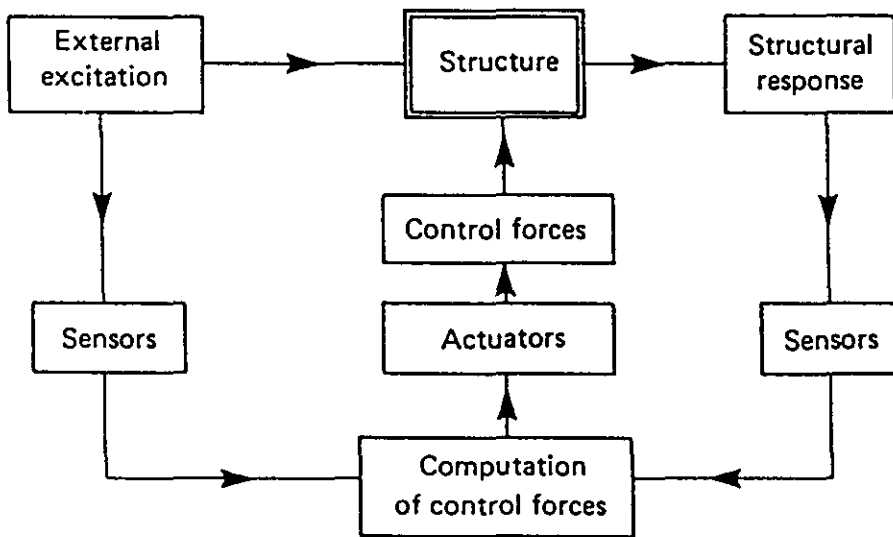


FIG. 2.2 SCHEMATIC DIAGRAM OF ACTIVE STRUCTURAL CONTROL SYSTEM (AFTER SOONG, 1988)

structure's special function and the inherent limitations to the amount of reduction in vibration levels that can be achieved restrict their practical applications. This is particularly the case in building design. Therefore, passive and active control technology is now gaining wide attention and acceptance in the building industry. A literature survey of this research area, which is closely related to this thesis, follows.

2.3 Literature Survey

2.3.1 Passive control

The successful application of passive control technology in machinery, automotive, space satellites and marine vessels encourages engineers and scientists to apply this technology to civil engineering structures which are massive and heavy. At present, passive control devices, as an additional energy absorber applicable to civil engineering structures against wind loading, are mainly impact dampers, viscoelastic dampers, tuned mass dampers and tuned liquid dampers.

2.3.1.1 Impact dampers

A typical impact damper shown in Fig. 2.3 consists of a chain, covered with a rubber sleeve and suspended with freedom to impact against a vertical channel and provide energy dissipation. Reed (1967) evaluated the effects of various chain-damper parameters such as clearance gap, chain length and weight, amplitude and frequency of vibration, by means of mechanical impedance measurements, and successfully fitted these dampers to a 20m high missile which would otherwise be vulnerable in the launch position. The dampers weighed about 5 percent of the total weight of the missile and increased the damping of the structure by a factor of about 3 except at small amplitudes. At small amplitudes, the chain fails to touch the channel and there is no effective increase in damping. An interesting characteristic of the chain damper is that the amount of energy absorbed by the chain dampers can remain a maximum over a quite wide frequency range, compared with tuned mass dampers. Therefore, this damper can

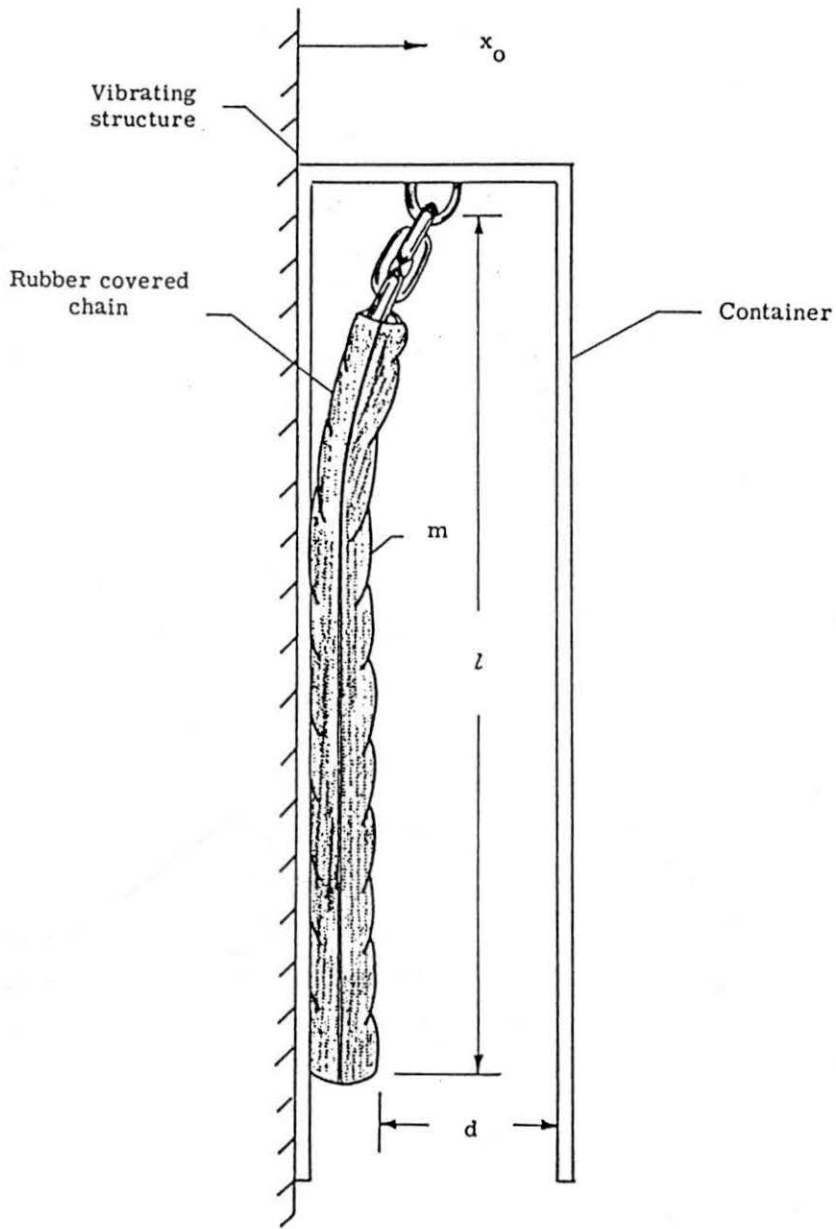


FIG. 2.3 CHAIN DAMPER CONFIGURATION
(AFTER REED, 1967)

suppress fundamental and higher mode vibrations at the same time if the ratio between the frequencies of the considered modes of a structure is lower than about 3. However, the impact noise and the required space for the installation of long and heavy chains limit their application to some special structures such as antennae and stacks. There are a number of other impact damper designs available but none have been as well documented as the chain type (Masri, 1967; Walshe and Wootton, 1970).

2.3.1.2 Viscoelastic dampers

One of the most promising approaches to added damping in tall buildings is the use of nonstructural viscoelastic dampers. Such dampers transfer part of the vibratory energy of the overall system into heat and dissipate this heat into the surroundings. A typical viscoelastic damper as shown in Fig. 2.4, which was used in the World Trade Centre, is described in Mahmoodi (1969), Feld (1971) and Architectural Record (1971). The force versus displacement characteristic of such a damper is in the form of a hysteresis loop. The enclosed area of the loop is a measure of the energy dissipated and therefore a measure of the physical performance of the damper, which is dependent on factors such as stiffness, geometry, operating temperature and the heat transfer to the connecting structures. These dampers can be located in the structure between any two points of relative displacement or between the structure and a support such that the viscoelastic material undergoes virtually pure shear deformation.

The World Trade Centre in New York City was one of the first major buildings to utilise viscoelastic damper system of the type shown in Fig. 2.4. Approximately 10,000 dampers were installed in the 110 storey tower, with about 100 dampers at the ends of floor trusses at each floor from the 8th to 107 th. Recently large viscoelastic dampers was used in the Columbia Center Building which is a 76-storey office tower located in downtown Seattle, Washington (Keel and Mahmoodi, Mahmoodi and Keel, 1986). The addition of only 260 viscoelastic dampers increased the critical damping ratio of the tower from 0.8 to 6.4 percent for frequent storm and 3.2 percent at design wind. Full scale measurements are being carried out after the completion of the building (Skilling et al., 1986).

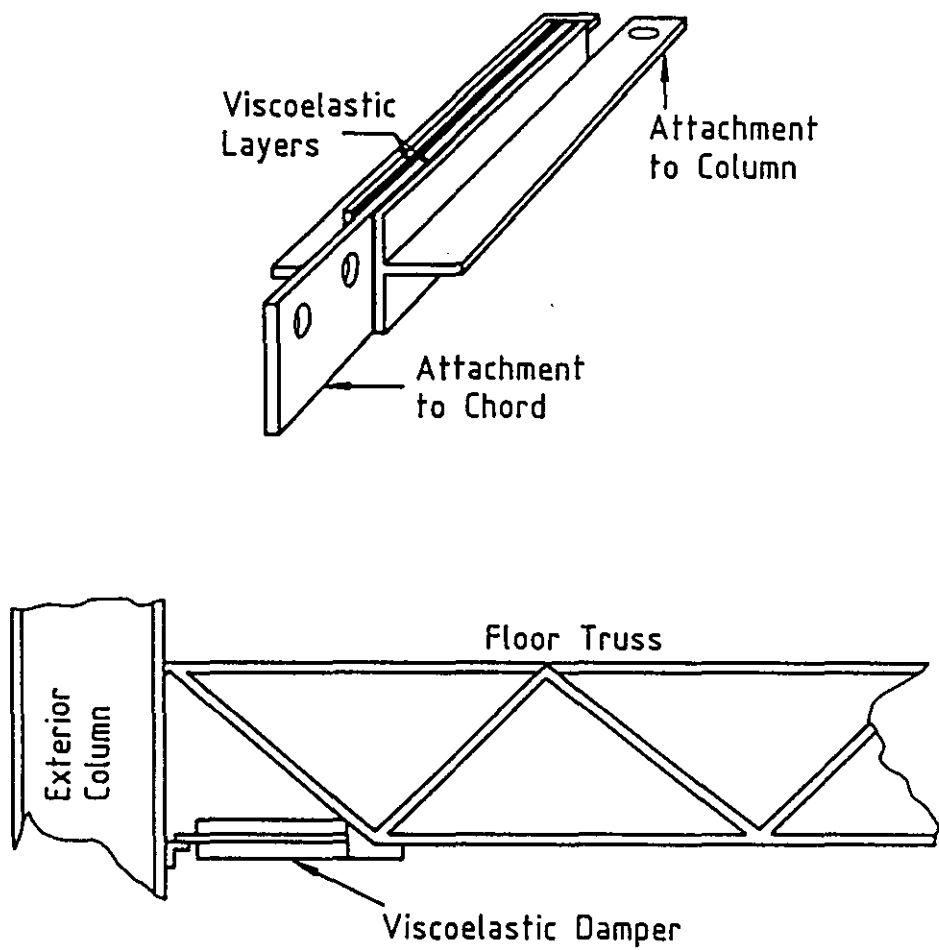


FIG. 2.4 VISCOELASTIC DAMPER USED IN THE WORLD TRADE CENTRE

Viscoelastic dampers or hydraulic dampers can also be incorporated with guy wires to form passive tendon devices which are usually used in radio masts, antennae, steel chimney stacks and bridges to suppress wind-induced vibrations.

Although viscoelastic dampers have been successfully used to suppress wind-induced vibration of tall buildings, there are still many problems worthy of further study. One of the major problems is that strong non-linear and other complex characteristics of the dampers, as well as the many dampers required to fit in one structure make it extremely difficult to predict the wind-induced response of structure-damper systems by wind tunnel test technique or computer structural analysis. Further information on viscoelastic dampers can be found in Johnson's thesis (1981), Mahmoodi and Keel (1989).

2.3.1.3 Tuned mass dampers

The concept of a tuned mass damper (TMD) as an added energy absorbing system dates back to 1909. The theory of the TMD was developed by Ormondroyd and Den Hartog (1928), and has been successfully applied in mechanical engineering systems (Den Hartog, 1955; Crandall and Marks, 1963). Attempts of applying large tuned mass dampers to civil engineering structures only began from 1970. Basically, a large TMD is a device consisting of a mass attached to a structure via a spring-dashpot system and energy is dissipated by the dashpot as relative motion develops between the mass and the structure. Four well known buildings and structures completed in 1970's are, equipped with large TMDs, the Sydney Tower, Sydney; the CN Tower, Toronto; the John Hancock Tower, Boston, and the Citicorp Center, New York City (Kwok, 1987).

Sydney Tower, the tallest structure in Australia, is 250m high with the base of the structure anchored on the roof of a 15 storey building. The Tower is one of the first structures in the world to have a large scale TMD installed. The 180 tonne doughnut-shaped water tank, as shown in Fig. 2.5, located near the top of the Tower and required by law for fire protection, was incorporated into the design of the TMD (Vickery and Davenport, 1970;

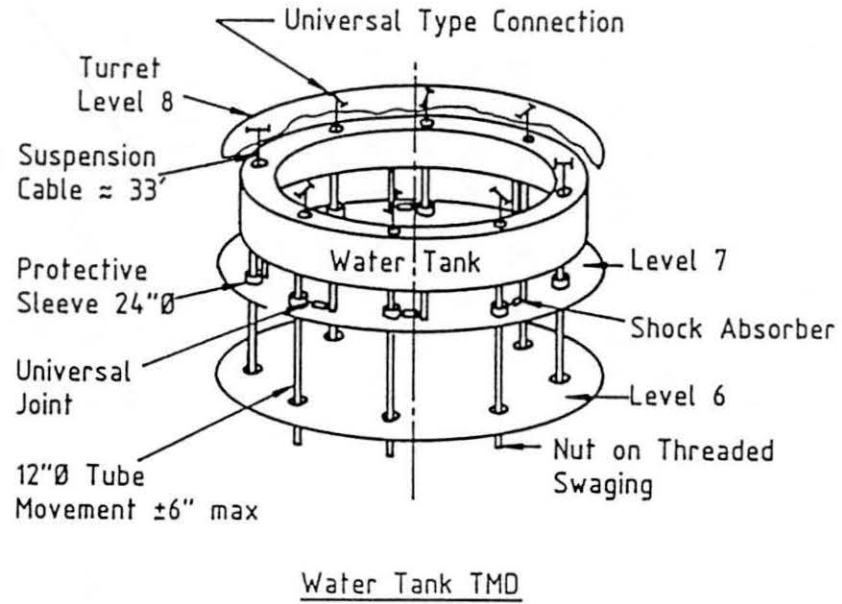
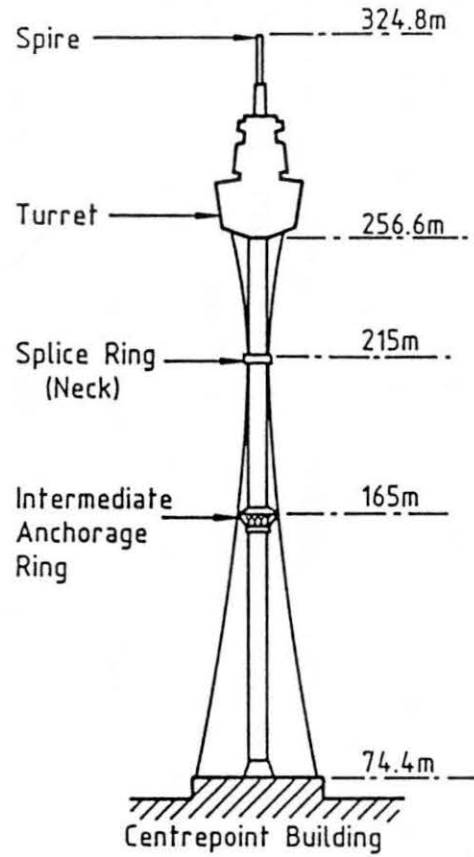


FIG. 2.5 SOME FEATURES AND PRINCIPAL DIMENSIONS OF SYDNEY TOWER (AFTER KWOK, 1983)

Engineering News Record, 1971). Energy associated with relative movements between the Tower and water tank is dissipated by 8 shock absorbers installed tangentially to the tank and anchored to the floor of the Turret. A 40 tonne secondary TMD was later installed during mid-December, 1981 on the Intermediate Anchorage Ring to further increase the damping level, particularly in the second mode of vibration (Kwok, 1983; Wargan, 1983).

The 102m steel antenna mast on top of the 553m CN Tower, the world's tallest free-standing structure, has two doughnut-shaped pendulum dampers to reduce the second and fourth modes of structural vibration (Engineering News Record, 1976). The circular steel rings are 2.45m and 3.05m in diameter, 0.36m wide and 0.31m deep, and together hold 18 tonnes of lead. Each ring is supported via universal joints by three steel beams attached to the side of the antenna mast, which allows pivoted motions in all directions. Shock absorbers are anchored on the side of the mast and attached to the center of each universal joint to dissipate energy.

The 278m tall Citicorp Centre employed a 373 tonne tuned mass damper system, as shown in Fig. 2.6, which is located on the 63rd floor (Isyumow et al., 1975; Engineering News Record, 1977; Peterson, 1979; Weisner, 1979). The mass rides on 12 low friction hydrostatic bearings and has a travel range of $\pm 1.14\text{m}$ in both the north-south and east-west directions. The damper stiffness is provided by nitrogen-charged pneumatic springs and the spring rate and hence the tuning frequency can be varied by adjusting the pre-charge pressure. The damper damping is provided by two hydraulic actuators. The TMD facility was used as an excitor to determine the natural frequency and damping of the building. The operational parameters of the TMD are: a mass ratio of 2%, damper damping of 14% of critical, and tuning ratio of 1. As a result, this gives a total damping of about 4% of critical, which should reduce the dynamic response by about 50%, according to the existing parametric study method of TMDs.

The 60 storey Hancock Tower in Boston used a tuned mass damper system similar to that in the Citicorp Centre after architects realised that the building had insufficient wind bracing to prevent occupant discomfort (Engineering News Record, 1975, 1977). Two 273 tonne TMDs were

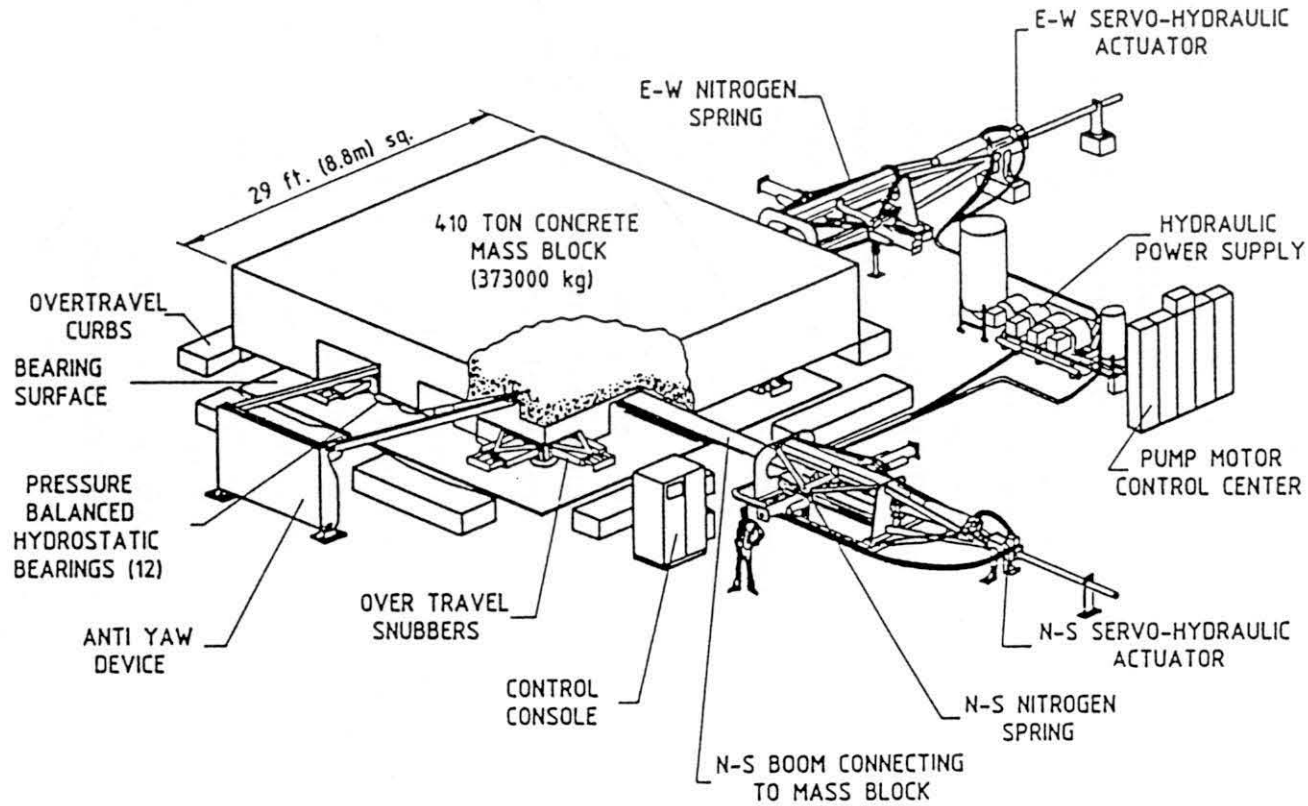


FIG. 2.6 TUNED MASS DAMPER SYSTEM IN CITICORP CENTRE (AFTER WEISNER, 1979)

installed 67m apart at either ends of the 58th floor. The dampers were designed to move only in the east–west direction and can be induced to work together to counteract swaying motions or in opposition to resist torsional motions.

The engineering design procedure of a TMD for suppressing wind–induced vibration of tall/slender structures usually is:

- (a) aeroelastic model test of the proposed structure without any TMD model in wind tunnel to determine whether added damping may be necessary, how much added damping may be needed, and what is the desired location of the TMD,
- (b) parametric studies of the TMD to decide TMD tuning, mass and damping for the required motion reduction,
- (c) if necessary, conducting aeroelastic model test in wind tunnel of the proposed structure with the TMD model to ensure the realisation of the required motion reduction,
- (d) After the completion of the main structure and before the installation of the real TMD, consider field measurement to determine the frequencies and dampings of the main structure and compare the measured results with the evaluated values,
- (e) Adjusting and setting the real TMD and then checking the various parameters of the structure–damper system and the performance of the TMD by using the TMD facility and full scale measurement.

Vickery and Davenport (1970) conducted aeroelastic model tests of Sydney Tower with and without auxiliary mass dampers and presented a method of performing parametric studies of TMDs in civil engineering structures based on an equivalent two–degree–of–freedom system, white noise excitation and the concept of effective damping. Kwok (1983), Kwok and Macdonald (1987) carried out field measurements of Sydney Tower prior to and after the installation the second TMD. Aeroelastic model tests of Citicorp Centre, which included the TMD test, were performed by Isyumov, Holmes, Surry and Davenport (1975). A detailed real TMD system design of Citicorp Centre, including passive spring system, mass block support bearings, control actuator, hydraulic power supply, electronic control and system installation, was described by Petersen (1979). Taking the Citicorp

Centre and Hancock Tower as a background, McNamara (1977), Luft (1979) and Wiesner (1979) further discussed the effectiveness and parametric studies of TMDs in reducing wind-induced building vibrations. However, all parametric studies of TMDs are based on sinusoidal or white noise excitation. Tanaka and Mak (1983) recognised the dependence of the optimised design parameters on the characteristics of random excitation and adopted a limited-band white noise excitation as wind excitation to perform parametric studies of TMDs. Other scholar's research, e.g, Kareem (1983) and Mataki et al. (1989), provided further understanding of the TMD performance.

Although great progress has been made of the application of large scale TMDs in civil engineering structures, many problems are worthy of further study. A system investigation of the TMD's effectiveness in suppressing wind-excited vibrations due to different mechanisms, including alongwind turbulence and incident turbulence in crosswind direction, crosswind wake excitation, lock-in and torsional excitation, has not been conducted, especially for tall buildings. In the existing TMD design procedure, the theoretical results of TMD parametric studies, without considering different wind excitation mechanisms and effects of building size, shape and surroundings on the wind loads, can be unreliable and inconsistent with experimental results obtained from aeroelastic model tests or prototype measurements. When a TMD is tuned to fundamental frequency of a structure, effects of vibration in higher modes and soil compliancy under the footing of the structure on the performance of a TMD should also be investigated. These problems form the main part of this thesis, and further critical review and detailed discussion are presented in Chapters 3, 4, 5, 8 and 9.

2.3.1.4 Liquid dampers

Liquid dampers consist of a container partially filled with liquid. When the container oscillates due to structural motions, the liquid damper absorbs and dissipates structural vibration energy by means of viscous action of the fluid, wave breaking, friction at the solid boundary and contamination at the liquid free surface. Motivation for applying liquid dampers in civil

engineering structures came from the spacecraft technology where torus-shape partially-filled ring-type nutation dampers are frequently used to control very long period librational motion (Amieux, 1972; Alfriend, 1974). This type of damper has several potential advantages, including low cost, easy installation, and a few maintenance requirements.

Modi and Welt (1988) carried out extensive parametric studies and wind tunnel tests of the nutation damper (doughnut-shape), and showed that the damper is effective for suppressing vortex-induced resonance and golloping instability of tall/slender structures. They also investigated the energy dissipation mechanism of the nutation damper using a nonlinear potential flow model in conjunction with boundary layer correction. Fujino et al. (1988) performed parametric studies and energy dissipation mechanism analysis of circular and rectangular liquid dampers (see Fig. 2.7) and called them the tuned liquid damper (TLD), for it is necessary to tune the liquid frequency to the natural frequency of the structure to attain large additional damping specially at small to moderate vibration amplitude. The tuned liquid damper is conceptually the same as the nutation damper. Circular tuned liquid dampers have been installed in Nagasaki Airport Tower (height 42m) and Yokohama Marine Tower (height 101m) in Japan. Fujii et al. (1990) measured the characteristics of the wind-induced vibration of both towers and confirmed that the tuned liquid dampers can effectively reduce wind-induced response of structures. The dynamic response analysis of the TLD-structure system is also discussed by Kareem (1990).

The energy dissipation mechanism of the circular, rectangular or doughnut-shape tuned liquid dampers is quite complicated and therefore causes considerable numerical difficulty in the solution of the equations of liquid motion. Sakai et al. (1989) investigated another type of tuned liquid damper which is called the tuned liquid column damper (TLCD) because the container shape is tube-like. The free vibration tests and frequency sweep tests of model TLCD showed that the TLCD can also effectively provide added damping for structures and the liquid motion in a TLCD can be simply discribed by one varying-quantity equation. Their investigation only considered simplified modelling of the main structure and wind excitation. In Chapter 8 of the thesis, a lumped multi-degree-of-freedom system was

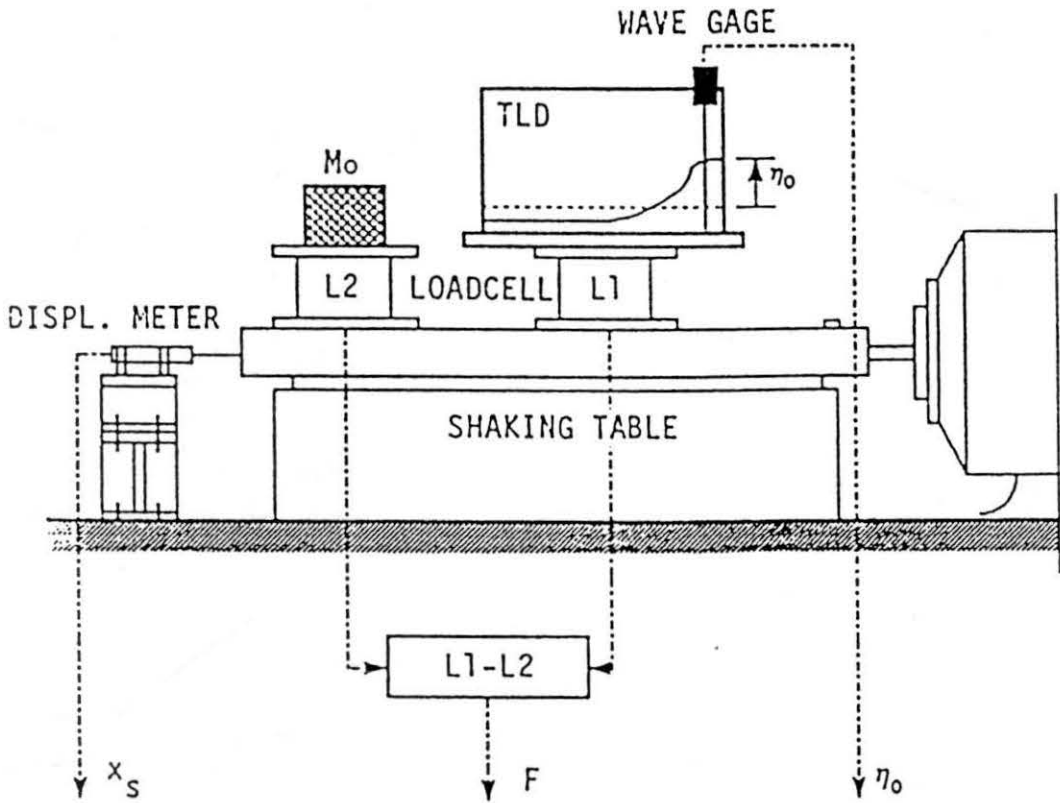


FIG. 2.7 EXPERIMENTAL APPARATUS FOR TUNED LIQUID DAMPER (AFTER FUJINO, 1989)

used to model the main structure and a random vibration analysis utilising transfer matrix formulation was carried out to investigate further the possible application of such tuned liquid column dampers in reducing the wind-induced response of slender structures.

2.3.2 Active control

Most passive dampers have a limitation of the motion reduction for a given tall/slender structure. If the required motion reduction exceeds the limit which the passive dampers can provide, an active or a semi-active control system may have to be considered. The idea of active control for civil engineering structures started to emerge around 1970. Work of Zuk (1968), Yao (1972), Roorda (1975), Yang (1975), Soong (1976) and Abdel-Rohman (1978) laid down the foundation for structural control. Since then, intensive research is being conducted and has expanded beyond narrow academic circles. Soong (1988) in a state-of-the-art review summarised recent advances in active and semi-active control technology for civil engineering structures and discussed possible future directions.

With particular reference to the application of active or semi-active control technology in reducing wind-induced vibration of tall/slender structures, control devices, control algorithms, experimental studies and existing obstacles are briefly described as follows:

(a) The forerunners of active or semi-active control devices to be applied to full scale structures against dynamic wind loads may be active tendon control systems, active or semi-active mass dampers, pulse generators, aerodynamic appendages and chambers, active liquid dampers and gyroscopes.

(b) Depending on the utilisation of the measured information from sensors, the control algorithms are classified as closed-loop control, open-loop control and closed-open-loop control. Based on control design criteria, there are a wide variety of control algorithms including optimal linear control, pole assignment, independent modal space control, instantaneous optimal control, bounded state control, sub-optimal control and non-optimal

control.

(c) The active or semi-active control experimental studies carried out to date have been severely limited in size and scope. The conducted experiments mostly concentrate on seismic-type loading supplied by a shaking table. Only one experimental study (Soong and Skinner, 1981), using aerodynamic appendages, was carried out in a wind tunnel. In this experiment, a scaled-down model of a tall structure and a closed-loop optimal linear control algorithm were used. A small metal appendage, located at the top of the model, was controlled by means of a solenoid activated by the sign of structurel velocity as sensed by a linear differential transformer. Recently, two active mass dampers have been installed on a slender eleven-storey building, which was constructed in the Kyobashi District of Tokyo, Japan, to confirm the effectiveness of active mass dampers in suppressing the vibrations from earthquake and strong winds (Kobori et al., 1990). One damper was located in the centre of the building to suppress the large lateral vibration, and another damper was fixed on the end of the building to reduce the torsion vibration. The composition and block diagram of the active mass damper system are shown in Fig. 2.8. Although the building is not a typical tall building, preliminary measurements of the building response under typhoon winds showed that the wind-induced vibration can be significantly reduced by active mass dampers.

(d) From a practical standpoint, a number of obstacles still remain. Amongst the major concerns are: time delay in processing measured information, in performing on-line computation and in executing the control forces as required; discrete-time formulation of active control algorithms since a digital computer is usually used for on-line computation and control execution; structural parametric uncertainties which will affect control sensitivity; reliability of an active control system which relies on external power sources and all the support utility systems; and cost and hardware development related to other allied areas such as computers, electronics, measurement techniques, instrumentation, materials research, etc. Therefore, simple active control systems using minimum number of actuators and sensors deserve more attention and further experimental verification must be

considered as the single most important task to be undertaken before full-scale testing is conducted.

As an approach to the experimental verification of the effectiveness of active control systems, a suboptimal closed-loop control system suggested by Roorda (1975), Yang (1982) and Samali (1985) was semi-analytically investigated in the thesis by means of the measured wind excitation spectra and tested models in the wind tunnel. Further explanation and review of the suboptimal closed-loop control system will be presented in Chapter 7.

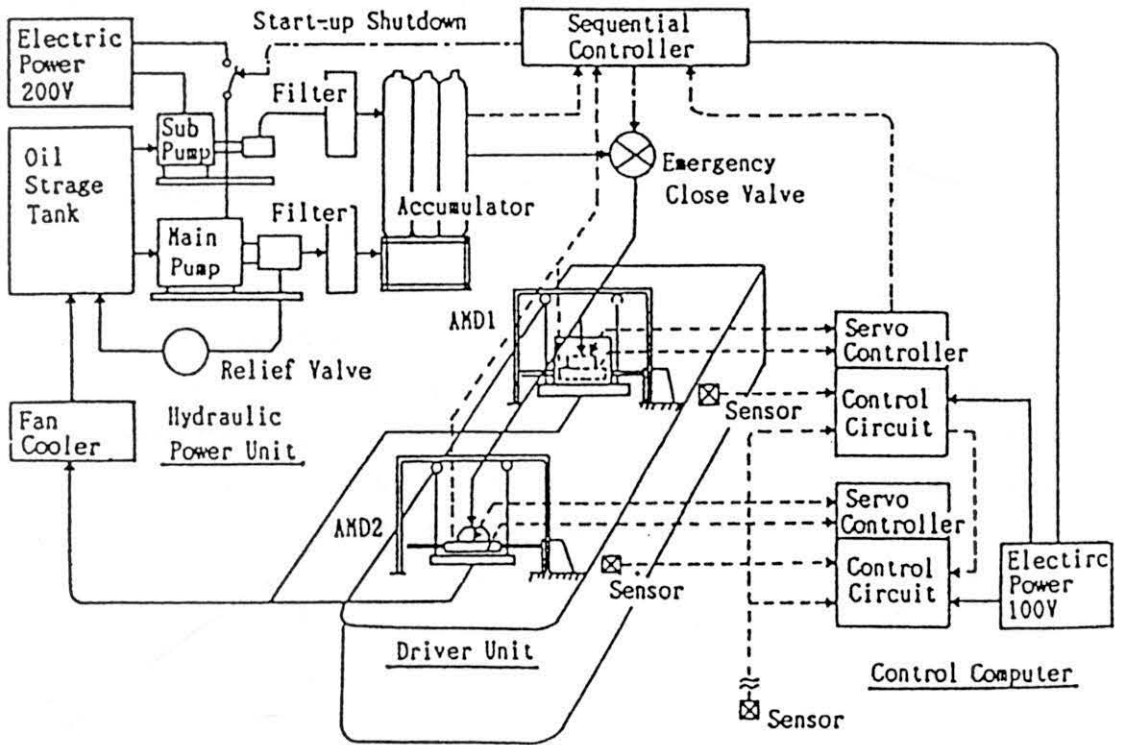


FIG. 2.8 BLOCK DIAGRAM OF THE ACTIVE MASS DAMPER SYSTEM OF KYOBASHI BUILDING (AFTER KOBORI, 1990)

Chapter 3

PASSIVE CONTROL OF WIND-INDUCED TRANSLATIONAL VIBRATION OF TALL BUILDINGS BY TUNED MASS DAMPERS

3.1 Introduction

Aeroelastic modelling in wind tunnel tests is of principal value in studies of tall/slender structures which are sensitive to wind-induced dynamic effects. The experimental results of an aeroelastic model can be used to determine whether a tuned mass damper may be needed to reduce excessive vibration of the corresponding prototype structure. If this is necessary, the aeroelastic test of the structure model with model tuned mass dampers may be conducted to demonstrate the effectiveness of the TMDs. However, few experimental investigations using wind tunnel tests have been made in order to determine the effects of different wind excitations acting on a tall building and the effectiveness of a TMD.

Based on the theoretical results of TMD parametric studies, it has been pointed out that added damping provided by a TMD is greater for harmonic force than for white noise excitation (Hirsch, 1979). Tanaka and Mak (1983) further considered wind excitation as band-limited white noise excitation, in which pure white noise and a simple harmonic excitation can be regarded as the two extremes of wide-band and narrow-band excitations respectively, in conducting the parametric study of a TMD. Their results showed that, for a given mass ratio, the narrower the bandwidth, the higher the added damping provided by the TMD. As the bandwidth becomes narrower, the maximum effective damping is more sensitive to the change of the mass ratio and the damper's optimum damping tends to stay with the lower mass ratio. In their study, the peak frequency of band-limited white noise excitation was chosen to coincide with the natural frequency of the primary system.

Actual wind excitations are, however, quite complex and most peak frequencies in measured wind excitation spectra do not coincide with the fundamental frequency of the structure, except for wind-induced lock-in excitation. Therefore, these theoretical models of wind excitations only approximately represent some extreme situations of actual wind excitations. An experimental investigation is necessary and seems to be the only way.

In this Chapter, a 1:400 scale aeroelastic model of the CAARC Standard Tall Building and tuned mass dampers of different parameters were designed and tested in a wind tunnel with properly simulated atmospheric boundary layer flow. The effectiveness of the tuned mass dampers under different wind excitation mechanisms, including alongwind turbulence, partial incident turbulence in crosswind direction, crosswind wake excitation and excitation due to crosswind displacement, are investigated. The displacement response signals of the building model with or without a damper were transferred to and processed by a mini-computer to obtain wind-induced response spectra and upcrossing probability distributions for exploring characteristics of the TMD. Although a 1:1000 scaled aeroelastic model of CAARC Standard Tall Building was chosen by Tanaka and Mak (1983) for the wind tunnel test to demonstrate the damper's effectiveness, the published experimental data are quite limited and the effects of different wind excitations on the effectiveness of TMDs were not discussed in terms of the experimental results.

A review of the scaling requirements for aeroelastic studies of tall building is arranged before the description of the experiment. The experimental results in this Chapter are used in Chapter 5 for the parametric study of TMDs.

3.2 Aeroelastic Model Requirements

Accurate estimates of wind effects on buildings and structures by direct measurements on small-scale models tested in a wind tunnel require satisfactory modelling of both the natural wind and the structure. The basic modelling requirements for aeroelastic tests, which are developed through

dimensional analysis and law of similarity, are that non-dimensional groups presented in Table 3.1 are maintained constant between model and prototype (Whitbread, 1963; Melbourne, 1972).

In practice it is rarely possible to satisfy all these requirements and some amount of compromise is necessary. An understanding of local full scale data is required to assess their relative importance so that some may be neglected.

The meaning of variables in Table 3.1 is explained in Table 3.2 and these non-dimensional groups can be divided into two sections: one deals with the modelling of the natural wind and the other the dynamic modelling of structures.

3.3 Modelling of Natural Wind

In some situations a more complete simulation of natural wind becomes necessary, including the modelling of the lateral and/or the vertical components of turbulence as well as the Reynolds stress. However, it is generally accepted (Isyumov, 1982; ASCE, 1987a) that the most important requirements for aeroelastic simulations of tall buildings with sharp-edges are similarity of

- (a) the vertical distribution of the mean wind speed, $\bar{V}(z)/\bar{V}_G$,
- (b) the intensity of the longitudinal turbulence, $\sigma_u(z)/\bar{V}(z)$,
- (c) the integral scale of the longitudinal turbulence, which is related to the corresponding power spectral density, $nS_{uu}(n,z)/\sigma_u(z)$.

Furthermore, it appears that primary attention needs to be given to the correct simulation of the turbulence intensity, the role of the turbulence integral scale being secondary (Isyumov, 1982).

3.3.1 Wind tunnel

Wind tunnels designed to simulate an atmospheric boundary layer with

**TABLE 3.1 NON-DIMENSIONAL GROUPS FOR WIND TUNNEL
MODELLING**

Non-Dimensional Group	Name (if in common usage)	Physical Meaning
$\frac{\bar{V}}{\bar{V}_G}$	Velocity profile	Velocity ratio which defines the velocity profile
$\frac{\sigma_u}{\bar{V}}$	Turbulence intensity	Expression related to turbulence energy
$\frac{nS_{uu}(n)}{\sigma_u^2}$	Normalised power spectral density	Expression related to turbulent energy distribution with respect to frequency
$\frac{n_{BL} L_{BL}}{\bar{V}}$	Strouhal number or reduced frequency (or inverse of reduced velocity)	Time scale
$\frac{\rho \bar{V} L_{BL}}{\mu}$	Reynold number	$\frac{\text{Inertia Force (Fluid)}}{\text{Viscous Force}}$
$\frac{P}{\frac{1}{2} \rho \bar{V}^2}$	Pressure coefficient (Euler No.)	$\frac{\text{Pressure Force}}{\text{Inertia Force (Fluid)}}$
$\frac{L_{BL}}{L_s}$	Length ratio	Ratio of lengths in boundary layer and structure
$\frac{n_{BL}}{n_0}$	Frequency ratio	Ratio of frequency or time in boundary layer and structure
$\frac{\rho_s}{\rho}$	Density Ratio	$\frac{\text{Inertia Force (Struc.)}}{\text{Inertia Force (Fluid)}}$
$\frac{\rho \bar{V}^2}{E}$	Cauchy Number	$\frac{\text{Inertia Force (Fluid)}}{\text{Inertia Force (Struc.)}}$
ζ_s	Damping ratio	$\frac{\text{Energy Dissipated/Cycle}}{\text{Total Energy of Oscillation}}$

TABLE 3.2 EXPLANATION OF VARIABLES INVOLVED IN TABLE 3.1

NOTATION	MEANING
\bar{V}_G	mean freestream longitudinal velocity or velocity at gradient height
\bar{V}	local mean longitudinal velocity
σ_u	standard deviation of velocity fluctuations
L_{BL}	length associated with the external air flow
n_{BL}	frequency associated with the external air flow
$S_{uu}(n)$	power spectral density of the longitudinal velocity
ρ	air density
μ	air viscosity
P	air pressure
L_s	length associated with the structure
n_0	frequency associated with the structure
ρ_s	density of the structure
E	elastic modulus of the structure
g	acceleration due to gravity
ζ_s	damping ratio for the structure

neutral thermal stratification are classified as boundary layer wind tunnels (BLWT). One type of wind tunnels has very long fetch of roughness elements in which a boundary layer is naturally developed. Another type is short working section wind tunnels with various types of passive or active augmentation devices to generate acceptable mean and turbulent flow conditions.

The No.2 BLWT at the School of Civil and Mining Engineering, the University of Sydney, is an open jet wind tunnel with a working section of 1.5m x 1.2m and approximately 4.5m long. The augmented method, consisted of vortex generators and floor-mounted roughness elements or carpet, was employed to generate a 1/400th scale model of the natural wind. The general arrangement of No.2 BLWT is shown in Fig. 3.1.

The experiments described in this Chapter were conducted only under a 1:400 scale wind model of the natural wind flow over suburban terrain (Terrain Category 3 as described in the Australian Wind Loading Code, AS 1170.2-1989). The fetch length was covered with 0.05m x 0.025m x 0.012m roughness elements at a density of 76 m⁻² which were preceded by 4 linearly-tapered vortex generators spanning the start of the working section. Measurements of the longitudinal component of the wind in the wind tunnel were taken with a calibrated hot-wire connected to a Disa Constant Temperature Anemometer and Lineariser. The hot wire signal was processed in real-time by a micro-computer and stored on a floppy-disc for power spectral analysis by a mini-computer.

3.3.2 Mean wind speed profile

Mean wind speed profiles at three lateral positions (see Fig. 3.1) are presented in Fig. 3.2. The profiles are closely represented by the power-law with an exponent $\alpha = 0.25$, i.e.,

$$\frac{\bar{V}(z)}{\bar{V}(z_r)} = \left(\frac{z}{z_r}\right)^\alpha \dots \dots \dots (3.1)$$

where z_r is a reference height = 0.5m.

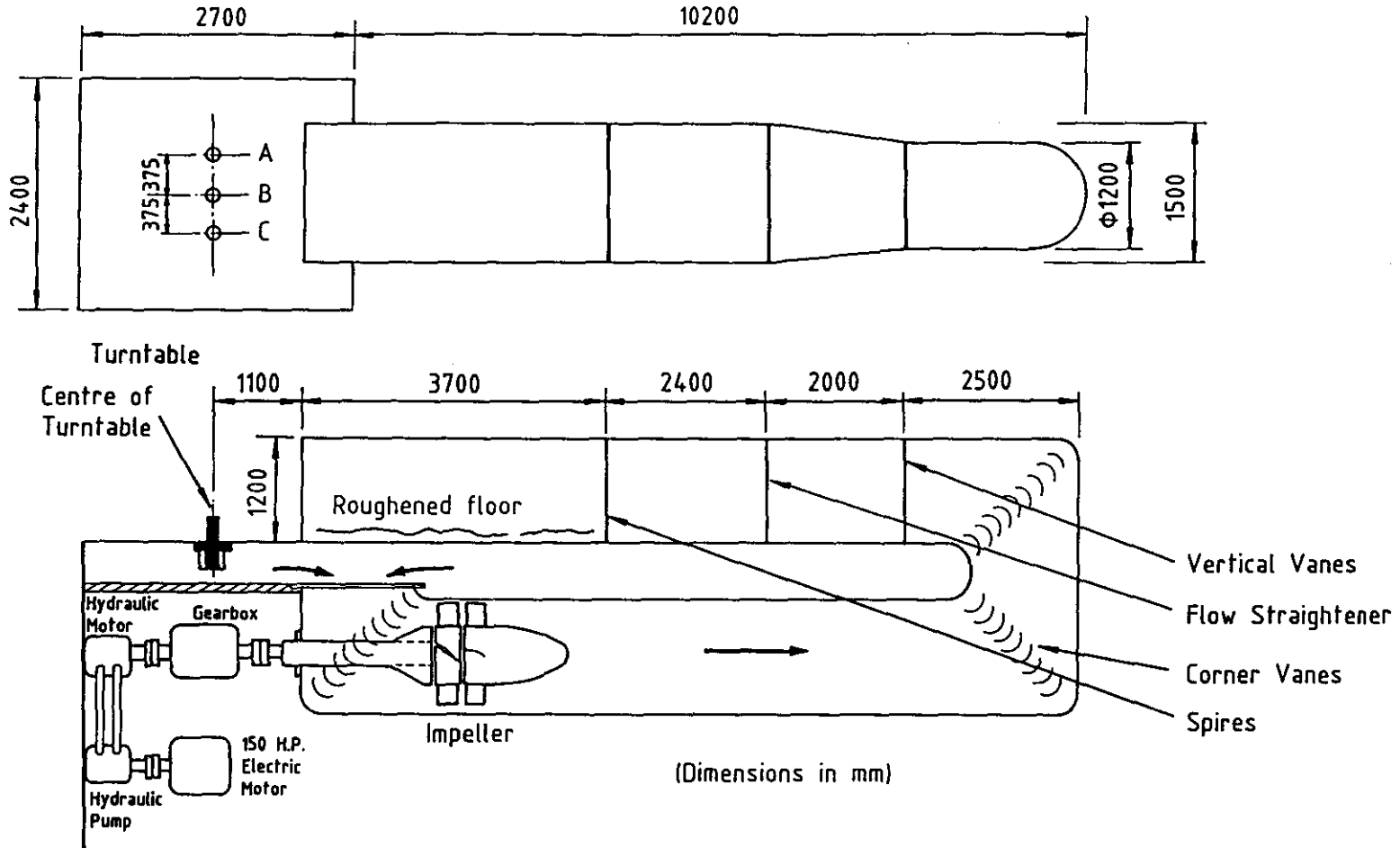


FIG.3.1 GENERAL ARRANGEMENT OF NO.2 BOUNDARY LAYER WIND TUNNEL

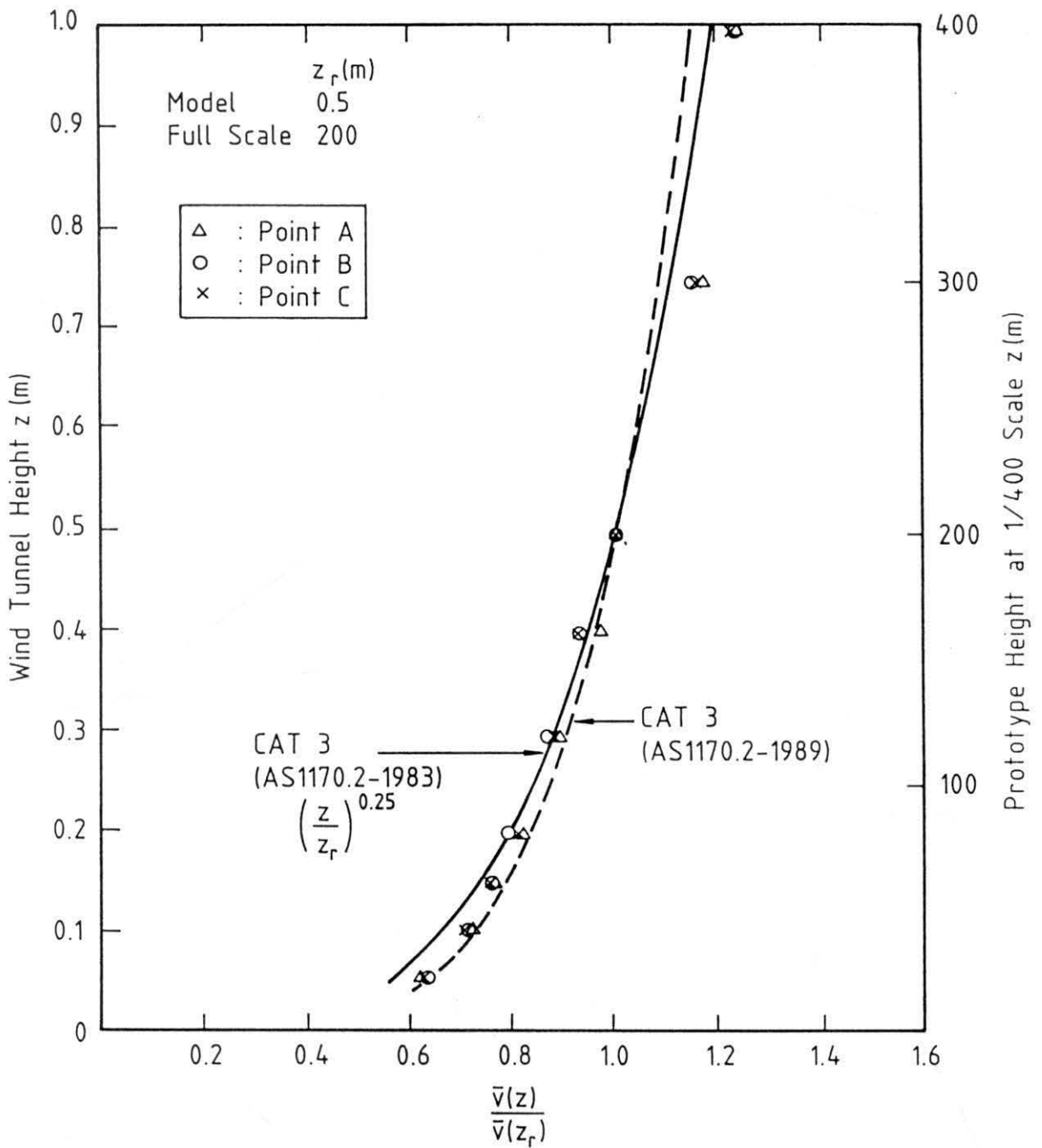


FIG.3.2 MEAN WIND VELOCITY PROFILES

The profiles were found to be consistent with the prototype profile suggested by AS 1170.2-1989. Variation in the immediate vicinity of the turntable centre, where the models were tested, was also small.

3.3.3 Longitudinal turbulence intensity profile

Turbulence intensity I_u is defined as the ratio of the standard deviation fluctuation σ_u to the mean speed \bar{V} , that is,

$$I_u(z) = \frac{\sigma_u(z)}{\bar{V}(z)} \dots \dots \dots (3.2)$$

The longitudinal turbulence intensity profiles at the same positions as those of the mean wind speed profiles are shown in Fig. 3.3, together with the prototype turbulence intensity profile provided by AS 1170.2- 1989 for comparison. Turbulence intensity is about 12% at the top of the model and the thickness of the boundary layer is found to be approximately 0.9m at the test section.

3.3.4 Integral length scale of longitudinal turbulence

The longitudinal turbulence spectrum is used to determine the distribution of turbulence energy as a function of frequency. The measured spectrum of the simulated boundary layer flow at the top of the model is given in Fig. 3.4. This spectrum is also compared, at 1/400 scale, with the Harris-Von Karman prototype empirical spectrum which may be expressed as follows (ESDU 74031, 1974):

$$\frac{nS_{uu}(n, h)}{\sigma_u^2(h)} = \frac{4 \left(\frac{n\ell_{ux}(h)}{\bar{V}(h)} \right)}{\left[1 + 70.8 \left(\frac{n\ell_{ux}(h)}{\bar{V}(h)} \right)^2 \right]^{5/6}} \dots \dots \dots (3.3)$$

where h is the height of the model and $\ell_{ux}(h)$ is the integral length scale of turbulence at h .

From Eq. 3.3 it is obvious that each spectrum can be described uniquely

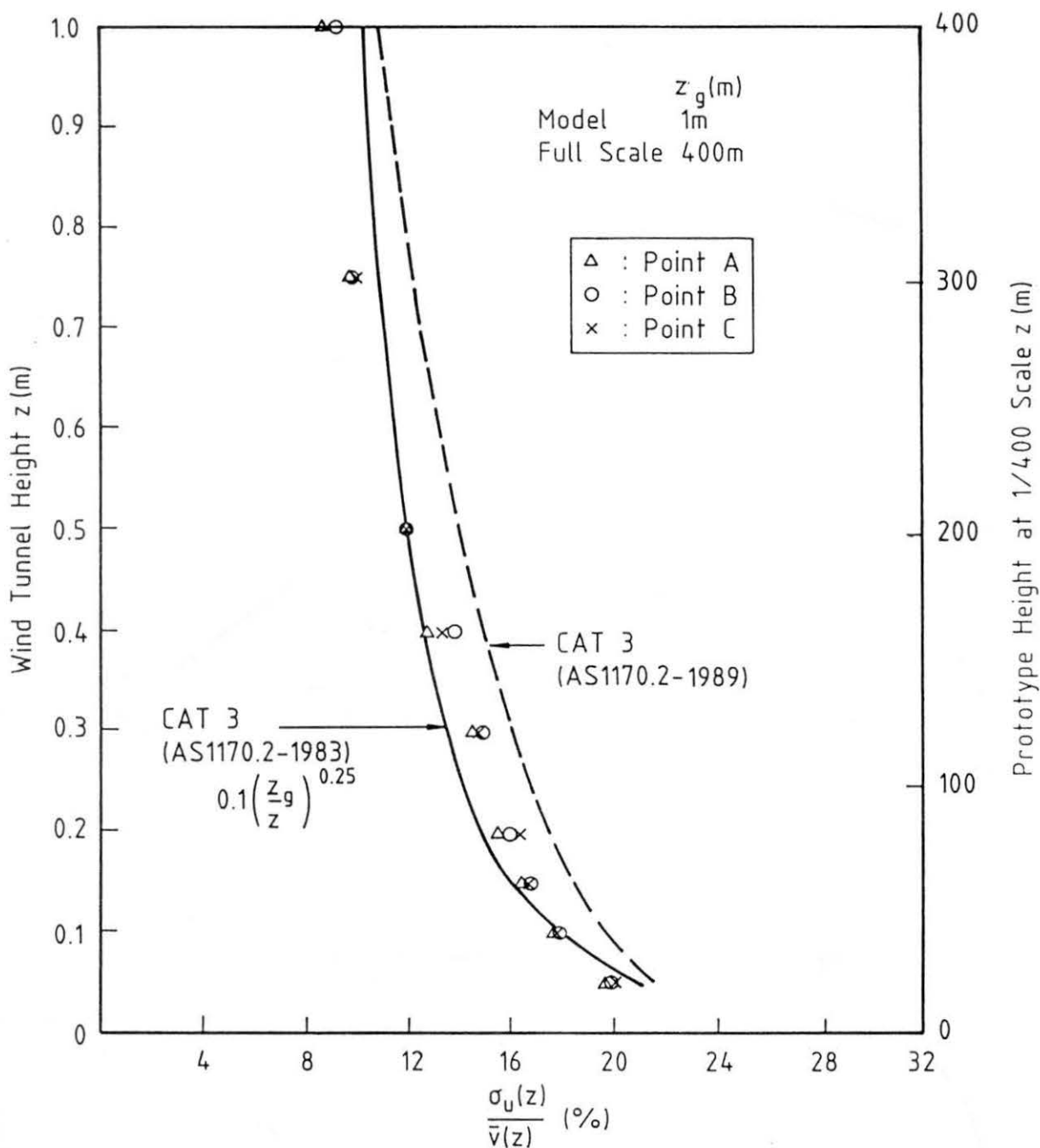


FIG.3.3 LONGITUDINAL TURBULENCE INTENSITY PROFILES

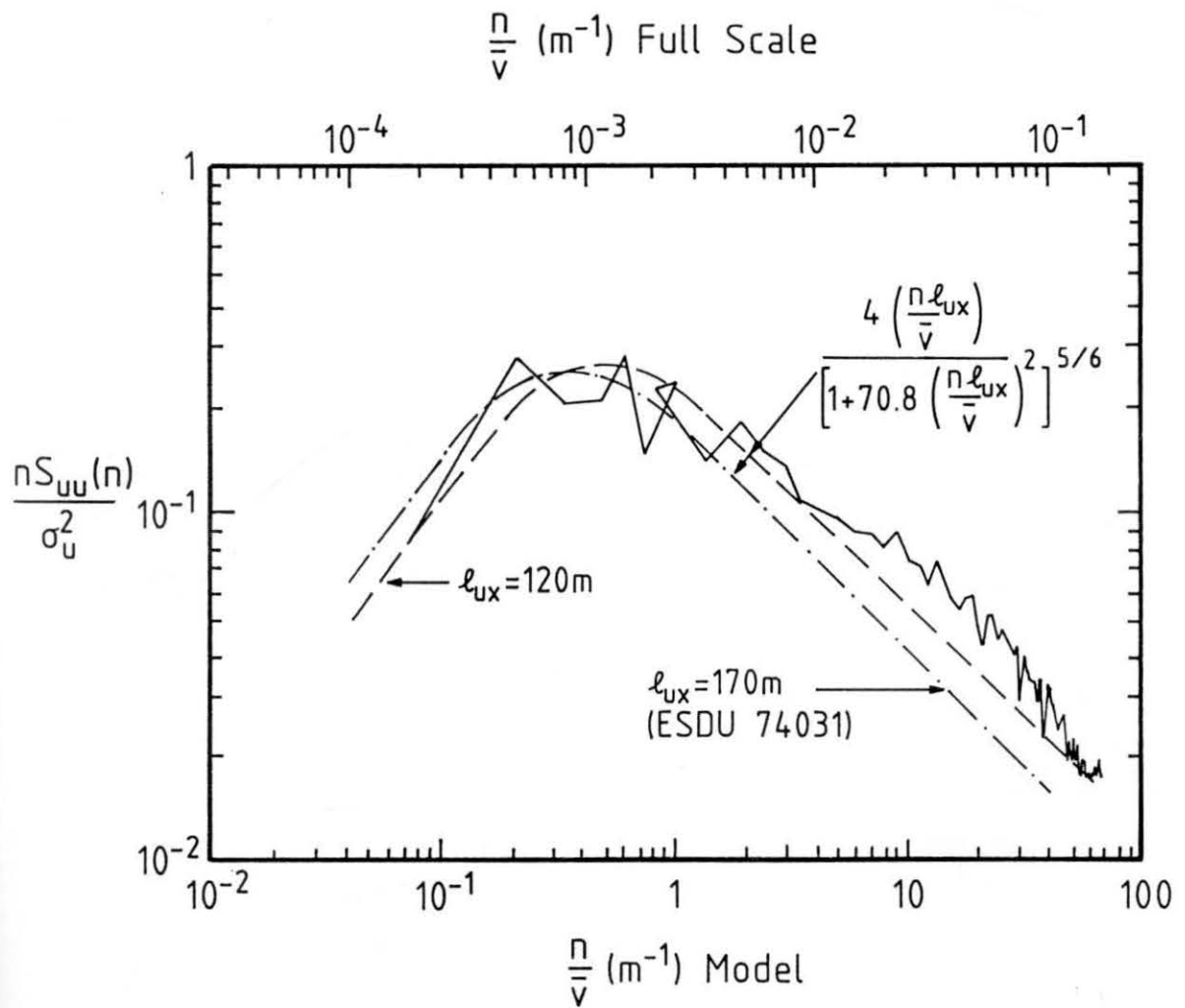


FIG.3.4 LONGITUDINAL TURBULENCE SPECTRUM AT 1/400 SCALE

by ℓ_{ux} . Therefore, the integral length scale of longitudinal turbulence ℓ_{ux} is also a typical length scale of the energy containing eddies, and it is found to be approximately 120 m at the top of the building model from the measured turbulence spectrum. The corresponding scale of the Harris-Von Karman spectrum under the same terrain category is 170 m as suggested in Engineering Science Data Unit (1974). There is a small mismatch by a factor of 1.4.

3.4 Aeroelastic Modelling of Buildings and Dampers

3.4.1 General description

Common types of aeroelastic model simulations for tall buildings are based on equivalent discrete representations which are designed to simulate, at a reduced scale, the dynamic properties of the more important modes of structural vibration. For most tall buildings of compact and torsionally stiff cross-section, the wind-induced response is primarily in the two orthogonal fundamental sway modes of vibration and the deflection of the fundamental mode can be approximated by a straight line pivoted near the base. Therefore, conventional aeroelastic models as shown in Fig. 3.5 are widely used in wind tunnel studies of tall buildings.

In this simulation, a rigid building model is attached to one end of an aluminium bar which is pivoted near the building base by a gimbal arrangement. The other end of the aluminium bar is restrained by appropriately selected springs, and an oil bath is used to simulate viscous structural damping. The other components are a ballast weight adjustable to achieve correct inertial scaling, and strain gauge bridges, which provide an indication of the wind-induced top deflection and base overturning moment of the building model. Results of a number of aeroelastic studies of tall buildings carried out at the Boundary Layer Wind Tunnel Laboratory at the University of Western Ontario indicate that this modelling technique adequately defines most significant components of the wind-induced dynamic response (Isyumov et al, 1975; Isyumov, 1982). A significant practical advantage of this approach is the freedom of readily varying the building

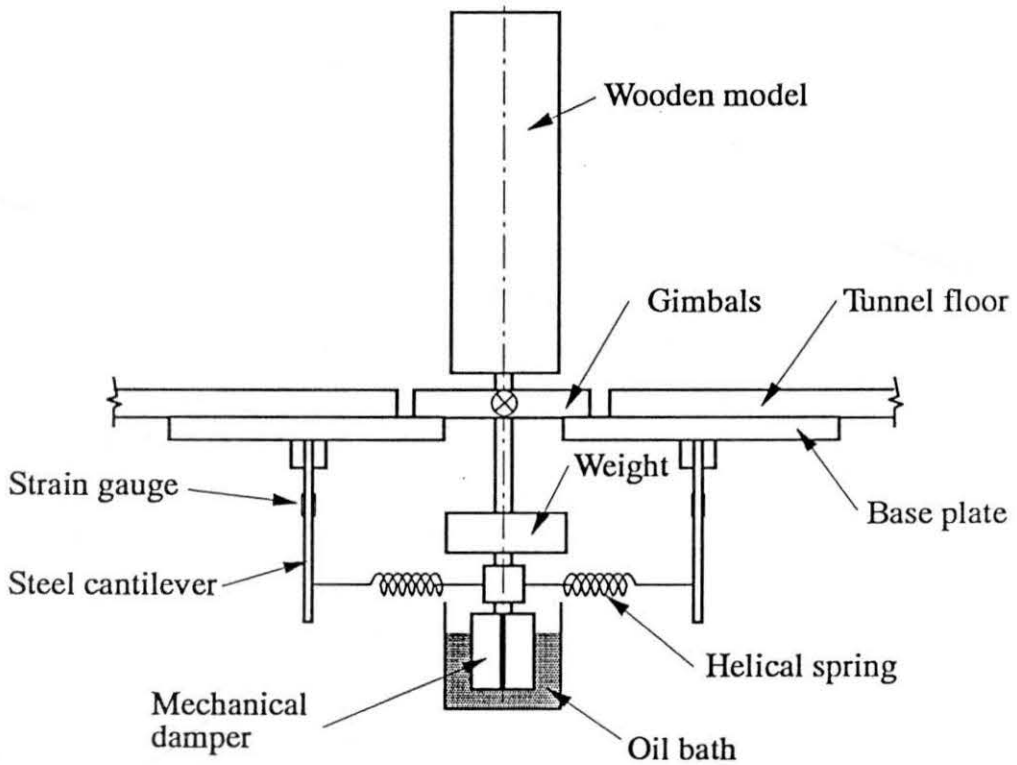


FIG. 3.5 SCHEMATIC REPRESENTATION OF AEROELASTIC TRANSLATION MODEL

mass, stiffness, damping and even the geometric properties. The experiments described in this Chapter were conducted by using this type of aeroelastic modelling technique.

In situations where the prototype mode shapes depart significantly from a straight line variation, a correction may be necessary to allow for differences between the model and prototype responses or excitations. This correction is discussed in Chapter 6. If torsional effects are judged to be important for some complex buildings, a similar aeroelastic test for pure torsion may be required, which is explained in the next Chapter. However, when the modes of vibration are highly 3-dimensional due to inertial and/or elastic coupling between various degrees of freedom, multi-degree-of-freedom aeroelastic models have to be used. The discussion of this aspect is beyond the aim of this thesis.

3.4.2 Derivation of scaling ratios

The geometric length scale λ_L is defined as

$$\lambda_L = \frac{L(\text{model})}{L(\text{prototype})} = \frac{L_m}{L_p} \dots \dots \dots (3.4)$$

To maintain equality of the ratio of overall building dimensions to the inherent lengths of the generated model of the natural wind, the length scaling parameter λ_L in this experiment was chosen as 1:400. Because the model blockage was less than 3% of the wind tunnel cross section and the wind tunnel was an open jet wind tunnel, no correction for the experimental results was considered.

The mass scaling parameter λ_M can be determined by the modelling criteria which implies equality of the bulk density ratio in model and in full scale, that is,

$$\lambda_M = \frac{L_m^3 \rho_{sm}}{L_p^3 \rho_{sp}} = \lambda_L^3 \lambda_{\rho_s} = \lambda_L^3 \quad (\text{for mass scale}) \dots \dots \dots (3.5)$$

$$\lambda_{I\theta} = \frac{L_m^5 \rho_{sm}}{L_p^5 \rho_{sp}} = \lambda_L^5 \lambda_{\rho_s} = \lambda_L^5 \text{ (for mass moment scale of inertia).} \quad (3.6)$$

Here the model air and structural densities are assumed to be equal to those of the prototype.

The time and velocity scales can be derived, in the simplest form, from the Strouhal number or the reduced velocity, that is,

$$\left(\frac{nL}{\bar{v}}\right)_{\text{model}} = \left(\frac{nL}{\bar{v}}\right)_{\text{prototype}} \quad (3.7)$$

Therefore, the relationship between the time scaling parameter λ_T and the velocity scaling parameter λ_V is

$$\lambda_T = \frac{n_p}{n_m} = \frac{\lambda_L}{\lambda_V} \quad (3.8)$$

where $\lambda_V = \bar{v}_m / \bar{v}_p$.

The Cauchy number can be expressed in the form

$$\left(\frac{\rho \bar{v}^2 L^3}{K_\theta}\right)_{\text{model}} = \left(\frac{\rho \bar{v}^2 L^3}{K_\theta}\right)_{\text{prototype}} \quad (3.9)$$

Therefore the rotation stiffness scaling parameter $\lambda_{K\theta}$ is

$$\lambda_{K\theta} = \frac{K_{\theta m}}{K_{\theta p}} = \lambda_V^2 \lambda_L^3 \quad (3.10)$$

Now the time scaling parameter is also be given by the period of oscillation so that

$$\lambda_T = \frac{\lambda_L}{\lambda_V} = \sqrt{\lambda_{I\theta} / \lambda_{K\theta}} \quad (3.11)$$

The velocity scale is then determined by the natural frequency of the model, which is in turn determined by the spring stiffness of the test rig or

vice versa. A more detailed derivation can be found in Melbourne (1972) and Isyumov (1982).

While structures with circular cross-section or rounded corners are very sensitive to Reynolds number, strict Reynolds number similarity is less significant for sharp-edged bodies. The flow around prismatic shapes is determined by the building geometry as flow separation tends to occur at the building corners. As a result, the influence of Reynolds number on the overall flow around rectangular and square building shapes, particularly in turbulent boundary layer flows, is generally not found to be significant.

3.4.3 Model building and tuned mass dampers

The CAARC Standard Tall Building was chosen to represent a typical highrise building. A 1:400 scaled aeroelastic model of this building was designed and mounted on the test rig as shown in Fig. 3.5. The model was of a rigid wooden construction and assumed to have a structural density of 180 kg/m^3 . The fundamental frequency of the prototype was chosen as 0.2 Hz and the corresponding structural damping was 1%. These parameters are reasonable values which fall within the range of the full scale data of modern tall buildings although full scale data are quite scattered.

The model tuned mass damper consisted of a small aluminium block cantilevered downward on a piano wire. The wire was covered with plastic tape to provide proper damping to the tuned mass damper. An adjustable mounting allowed the length of the cantilever to be varied, facilitating fine tuning of the damper frequency. The base of the cantilever was positioned at the centre of the top cover of the building model. These arrangements are similar to that described by Isyumov et al. (1975). The physical dimensions of the building model and three tuned mass damper models are listed in Table 3.3. The mass ratios (i.e., damper mass over building first mode generalised mass) are, respectively, 2.5%, 3.5% and 4.6%. The dampers were approximately tuned to the natural frequency of the building model, and the dampings of the dampers corresponded to viscous dampings of about 3.2% to 4.2% of critical. These properties were expected to lead to a significant reduction of building vibration based on preliminary

TABLE 3.3 PHYSICAL PROPERTIES OF THE BUILDING AND TUNED MASS DAMPERS MODELS

Building Model	Size	0.465x0.1125x0.075 (m)
	Generalised Mass	0.2375 (kg)
	Natural Frequency	5.92 (Hz) x-x, y-y
	Structural Damping	0.010 of critical, x-x, y-y
Tuned Mass Damper Model 1 (TMD 1)	Mass	0.0059 (kg)
	Frequency	6.1 (Hz)
	Damping	0.032 of critical
Tuned Mass Damper Model 2 (TMD 2)	Mass	0.0082 (kg)
	Frequency	6.2 (Hz)
	Damping	0.040 of critical
Tuned Mass Damper Model 3 (TMD 3)	Mass	0.0110 (kg)
	Frequency	6.0 (Hz)
	Mass	0.042 of critical

parametric studies of TMDs and experimental conditions.

3.5 Experimental Arrangements

The whole testing rig with the building model was mounted on the turntable of the wind tunnel so that the wind direction could be varied relative to the model. The signal output from the strain gauge bridges was low-pass filtered at 30Hz to attenuate the high instrumentation noise. It was then digitised by means of an analogue to digital converter, and sampled by a micro-computer. The aeroelastic model was calibrated to relate the output data from the micro-computer to applied top displacements in both alongwind and crosswind directions. The dampings and natural frequencies of the building model with or without the TMDs were determined from the decay of free vibration (see Fig. 3.6). A small vibration table was used to measure the natural frequency of each damper by using resonant method and two methods were used to determine the damper damping: one used a non-contact laser displacement sensor to obtain the decay of free vibration; the other used the free decay vibration theory of the two-degree-of-freedom system which is presented in Appendix A.

The mean (static) and standard deviation (dynamic) alongwind displacement responses \bar{x} and σ_x , and the standard deviation crosswind displacement response σ_y at the top of the building model without, then with, tuned mass dampers were measured at reduced wind velocities $\bar{V}/(n_0 b)$ ranging from 4 to 18 and at a structural damping value of 1% of critical damping. This wind velocity range included the critical reduced velocity of the building model. It should be noted that the reduced velocities were based on the width of the building, b , normal to the wind. \bar{V} is the mean wind velocity at the top of the building and n_0 is the natural frequency of the building without any dampers. These measurements were made with the on-line digital computer data acquisition system for a period of time corresponding to approximately one and half hour in full scale. The velocity fluctuations in the near wake of the building model were also measured using a vertically-aligned hot-wire. Some of the displacement response signals and the hot-wire signals were saved in real-time by the

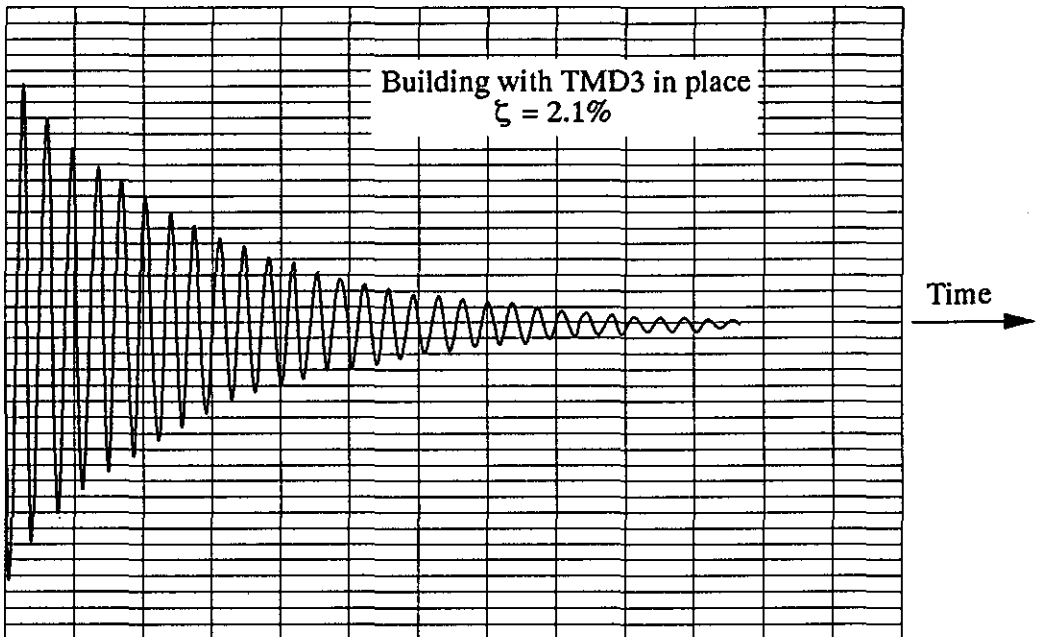
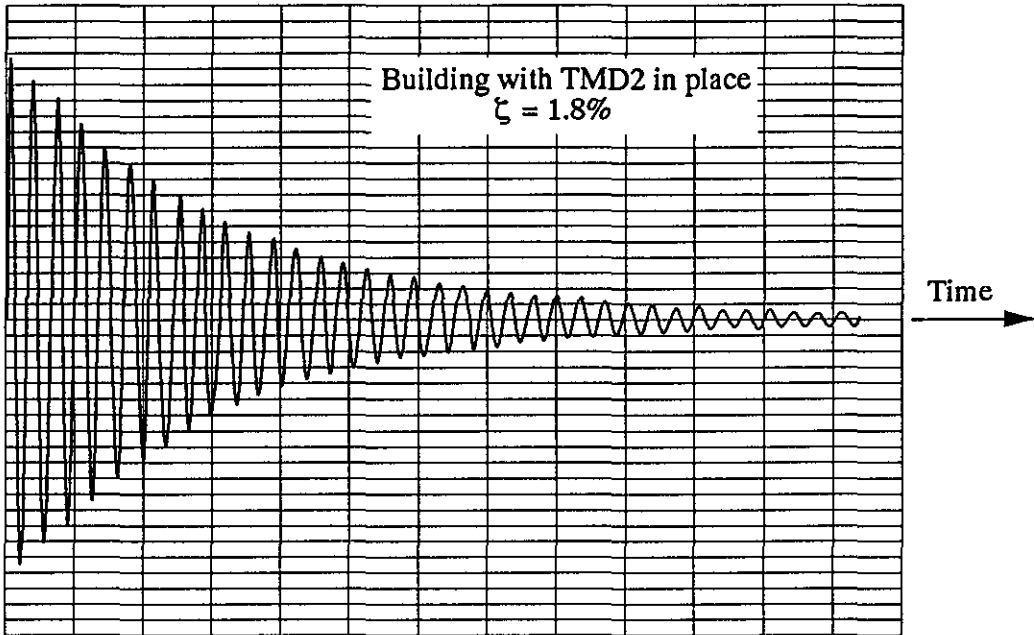


FIG. 3.6a FREE VIBRATION DECAY TRACES SHOWING EFFECTIVENESS OF TUNED MASS DAMPERS

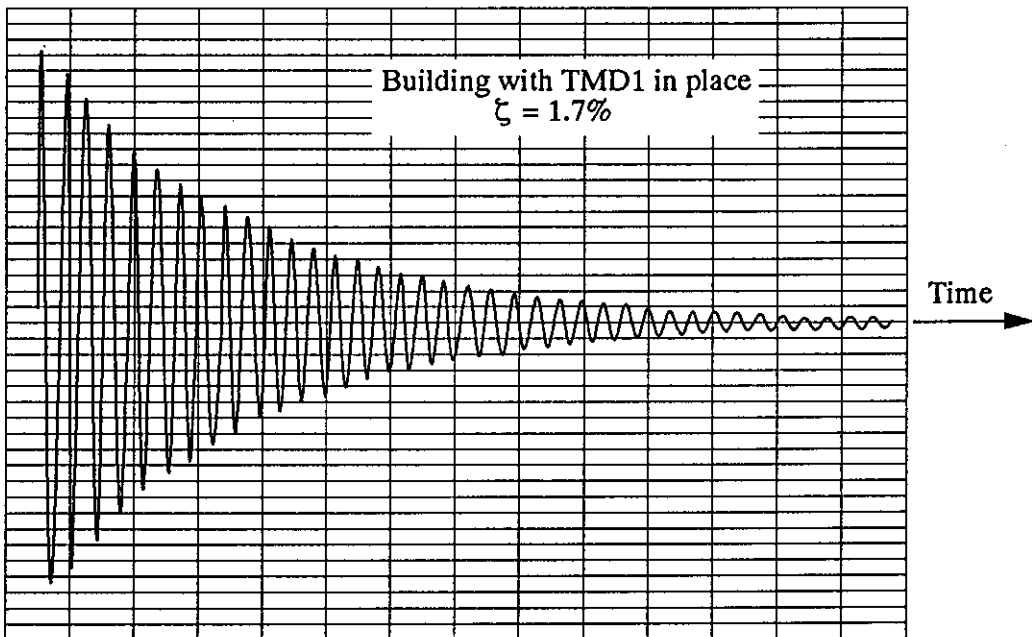
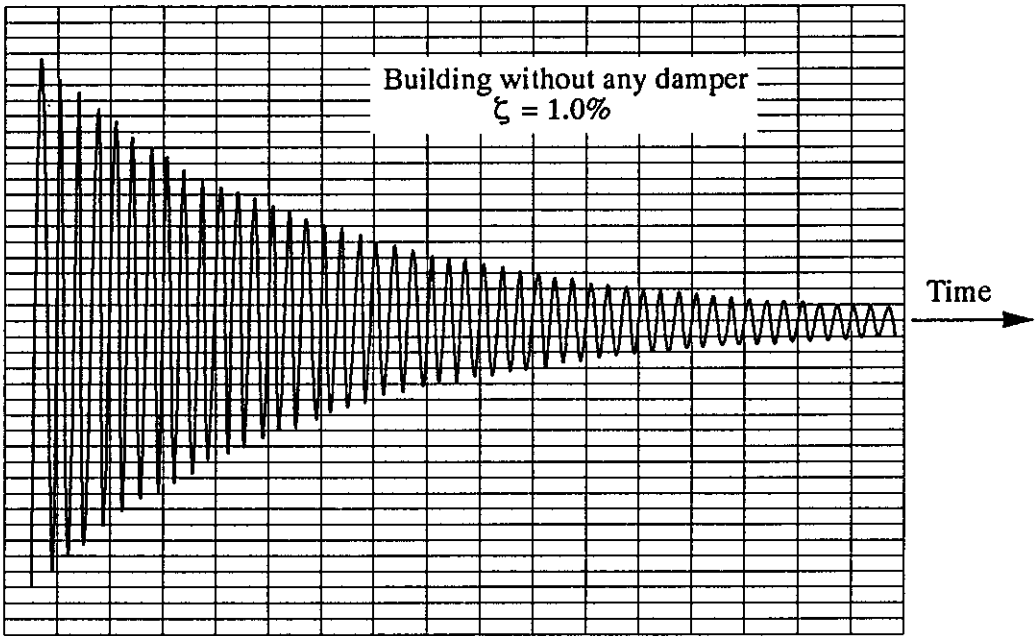


FIG. 3.6b FREE VIBRATION DECAY TRACES SHOWING EFFECTIVENESS OF TUNED MASS DAMPERS

micro-computer, and then the saved data were transferred to and processed by a mini-computer to obtain various power spectral densities and probability distribution analysis of peaks.

3.6 Experimental Results and Analysis

3.6.1 Alongwind responses

The experimental results showed that the mean alongwind displacement responses at the top of the building model were not reduced by any TMDs whether the incident wind was normal to the wide face of the building model or normal to the narrow face of the model. The reductions in standard deviation of alongwind displacement responses were generally in the range of 20% to 40% even though the parameters of the three tuned mass dampers tested were not optimum (see Fig. 3.7). Here the standard deviation responses were normalised as σ_x/b and were presented as a function of reduced wind velocity for the plain model (i.e., without any dampers) and the building model with the TMDs. Logarithmic scale is used to represent the normalised response in order to accommodate the large variation in response amplitude. It is observed that the third tuned mass damper was the most effective, which corresponded to the largest damping value as measured by the free decay vibration of the model systems and the largest mass ratio.

3.6.2 Crosswind responses

The normalised standard deviation crosswind displacement responses σ_y/b are presented in Fig. 3.8. With the incident wind normal to the wide face of the building model, there was a significant peak in the crosswind response of the plain building at reduced wind velocities close to a critical value of about 10. This represents the wind condition at which the vortex shedding frequency is very close to the natural frequency of the building, i.e., the building is operating near the peak of the wake energy spectrum. It is fairly obvious that the variation of crosswind response with reduced velocity can not be described by a simple relationship. The use of the

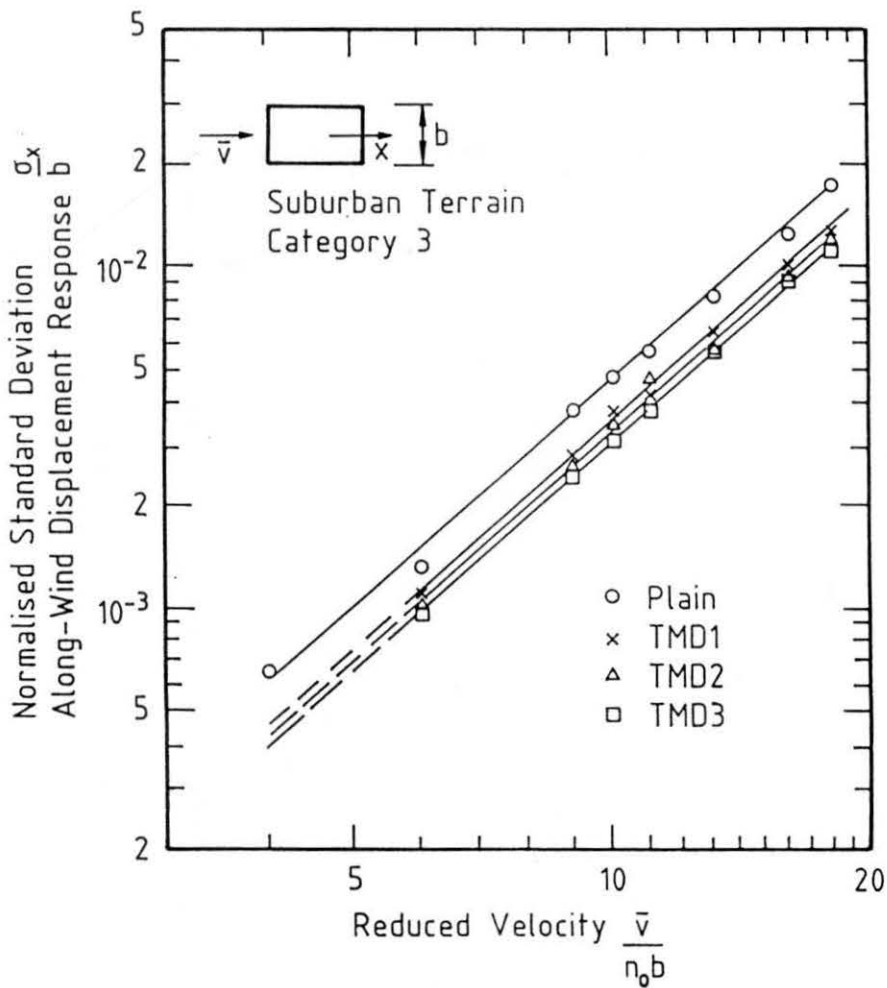
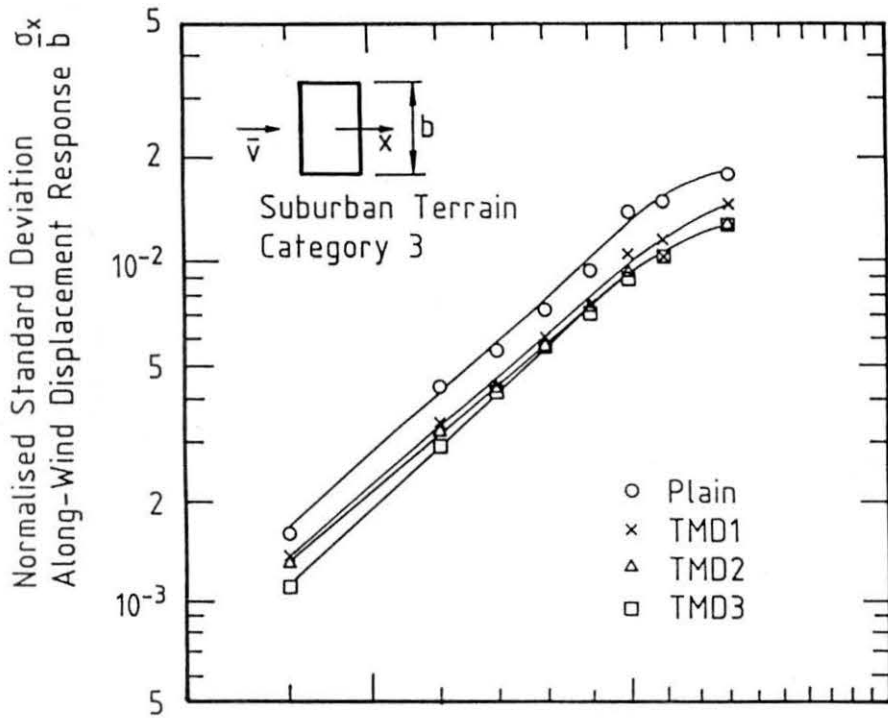


FIG.3.7 STANDARD DEVIATION ALONG-WIND RESPONSES

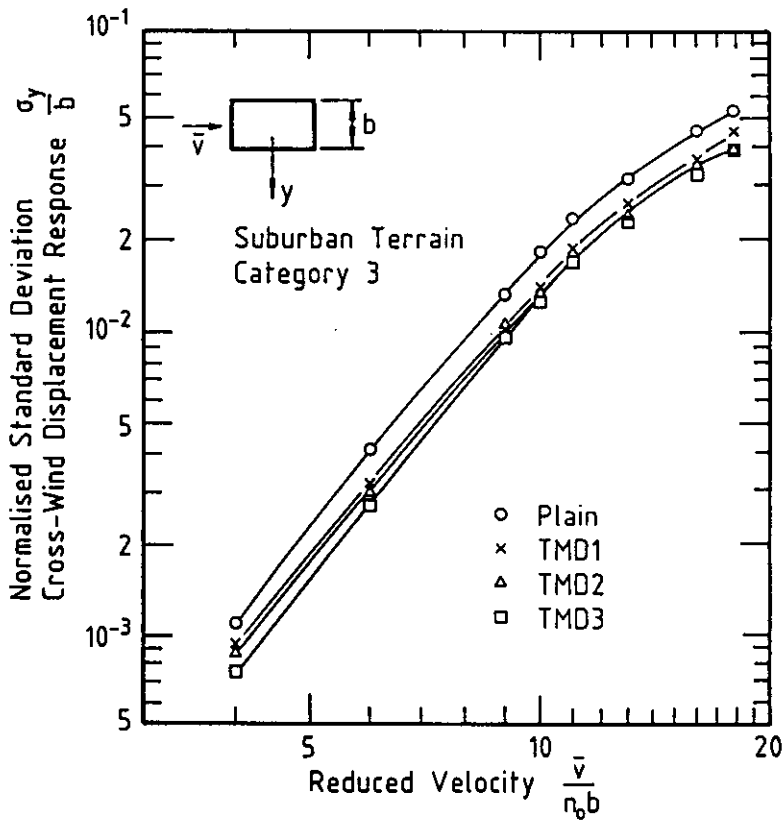
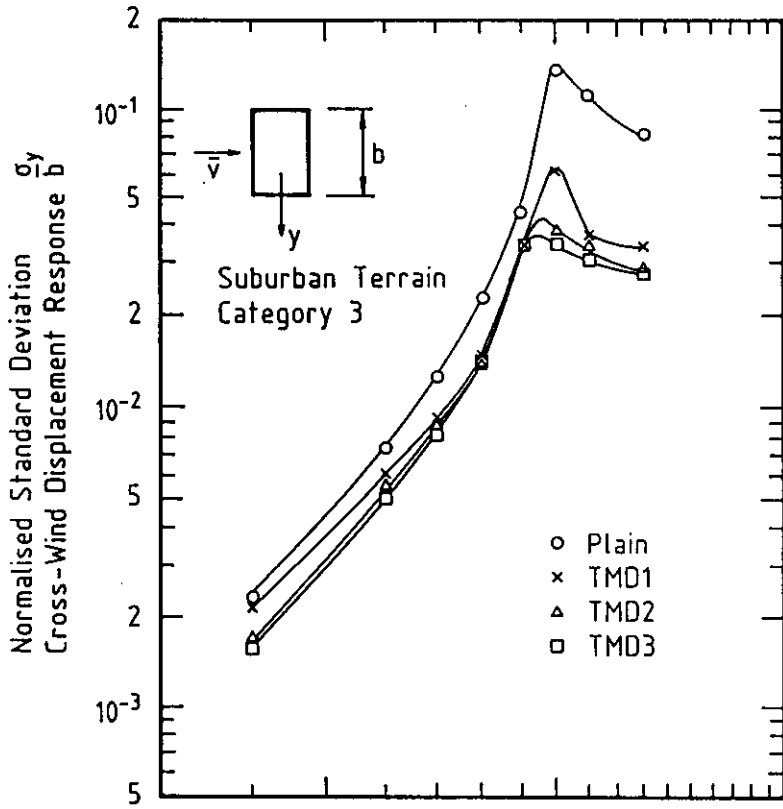


FIG.3.8 STANDARD DEVIATION CROSS-WIND RESPONSES

TMDs was found to be effective in reducing the response within the studied range of reduced velocities. There is up to a 30% reduction in wake-excited response at the low range of reduced velocities. At reduced velocities close to and above the critical value of about 10, there are considerable reductions in response by a factor of 2 or more. It is noted that the geometrical configurations of the building related to the wind excitation and hence the aerodynamics are the same for the plain model and for the model with the TMDs in place. Such a significant decrease reflects the change in aeroelastic aspect, in particular the lock-in mechanism. At the larger response amplitude of the plain model, the displacement-dependent lock-in excitation was dominant which results in a negative aerodynamic damping term and the most excitation energy was concentrated on or near the natural frequency of the building. Whereas when the TMD was fitted, the response amplitude of the model system was much smaller and might drop below the level in which the lock-in effects become significant. The significant decrease in response amplitude observed here suggests that the TMD was more effective in suppressing the vibration caused by the lock-in excitation than that caused by the wake excitation. It is noted that the relative displacement of the damper to the building would be much larger under lock-in excitation than that under wake excitation.

With the incident wind normal to the narrow face of the building, crosswind responses were caused by both incidence turbulence and wake excitation. There was no significant response peak to indicate a dominant critical velocity effect. The long afterbody of the building is believed to have a disruptive effect on the vortex shedding process. With tuned mass dampers, there was up to a 30% reduction in response.

3.6.3 Wake spectra

For most modern tall buildings, one of the most common sources of crosswind excitation is associated with vortex shedding and this is often referred to as wake excitation. It is of considerable interest to investigate the wake characteristic around an oscillating body, in particular when the vortex shedding frequency is close to the fundamental frequency of the body vibration. Under these operating conditions, large amplitude crosswind

response due to lock-in may occur.

Velocity fluctuation in the near wake of the tested building was measured with a vertically-aligned hot-wire which is the most common type of instrumentation used in investigation of this nature. The hot wire was located at $3/4$ of the height of the building model where the flow was not expected to be affected by flow entrainment from the top of the building, and at just outside the wake region within which the signals are likely to be confused by flow reversals, but close enough to detect any periodicity in the velocity fluctuations associated with the vortex shedding process (Kwok, 1977). Although the relationship between velocity in the near wake and crosswind excitation is still poorly defined, a wake spectrum is thought to be a reasonable representation of the wake energy. Wake spectra for the building model without the TMD and with the third TMD are presented in Fig. 3.9. When the incident wind, at a reduced velocity of about 10, was normal to the wide face of the building model, the wake spectrum, as shown in Fig. 3.9, for the plain model showed a peak at the reduced velocity of about 10 (reduced frequency was about 0.10). This is thought to be associated with the interaction between the model displacement and the wake, and the motion-dependent lock-in excitation may be significant. Compared with this, the peak of the wake spectrum for the model with the TMD was smaller than the peak for the plain model. This is consistent with the smaller standard deviation crosswind displacement response of the model with the TMD discussed earlier.

With the incident wind normal to the narrow face of the building model and at a reduced velocity of about 13, the wake spectrum for the plain model was similar to the wake spectrum for the model with the TMD in place, and both spectra did not show a peak at the corresponding reduced frequency. This indicates that under motion-independent wind excitation the tuned mass damper can reduce the displacement response of the building only through the change of structural properties rather than the change of wind excitation.

Overall, the measured wake energy spectra correlate well with the measured response characteristics discussed earlier.

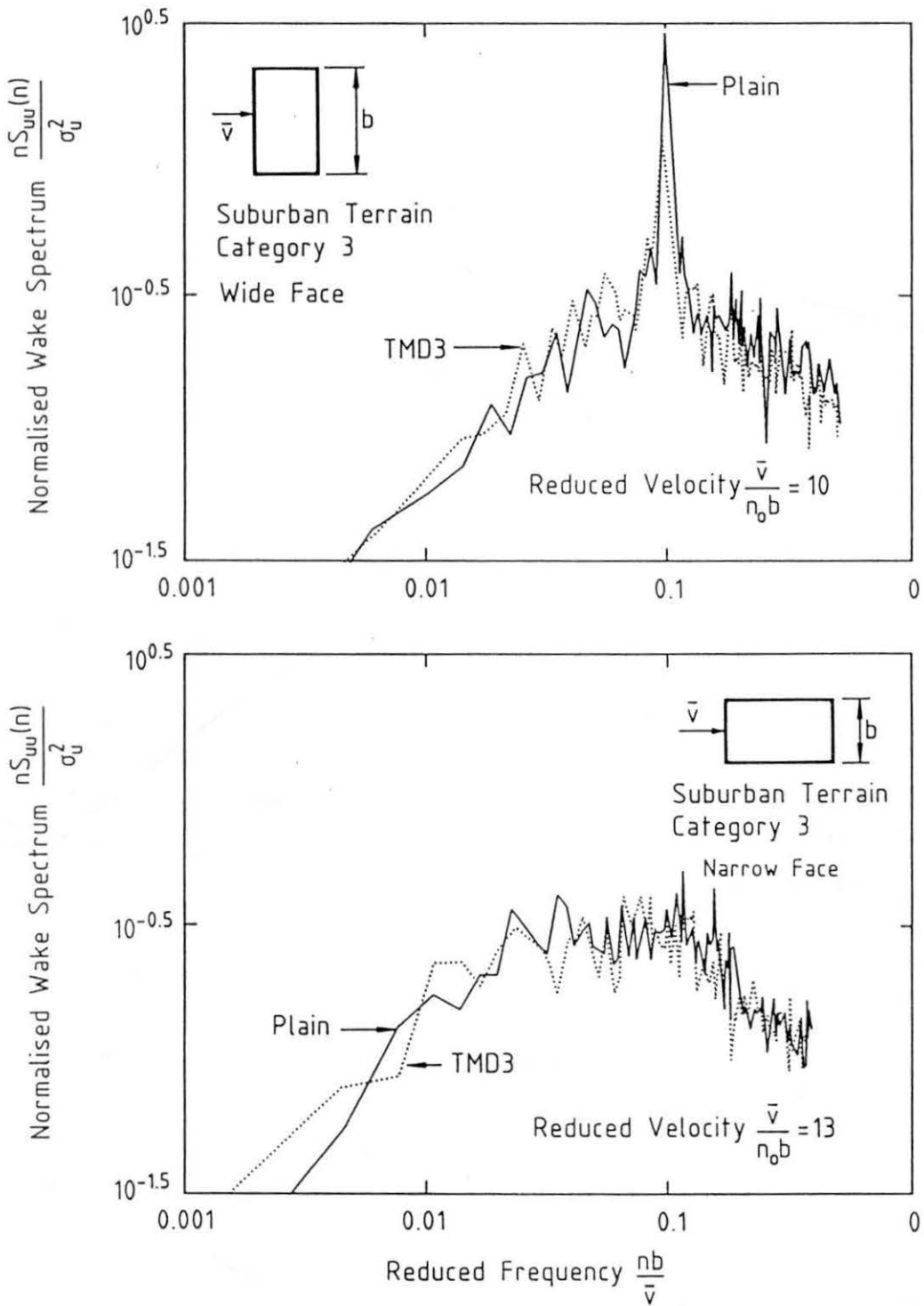


FIG.3.9 WAKE SPECTRA

3.6.4 Probability distributions of peaks

Wind-excited tall buildings behave essentially like a lightly damped system oscillating at a fundamental frequency. It is therefore more convenient to express the probability distribution of the response of a tall building in terms of the distribution of the response peaks, i.e., the proportion of peak values exceeding a given response amplitude, rather than on a time basis. The probability analysis of response peaks can be performed by digital analysis, and the results can be used to determine the variations from that of a normally distributed Gaussian process and to identify the crosswind excitation mechanism. The theory of probability distributions of peaks and description of the digital analysis process can be found in Melbourne (1977) and Kwok (1977).

It was found that for all tested models with or without the TMDs in the reduced wind velocity range from 4 to 18, the alongwind responses were normally distributed. With the narrow face of the building model normal to the wind, the crosswind responses were also essentially normally distributed. However, with the wide face normal to the wind and at close to the critical reduced wind velocity, the probability distribution of the crosswind response peaks of the plain model showed a significant departure from a normally distributed process and approached to that for a sine wave. As shown in Fig. 3.10, the motion-dependent lock-in excitation mechanism which was evident in the plain model has been significantly disrupted by the introduction of the TMDs to the plain model as the responses of the model with the TMDs remained essentially normally distributed.

3.6.5 Normalised displacement response spectra

The top displacement spectra of the building model without a damper and with the third tuned mass damper were obtained by Fast Fourier Transformation of the recorded displacement response signals. The spectra were normalised by σ_{x_0} for alongwind spectra and by σ_{y_0} for crosswind spectra, in which σ_{x_0} and σ_{y_0} were the alongwind standard deviation and crosswind standard deviation of the plain model. It was found that the alongwind displacement response spectra, corresponding to alongwind

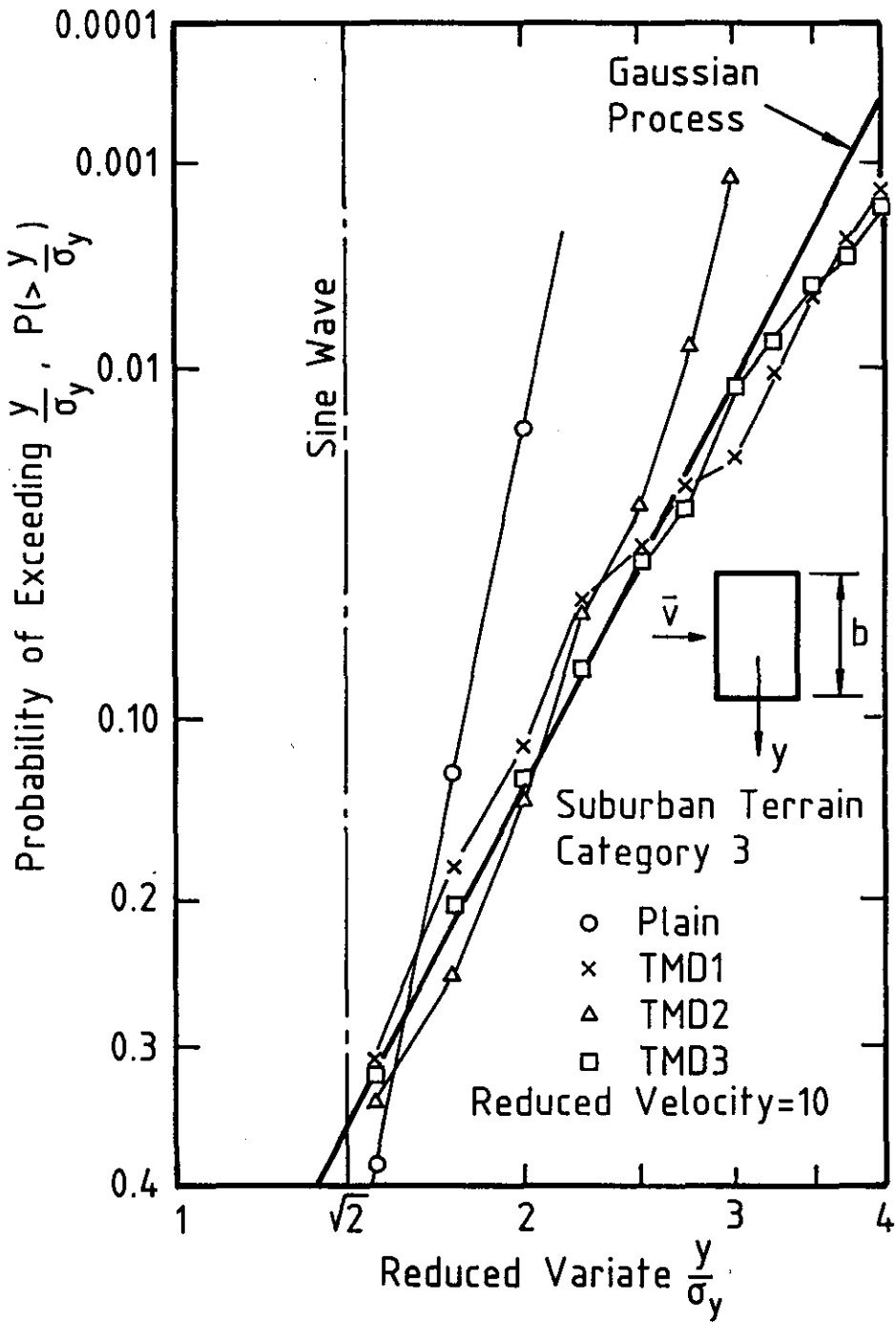


FIG.3.10 PROBABILITY DISTRIBUTIONS OF CROSSWIND RESPONSE PEAKS (WIDE FACE)

turbulence buffeting, were different from the crosswind displacement response spectra, which were related to crosswind wake excitation, as shown in Fig. 3.11. The alongwind displacement spectra indicate that the alongwind turbulence energy is mainly distributed within the low frequency range while the energy distribution of crosswind wake excitation depends on the structural properties. It is consistent with the corresponding alongwind and crosswind force spectra provided by Kwok (1988). It is also obvious that the reductions in energy amplitudes at the natural frequency of the model by use of the TMD are significant.

3.6.6 Effect of angle of wind incidence

In the design of tall buildings, strong wind from all possible wind directions has to be considered. Fig. 3.12 shows the effect of angle of wind incidence on the dynamic response along one of the body axes of the building model at reduced wind velocities of 6 and 10. As the angle of wind incidence increases, there is an increased tendency for the separated shear layer to re-attach onto the windward face of the building. The effect of shear layer re-attachment is a reduction in excitation force and hence a decrease in response. This trend can be observed over the first 15–30 degrees. As for the effectiveness of the TMDs in reducing the structural dynamic responses, it is obvious that this effectiveness is maintained at all concerned angles.

3.7 Conclusions

The results of the aeroelastic test of the CAARC Standard Tall Building model demonstrated the effectiveness of the TMD system in reducing the dynamic response of the building induced by wind excitation with different mechanisms. The TMD system reduced the vibration caused by alongwind turbulence, partial incidence turbulence in crosswind direction and crosswind wake excitation by 20% to 40%. The TMD system was found to be more effective in suppressing the vibration caused by the lock-in excitation by a factor 2 or more. The effectiveness of the TMD system can be maintained under various wind directions.

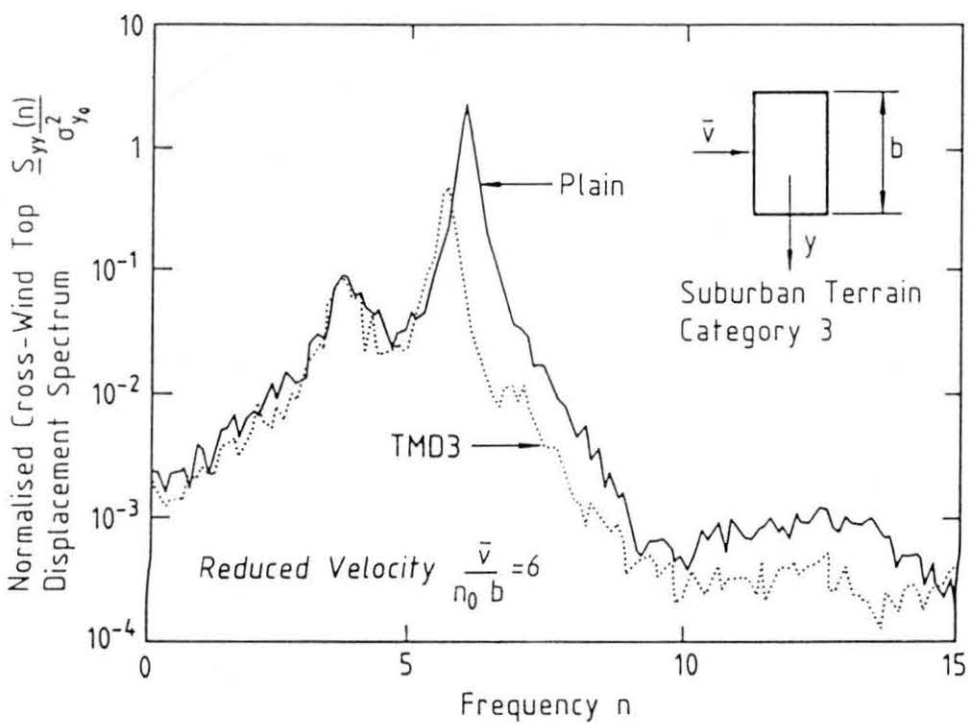
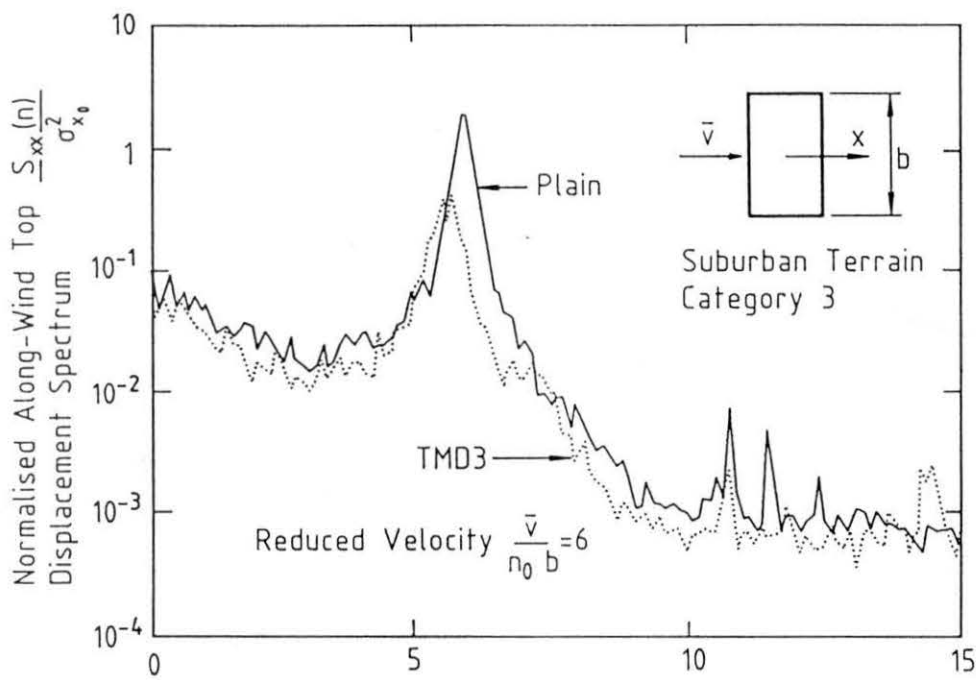


FIG.3.11 DISPLACEMENT SPECTRA

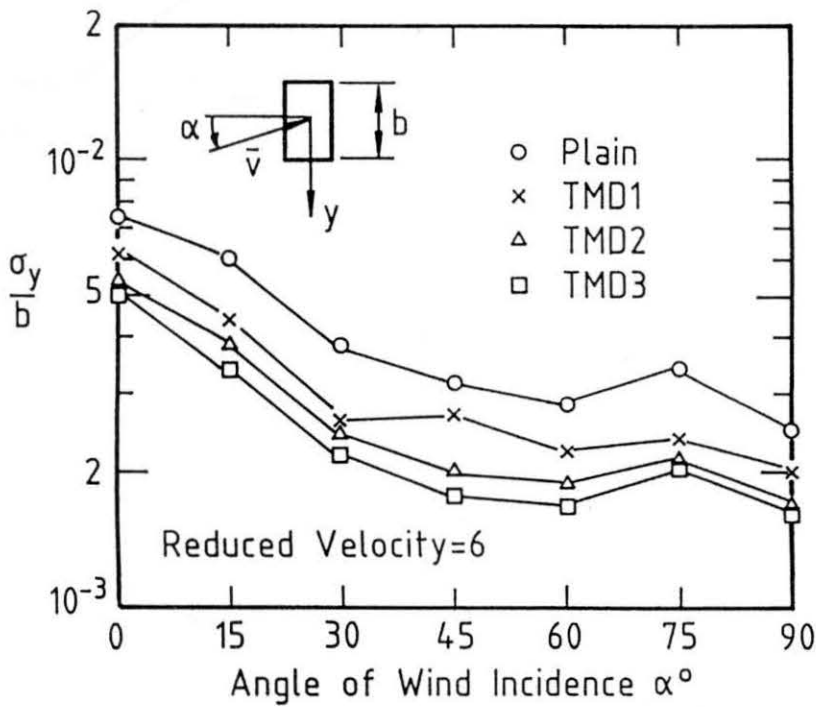
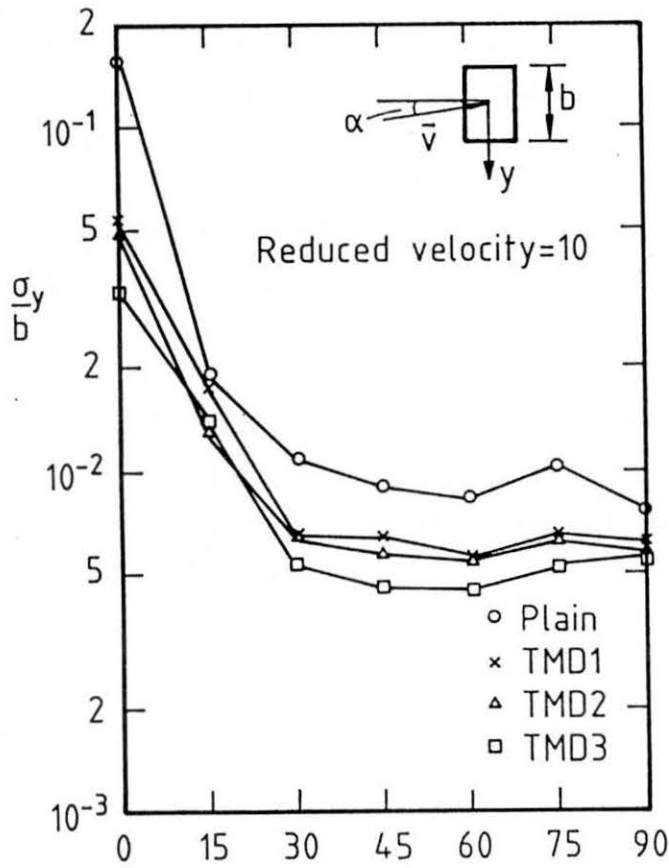


FIG.3.12 EFFECT OF ANGLE OF WIND INCIDENCE

The use of the TMD, as an added energy absorbing system, usually increased the overall effective damping of buildings rather than change the wind loads acting on the building. However, under motion-dependent lock-in excitation, not only can the tuned mass damper absorb most of the vibrational energy which concentrates at the natural frequency of the building, it can also change both the magnitude and mechanism of the external excitation.

The experimental results described in this Chapter should be compared with the theoretical results obtained by using harmonic and white noise excitation models to examine the reliability of theoretical predictions. Chapter 5 deals with this problem.

Chapter 4

WIND-INDUCED TORSIONAL VIBRATION OF TALL BUILDINGS AND ITS PASSIVE CONTROL BY TUNED MASS DAMPERS

4.1 Introduction

Full scale building response measurements have shown that wind loads acting on modern tall buildings may cause significant torsional moments and motions (Hart, DiJulio and Lew, 1975; Jeary, Lee and Sparks, 1979). At least two major buildings which have suffered permanent structural damage as a result of wind action (Mayer-Kaiser, Miami; Great Plains Life, Lubbock, Texas) exhibited marked permanent deformations in torsion (Vickery, 1979). Because of human biodynamic sensitivity to angular motion, the torsional motion can be often perceived by a visual-vestibular mechanism at motion thresholds which are an order of magnitude smaller than those for translational motion (Kareem, 1985). Recent trends towards more complex building shapes and structural systems further accentuate eccentricities between the mass centre, elastic centre and instantaneous point of application of aerodynamic loads, and significantly increase torsional responses. Wind-induced torsional effects on tall buildings cannot be completely ignored.

Foutch and Safak (1981) attempted to estimate theoretically the torsional dynamic response of an idealised single-mass structure subjected to a normally-incident wind. Patrickson and Friedmann (1979) as well as Yang, Lin and Samali (1981) investigated the importance of the coupled response of tall buildings caused by an offset between the centre of mass, stiffness and aerodynamic forces. Theoretical estimates of dynamic torque were also discussed by Torkamani and Pramono (1985). Their results indicated that the torsional response contributed significantly towards the overall dynamic

response of structures and buildings. Inclusion of coupling between the lateral and torsional degrees-of-freedom further increased the torsional response. However, owing to the absence of sufficient information on aerodynamic loads, these theoretical methods are not presently usable for design purposes.

Reinhold et al. (1979) first used a direct pressure measurement technique to determine mean and dynamic torsional moments on a rigid square building model. Isyumov and Poole (1983) then adopted a similar technique to examine the anatomy of the torsional moments on buildings of square and rectangular cross-section. Tallin and Ellingwood (1985), Kareem (1985), and Islam, Ellingwood and Corotis (1990) further utilised pressure measurement results of wind loads to analyse wind induced coupled lateral-torsional motion of tall buildings. On the other hand, Tschanz and Davenport (1983) used a base force balance technique to develop a generalised torsional force. Both pressure measurement and force balance techniques disregard aeroelastic effects such as aerodynamic damping. Based on the results of multi-degree-of-freedom (MDOF) aeroelastic model tests, empirical relations for estimating mean, standard deviation and peak base torques in the respective most unfavorable wind directions were presented by Greig (1980) and Isyumov (1982). An improved version of the empirical formulae, based on an expanded data consisting of 15 building studies, has also been presented by Isyumov in the ASCE State-of-the-art report (1987). Because present MDOF aeroelastic model tests are quite complicated, time-consuming and expensive, it is difficult to get enough experiment results to support the empirical formulae. Therefore, Lythe and Surry (1990) used a large data base measured experimentally in wind tunnel rigid model tests to develop an improved estimation method for mean torque. This involved evaluating various definitions of the torsion coefficient and classifying building shapes in order to decrease the variability of the associated coefficients.

In order to find a convenient and efficient way to predict the mean and dynamic torsion responses, to explore the mechanisms of the torsional excitation, and to demonstrate the effectiveness of active and passive systems to control torsional motion of tall buildings to wind, an aeroelastic model

for pure torsion vibration has been developed in this research project. The principle of the aeroelastic model is similar to that of the conventional "stick" aeroelastic model for translational motions of buildings. The model design and construction requirements are modest and consequently there are both timing and economic advantages. The torsional mass moment of inertia, stiffness, damping and even geometric properties of building models can be readily changed. Information on the sensitivity of the wind induced response to changes in the building configuration and surroundings can be provided, some aeroelastic effects can be considered and the effectiveness of active and passive systems to control dynamic motion of buildings can be demonstrated. The principal disadvantage of this type of simulation is that there is a mis-match between the model and prototype torsional mode shapes. Like base force balance technique (Tschanz and Davenport, 1983), errors caused by the mode shape discrepancy must be estimated.

In this Chapter, the aeroelastic model for pure torsion vibration is described. The experimental results, using this technique, were compared, wherever possible, with other wind tunnel test techniques, e.g., direct pressure measurement technique and multi-degree-of-freedom aeroelastic models. The comparisons included the mechanism of torsional excitation, torsional response of tall buildings, sensitivity of the torsional response to eccentricity between centres of twist and building geometry. The probability distribution of the torsional response peak and the torsional aerodynamic damping of a prism were evaluated. The effectiveness of tuned mass dampers in suppressing the torsional vibration of the building was also investigated. The torsional experiment results, combined with the translational experiment results in Chapter 3, provide a data base for Chapters 5 and 7 to conduct parametric studies of passive tuned mass dampers and preliminary studies of active mass dampers. The discussion of the mode shape correction for both pure torsion model and translation model is given in Chapter 6.

4.2 Experimental Techniques

4.2.1 Modelling of turbulent boundary layer wind

Wind tunnel tests of pure torsion vibration of tall buildings were also performed in the No. 2 Boundary Layer Wind Tunnel. A 1:400 scale wind model of natural wind flow over open country terrain (Terrain Category 2 as described in the Australian Wind Loading Code, AS 1170.2 -1989) was developed by using an augmented growth method which included a set of four 1.2m high linearly-tapered vorticity generators spanning the start of the working section and low-pile carpet covering a fetch length of approximately 4.5m.

The mean wind velocity profiles and longitudinal turbulence intensity profiles at three lateral positions are presented in Figs. 4.1 and 4.2. The mean velocity profiles are closely represented by the power law with an exponent $\alpha = 0.15$. The turbulence intensity was about 10% at the top of the model and the thickness of the boundary layer was found to be approximately 0.9m at the test section. These profiles were found to be consistent with profiles suggested by AS 1170.2-1989. The longitudinal velocity spectrum of the simulated boundary layer flow is presented in Fig. 4.3 and is compared with the Harris-Von Karman prototype empirical spectrum (see Eq. 3.3). The integral length scale of turbulence of the measured velocity spectrum was found to be approximately 120m at the top of the building model while that of the Harris-Von Karman spectrum under the same terrain category is 200m, as suggested in Engineering Science Data Unit (1974). The distortion of the scale of turbulence by a factor of 1.7 seems to be acceptable (Laneville and Williams, 1979; Surry, 1982).

4.2.2 Model building and tuned mass damper

The building model was a 9.1 x 18.9 x 48.1 cm tall rectangular prism which has an equivalent full scale height of 192.4 m, width of 75.6 m and depth of 36.4 m according to the wind model scale of 1/400. The size of the building model was nearly the same as that used by Isyumov and Poole (1983) for torsional studies. The model blockage was about 5% of the wind tunnel cross section, but, after considering the open jet wind tunnel being used, correction was not to be included. The building model was of a rigid wooden construction and there was a space near the top of the model so that a mass damper could be arranged inside (see Fig. 4.4). The top cover

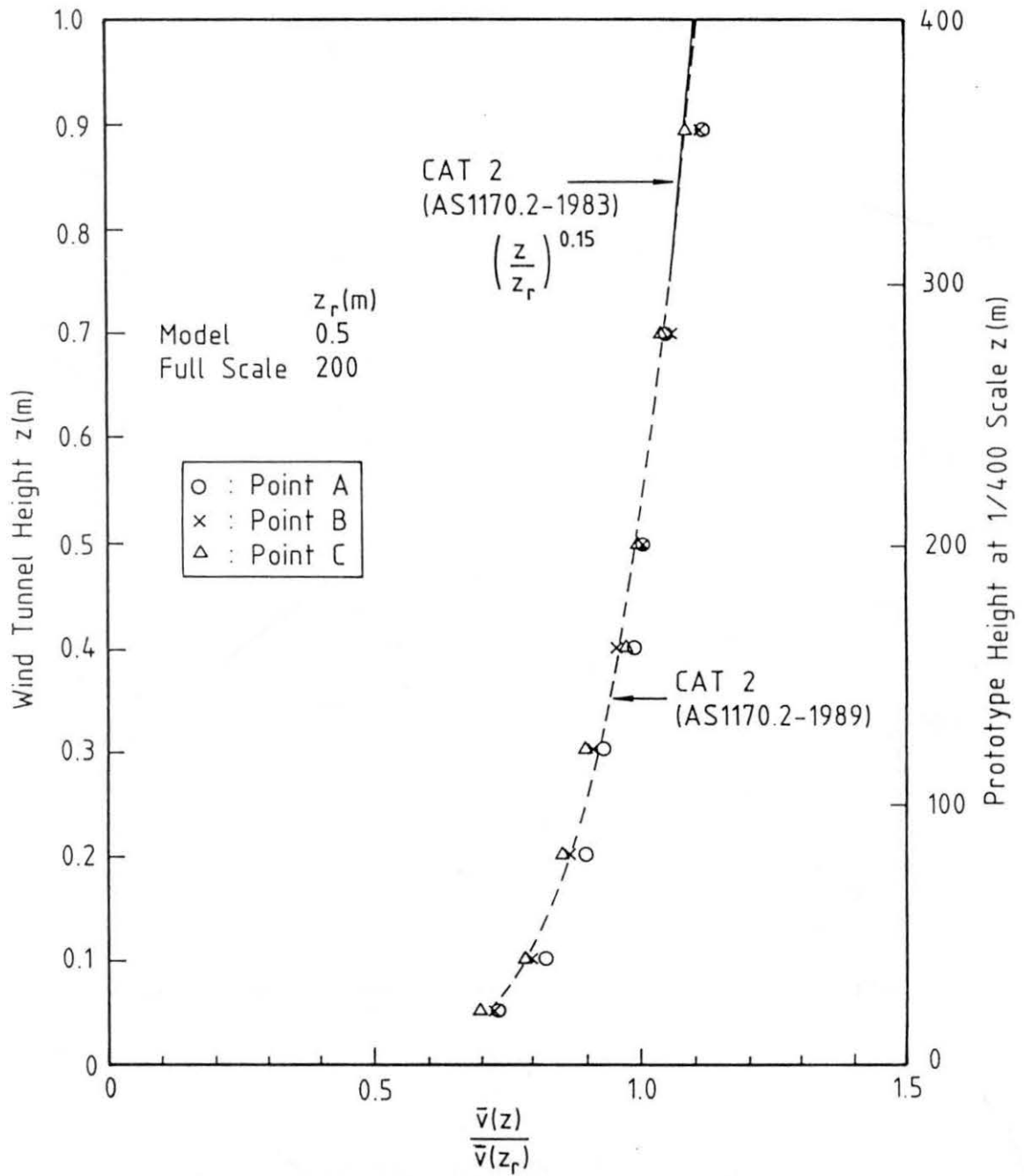


FIG.4.1 MEAN WIND VELOCITY PROFILES
 (CATEGORY 2)

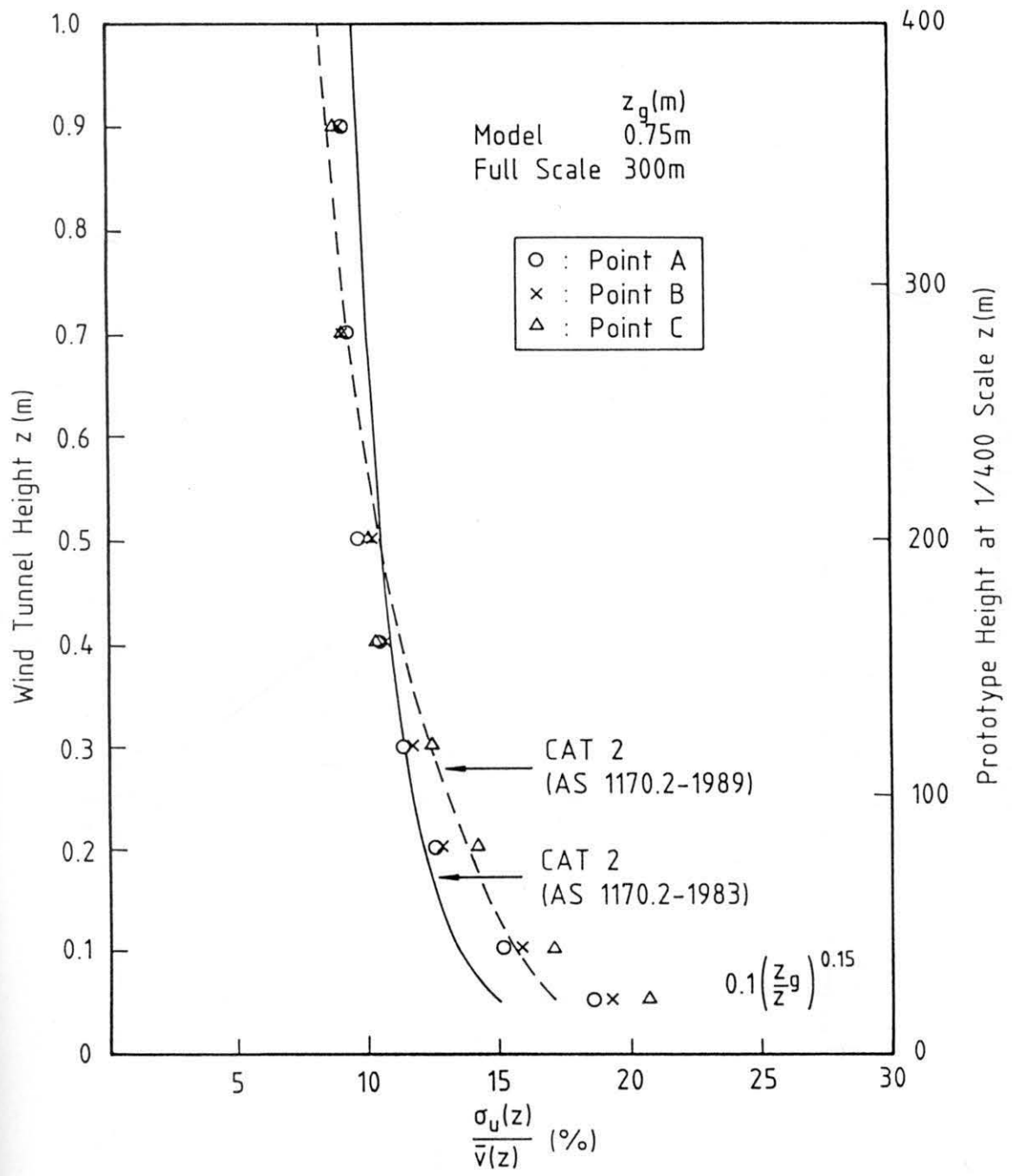
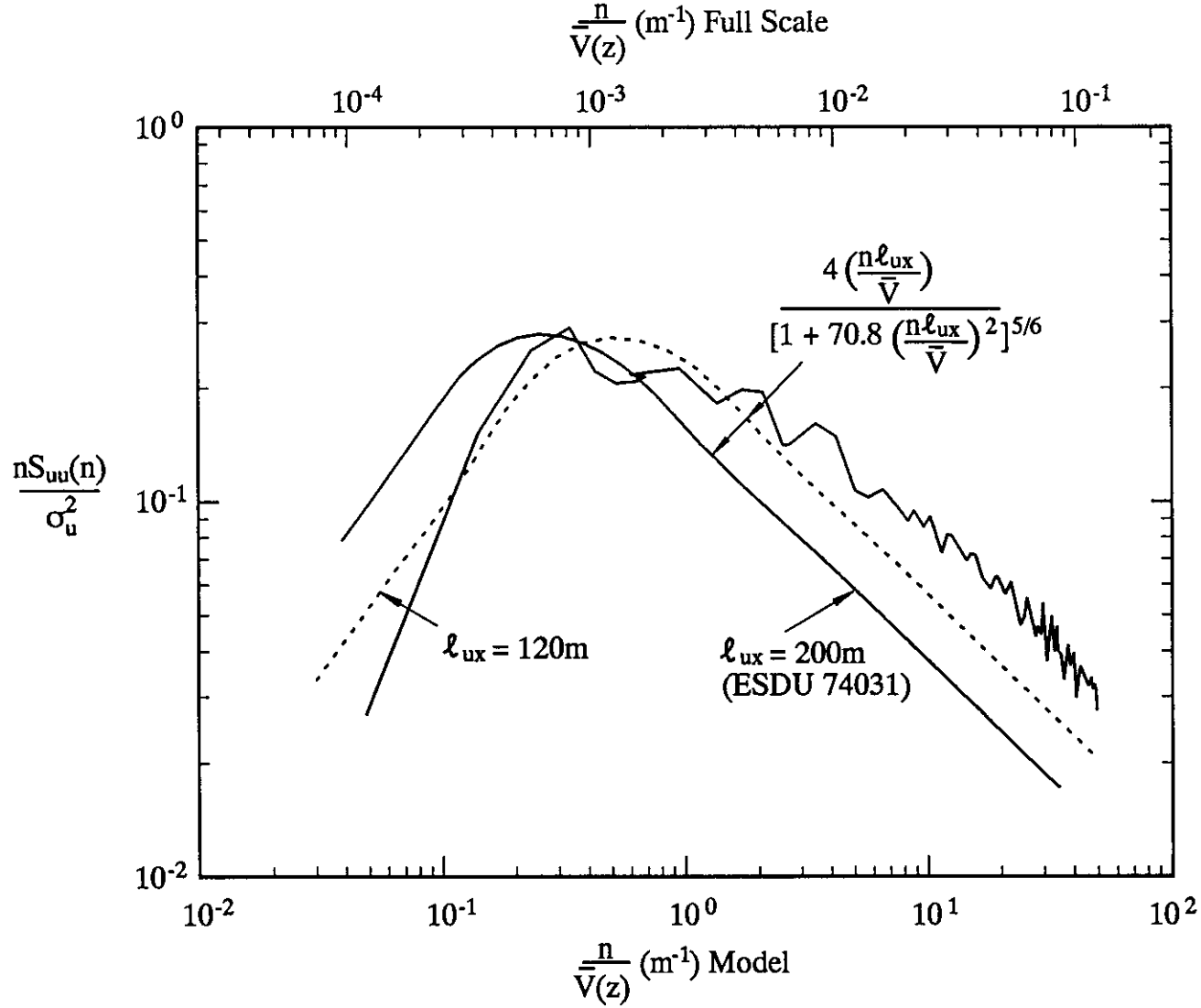


FIG.4.2 LONGITUDINAL TURBULENCE INTENSITY PROFILES
(CATEGORY 2)



**FIG.4.3 LONGITUDINAL TURBULENCE SPECTRUM AT 1/400 SCALE
(CATEGORY 2)**

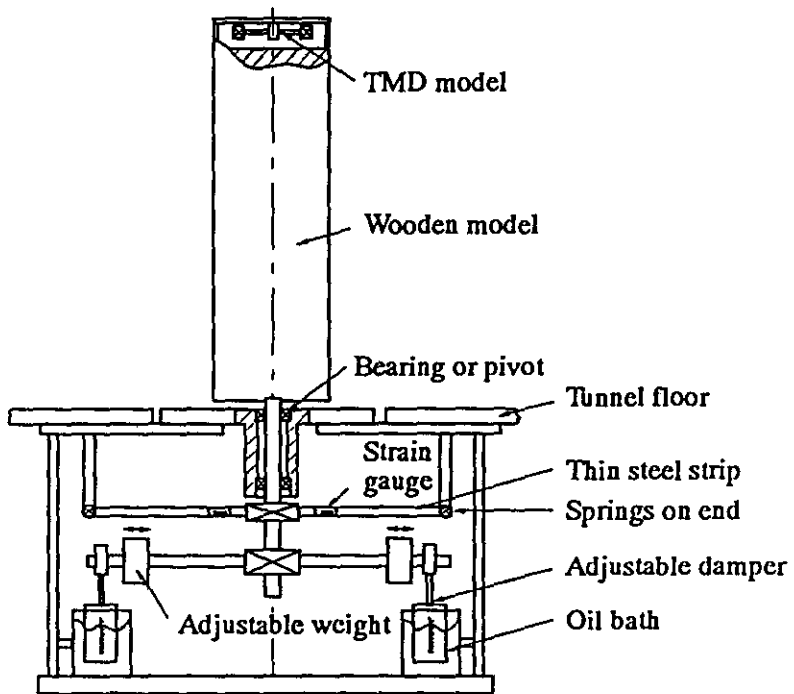


FIG. 4.4 SCHEMATIC REPRESENTATION OF AEROELASTIC TORSION MODEL

of the building model was made of transparent plastic and, therefore, the motion of the mass damper could be seen during the testing. The building prototype was assumed to have a structural damping ratio of 1.2% of critical damping and a fundamental frequency of 0.4 Hz. Aeroelastic model requirements are the same as those described in Chapter 3. For the basic model tests, the elastic centre of the building model was coincident with the mass or geometric centre of the model. However, for the eccentric model tests, both centres did not coincide with each other.

The model tuned mass damper consisted of two identical small brass blocks which were fixed at both ends of a very thin steel strip. The centre of the thin steel strip was positioned under the top cover of the building model and was usually kept on the vertical elastic axis of the model (see Fig. 4.4). The damping of the model tuned mass damper was provided by covering the steel strip with plastic tape. The physical dimensions of the building and tuned mass damper model are listed in Table 4.1.

4.2.3 Testing rig and data acquisition

A photograph of the aeroelastic torsion testing rig is shown in Plate 4.1. It is also schematically shown in Fig. 4.4. The building model was fixed on an aluminium bar which was mounted on two precision bearings or flexural pivots, thus maintaining a constant magnitude mode shape. The model was further restrained by a flexible steel strip and four helical springs, which provided the required torsional stiffness. Strain gauges attached to the flexible steel strip were used to provide an indication of wind induced twist angle and base torque. Two oil baths were designed to simulate viscous structural damping of torsional motion, while two ballast weights could be adjusted to achieve correct inertial scaling. The rig was designed so that it could be readily adjusted to model the different parameters of different types of buildings.

The natural frequency of the building model was about 8 Hz. The signal output from the strain gauge bridge was low-pass filtered at 30 Hz to attenuate instrumentation and environment noise of a greater frequency. The resulting signal was then digitised by means of an analogue to digital

TABLE 2. PHYSICAL PROPERTIES OF THE MODEL (TORSION)

Basic Building Model	Size	0.481x0.189x0.091 (m)
	Generalised Mass Moment of Inertia	$6.34 \times 10^{-3} \text{ kg.m}^2$
	Natural Frequency	7.68 (Hz)
	Structural Damping	0.012 of critical
Eccentric Building Model	Size	0.481x0.189x0.091 (m)
	Generalised Mass Moment of Inertia	$7.06 \times 10^{-3} \text{ kg.m}^2$
	Natural Frequency	7.32 (Hz)
	Structural Damping	0.012 of critical
Tuned Mass Damper	Mass Moment of Inertia	$8.40 \times 10^{-5} \text{ kg.m}^2$
	Frequency	7.40 (Hz)
	Damping	0.048 of critical

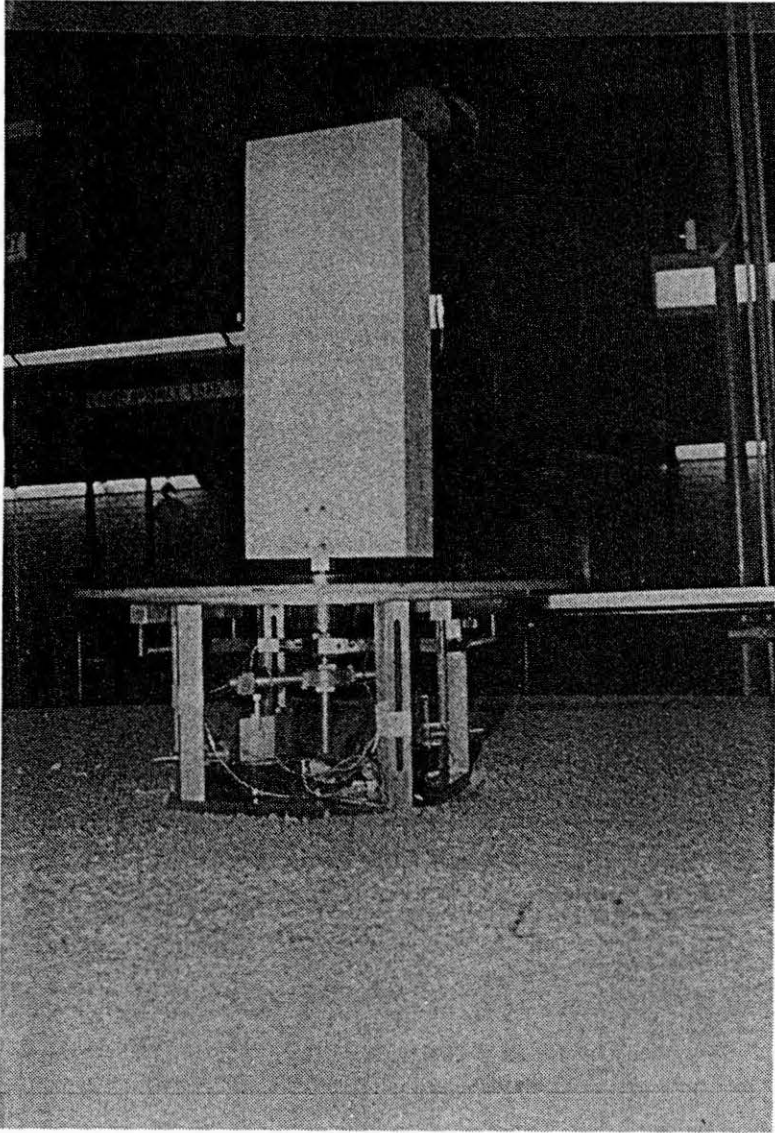


PLATE 4.1 AEROELASTIC TORSION TESTING RIG

converter, and sampled by a micro-computer. A pitot-static tube, which was located 1.3m away from the model, was used to measure mean velocities in the wind tunnel during the testing. Same data acquisition system has been used for the translational experiments in Chapter 3 and the system arrangement is shown in Plate 4.2. The twist angle and base torque were calibrated against the output from the strain gauge bridge. A typical calibration curve is shown in Fig. 4.5. The calibration of the damper properties was conducted in the same way as described in Chapter 3.

4.2.4 Experimental program

The mean (static) and standard deviation (dynamic) twisting angle responses $\bar{\theta}$ and σ_{θ} as well as base torque responses \bar{T} and σ_T were measured at reduced wind velocities $V_r (= \bar{V}/n_0 b$ or $\bar{V}/n_0 L$) ranging from 1 to 4.5 (wide face) and 2 to 10 (narrow face). The reduced velocities were based on the width of the building, b , normal to the wind and, in some cases, based on the length parameter $L (= \int |r| ds / A^{1/2})$ as suggested by Greig (1980). \bar{V} is the mean wind velocity at the top of the building; n_0 is the natural frequency of the torsional vibration of the building without any dampers; ds is the elemental length of the building perimeter; $|r|$ is the torque arm of the element ds and A is the cross-sectional area of the building. The torsional response signals were processed in real-time by a computer and the data were transferred and analysed further to obtain response and excitation spectra, probability distributions of the responses and other statistical quantities. The total test consisted of basic model tests and eccentric model tests with and without the tuned mass damper.

4.3 Basic Model Tests

4.3.1 Torsional response

The experimental results showed that instantaneous unbalanced fluctuating wind force caused fluctuating responses on a symmetrical building and the fluctuating responses of the building increased with increasing reduced wind velocities. With the incident wind normal to the wide face of

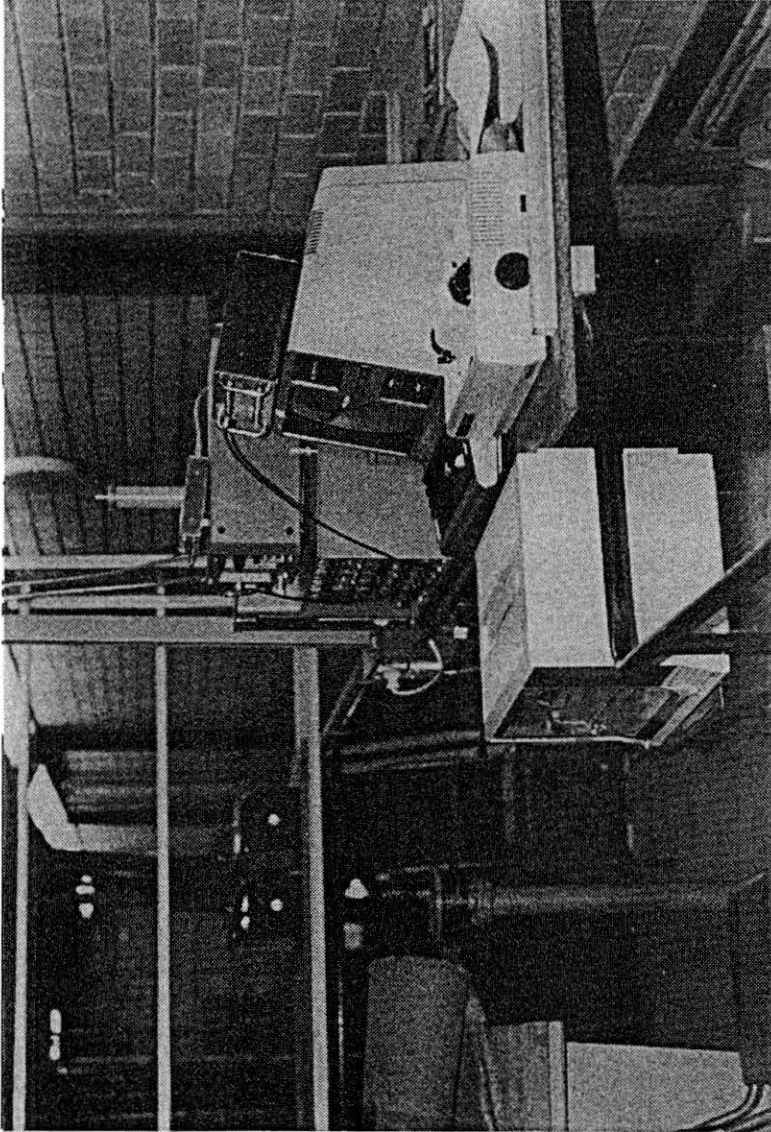


PLATE 4.2 DATA ACQUISITION SYSTEM

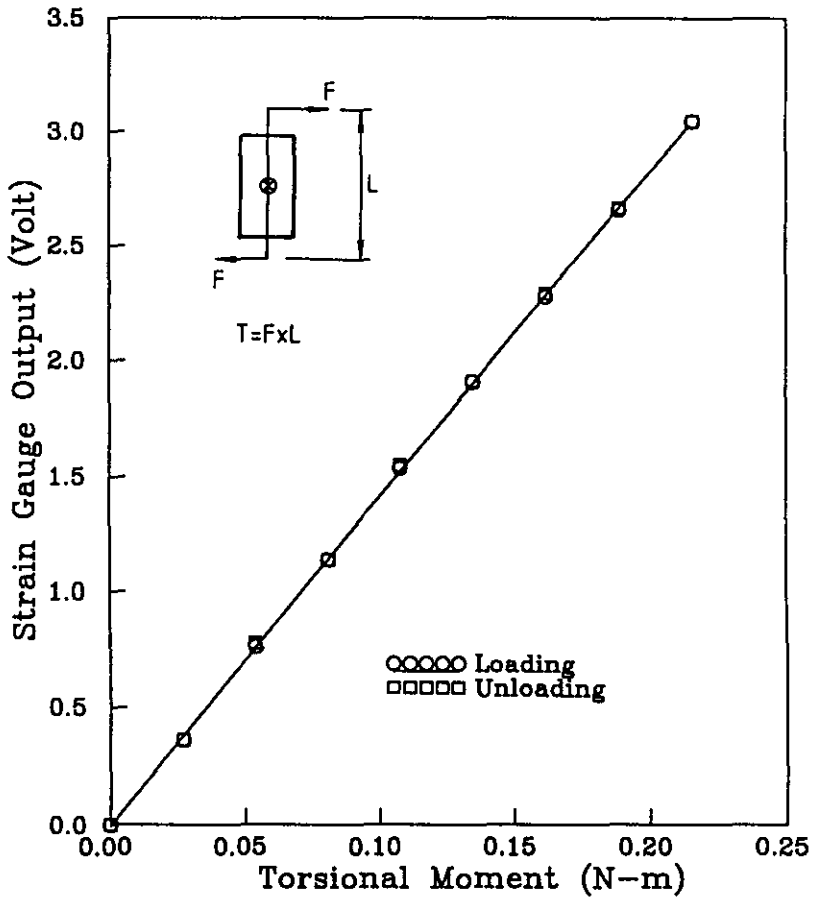


FIG. 4.5 A TYPICAL CALIBRATION OF STRAIN GAUGE BRIDGE ON TESTING RIG

the building, the standard deviation twist angle responses σ_θ were proportional to $V_f^{2.35}$ shown in Fig. 4.6. With the incident wind normal to the narrow face of the building, as shown in Fig. 4.7, the responses σ_θ were not uniformly proportional to $V_f^{2.68}$ as suggested by Isyumov (1987). Compared with the standard deviation twist angle responses, the mean twist angle responses $\bar{\theta}$ for the two orientations were too small at the low reduced wind velocity range to be correctly detected by the existing test instrument. The pressure distribution on a rectangular building is expected to be nearly symmetrical for a wind direction perpendicular to any face, and the mean torque is approximately zero. This is consistent with the surface pressure data reported by Miyata and Miyazaki (1979).

In the design of tall buildings, strong wind from all possible wind directions has to be considered. Figs. 4.8 and 4.9 show the effect of angle of wind incidence on the mean and standard deviation base torque responses, respectively, along one of the body axes of the building model at reduced wind velocities of 4 and 8. Here the torque responses were normalised by $\frac{1}{2}\rho\bar{V}^2b^2h$, while reduced wind velocities were normalised by n_0b . ρ and h are, respectively, the air density and the building height. It was found that, as the angle of wind incidence was changed from 0° to 90° , the dynamic torque decreased from a maximum at around 0° to a minimum at around 45° and then increased slightly for higher values of angle. However, the peak values of the mean torque occurred at around 10° or 60° (in the opposite direction), at which the wind directions were not aligned with the axes of the model symmetry. These trends of torsional responses with wind direction were consistent with those obtained by Isyumov and Poole (1983), using the direct pressure measurement technique, on a rigid model of nearly the same proportion. Furthermore, it was found that the variation of reduced wind velocity only slightly affect the normalised mean base torque within the studied range of angles. This is, however, not true for the normalised dynamic base torque.

After a series of wind tunnel tests based on multi-degree-of-freedom aeroelastic models, Greig in his master thesis (1980) and Isyumov in the ASCE State-of-the-art report (1987) presented the following empirical relations for estimating the mean and standard deviation base torques in the

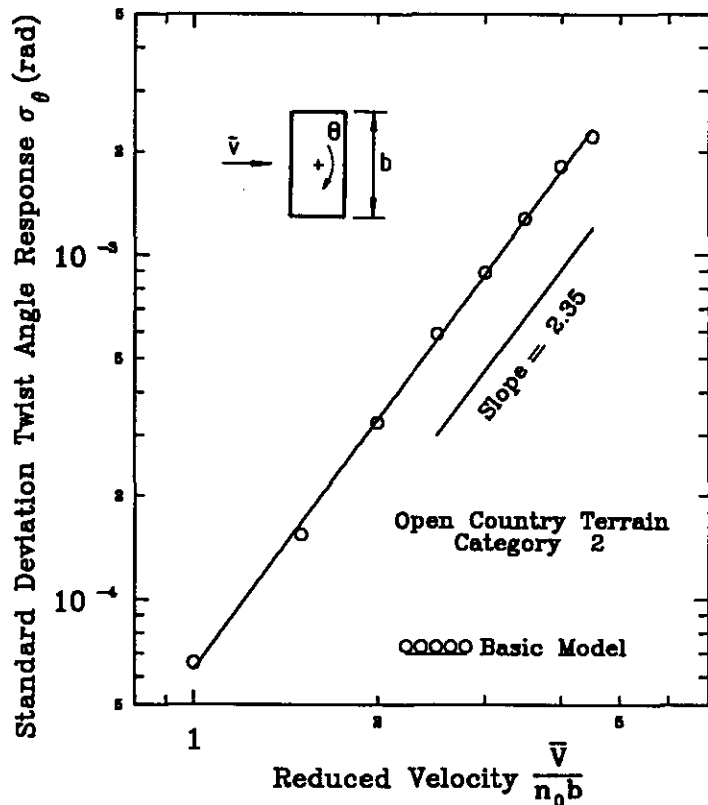


FIG. 4.6 STANDARD DEVIATION TORSIONAL RESPONSE (BASIC MODEL + WIDE FACE)

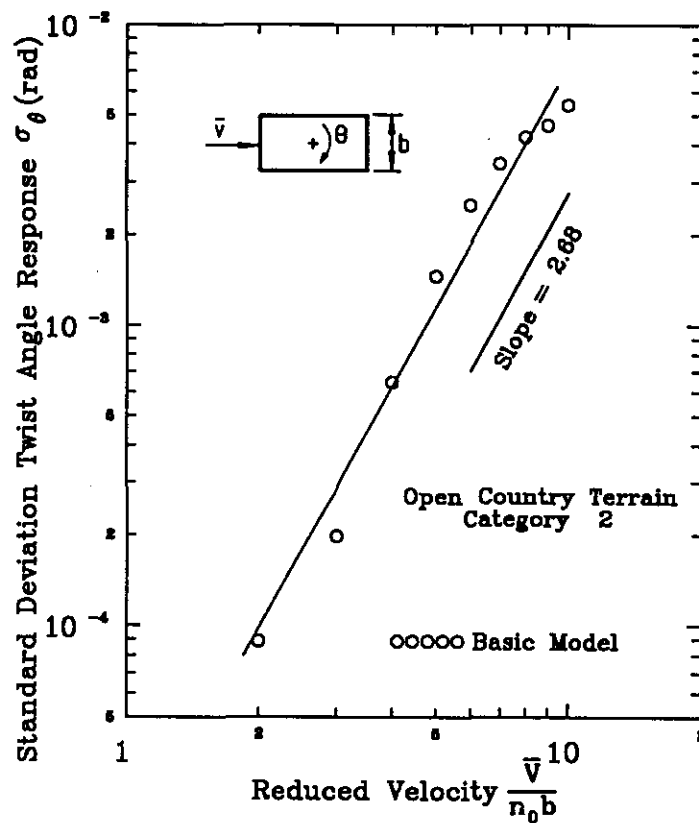


FIG. 4.7 STANDARD DEVIATION TORSIONAL RESPONSES (BASIC MODEL + NARROW FACE)

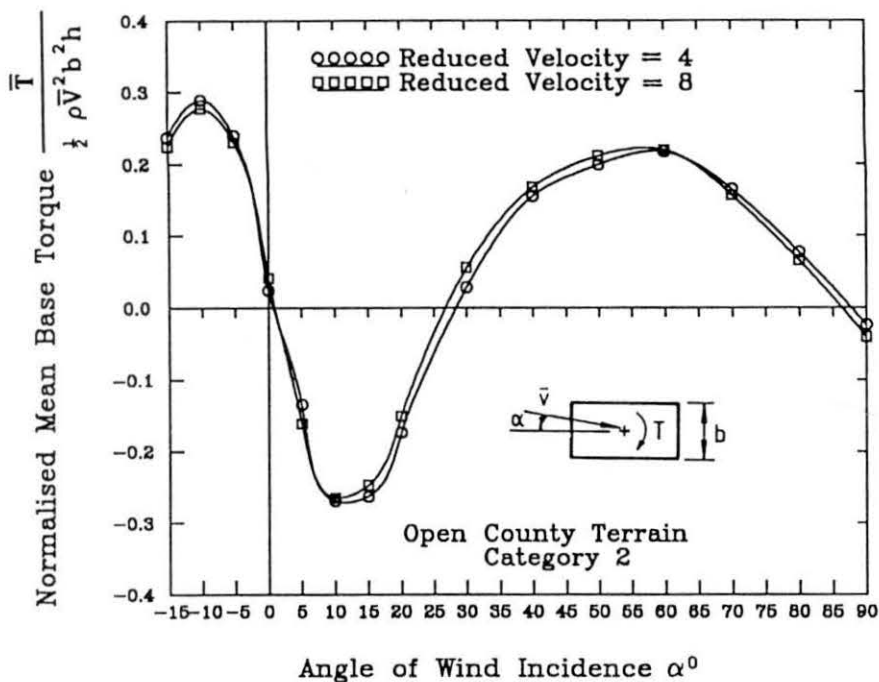


FIG. 4.8 EFFECT OF ANGLE OF WIND INCIDENCE ON MEAN TORQUE (BASIC MODEL)

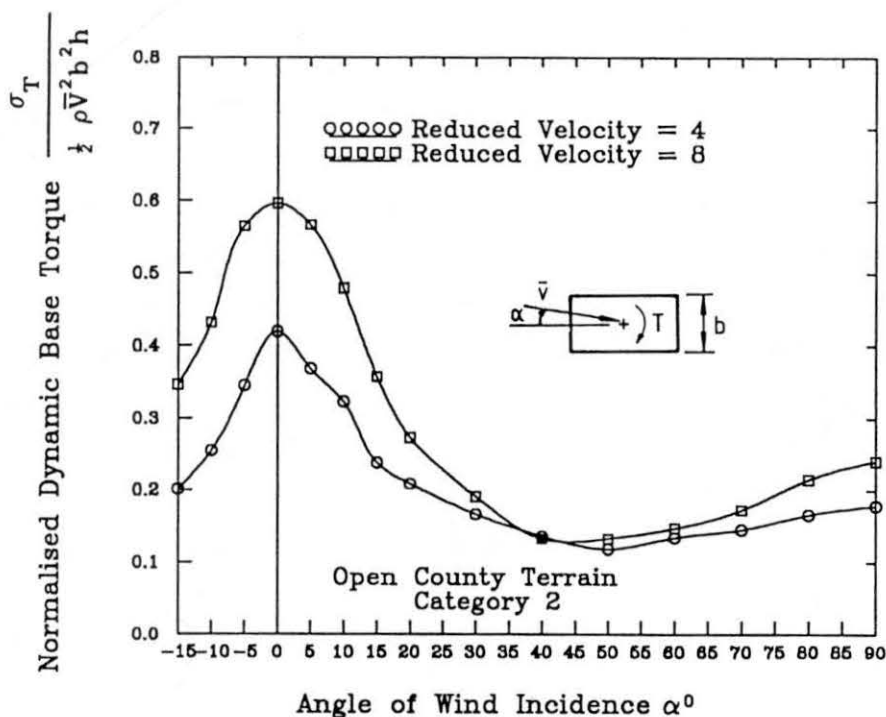


FIG. 4.9 EFFECT OF ANGLE OF WIND INCIDENCE ON DYNAMIC TORQUE (BASIC MODEL)

respective most unfavorable wind directions:

$$\bar{T}_{\max}(\bar{V}) = 0.038\rho L^4 h n_0^2 V_r^2 \quad \dots \dots \dots (4.1)$$

$$\sigma_{T\max}(\bar{V}) = 0.00167\zeta^{-\frac{1}{2}}\rho L^4 h n_0^2 V_r^{2.68} \quad \dots \dots \dots (4.2)$$

where

$$V_r = \frac{\bar{V}}{n_0 L} \quad \dots \dots \dots (4.3)$$

$$L = \frac{\int |r| ds}{A^{\frac{1}{2}}} \quad \dots \dots \dots (4.4)$$

and ζ is the critical damping ratio in the fundamental torsional mode of vibration.

It should be noted that effects of terrain categories, immediate surroundings and other fluctuating wind force characteristics on the torsional responses of buildings are not directly reflected in the above formulae.

For the rectangular symmetric building studied, the most unfavorable wind direction for the mean base torque was 10° . Fig. 4.10 shows that the mean torques in this orientation were proportional to V_r^2 and in good agreement with the predicted values obtained by Eq. 4.1. However, Fig. 4.11 shows that the standard deviation torques at the most unfavorable wind direction, i.e., $\alpha = 0^\circ$, were not uniformly proportional to $V_r^{2.68}$ and were approximately 2 times the results obtained by Eq. 4.2 on average. This was attributed mainly to the mis-match of mode shape of the present "stick" aeroelastic rig and partly to the simplicity of the empirical formulation. It will be seen in Chapter 6 that the error shown in Fig. 4.11 can be adjusted by the mode shape correction factors to some extent, but the variation trend of the dynamic torque with reduced velocity still is not uniformly proportional to $V_r^{2.68}$ as suggested by Isyumov.

4.3.2 Response and excitation spectra

The twist angle response spectra of the building model were obtained by Fast Fourier Transformation of the recorded response signals.

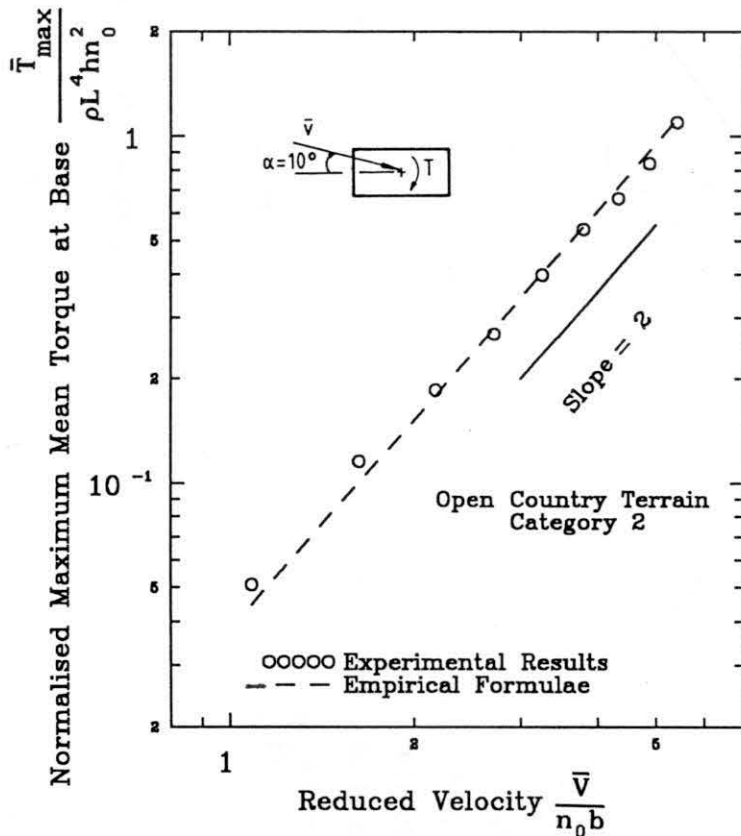


FIG. 4.10 COMPARISON OF MAXIMUM MEAN TORQUE

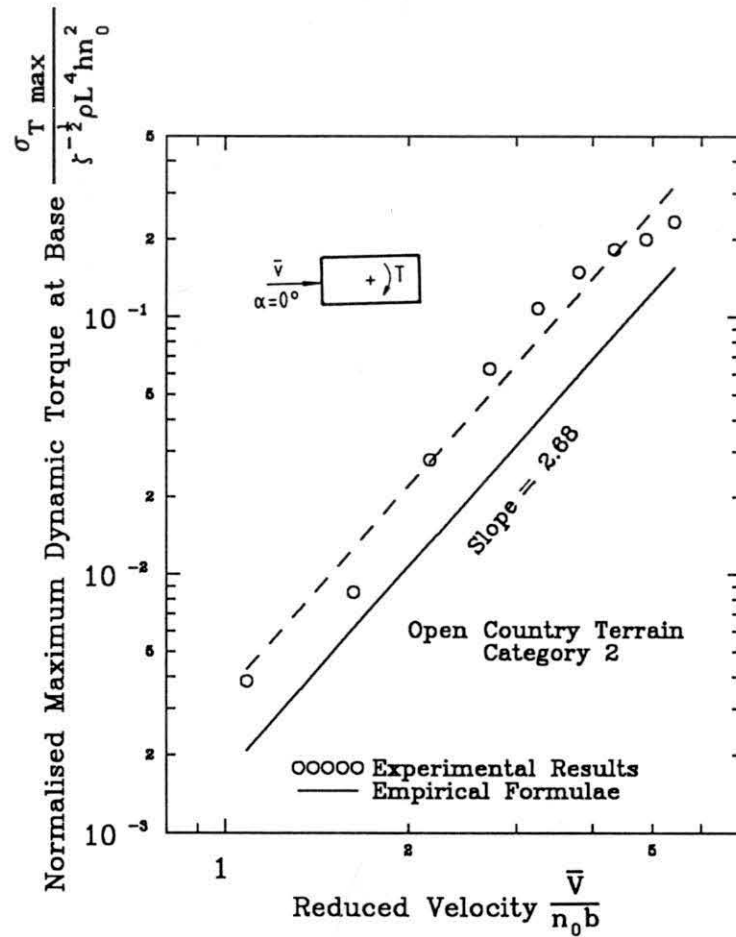


FIG. 4.11 COMPARISON OF MAXIMUM DYNAMIC TORQUE

Normalised response spectra, corresponding to the wide and narrow faces of the building model, are presented in Fig. 4.12. The shapes of these spectra were different but the largest peaks were both located at the natural frequency of the building model.

The difference between the response spectra was attributed to different torsion excitation mechanisms, which can be identified by analysing generalised torsional excitation spectra. The procedure to obtain generalised torsional spectra was similar to that suggested by Saunders and Melbourne (1975) for crosswind force spectra. As shown in Fig. 4.13, with the incident wind normal to the wide face of the building, the generalised torsional excitation spectrum has a dominant peak at a reduced frequency of about 0.1 at which there is concentrated excitation energy associated with the vortex shedding process. With the incident wind normal to the narrow face of the building, the peak in the torsional excitation spectrum was relatively broad and, at the reduced wind velocity of 8, two peaks could be readily identified at the reduced frequencies of about 0.04 and 0.15. From the viewpoint of energy distribution, both spectral shapes look more similar to the corresponding crosswind force spectral shapes than the alongwind force spectral shapes (Kwok et al., 1988) of a rectangular section building. Therefore, the mechanisms of torsional excitation of rectangular section buildings might be closely related to those of crosswind excitation. By correlation analysis of fluctuating pressure distribution on a square section building (Reinhold, 1983) and base dynamic moments obtained by base force balance technique (Thoroddsen, Peterka and Cermak, 1988), the same conclusion was reached. The effect of angle of wind incidence on the excitation spectral shape is highlighted by using Fig. 4.14. It is obvious that different wind directions caused different generalised torsional excitation on the rectangular building. Further discussion of torsional excitation mechanisms can be found in the section on eccentric model tests.

4.3.3 Probability distributions of peaks

As discussed in Chapter 3, for most tall buildings under normal strong wind conditions, the alongwind and crosswind response processes are usually well represented by a normal, that is Gaussian, distribution. However,

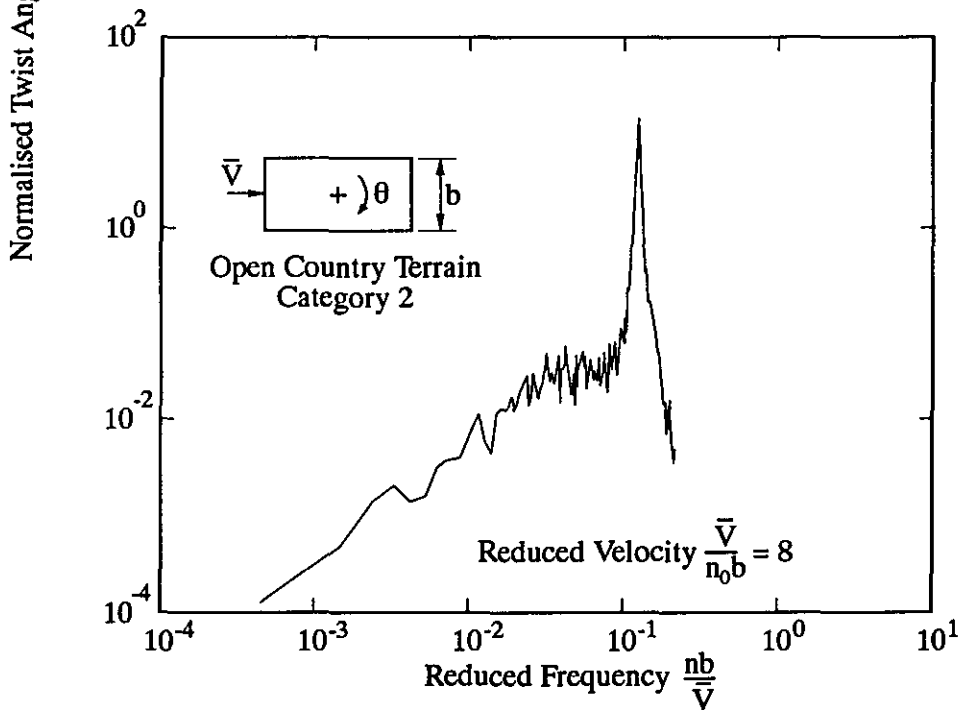
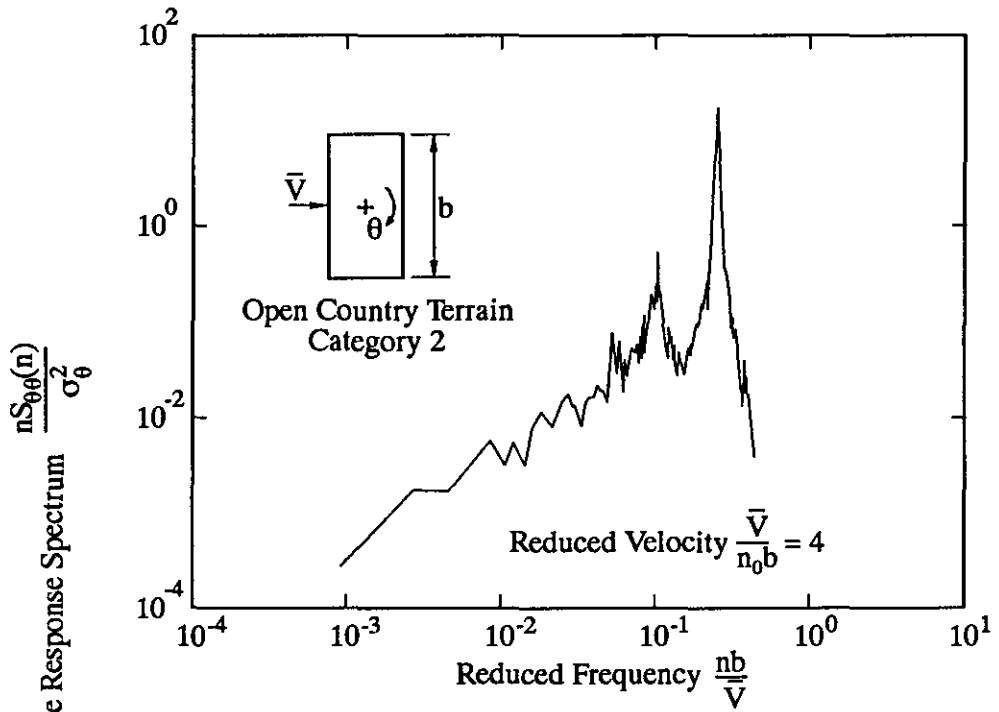


FIG.4.12 TWIST ANGLE RESPONSE SPECTRA

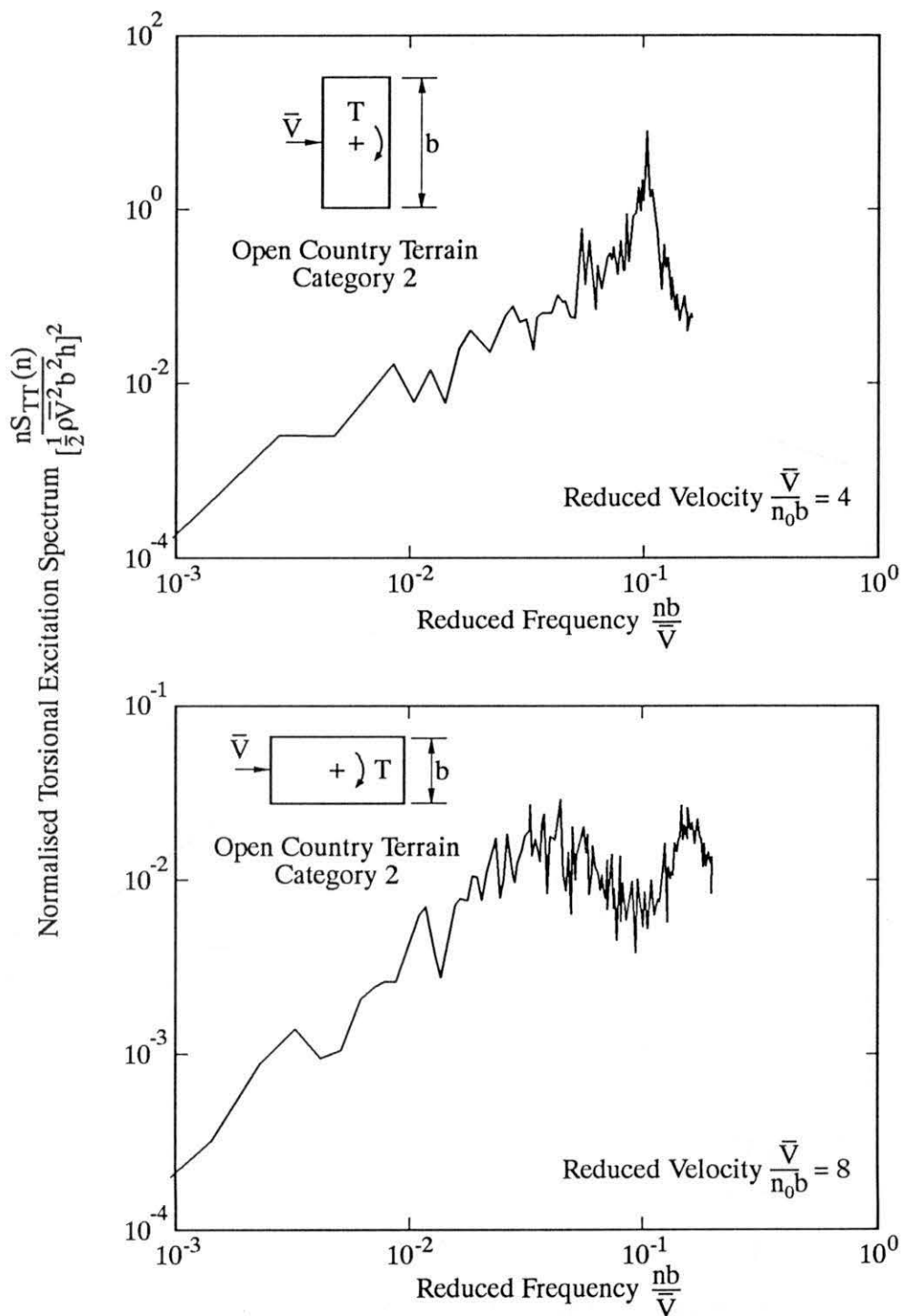


FIG.4.13 TORSIONAL EXCITATION SPECTRA (Basic Model)

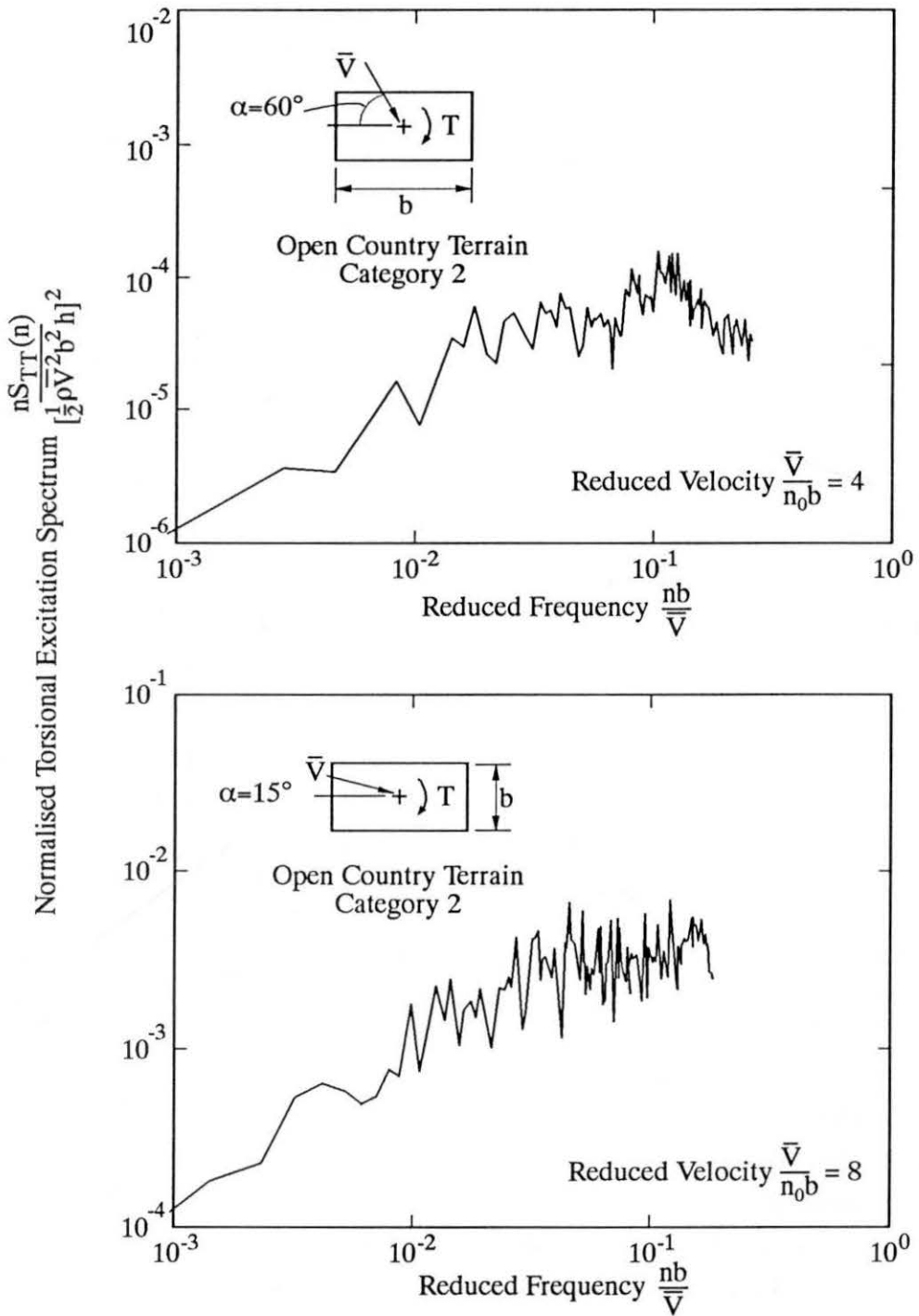


FIG.4.14 VARIATION OF TORSIONAL EXCITATION SPECTRA WITH WIND DIRECTIONS

under conditions where there is a significant interdependence of variables in the crosswind excitation and response processes, such as displacement dependent lock-in, the response process will depart from being normally distributed and in extreme case approaches that of a sine wave. Therefore, probabilistic analysis of the response peaks can be used to identify the response characteristic as well as the mechanism of the excitation.

The same method was used to analyse the torsional response characteristics. It is expected that the torsional response processes within the studied reduced wind velocity range are also normal distribution, since the torsional excitation acting on a rectangular building is believed to be closely related to the corresponding crosswind wake excitation. The results of probabilistic analysis of the torsional response showed that in the reduced wind velocity range studied, the torsional responses were essentially normally distributed, as shown in Figs. 4.15 and 4.16, whether the incident wind was normal to the wide face or narrow face of the model. This is also clearly demonstrated in the traces of the torsional motions as shown in Fig. 4.17. However, because of the limited wind velocity in the present wind tunnel, the critical wind speed which may be associated with displacement dependent lock-in could not be obtained to demonstrate the torsional response distribution under this special wind speed.

4.3.4 Aerodynamic damping

As a building moves through the fluid in response to the wind loading, an aeroelastic force which depends on the building motion may be generated. This force is usually referred to as the aerodynamic damping force and estimated by an aerodynamic damping. Aerodynamic dampings of prismatic bodies in the drag and lift directions have been discussed by Davenport (1979), Kareem (1982), and others although the relevant data are still not plentiful. However, very little information on torsional aerodynamic damping of a prism is available.

By analysing the decay curve of the torsional response autocorrelation function, torsional aerodynamic damping was approximately evaluated. Figs. 4.18 and 4.19 show log plots of the autocorrelation envelopes of the torsional

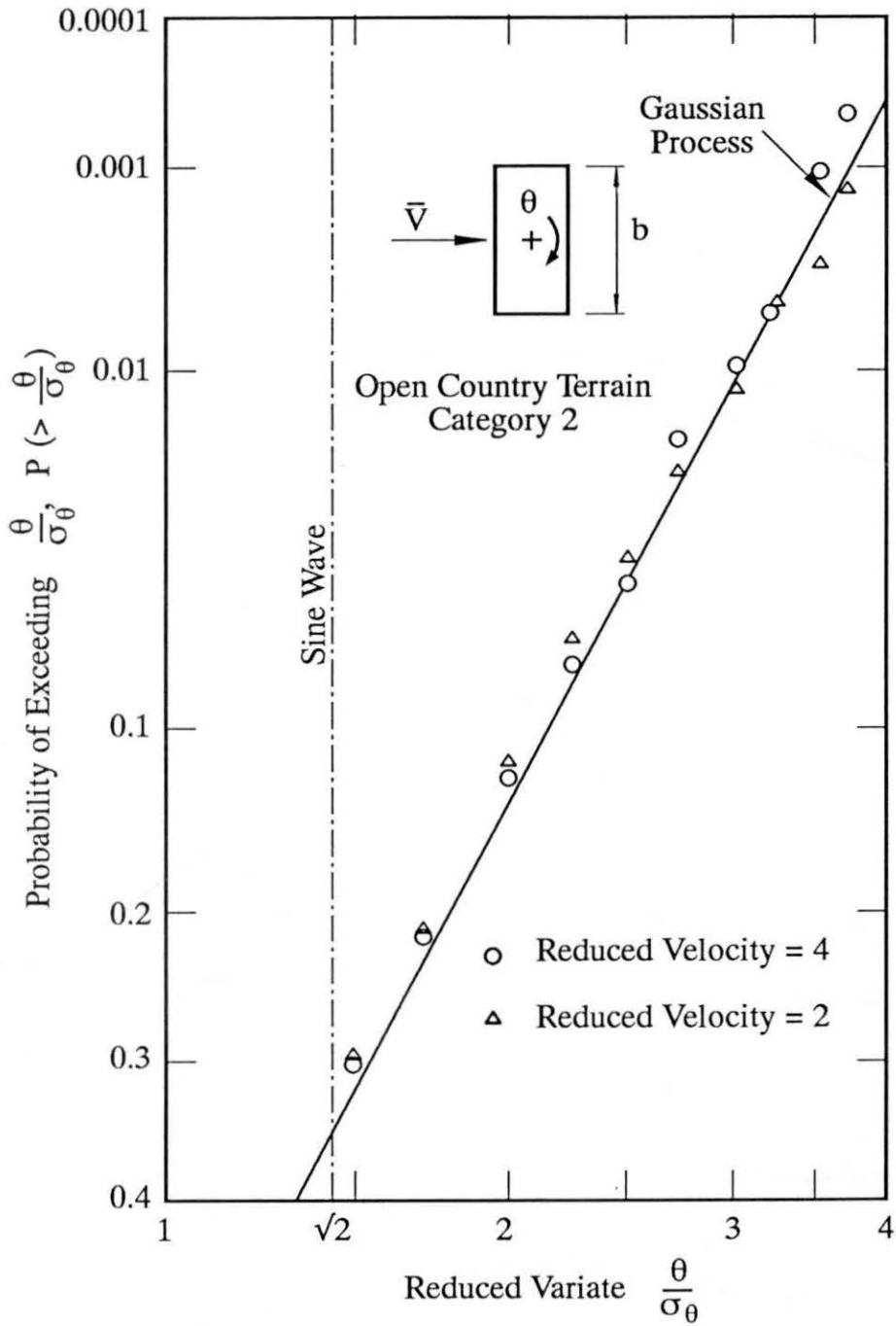


FIG.4.15 PROBABILITY DISTRIBUTIONS OF TORSIONAL RESPONSE PEAKS (Basic Model + Wide Face)

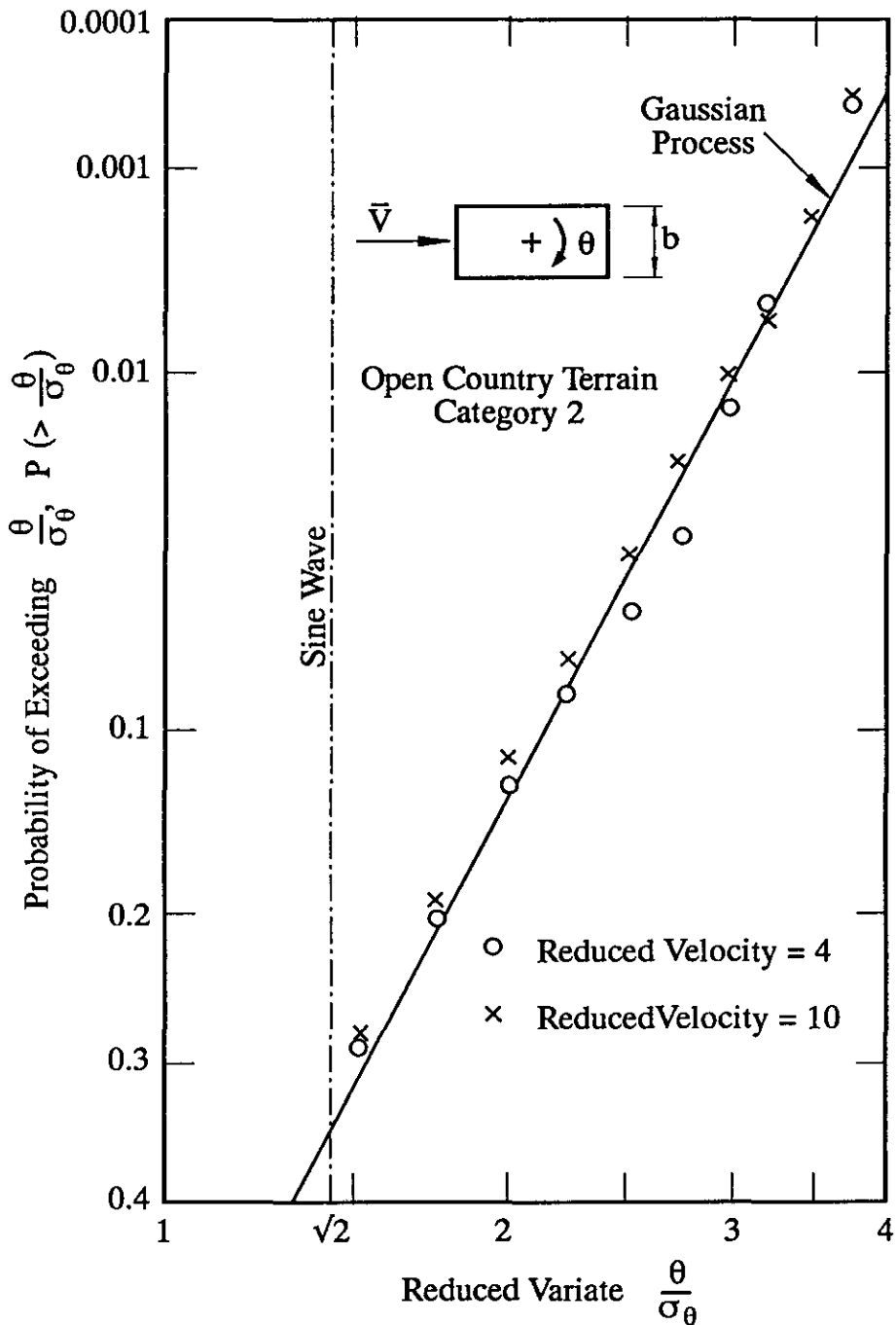


FIG.4.16 PROBABILITY DISTRIBUTIONS OF TORSIONAL RESPONSE PEAKS (Basic Model + Narrow Face)

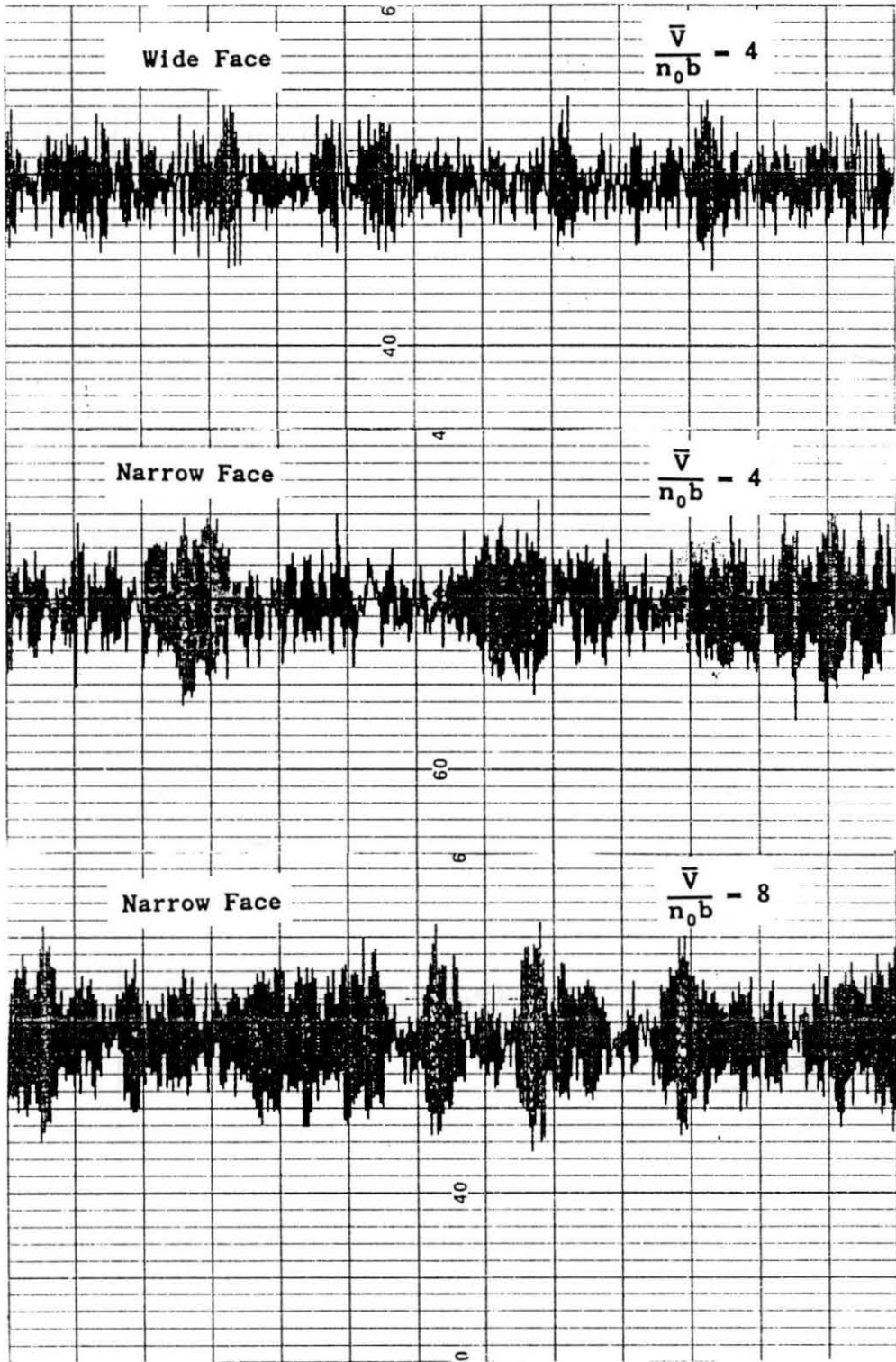


FIG. 4.17 TRACES OF TORSIONAL RESPONSES (BASIC MODEL)

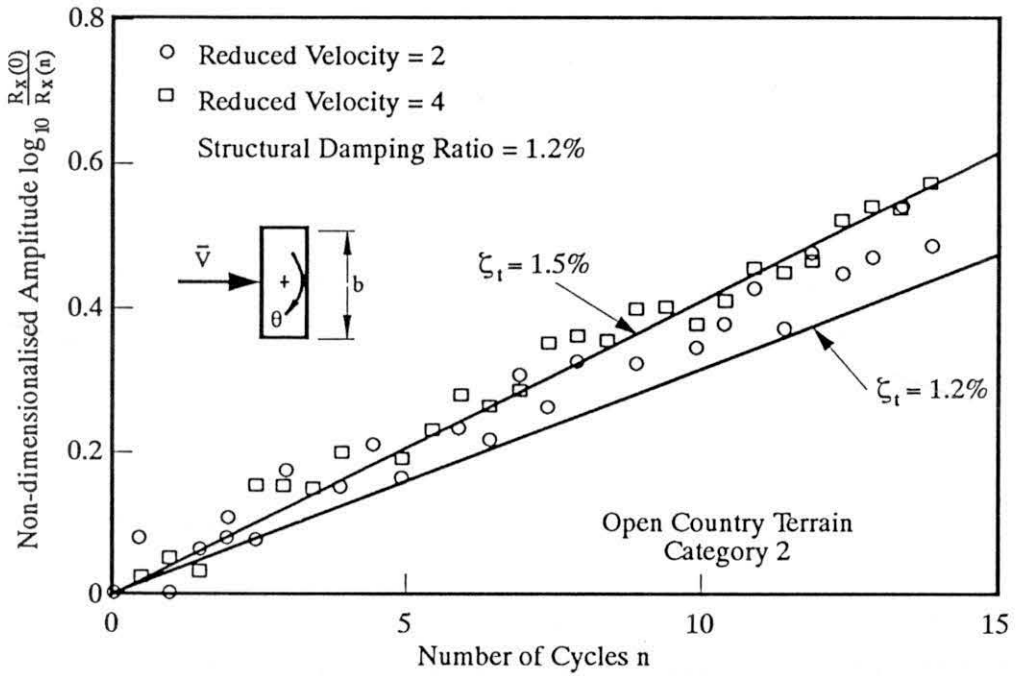


FIG.4.18 AUTOCORRELATION ENVELOPE OF TORSIONAL RESPONSE (WIDE FACE)

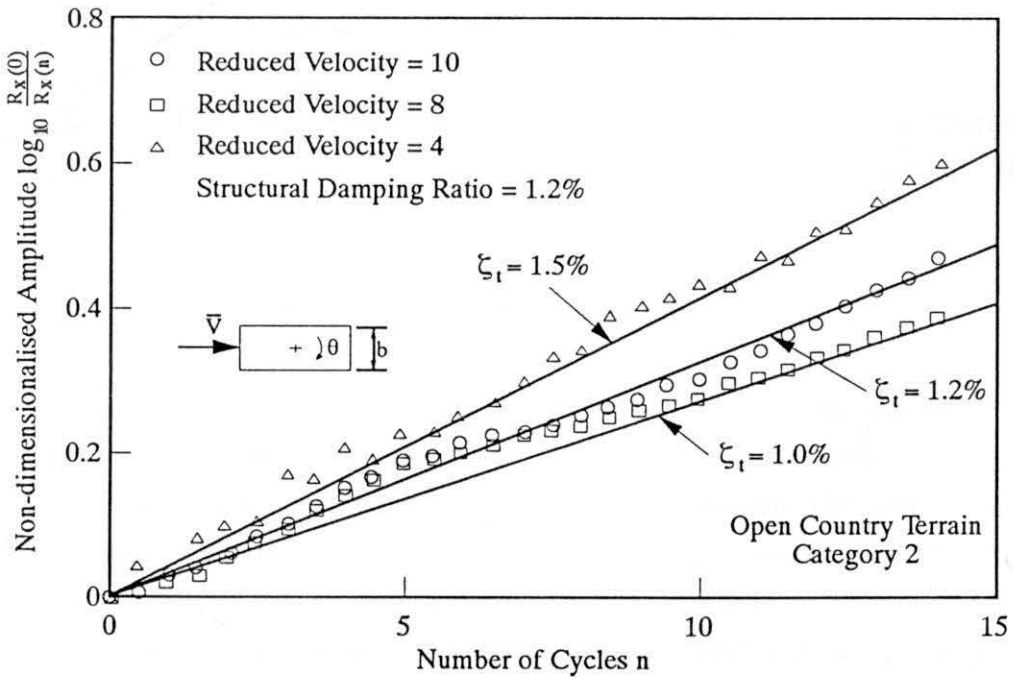


FIG.4.19 AUTOCORRELATION ENVELOPE OF TORSIONAL RESPONSE (NARROW FACE)

responses with the wind incidence normal to the narrow or wide face of the building. In these figures the total damping of the building, ζ_t , is the sum of the structural damping ζ_s and the aerodynamic damping ζ_a . It was found that the torsional aerodynamic damping was small in both wind directions and for all the studied reduced wind velocities. The maximum positive aerodynamic damping ratio was less than 0.4 %, and there was a negative aerodynamic damping ratio of approximately -0.2 % at a reduced velocity of 8 and with the wind incidence normal to the narrow face of the building. However, larger negative aerodynamic damping may occur at reduced wind velocities higher than the studied range.

4.4 Eccentric Model Tests

The torsional responses of tall buildings can be amplified by asymmetrical wind pressure loading about the elastic axis, or inertial loading resulting from non-coincidence of the centre of mass with the elastic axis. In order to estimate this influence and further investigate the torsional excitation mechanism, the elastic centre of the basic model was shifted away from the mass (geometry) centre of the basic model by about 10% of the width of the model, in the longer axis of the model section. As a result, the building model generalised mass moment of inertia increased by 9.8% and the corresponding natural frequency decreased by 4.6%. None of the other parameters was changed.

4.4.1 Effect of eccentricity on torsional excitation

For incident wind normal to the narrow face of the eccentric model, two wind directions, i.e., 0° and 180° , were considered. These two orientations indicated a change of the offset between the centre of mass, stiffness and aerodynamic forces. Therefore, there would be some difference between the corresponding torsional excitation spectra. Compared with the basic model excitation spectrum, generalised torsional excitation spectra for these two orientations and at the reduced velocity of 8 also have two obvious peaks, but the two peak values were different for different eccentricity levels, as shown in Fig. 4.20. With the forward shift of the

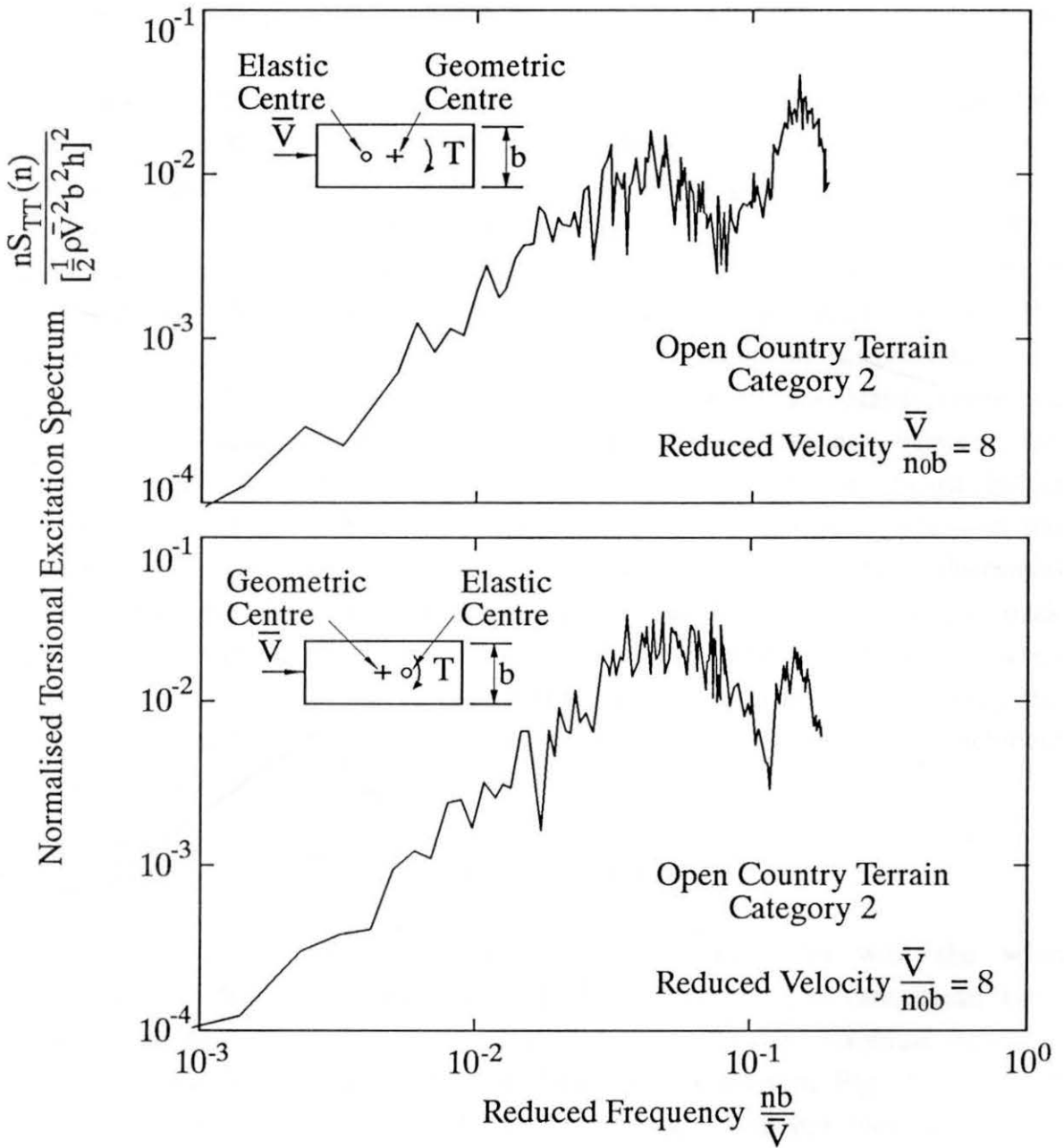


FIG.4.20 TORSIONAL EXCITATION SPECTRA (ECCENTRIC MODEL)

elastic centre of the building model, the magnitude of the first peak decreased, but the second peak values increased. The situation was reversed for the backward shift of the elastic centre. Combined with the experimental results obtained by Isyumov and Poole (1983), it is thought that the first peak is related to cross-wind excitation due to incident turbulence, which is mainly distributed on the windward halves of the two side faces of the building. The second peak is thought to be caused by flow re-attachment intermittencies on the leeward halves of the two side faces of the building. Note that the wind load magnitude and distribution on the surface of the building can be considered to be unchanged for both orientations. The forward shift and backward shift of the elastic centre of the building model caused a change of the relative distance between the elastic centre and wind forces respectively acting on the windward halves and the leeward halves of the building. As a result, two peak values in the generalised torsional excitation spectra increased or decreased correspondingly. It is also noted that the frequency around the second peak was close to the natural frequency of the building model. Therefore, when wind incidence was normal to the narrow face of a rectangular building, the energy absorbed by the building mostly came from the flow re-attachment intermittence which is related to the second peak.

4.4.2 Effect of eccentricity on torsional response

Compared with the test results of the basic model with the wind incidence normal to the wide face of the model, a significant mean twist angle response occurred and the variation of the mean response with the reduced velocity was still proportional to V_r^2 as shown in Fig. 4.21. From Fig. 4.22, it is shown that the dynamic twist angle response increased by up to 40%.

The effect of angle of wind incidence on the torsional response of the eccentric model is shown in Figs. 4.23 and 4.24. The maximum dynamic torque still occurred at around 0° or 180° while the maximum mean torque was located at 120° . At the reduced wind velocity of 8, the maximum dynamic torque of the eccentric model increased by 30% and the maximum mean torque increased by a factor of 2 or more, compared with the values

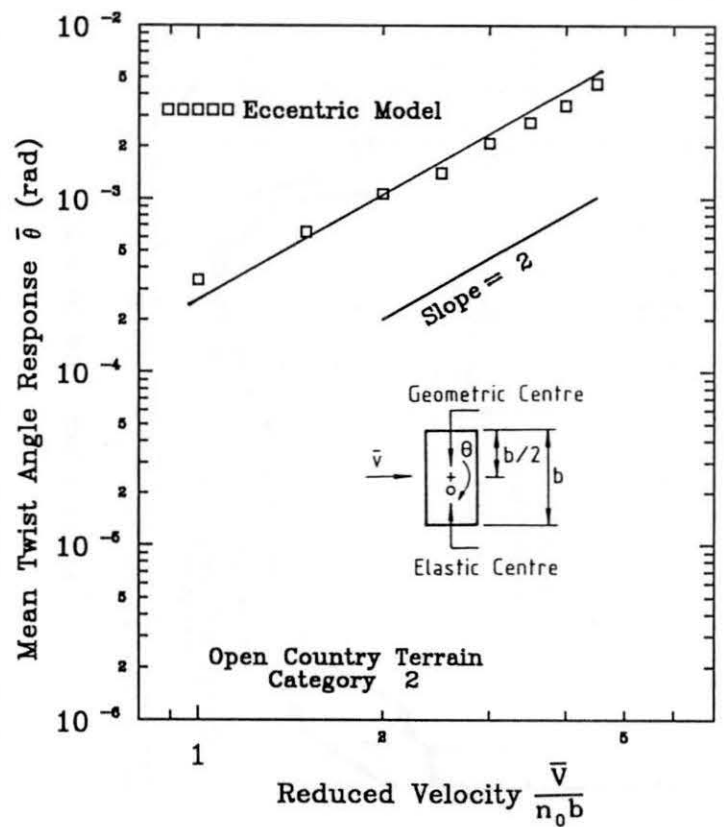


FIG. 4.21 MEAN TORSIONAL RESPONSES (ECCENTRIC MODEL + WIDE FACE)

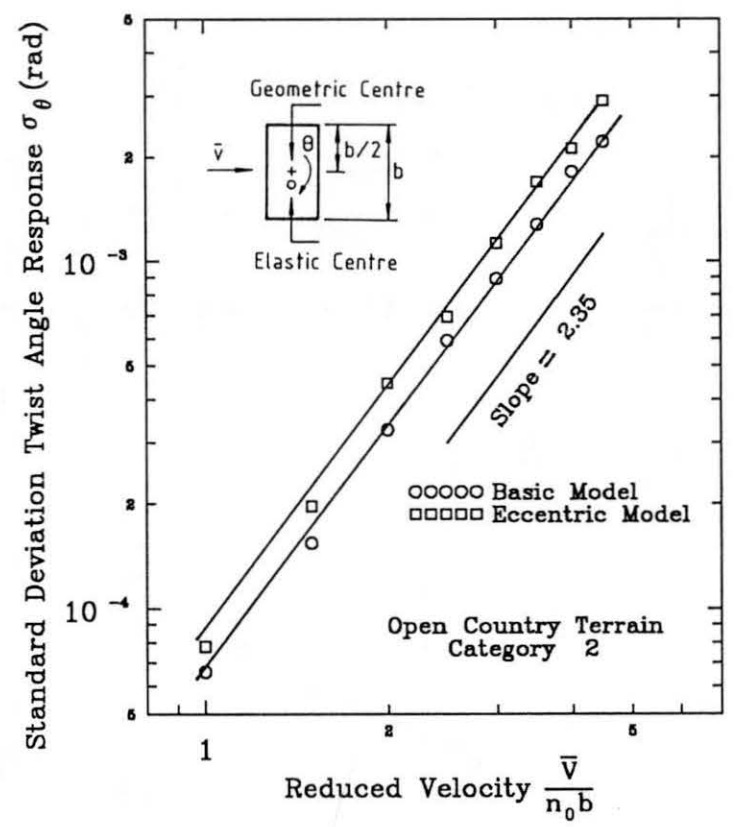


FIG. 4.22 COMPARISON OF STANDARD DEVIATION TORSIONAL RESPONSES (WIDE FACE)

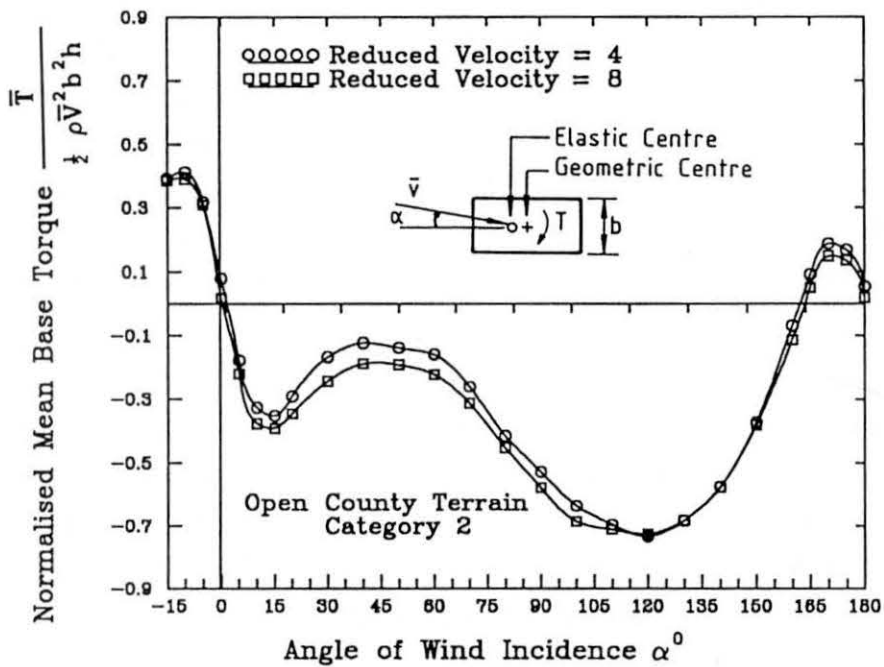


FIG. 4.23 EFFECT OF ANGLE OF WIND INCIDENCE ON MEAN TORQUE (ECCENTRIC MODEL)

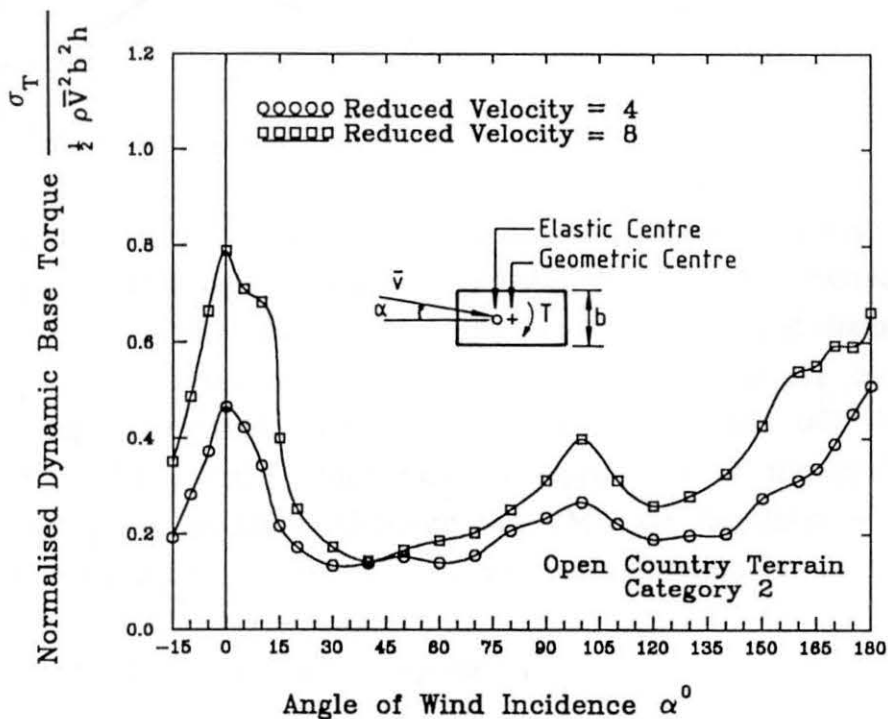


FIG. 4.24 EFFECT OF ANGLE OF WIND INCIDENCE ON DYNAMIC TORQUE (ECCENTRIC MODEL)

of the basic model. Again the variation of the reduced wind velocity did not change the normalised mean torque, but did change the normalised dynamic torque. This is consistent with the variations of the mean and dynamic torques with reduced velocity, that is, the former was proportional to V^2 and the latter was not. In addition, the probability analysis of the eccentric model response peaks showed that the dynamic torque responses of the eccentric model were also normally distributed despite the significant increases in the dynamic response. A typical probability distribution of the torsional response peak is shown in Fig. 4.25.

It is noted that the length parameter L in Eq. 4.4 is a measure of the effective eccentricity of the aerodynamic force as discussed by Greig (1980) and, therefore, it can also be used in the response analysis of the eccentric model. Experimental results of the dynamic base torque of the eccentric model were compared with the results obtained by Eq. 4.3 as shown in Fig. 4.26. The difference between the experimental and empirical values for the eccentric model was slightly larger than that for the basic model. However, after considering Lythe and Surry's work (1991) on various definitions of the torsion coefficient, more such experiments in the future are still needed to evaluate the definition of the length parameter L .

4.5 Eccentric Model with Tuned Mass Damper

As described in Chapters 2 and 3, tuned mass dampers as an energy dissipation device can be used to increase the overall effective damping of the main building and accordingly to reduce wind-induced building vibration. However, most studies of the TMD system are concentrated on suppressing alongwind and crosswind vibrations of tall buildings and structures. Very little information on suppression of torsional vibration of tall buildings is available, although the TMD on the John Hancock Tower was designed mainly to suppress the torsional vibration of the tower.

4.5.1 Comparison of torsional responses

As a preliminary study, a symmetric tuned mass damper, with about

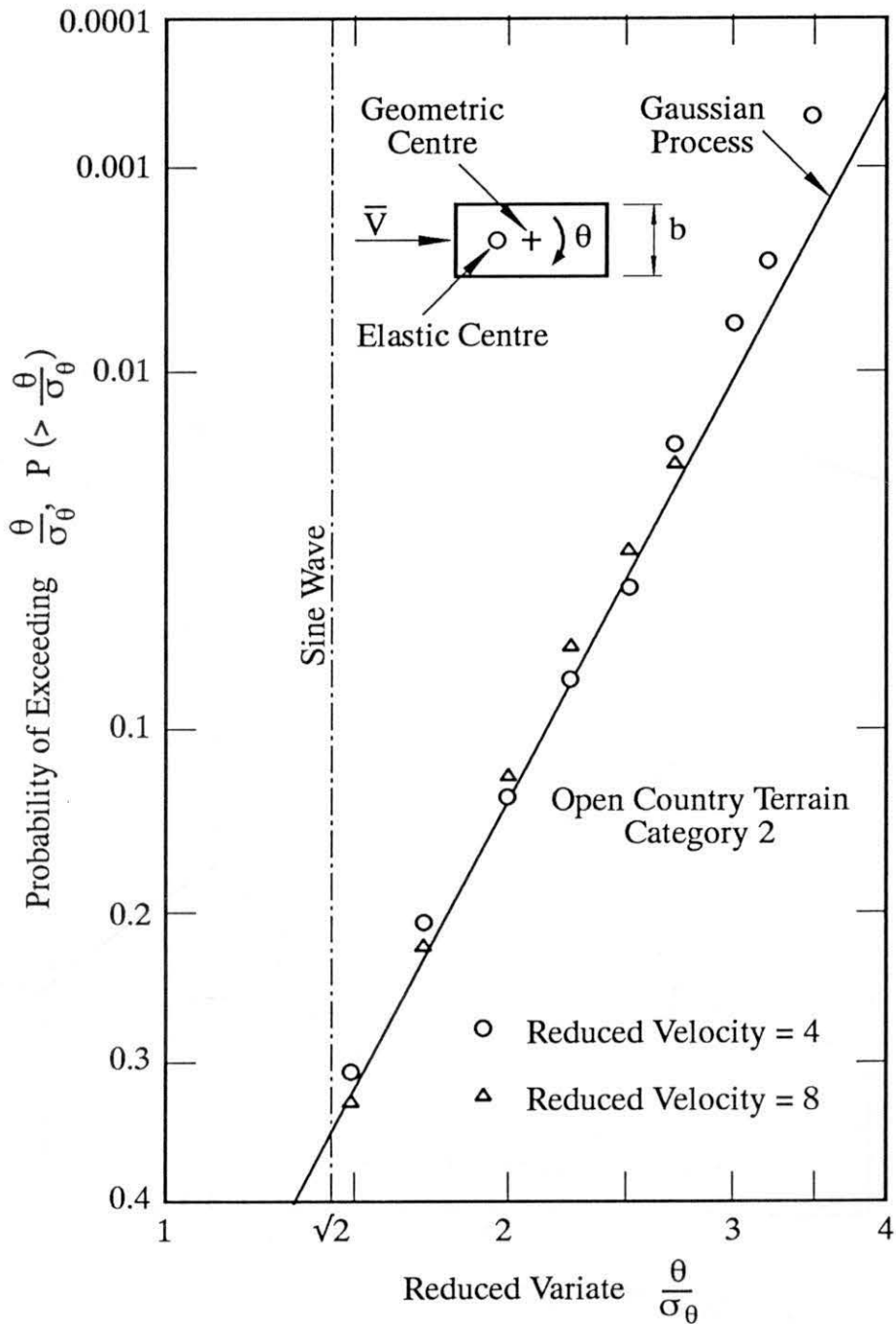


FIG.4.25 PROBABILITY DISTRIBUTIONS OF TORSIONAL RESPONSE PEAKS (Eccentric Model)

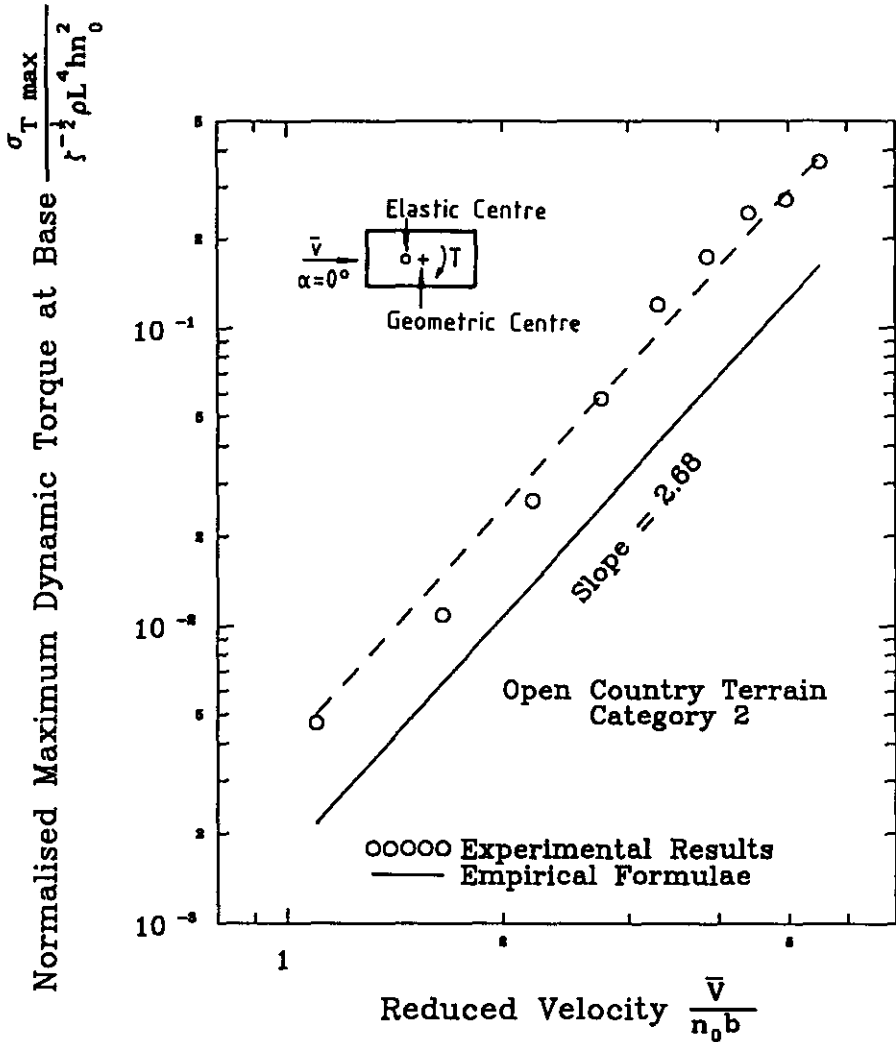


FIG. 4.26 COMPARISON OF MAXIMUM DYNAMIC TORQUE (ECCENTRIC MODEL)

1.2% of the building model generalised mass moment of inertia or about 3.6% of the building model generalised mass, was positioned under the top cover of the building model. The damper damping was 4.8% of critical and the total system then had 2.9% of critical damping as shown in the free vibration decay curve in Fig. 4.27. The experimental results showed that a TMD can effectively suppress wind-induced torsional vibration within the studied range of wind reduced velocities and angles of wind incidence. Figs. 4.28 and 4.29 show that there is up to a 30% reduction in response for wind incidence normal to the wide face of the model and a 45% reduction for wind incidence normal to the narrow face of the model, even though the parameters of the tuned mass damper tested were not optimum. Fig. 4.30 shows that the effectiveness of the TMD can be maintained at all concerned angles of wind incidence.

4.5.2 Comparison of response spectra

The twist angle response spectra of the building model with and without a damper were compared for the incident wind normal to the wide and narrow faces of the building model, as shown in Figs 4.31 and 4.32. Both spectra were normalised by $\sigma_{\theta_0}^2$, which was the standard deviation twist angle of the plain model without the damper, in order to have an apparent comparison of the spectral amplitude. It is obvious that the reduction in energy amplitudes around the natural frequency of the building was quite significant for both orientations. Further analysis of the effectiveness of the TMD to reduce the torsional vibration of the tall building will be performed in next Chapter.

4.6 Conclusions

The aeroelastic modelling technique for pure torsion vibration as described in this Chapter was found to be a convenient and efficient way to explore the mechanism of torsional excitation and to predict the torsional response of tall buildings to wind. This technique allows some aeroelastic effects to be considered and the effectiveness of passive control systems can also be readily demonstrated.

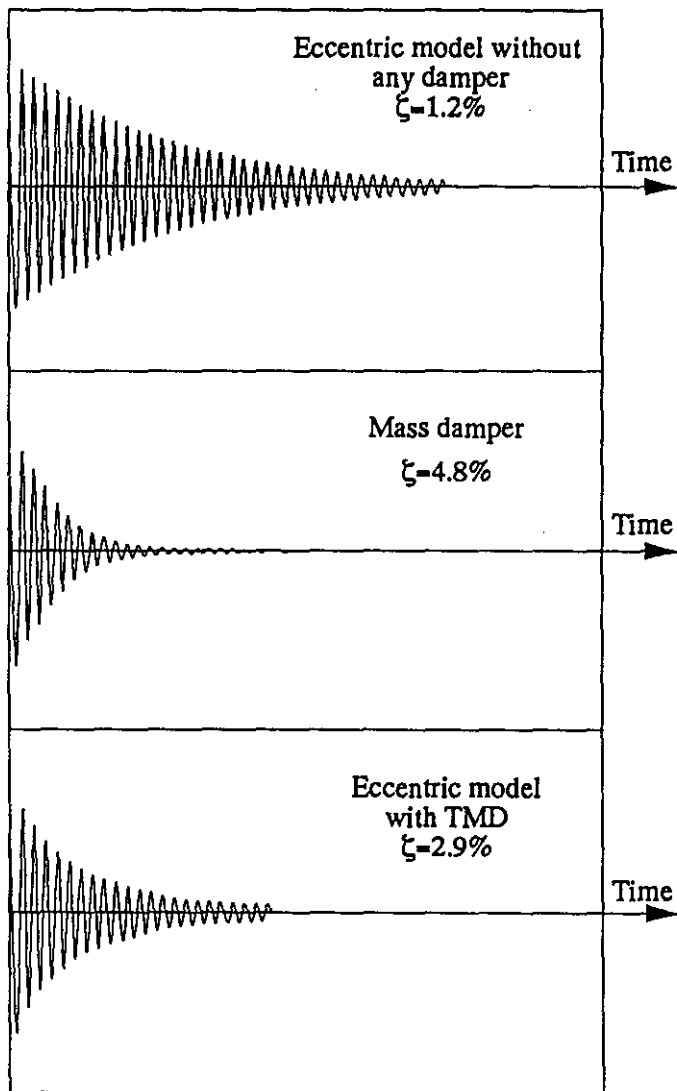


FIG. 4.27 TORSIONAL FREE VIBRATION DECAY TRACES SHOWING EFFECTIVENESS OF TUNED MASS DAMPER

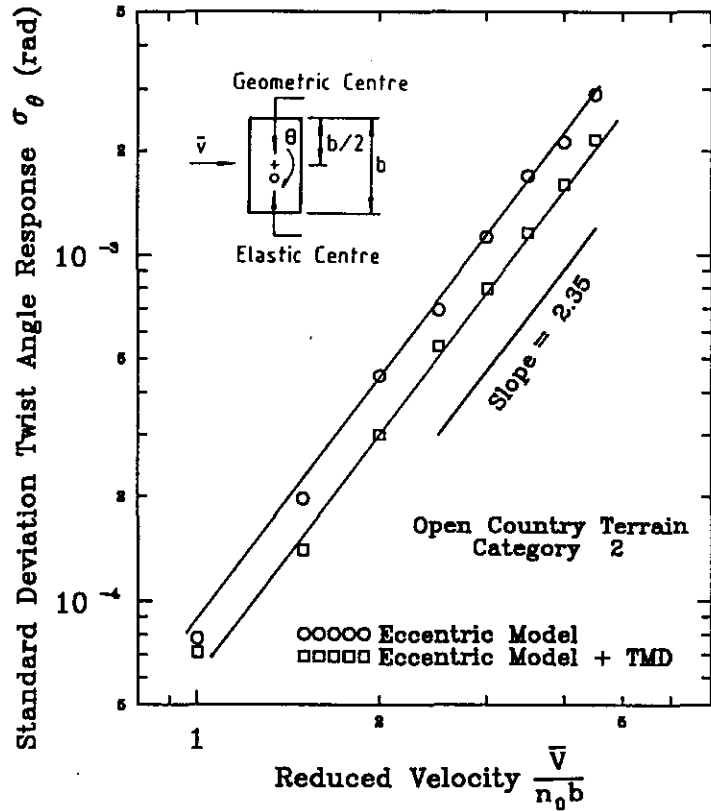


FIG. 4.28 STANDARD DEVIATION TORSIONAL RESPONSES (WIDE FACE WITH TMD)

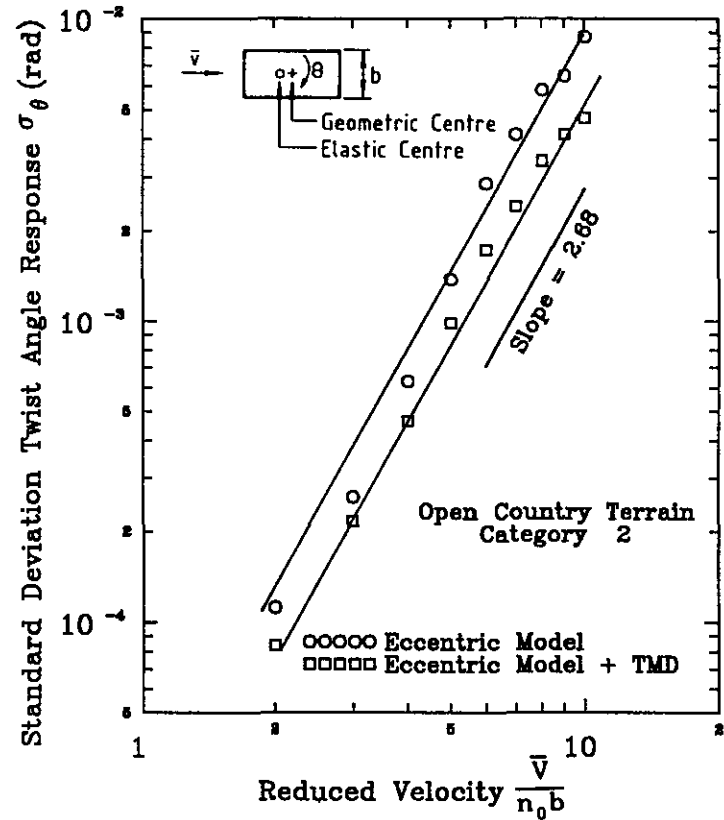


FIG. 4.29 STANDARD DEVIATION TORSIONAL RESPONSES (NARROW FACE WITH TMD)

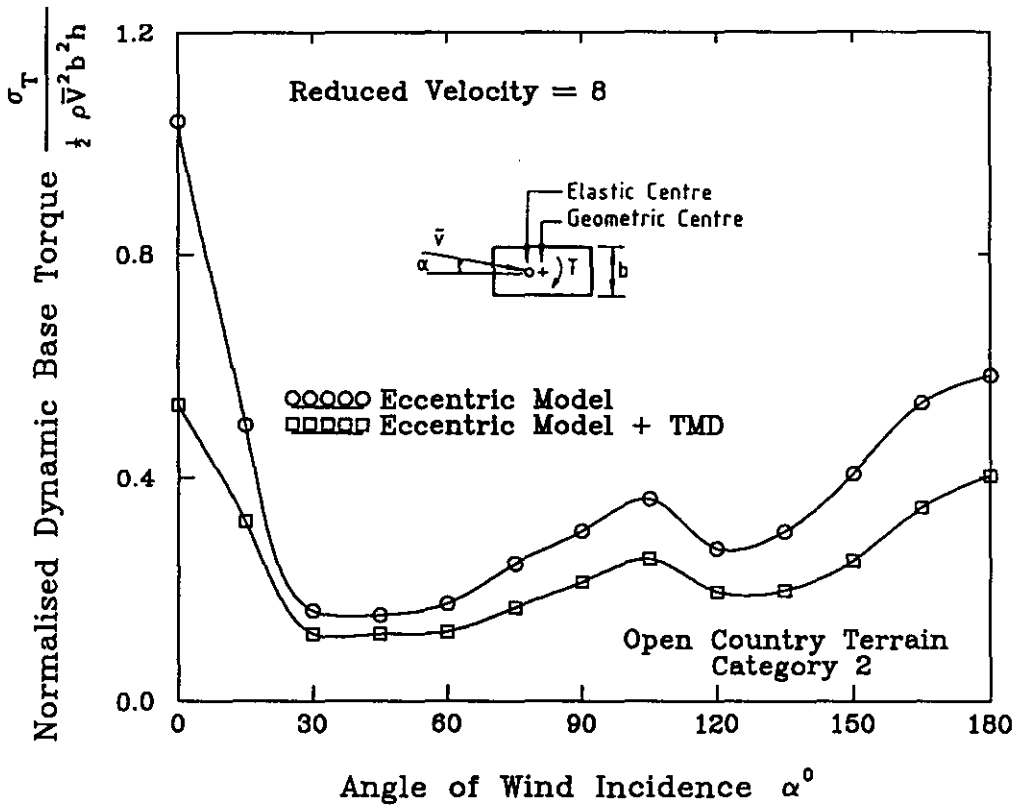


FIG. 4.30 EFFECT OF ANGLE OF WIND INCIDENCE AND TMD

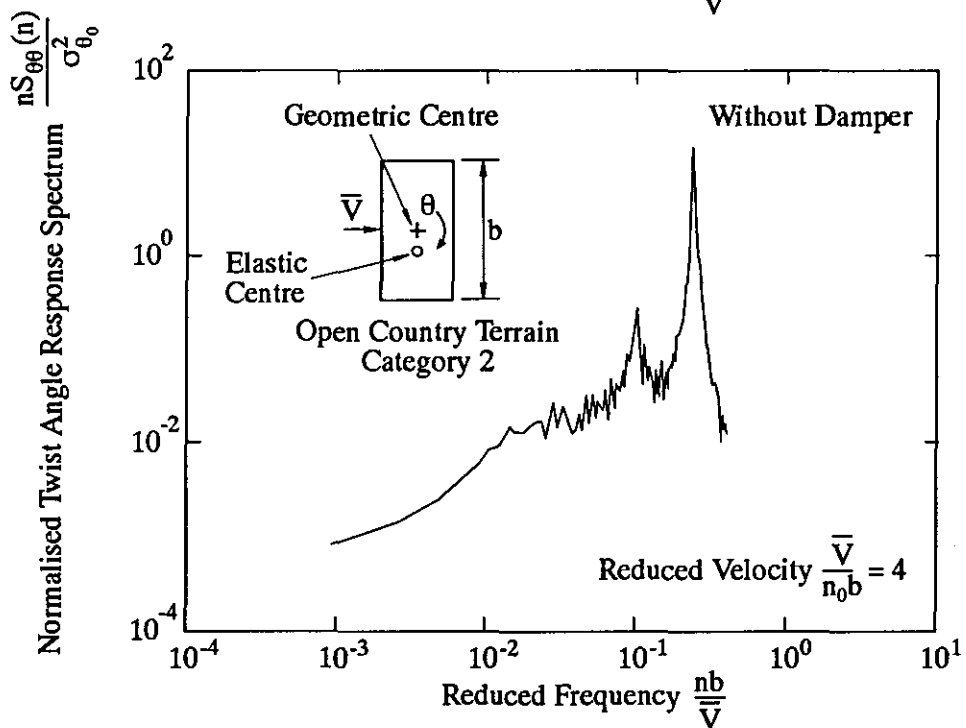
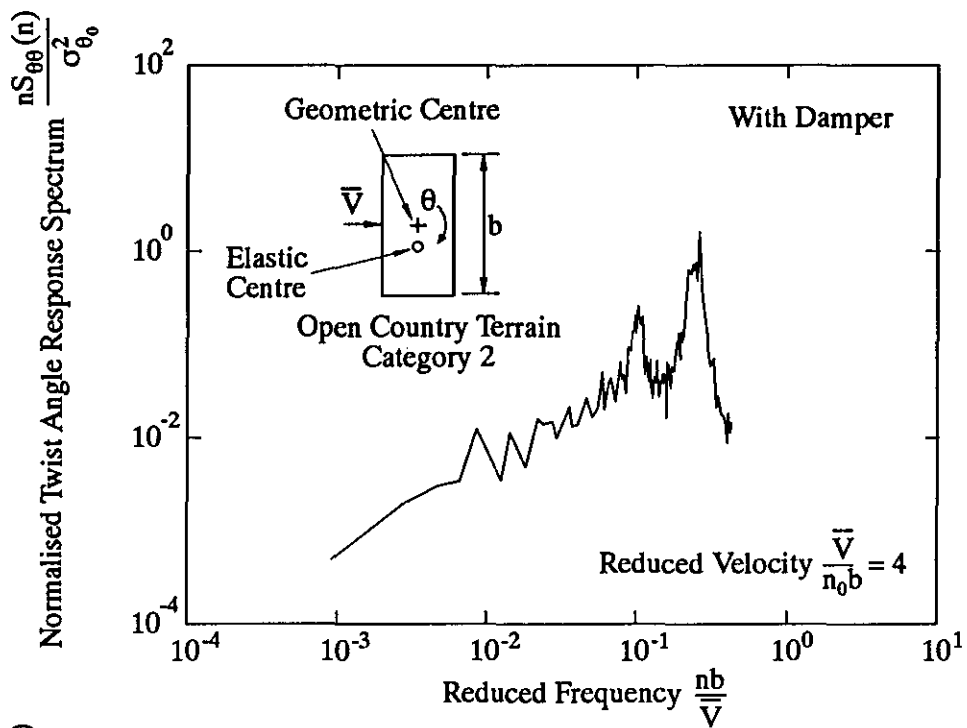


FIG.4.31 COMPARISON OF TWIST ANGLE RESPONSE SPECTRA
(Wide Face + TMD)

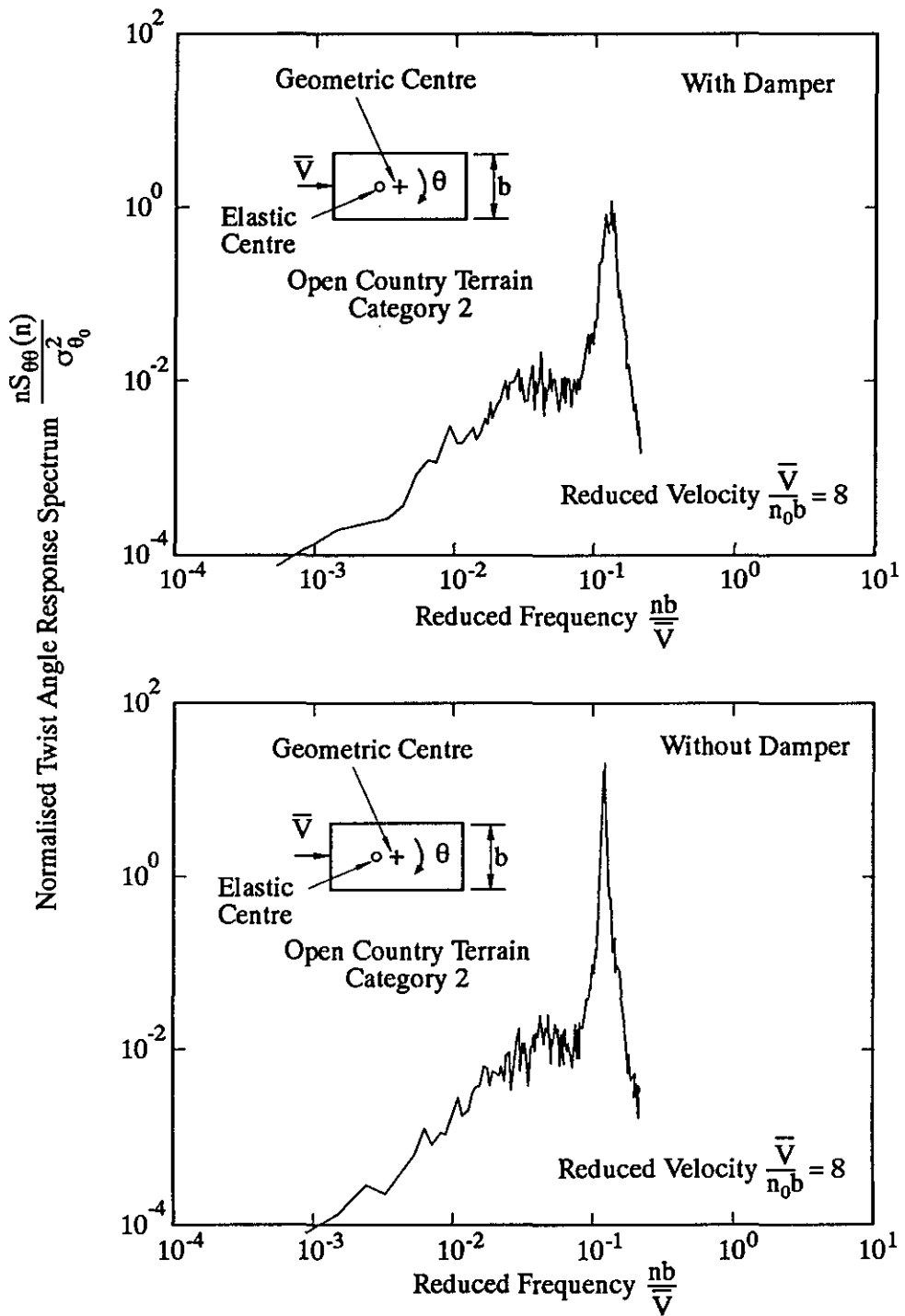


FIG.4.32 COMPARISON OF TWIST ANGLE RESPONSE SPECTRA
(Narrow Face + TMD)

From the basic model tests, it was shown that the maximum dynamic response usually occurred at around 0° , i.e., with wind incidence normal to the narrow face of the rectangular building. The maximum mean torque occurred at 10° and 60° . It was shown that the experimental results of the maximum mean torque were in good agreement with the empirical values suggested by Greig and Isyumov. However, there was some difference in the maximum dynamic torque. Experimental results also showed that the torsional responses were essentially normally distributed and the torsional aerodynamic damping was small in the reduced wind velocity range studied.

With the wind incidence normal to the wide face of the building, vortex shedding is the dominant mechanism of torsional excitation. With the wind incidence normal to the narrow face, there are two important excitation mechanisms: incident turbulence which exerts its influence mainly distributed on the windward halves, and flow re-attachment intermittencies on the leeward halves of the two side faces of the building.

For the eccentric model with a 10% geometric eccentric ratio, the maximum dynamic torque still occurred at around 0° or 180° while the maximum mean torque was located at 120° . At a reduced wind velocity of 8, the maximum dynamic torque of the eccentric model increased by 30% and the maximum mean torque increased by a factor of 2 or more, compared with the values of the basic model.

For the eccentric model with a TMD, the results showed that a TMD can effectively suppress wind-induced torsional vibration. There was up to a 30% reduction in response for wind incidence normal to the wide face of the building and a 45% reduction for wind incidence normal to the narrow face of the building, even though the parameters of the TMD tested were not optimum. Because the torsional excitation spectra were different for both wind directions, it can be concluded that the effectiveness of the TMD was dependant on the type of torsional excitation.

Chapter 5

A SEMI-ANALYTICAL METHOD OF PERFORMING PARAMETRIC STUDY OF TUNED MASS DAMPERS

5.1 Introduction

A theoretical treatment of the response of a one degree of freedom system with an auxiliary mass damper to sinusoidal excitation has been discussed by Den Hartog (1956) in detail. The application of this theory to parametric studies for large scale TMDs in reducing wind-induced slender structure motion was first presented by Vickery and Davenport (1970). The work of Isyumov et al. (1975), McNamara (1977), Wiesner (1979), Luft (1979) and others further improved the procedure of the parametric studies for large scale TMDs. The main aspects of this procedure can be summarised as follows:

(a) Letting the i th mode of a slender structure fitted with an auxiliary mass damper be equivalent to a two degree of freedom system as shown in Fig. 5.1. The equivalent mass M_{ei} and the equivalent stiffness K_{ei} for the i th mode of a slender structure of height h and a mass per unit height of $m(z)$ can be calculated by the following formulae:

$$M_{e_i} = \frac{\int_0^h m(z) \Phi_i^2(z) dz}{\Phi_i^2(z_d)} \dots \dots \dots (5.1)$$

$$K_{e_i} = (2\pi n_i)^2 M_{e_i} \dots \dots \dots (5.2)$$

where $\Phi_i(z)$ is the modal shape for the i th mode; z_d is the height at which

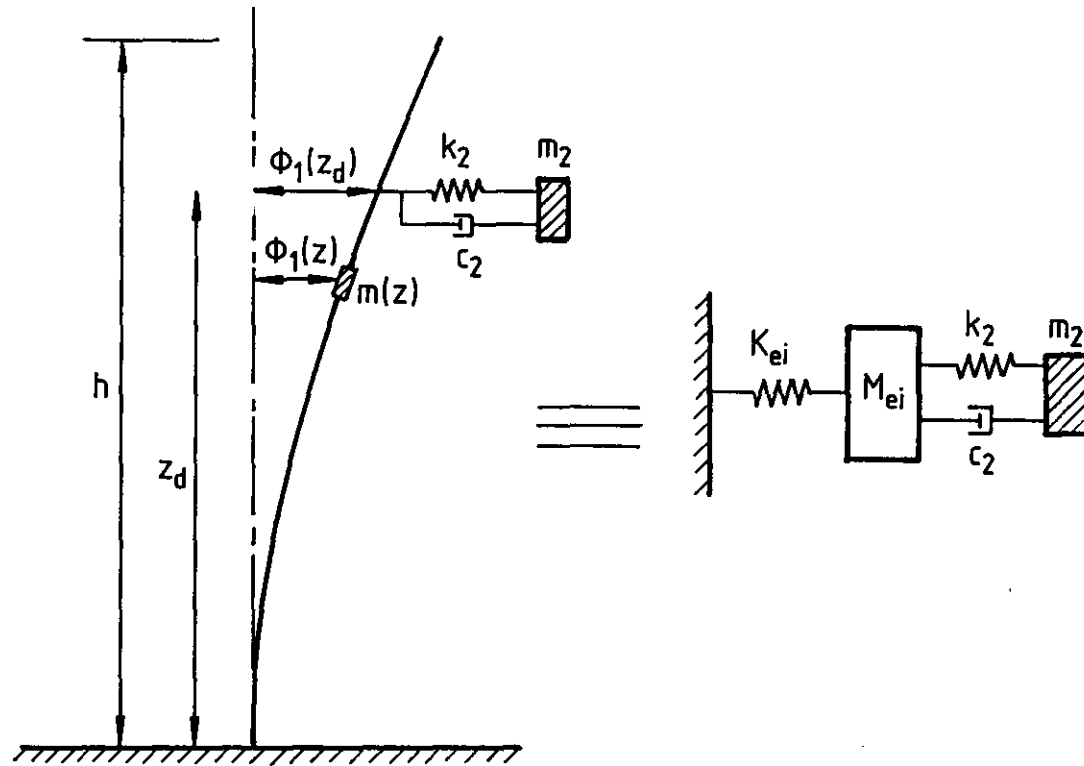


FIG.5.1 EQUIVALENT TWO DEGREE OF FREEDOM SYSTEM FOR THE ITH MODE

the auxiliary mass damper is located; and n_i is the frequency of the i th mode without the auxiliary mass.

(b) Assuming that the actual i th mode generalised wind loads F_i acting on the equivalent mass can be represented by a random white noise excitation, the displacement response variance of the equivalent mass M_{ei} and the relative displacement response variance of the mass damper, as shown in Fig. 5.1, can be expressed as:

$$\sigma_{y_i}^2 = \frac{S_o}{K_{e_i}^2} \int_0^\infty |H_{y_i F_i}(n)|^2 dn \quad \dots \dots \dots (5.3)$$

$$\sigma_z^2 = \frac{S_o}{K_{e_i}^2} \int_0^\infty |H_{z F_i}(n)|^2 dn \quad \dots \dots \dots (5.4)$$

where S_o is a constant which reflects the intensity of the white noise excitation; $|H_{y_i F_i}(n)|$ and $|H_{z F_i}(n)|$ are the mechanical admittance functions of the equivalent TMD-structure system. These expressions are derived in the next section.

(c) Introducing the concept of the effective damping, i.e., the performance of the combined system with a TMD as if the behavior were a single degree-of-freedom system with a single damping parameter ζ_{ei} . This can be accomplished by equating the response of the combined system to that of a single degree-of-freedom system with the same frequency. That is,

$$\zeta_{e_i} = \frac{\pi n_i}{4 \int_0^\infty |H_{y_i F_i}(n)|^2 dn} \quad \dots \dots \dots (5.5)$$

Obviously, the derivation of Eq. 5.5 was also based on the assumption of white noise excitation.

In terms of the above described approach and computer optimisation technique, for a given mode and a given mass ratio of a structure-TMD

system, contours of effective damping and relative damper movement for a range of frequency ratio and damper damping can be presented. By analysing these contours and wind tunnel test results of the structure, optimum parameters of the TMD can be decided.

The response of a tall building to the action of wind is confined primarily to the fundamental mode of vibration. As a result, a TMD is usually used to suppress the fundamental mode vibration and the above described procedure is applicable to the fundamental mode only.

It should be noted that, even for isolated simple rectangular buildings such as those described in Chapters 3 and 4, the mechanisms of the actual wind excitations acting on the buildings were quite complicated. Additional changes of building size, shape and surroundings as well as wind directions will affect wind loads further. The wind tunnel test results of translational and torsional vibrations of the tall buildings also showed that the effectiveness of a TMD was dependant on the type of alongwind, crosswind and torsional excitations. Hence the theoretical results of TMD parametric studies based on white noise excitation may not be reliable and consistent with experimental results obtained from aeroelastic model tests or propotype measurements. The reliability of large scale TMDs is affected by this assumption in the existing design procedure.

In this Chapter, a semi-analytical method, combining experimental and analytical techniques, is proposed. The semi-analytical results obtained by this method are compared with the experimental results which have been obtained and presented in Chapters 3 and 4. Selection diagrams of optimum parameters for the tested building-TMD systems are presented as examples of a general selection procedure of TMD parameters. The assumption of white noise excitation as actual wind excitation is also examined by comparing the theoretical results with the experimental results and the semi-analytical results.

5.2 Basic Theory

It has been recognised that the dominant aspects of wind action on tall buildings can be studied with relatively simple aeroelastic models which provide information that can be scaled up to the prototype process (Isyumov, 1982). The conventional aeroelastic model used in wind tunnel studies of tall buildings for 2 orthogonal fundamental sway modes of vibration has been discussed in detail in Chapter 3. The aeroelastic model for pure torsional vibration of tall buildings was also explained in Chapter 4. The following description of the semi-analytical method is based on the above aeroelastic models. The coupled effects between three fundamental modes of vibration are not considered in the thesis.

5.2.1 Translational vibration

Without a tuned mass damper, the translational vibration of the building model shown in Fig. 3.5 is governed by the equation

$$m_1^* \ddot{y}_1 + c_1^* \dot{y}_1 + k_1^* y_1 = F_1^*(t) \quad \dots \dots \dots (5.6)$$

where m_1^* , c_1^* , k_1^* , F_1^* , and y_1 are the first mode generalised mass, damping, stiffness, force and top displacement of the tested building in alongwind (crosswind) direction, respectively; a dot represents the first-order derivative with respect to time.

When $F_1^*(t)$ is a stationary random process, the power spectral density of the top displacement response, y_1 , of the building model is given by

$$S_{y_1}(n) = \frac{S_{F_1}(n) |H(n)|^2}{(k_1^*)^2} \quad \dots \dots \dots (5.7)$$

where $|H(n)|^2$ is the mechanical admittance function of the building model without a damper, i.e.,

$$|H(n)|^2 = \frac{1}{[1 - (\frac{n}{n_0})^2]^2 + 4\zeta^2 (\frac{n}{n_0})^2} \quad \dots \dots \dots (5.8)$$

in which

$$\zeta = \text{critical damping ratio} = \frac{c_1^*}{2\sqrt{m_1^* k_1^*}}$$

$$n_0 = \text{natural frequency} = \frac{1}{2\pi} \sqrt{k_1^*/m_1^*}$$

$S_{F_1}(n)$ = generalised wind force spectrum.

Since the power spectral density, $S_{y_1}(n)$, can be obtained by Fast Fourier Transformation of the corresponding recorded displacement response signals in wind tunnel tests, the generalised wind force spectrum, $S_{F_1}(n)$, can be determined by using Eq. 5.7 such that

$$S_{F_1}(n) = \frac{(k_1^*)^2 S_{y_1}(n)}{|H(n)|^2} \dots \dots \dots (5.9)$$

For the building model with a tuned mass damper, the equations of translational motion of the system are

$$\left. \begin{aligned} m_1^* \ddot{y}_1 + c_1^* \dot{y}_1 + k_1^* y_1 - c_2^* \dot{z} - k_2^* z &= F_1^*(t) \\ m_2^* \ddot{z} + c_2^* \dot{z} + k_2^* z &= -m_2^* \ddot{y}_1 \end{aligned} \right\} \dots \dots \dots (5.10)$$

where $z(t)$ is the relative displacement of the damper with respect to the building top cover, i.e., $z(t) = y_2(t) - y_1(t)$; y_2 is the absolute displacement of the damper; m_2 , c_2 and k_2 are the mass, damping and stiffness of the damper.

It is noted that Eq. 5.10 is, in fact, the motion equation of the equivalent two degree of freedom system as mentioned in the Introduction of this Chapter. Through wind tunnel tests it is now possible to use simulated wind loads, as described in Eq. 5.9, instead of white noise excitation. By means of random vibration theory, the power spectral density

functions of the building top displacement response, y_1 , and the relative displacement response, z , of the damper can be given by

$$S_{y_1}^c(n) = \frac{S_{F_1}(n) |H_{y_1 F_1}(n)|^2}{(k_1^*)^2} \dots \dots \dots (5.11)$$

$$S_z^c(n) = \frac{S_{F_1}(n) |H_{z F_1}(n)|^2}{(k_1^*)^2} \dots \dots \dots (5.12)$$

where the mechanical admittance functions

$$|H_{y_1 F_1}(n)|^2 = \frac{(\chi^2 - \lambda^2)^2 + 4\lambda^2\chi^2\zeta_2^2}{a^2 + b^2} \dots \dots \dots (5.13)$$

$$|H_{z F_1}(n)|^2 = \frac{\lambda^4}{a^2 + b^2} \dots \dots \dots (5.14)$$

and in which

$$\left. \begin{aligned} a &= \lambda^4 - \lambda^2(1 + \chi^2 + \mu\chi^2 + 4\zeta_2\chi) + \chi^2 ; \\ b &= 2\lambda[\zeta_2\chi(1 - \lambda^2 - \mu\lambda^2) + \zeta(\chi^2 - \lambda^2)] ; \\ \mu &= \frac{m_2}{m_1^*} ; \quad \chi = \frac{n_2}{n_0} ; \quad \zeta_2 = \frac{c_2}{2\sqrt{m_2 k_2}} ; \\ \lambda &= \frac{n}{n_0} ; \quad n_2 = \frac{1}{2\pi} \sqrt{k_2/m_2} \end{aligned} \right\} \dots \dots \dots (5.15)$$

Substituting Eq. 5.9 into Eqs. 5.11 and 5.12, one can obtain

$$S_{y_1}^c(n) = \frac{|H_{y_1 F_1}(n)|^2}{|H(n)|^2} S_{y_1}(n) \dots \dots \dots (5.16)$$

$$S_z^c(n) = \frac{|H_{z F_1}(n)|^2}{|H(n)|^2} S_{y_1}(n) \dots \dots \dots (5.17)$$

Note that $S_{y_1}^c(n)$ is the power spectral density of the top displacement of

the building model with a damper while $S_{y_1}(n)$ is the same term without a damper.

The corresponding standard deviations are

$$\left. \begin{aligned} \sigma_{y_1}^c &= \left[\int_0^\infty S_{y_1}^c(n) dn \right]^{\frac{1}{2}} \\ \sigma_z^c &= \left[\int_0^\infty S_z^c(n) dn \right]^{\frac{1}{2}} \end{aligned} \right\} \dots \dots \dots (5.18)$$

The normalised standard deviation responses are defined as

$$\left. \begin{aligned} \frac{\sigma_{y_1}^c}{\sigma_{y_1}} &= \frac{\left[\int_0^\infty S_{y_1}^c(n) dn \right]^{\frac{1}{2}}}{\left[\int_0^\infty S_{y_1}(n) dn \right]^{\frac{1}{2}}} \\ \frac{\sigma_z^c}{\sigma_{y_1}^c} &= \frac{\left[\int_0^\infty S_z^c(n) dn \right]^{\frac{1}{2}}}{\left[\int_0^\infty S_{y_1}^c(n) dn \right]^{\frac{1}{2}}} \end{aligned} \right\} \dots \dots \dots (5.19)$$

where σ_{y_1} is the standard deviation of top displacement of the building model without a damper.

5.2.2 Torsional vibration

The equation of torsional vibration of the building model without a damper, as shown in Fig. 4.4, is

$$m_{t_1}^* \ddot{\theta}_1 + c_{t_1}^* \dot{\theta}_1 + k_{t_1}^* \theta_1 = T_1^*(t) \dots \dots \dots (5.20)$$

where $m_{t_1}^*$, $c_{t_1}^*$, $k_{t_1}^*$, T_1^* , and θ_1 are the generalised mass moment of inertia, damping, torsional stiffness, torque and twist angle, respectively.

It is obvious that Eq. 5.20 is the same as Eq.5.6 if the parameters in Eq. 5.6 are properly interpreted by using the notation in Eq. 5.20. Furthermore, Eq. 5.10 can also be applied to the torsional vibration of the building-TMD system if the parameters in Eq. 5.10 are interpreted as those notations related

to torsional vibration. As a results the above derived equations for alongwind (crosswind) vibration can be applied to torsional vibration without any difficulties. The normalised standard deviation responses of the torsional vibration of the building-TMD system are

$$\left. \begin{aligned} \frac{\sigma_{\theta_1}^c}{\sigma_{\theta_1}} &= \frac{[\int_0^\infty S_{\theta_1}^c(n) dn]^{\frac{1}{2}}}{[\int_0^\infty S_{\theta_1}(n) dn]^{\frac{1}{2}}} \\ \frac{\sigma_{z\theta}^c}{\sigma_{\theta_1}^c} &= \frac{[\int_0^\infty S_{z\theta}^c(n) dn]^{\frac{1}{2}}}{[\int_0^\infty S_{\theta_1}^c(n) dn]^{\frac{1}{2}}} \end{aligned} \right\} \dots \dots \dots (5.21)$$

In the semi-analytical method, Eqs. 5.16, 5.17, 5.19 and 5.21 are basic equations for TMD parametric studies of translational and torsional vibrations. By using measured wind response spectra of the plain buliding (without any damper) tested in a wind tunnel, parametric studies of a TMD specially for the tested building can be performed without conducting a series of wind tunnel tests of the building with different TMDs. The experimental verification of the semi-analytical method is presented in the next section before extensive parametric studies of the TMD are conducted.

5.3 Experimental Verification of the Method

Through the plain building model (i.e., without a damper) calibration and wind tunnel test, one can obtain the power spectral density function, $S_{y_1}(n)$ or $S_{\theta_1}(n)$, of the top displacement (or twist angular displacement) of the plain model as well as the relevant structural parameters of the plain model. One can also obtain the damper parameters by the calibration of the damper. Therefore, the normalised standard deviation responses of the building model with TMDs can be calculated by use of Eq. 5.19 or Eq. 5.21. On the other hand, wind tunnel tests of the building model with the TMDs in place can provide the experimental results for the normalised standard deviation responses of the building model with the TMDs. A comparison between the semi-analytical and experimental results can be made. For

the two rectangular building models studied in Chapter 3 and Chapter 4, respectively, the comparison of results are summarised in the following.

5.3.1 Alongwind vibration

Table 5.1 shows the comparison between semi-analytical and experimental results in alongwind direction. The semi-analytical results were in agreement with the experimental results for different reduced velocities and different angles of wind incidence. The maximum relative error was 9%. The comparison with the results based on white noise excitation is given in section 5.5.

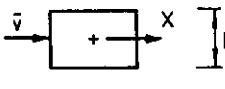
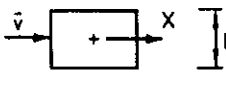
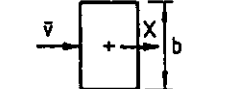
5.3.2 Crosswind vibration

The first two columns of Table 5.2 show that the comparison in crosswind direction is also satisfactory for different reduced velocities and different angles of wind incidence when the reduced wind velocities are below the critical reduced velocity, which is 10 in the corresponding experiment. Close to the critical reduced velocity, displacement dependent lock-in excitation was found to be significant for the building model in a suburban turbulent boundary layer flow, as discussed in Chapter 3. As a result, there are large differences between the semi-analytical and experimental results, which can be seen from the last column of Table 5.2. This difference indicates that the linear random wake excitation process cannot adequately account for the crosswind responses, and the derived linear random vibration equations also cannot be used to conduct the TMD parametric studies when displacement dependent lock-in excitation is significant. In this case, a nonlinear lock-in force model is needed to achieve a satisfactory comparison between the semi-analytical and experimental results. However, it is difficult to present such a nonlinear model for the building-TMD system at this stage.

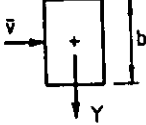
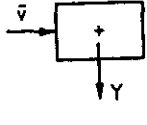
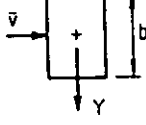
5.3.3 Torsional vibration

For the torsional vibration, Table 5.3 shows that the semi-analytical results are in good agreement with the experimental results for different

TABLE 5.1 COMPARISON BETWEEN SEMI-ANALYTICAL,
THEORETICAL AND EXPERIMENTAL RESULTS
(ALONGWIND)

$\sigma_{x_1}^c / \sigma_{x_1}$		Type	Reduced Velocity		
			= 9	= 13	= 6
Model					
TMD 1	Experimental	0.774	0.860	0.796	
	Analytical	0.746	0.786	0.862	
	White Noise	0.515	0.515	0.515	
TMD 2	Experimental	0.759	0.809	0.854	
	Analytical	0.739	0.772	0.846	
	White Noise	0.522	0.522	0.522	
TMD 3	Experimental	0.692	0.703	0.718	
	Analytical	0.699	0.717	0.744	
	White Noise	0.481	0.481	0.481	

**TABLE 5.2 COMPARISON BETWEEN SEMI-ANALYTICAL,
THEORETICAL AND EXPERIMENTAL RESULTS
(CROSSWIND)**

$\sigma_{y_1}^c / \sigma_{y_1}$		Type	Reduced Velocity = 6	Reduced Velocity = 9	Reduced Velocity = 10
					
Model					
TMD 1	Experimental		0.774	0.722	0.333
	Analytical		0.771	0.801	0.754
	White Noise		0.515	0.515	0.515
TMD 2	Experimental		0.726	0.733	0.289
	Analytical		0.758	0.807	0.665
	White Noise		0.522	0.522	0.522
TMD 3	Experimental		0.704	0.742	0.230
	Analytical		0.696	0.799	0.414
	White Noise		0.481	0.481	0.481

**TABLE 5.3 COMPARISON BETWEEN SEMI-ANALYTICAL,
THEORETICAL AND EXPERIMENTAL RESULTS
(TORSION)**

Type	$\sigma_{\theta_1}^c / \sigma_{\theta_1}$	Experimental	Analytical	White Noise
Reduced Velocity = 2		0.675	0.722	0.565
Reduced Velocity = 4		0.756	0.725	0.565
Reduced Velocity = 4		0.737	0.736	0.565
Reduced Velocity = 8		0.585	0.567	0.565
Reduced Velocity = 4		0.787	0.769	0.565
Reduced Velocity = 8		0.693	0.739	0.565

Note: + Geometric Centre
o Elastic Centre

reduced velocities and different wind incidence. The maximum relative error was only 7%. The agreement also indicated that the torsional excitation due to torsional motion of the building is not significant in the reduced wind velocity range considered in this study. However, torsional excitation dependent on torsional motion may be significant at higher reduced wind velocities than the studied range.

Generally speaking, for alongwind turbulence excitation, crosswind wake excitation and torsional excitation, the proposed approach is quite satisfactory if the system is linear and the mechanical admittance function as determined from measured values of frequency and damping is not changed aerodynamically.

5.4 TMD Parametric Studies with Semi-Analytical Method

5.4.1 Estimate of TMD parameters

The comparison between the semi-analytical and experimental results has shown that the proposed approach is quite satisfactory. Therefore, one can now conduct parametric studies of a TMD with the measured response spectra of the plain buildings and without performing a series of wind tunnel tests of the building with different TMDs.

The first step of parametric studies of a TMD is to decide which alongwind, crosswind or torsional response spectra of the corresponding plain building are selected as input spectra in Eqs. 5.16 and 5.17. This selection is usually determined by the most unfavourable orientations of the plain building responses for different design wind velocities. In this study, one alongwind response spectrum, for incident wind normal to the narrow face of the CARRC model and at a reduced velocity of 9, was selected as input spectrum in alongwind direction. The crosswind response spectrum was for incident wind normal to the wide face of the model and at a reduced velocity of 6. Two twist angle response spectra of the plain building model were selected as torsional input spectra: one for incident wind normal to the wide face of the model and at a reduced wind velocity of 4; another for

incident wind normal to the narrow face and at a reduced velocity of 8. The second step in parametric studies of a TMD is to run a computer program which is structured according to the basic theory. During running of the program, the structural parameters of the plain building are kept unchanged, and only the tuning frequency χ , mass ratio μ (or mass moment ratio of inertia) and damper damping ζ_2 are changed.

Fig. 5.2 shows the importance of tuning, and the effect of mass ratio μ and damper damping ζ_2 variations on the alongwind and crosswind response ratios, while Fig. 5.3 shows the same evidence for torsional vibration control. Figs. 5.4 and 5.5 show, for a tuning ratio of 1.0, how the response ratio and the damper displacement ratio in alongwind and crosswind directions are affected by damper damping ζ_2 . The same investigation was carried out for the torsional excitation and the results are shown in Figs. 5.6 and 5.7. From these diagrams, it was found that the tuned mass damper resulted in slightly different motion reductions for both alongwind and crosswind excitations, but for different torsional excitation spectra the tuned mass damper has a different effectiveness. The TMD system was more effective in reducing the torsional vibration with the wind incidence normal to the narrow face of the building model than that with the wind incidence normal to the wide face of the model. It is also evident from these diagrams that, for a given mass ratio, there is one tuning ratio and one damping value which lead to maximum motion reduction.

In the semi-analytical method, the contour of the effective damping, as discussed in the Introduction of this Chapter, can be replaced by the contour of the building response ratio. Figs. 5.8 and 5.9 show the contours of the building torsional response ratio and the relative damper motion ratio for a range of frequency ratio and damper damping and for a mass moment ratio of inertia of 0.04. The input twist angle response spectrum is for wind incidence normal to the wide face of the plain building and at a reduced wind velocity of 4. From these figures, it is seen that the minimum value of the building twist angle response ratio was around 0.63 for the mass moment ratio of inertia of 0.04. The corresponding relative damper movement was around 2.5 time the dynamic twist angle response of the building. It is interesting to note that when the damper damping ratio ζ_2

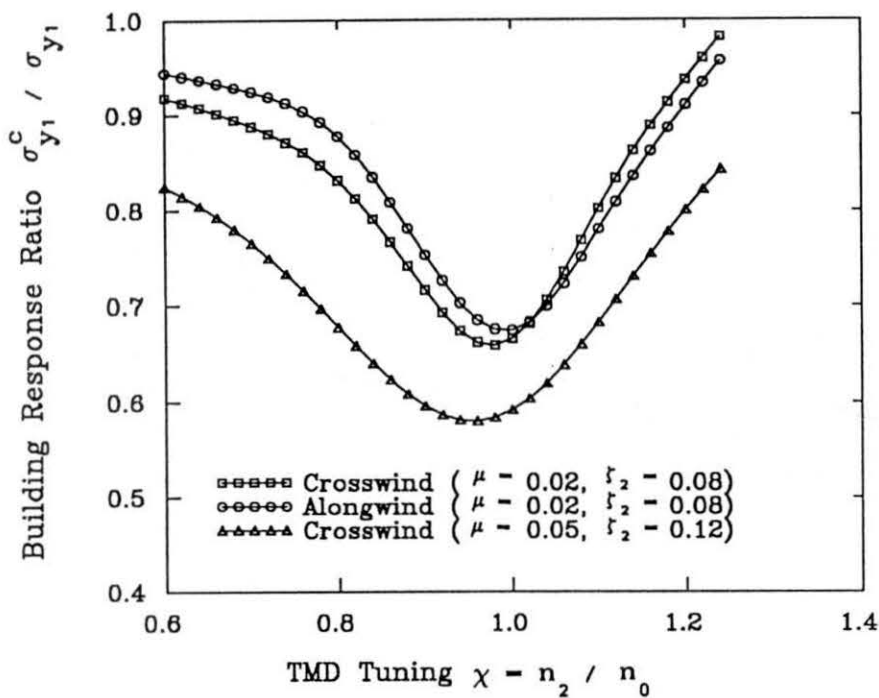


FIG. 5.2 TMD PARAMETER STUDY: $\sigma_{y_1}^c / \sigma_{y_1}$ versus χ

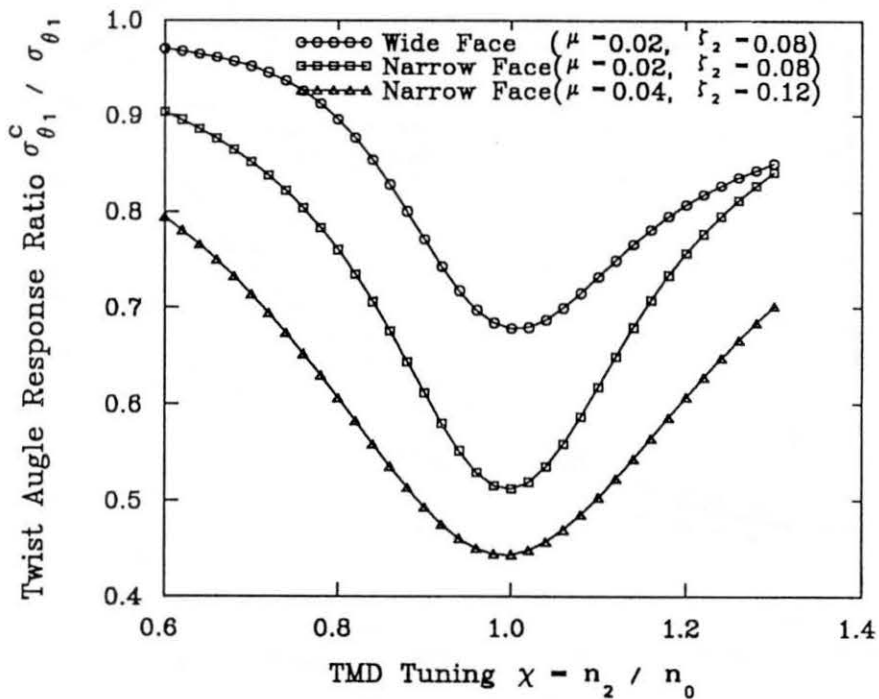


FIG. 5.3 TMD PARAMETER STUDY: $\sigma_{\theta_1}^c / \sigma_{\theta_1}$ versus χ

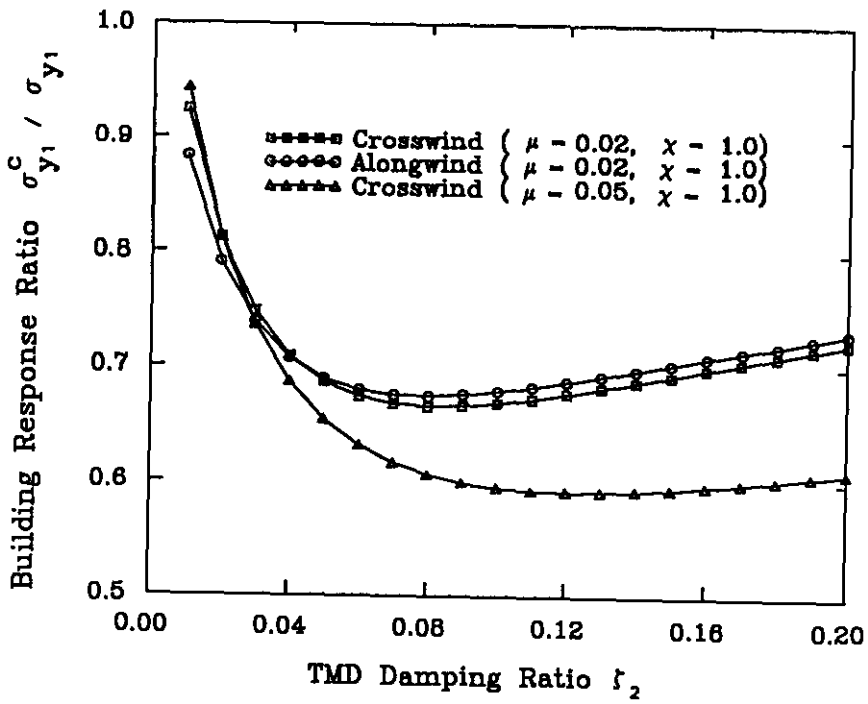


FIG. 5.4 TMD PARAMETER STUDY: $\sigma_{y_1}^c / \sigma_{y_1}$ versus ζ_2

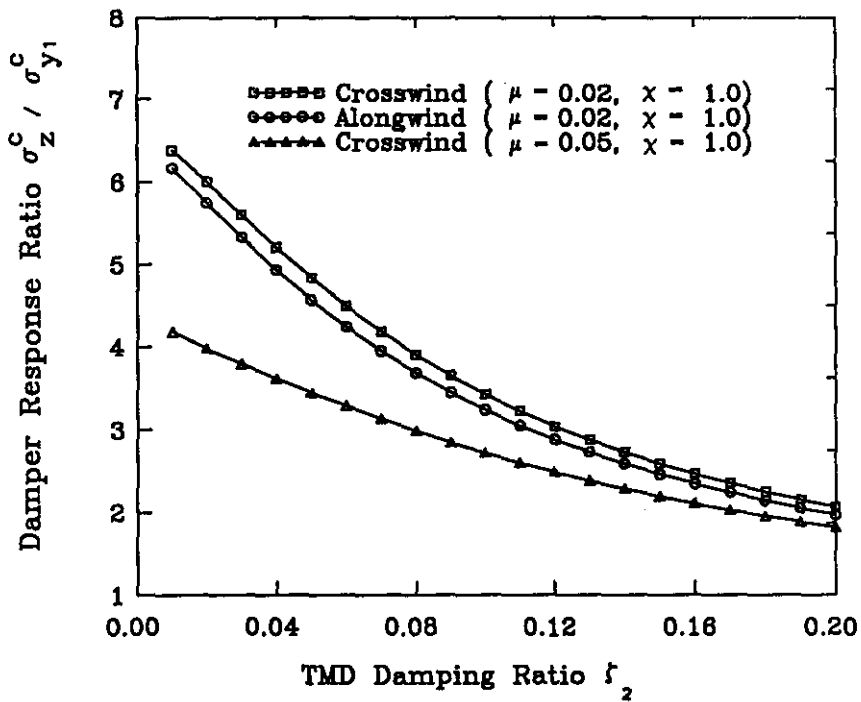


FIG. 5.5 TMD PARAMETER STUDY: $\sigma_z^c / \sigma_{y_1}^c$ versus ζ_2

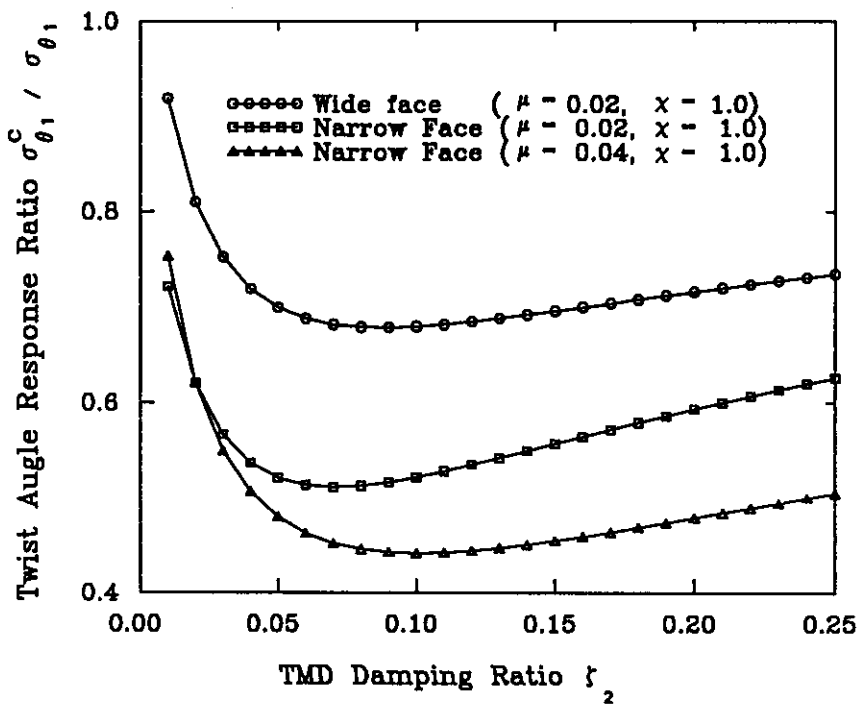


FIG. 5.6 TMD PARAMETER STUDY: $\sigma_{\theta_1}^c / \sigma_{\theta_1}$ versus ζ_2

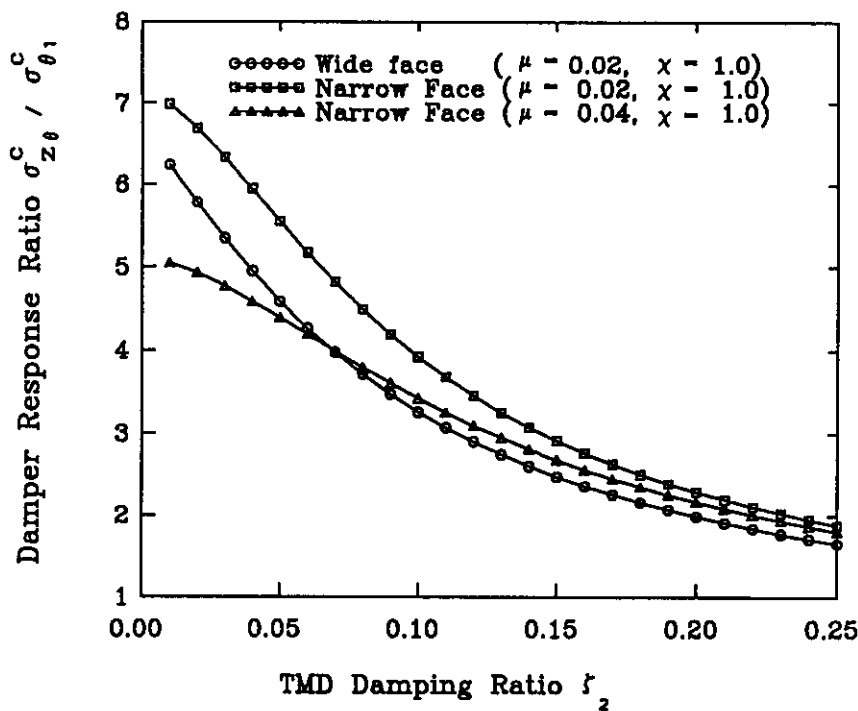


FIG. 5.7 TMD PARAMETER STUDY: $\sigma_z^c / \sigma_{\theta_1}^c$ versus ζ_2

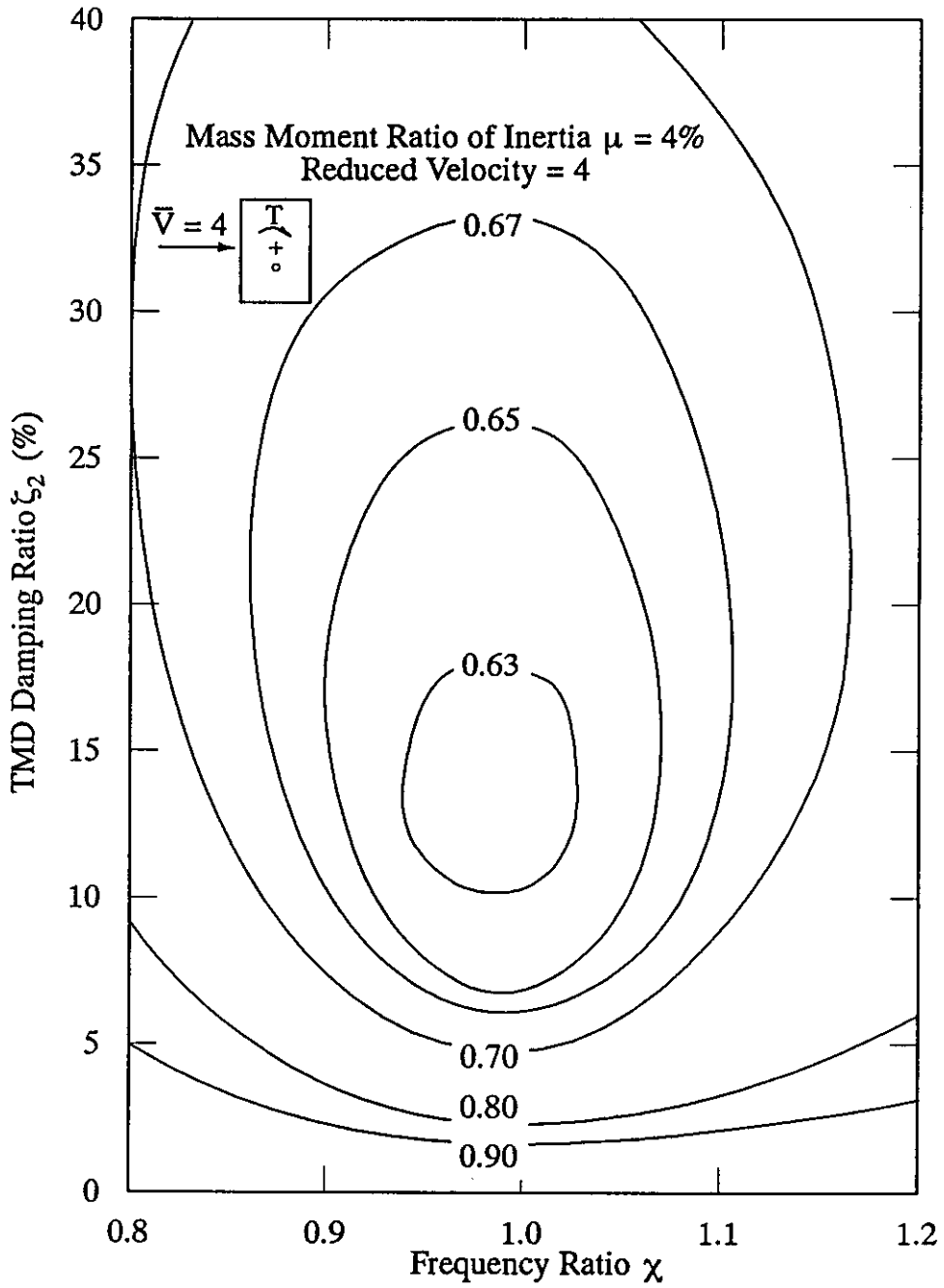


FIG. 5.8 ESTIMATE OF BUILDING RESPONSE RATIO $\sigma_{\theta_1}^c / \sigma_{\theta_1}$

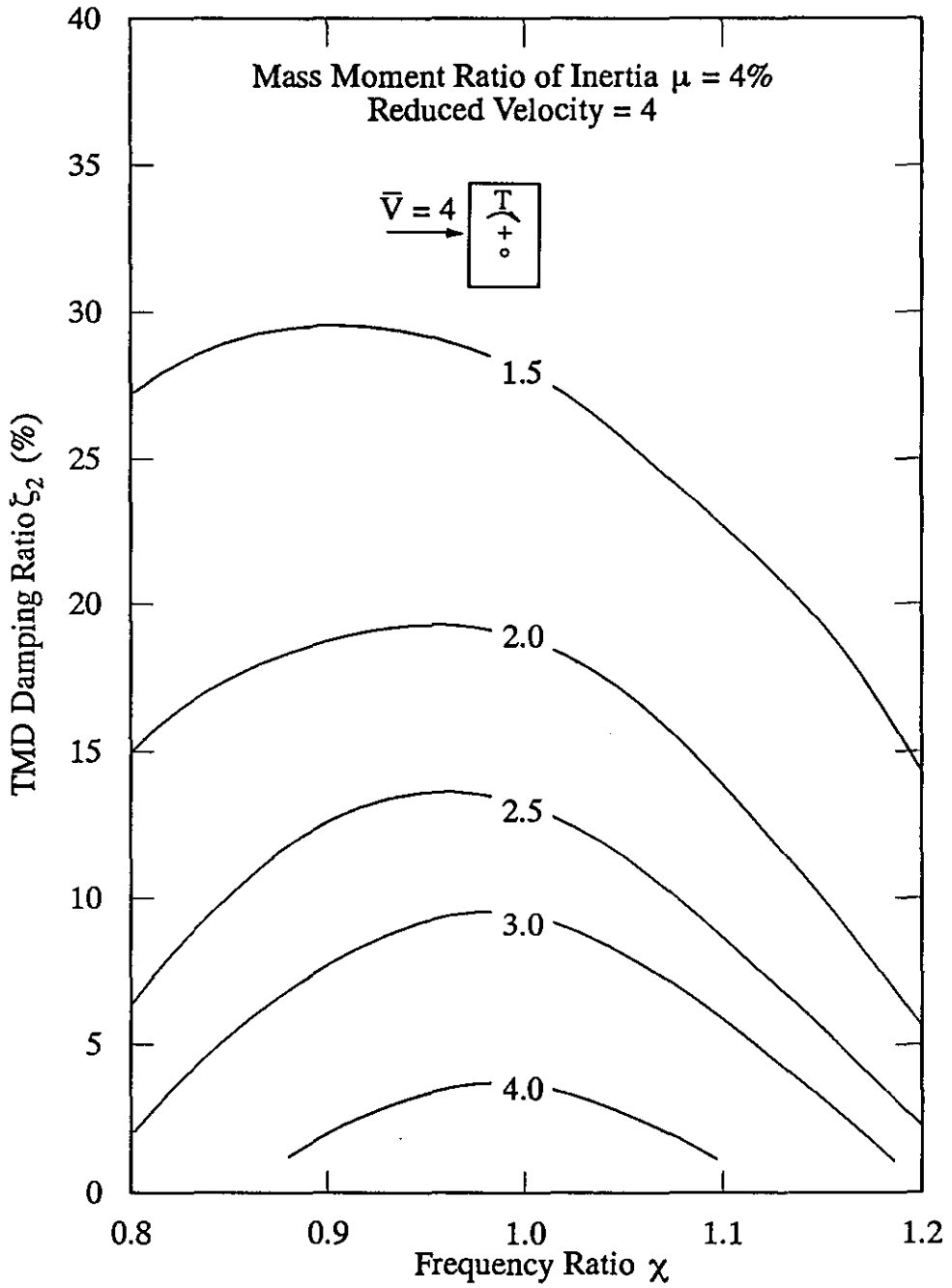


FIG. 5.9 ESTIMATE OF DAMPER RELATIVE MOTION $\sigma_{z\theta}^c / \sigma_{\theta_1}^c$

was larger than 10% the minimum building response can be attained over a relative wide range of values of frequency ratio. However, this case is not true for smaller mass moment ratio of inertia.

5.4.2 Selection of optimum TMD parameters

An optimisation parametric study was conducted by numerical computation to determine TMD tuning and damping required to produce the smallest building dynamic response for each of a number of mass (or mass moment of inertia) ratios. Hooke-Jeeves numerical computation optimum method (Murray, 1972) was used in the present computer program.

Figs. 5.10 and 5.11 show that optimum tuning ratio decreases with increasing mass ratio. Under torsional excitations the decreasing tendency is quite different for the wind incidence normal to the narrow face and the wide face of the building model. This difference may cause some problems when global optimum parameters are expected. Figs. 5.12 and 5.13 show that optimum damper damping increases as mass ratio increases. Figs. 5.14 and 5.15 show how optimum building response is affected by mass ratio and Figs. 5.16 and 5.17 show the variation of mass damper displacement (twist angular displacement) ratio with mass ratio. It is clear from Figs. 5.14 to 5.17 that increase in the mass ratio (or mass moment ratio of inertia) produces smaller response reduction when the mass ratio is larger than 4 per cent. It is also obvious that there is a limit to the motion reduction for a given tall building.

From these diagrams, a designer can determine whether there is a passive tuned mass damper which can be practically used to obtain the required building motion reduction. If it is possible, the designer can then choose the optimum design parameters of the tuned mass damper system according to these diagrams. That is first to decide the required mass ratio or mass moment ratio of inertia according to the required building motion reduction from the diagrams of optimum building response ratio versus mass ratio, or according to the restricted damper relative displacement from the corresponding diagram. By using the chosen mass ratio, the optimum damper damping and frequency tuning of the studied building-TMD system

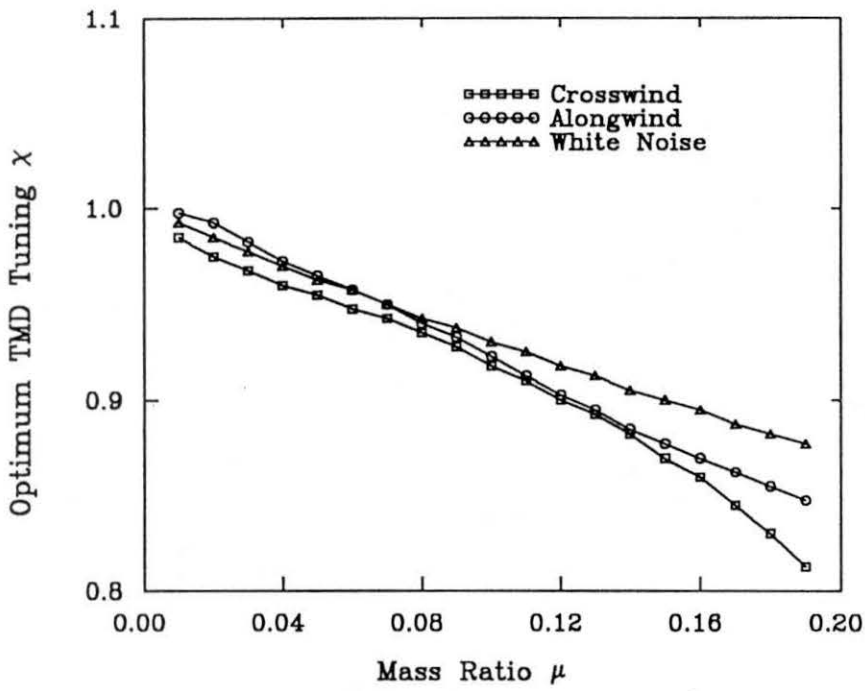


FIG. 5.10 TMD OPTIMIZATION STUDY: χ versus μ

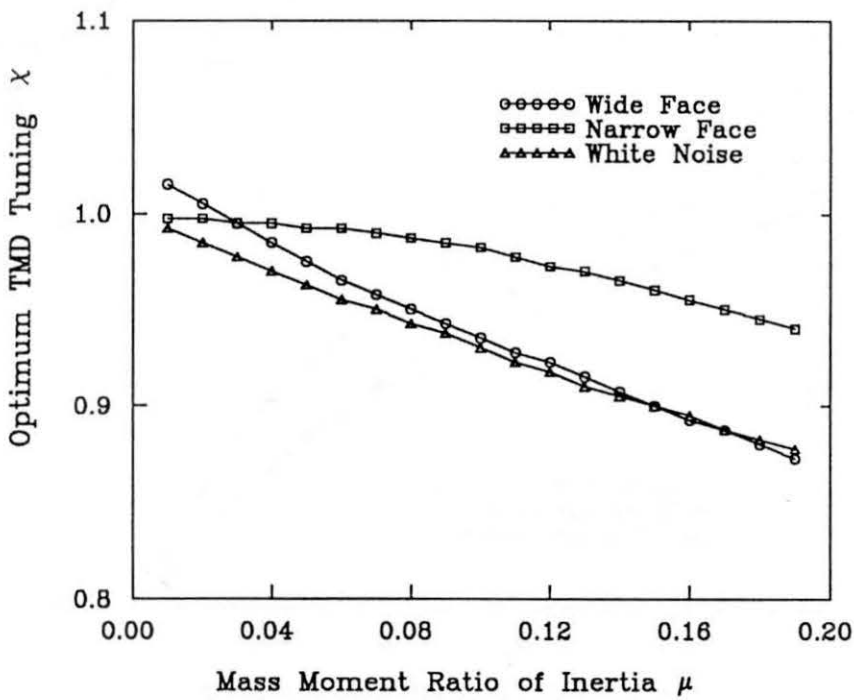


FIG. 5.11 TMD OPTIMIZATION STUDY: χ versus μ

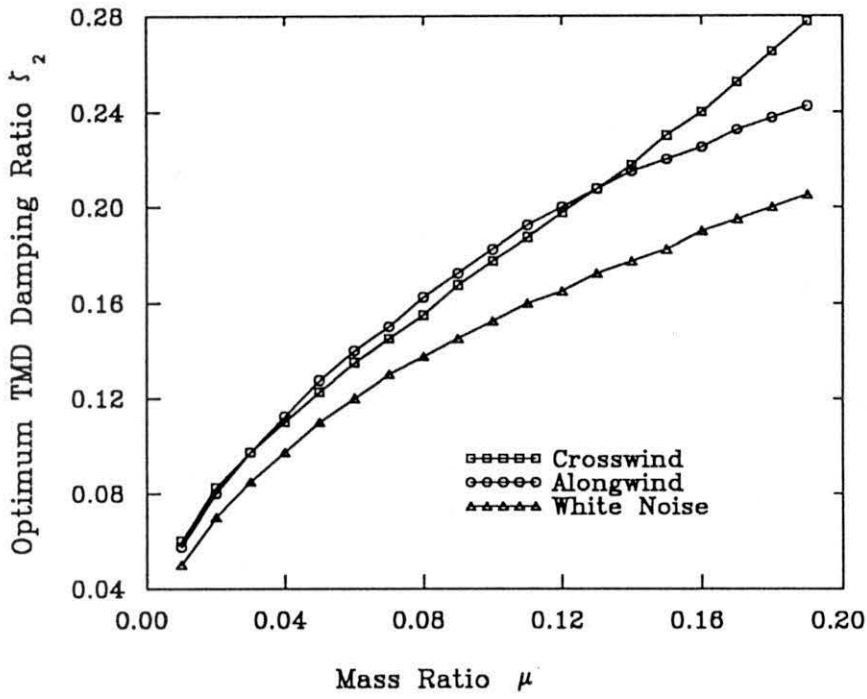


FIG. 5.12 TMD OPTIMIZATION STUDY: ζ_2 versus μ

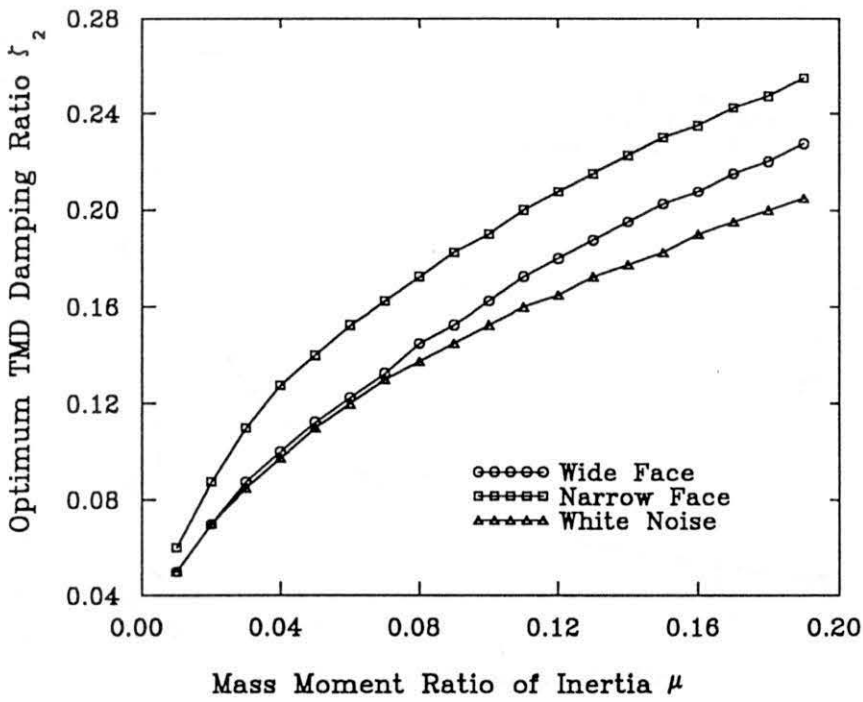


FIG. 5.13 TMD OPTIMIZATION STUDY: ζ_2 versus μ

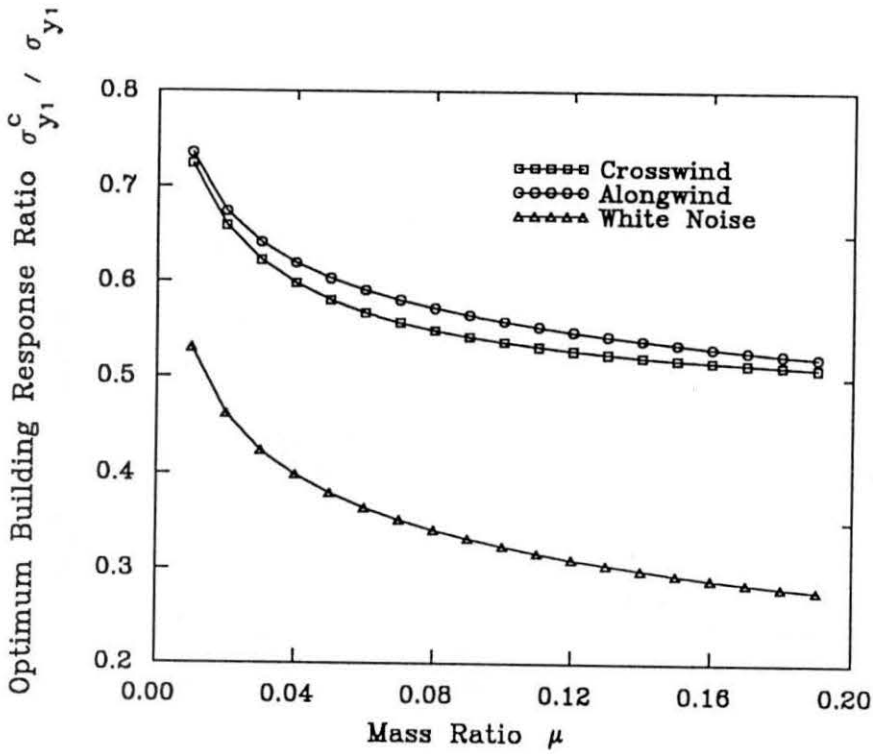


FIG. 5.14 TMD OPTIMIZATION STUDY: $\sigma_{y_1}^c / \sigma_{y_1}$ versus μ

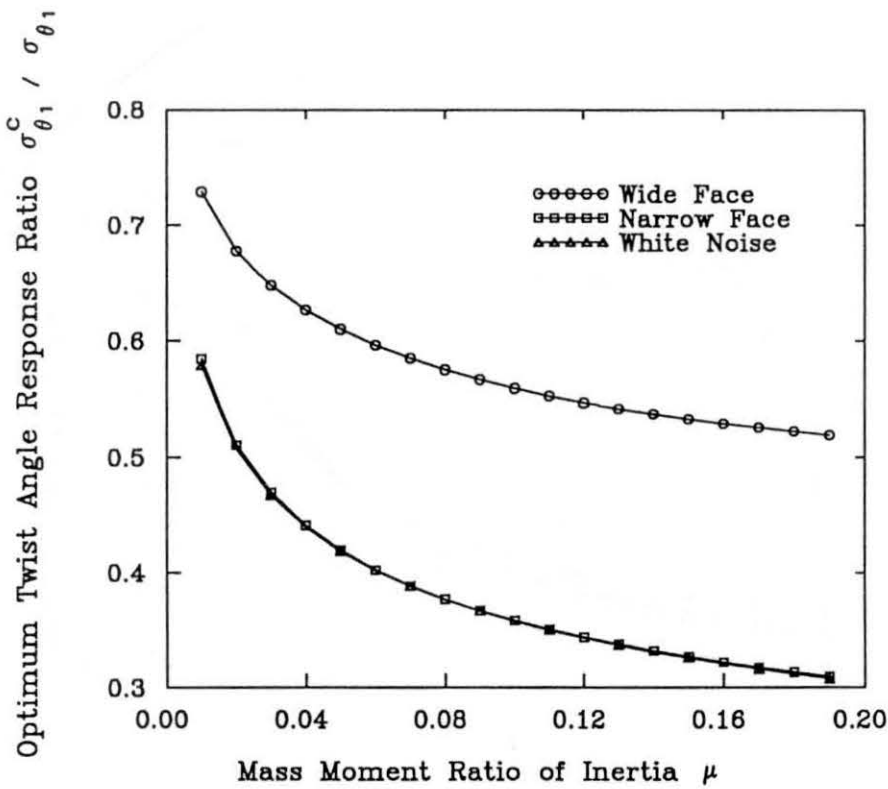


FIG. 5.15 TMD OPTIMIZATION STUDY: $\sigma_{\theta_1}^c / \sigma_{\theta_1}$ versus μ

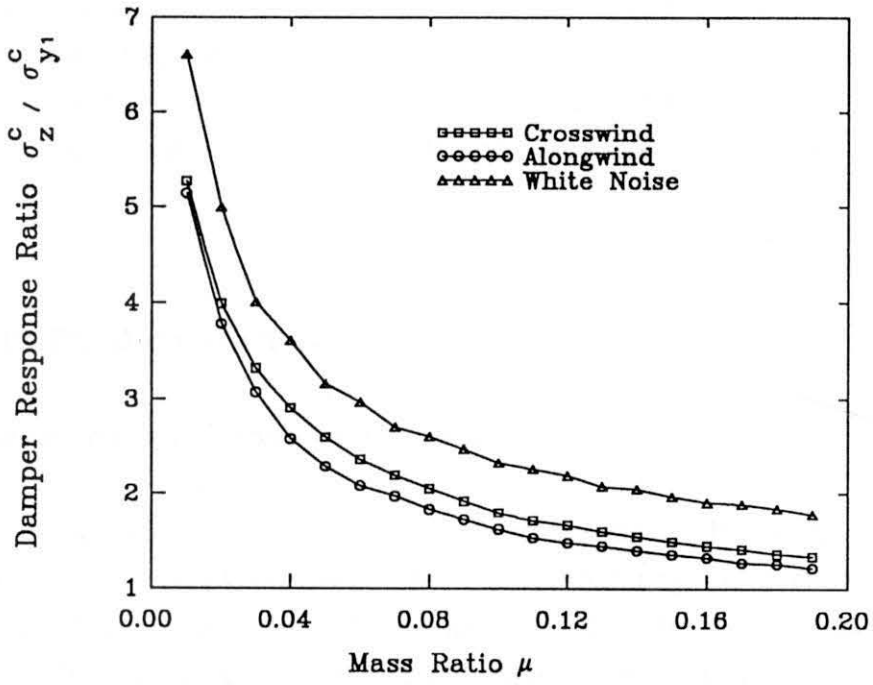


FIG. 5.16 TMD OPTIMIZATION STUDY: $\sigma_z^c / \sigma_{y1}^c$ versus μ

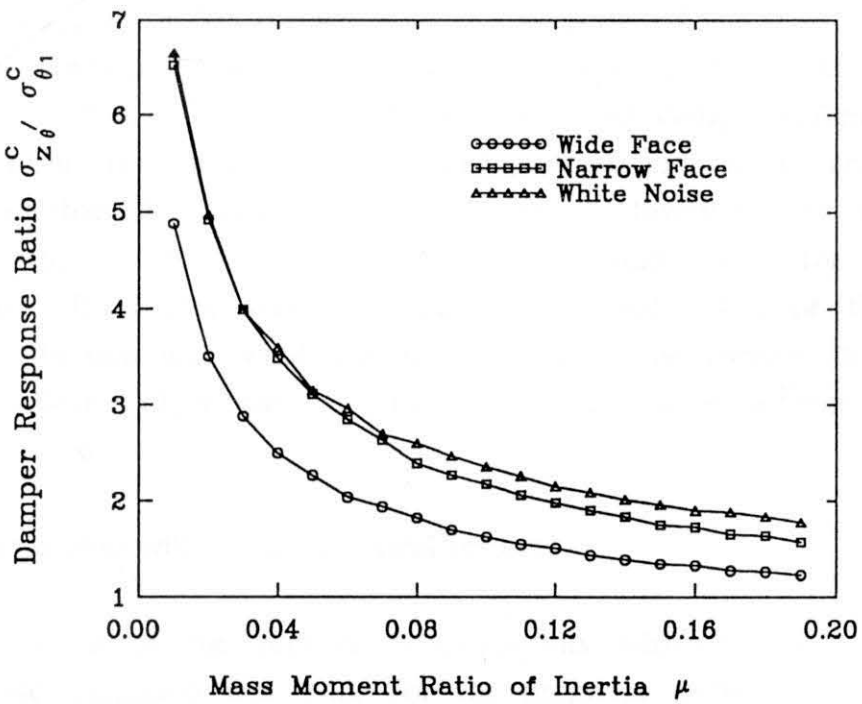


FIG. 5.17 TMD OPTIMIZATION STUDY: $\sigma_z^c / \sigma_{\theta 1}^c$ versus μ

then can be easily found in the selection diagrams of the TMD optimum parameters. Sometimes, some compromise has to be made and selection of TMD optimum parameters has to be given up because of some practical constraints such as a space for the TMD. In this situation, contours of building response ratio and relative damper movement, as shown in Figs. 5.8 and 5.9, can be used.

5.5 Results Based on White Noise Excitation

5.5.1 Comparison with experimental results

The theoretical results of the building responses by using white noise excitation were compared with the corresponding experimental results obtained in Chapters 3 and 4. By using the same physical dimensions of the building model and three tuned mass damper models as listed in Table 3.3, it was found that the theoretical results of the building response ratios, $\sigma_{x_1}^c/\sigma_{x_1}$, or $\sigma_{y_1}^c/\sigma_{y_1}$, were 0.515, 0.522 and 0.481 corresponding to TMD1, TMD2 and TMD3, respectively, for white noise excitation. For the torsional vibration of the building tested in Chapter 4, the torsional response ratio, $\sigma_{\theta_1}^c/\sigma_{\theta_1}$, was 0.565 for white noise excitation. Comparing these results with the semi-analytical and experimental results, which are shown in Tables 5.1 to 5.3, it is evident that the tuned mass damper system is usually less efficient for alongwind turbulence, crosswind wake and torsional excitations than for white noise excitation. However, the tuned mass damper system is more efficient for lock-in excitation than for white noise excitation. It is also seen that the experimental result of the building torsional vibration with wind incidence normal to the narrow face and at a reduced velocity of 8 was nearly the same as the theoretical result by using white noise excitation.

5.5.2 Comparison with semi-analytical results

Comparison of the semi-analytical results with the results obtained using white noise excitation was made for the optimum parametric studies. As shown in Figs. 5.10 to 5.17, it can be seen that the changes of the optimum

TMD tuning χ , TMD damping ratio ζ_2 , building response ratios and damper response ratios with mass ratio μ (mass moment ratio of inertia) are the same for both the actual wind excitations and white noise excitation. However, the optimum values of these quantities, except for the building torsional vibration with wind incidence normal to the narrow face and at a reduced velocity of 8, are quite different. Once again the tuned mass damper systems are less efficient for alongwind turbulence, crosswind wake excitation and sometimes torsional excitation than for white noise excitation. It is believed that the relative locations of the peaks in the wind excitation spectra to the natural frequencies of the building-TMD system and the values of the spectral peak are two important factors which cause the difference between the theoretical and experimental results and affect the effectiveness of the tuned mass damper.

5.5.3 Displacement and acceleration responses

In the present design of tall buildings, TMD effects are usually called upon for serviceability purposes only (ASCE State-of-the art report, 1987). The serviceability of a building is mainly affected by excessive accelerations experienced at the top floors in wind storms which may cause discomfort to the building occupants. Therefore, the parametric studies of building-TMD systems should be based on building acceleration (or twist angular acceleration) responses rather than building displacement (or twist angular displacement) responses. However, results of most parametric studies of TMDs are presented directly or indirectly by using building displacement response ratios. For white noise excitation, the building acceleration spectrum $(2\pi n)^4 S_{y_1}(n)$ can be replaced by $(2\pi n_0)^4 S_{y_1}(n)$ and as a result the acceleration response ratio is nearly the same as the corresponding displacement response ratio. In the semi-analytical method, such a viewpoint is examined. Figs. 5.18 to 5.21 show the optimum response ratio of the building twist angular acceleration and the corresponding optimum frequency tuning, optimum damper damping ratio and damper relative twist angular acceleration. They were obtained in terms of a torsional twist angular displacement response spectrum with wind incidence normal to the wide face of the building and at a reduced velocity of 4. The same quantities which are related to white noise excitation are also plotted in the same figures. It

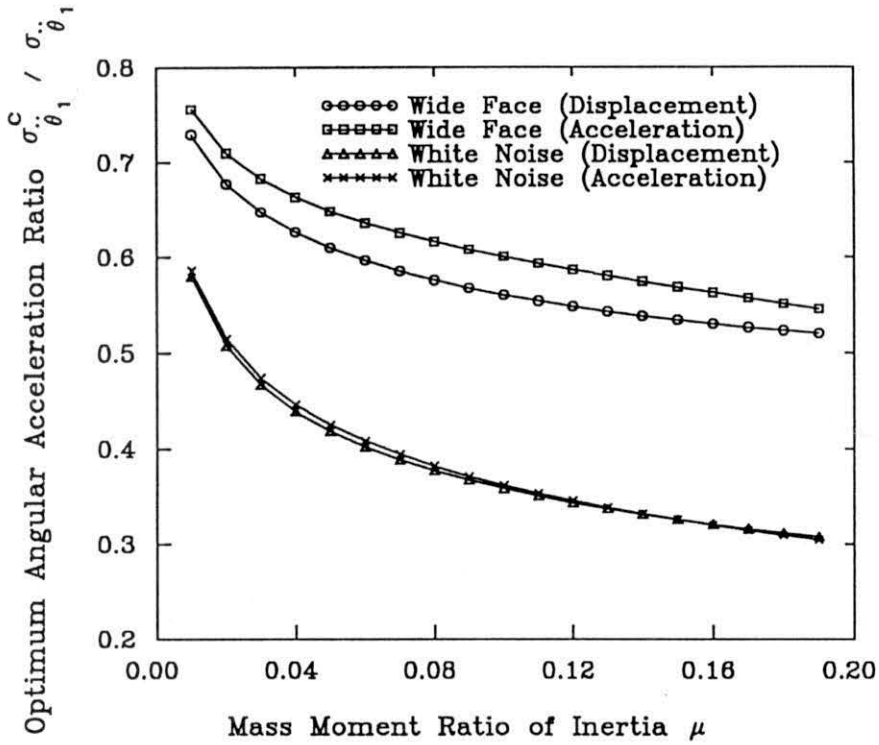


FIG. 5.18 ANGULAR ACCELERATION STUDY: $\sigma_{\theta_1}^c / \sigma_{\theta_1}$ versus μ

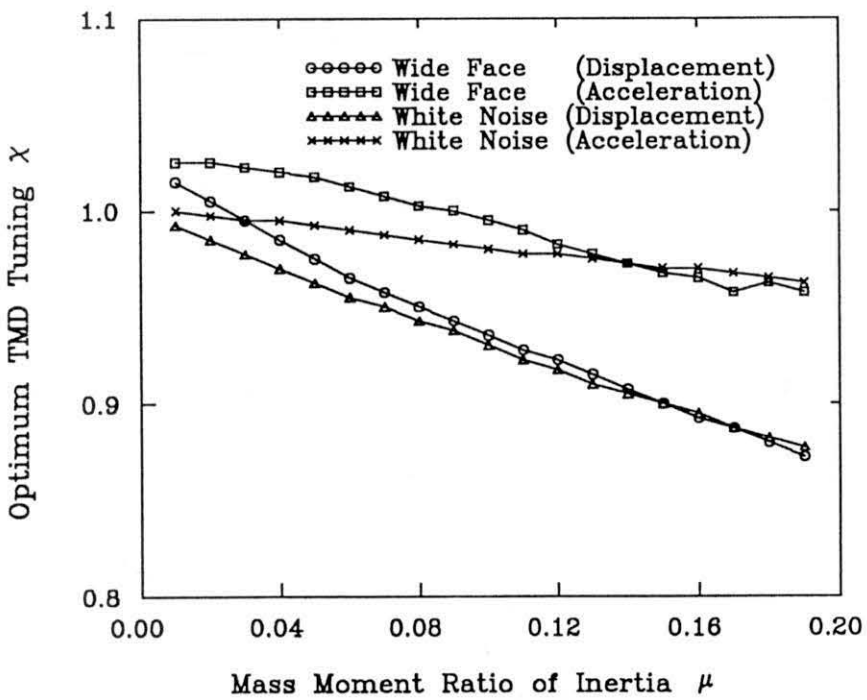


FIG. 5.19 ANGULAR ACCELERATION STUDY: χ versus μ

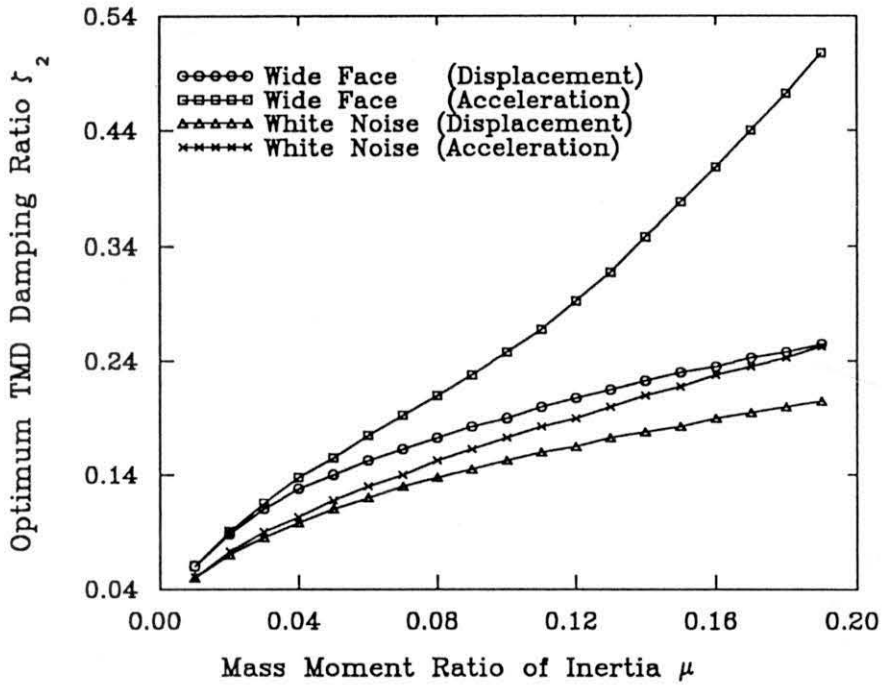


FIG. 5.20 ANGULAR ACCELERATION STUDY: ζ_2 versus μ

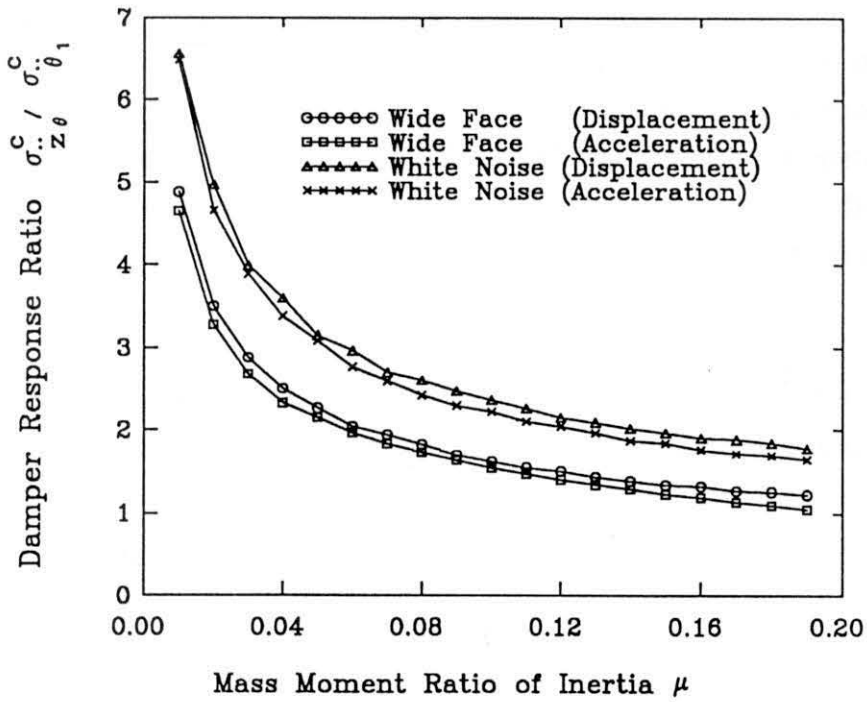


FIG. 5.21 ANGULAR ACCELERATION STUDY: $\sigma_z^c / \sigma_{\theta_1}^c$ versus μ

is found that, for white noise excitation, the acceleration response ratios of both the building and the damper are nearly the same as the displacement response ratios. However, there were some differences of both the optimum frequency tuning and damper damping ratios. For the semi-analytical method, the errors caused by the displacement response ratio instead of the acceleration response ratio were slightly larger than those for white noise excitation, but the optimum damper damping ratios were quite different. It seems to be reasonable to use acceleration responses in parametric studies of TMDs.

5.6 Discussions

In the design of tall buildings, parametric studies of TMDs by using the proposed semi-analytical method usually follow the wind tunnel tests. Once the acceleration levels of the tall building in most unfavorable orientations are found to be beyond discomfort threshold and a passive TMD is decided to be used to reduce the excessive acceleration levels, the corresponding building displacement (twist angular displacement) response signals should be recorded and processed to obtain the response spectra. The measured response spectra, building generalised mass (or mass moment of inertia) and damping ratio ζ_1 , are then input into a computer program designed for TMD parametric studies by using the semi-analytical method to obtain selection diagrams or contours of the TMD optimum parameters. From these diagrams or contours, and considering other practical limitations, a designer or consultant can finally determine the TMD parameters of the tall building.

The proposed semi-analytical method can also be used in force balance techniques. In the force balance technique, the measured excitation spectra can be used to replace the response spectra and the computer program modified slightly. If a TMD is required to reduce higher mode vibrations of the tall building, a multi-degree-of-freedom aeroelastic model in wind tunnel tests might be needed to obtain building response signals and to conduct the TMD parametric studies in the higher mode vibrations.

For a very slender tall building which endures motion-dependant lock-in excitation, a linear sinusoidal vibration equation cannot provide a satisfactory results and a non-linear random vibration equation of the building-TMD motion is needed to obtain accurate prediction of the building motion reduction. This represents a much more difficult problem which requires further study.

5.7 Conclusions

A semi-analytical method of performing parametric studies of TMDs, which combines experimental and analytical techniques, was proposed in this thesis. The semi-analytical method overcomes the uncertainties of the comparison between theoretical and experimental results of the coupled building-TMD system, and provides a reliable estimate of the reduction of building motion and optimum design parameters of the TMD without having to perform a series of wind tunnel tests of the building with different TMDs. This technique is based on modal analysis, random vibration theory, and direct measurement in the wind tunnel of wind induced alongwind, crosswind or torsional response (or excitation) spectra of the plain building without the damper. The effects of wind intensity and direction, surrounding environment, building size, shape, mass, stiffness, and natural damping on the response reduction of the building can readily be investigated.

The results obtained by this semi-analytical technique were in good agreement with the corresponding experimental results. When both sets of results were compared with those using white noise excitation as wind excitation, it was found that the tuned mass damper system was less efficient for alongwind turbulence, crosswind wake and torsional excitations acting on tall buildings than for white noise excitation, but it was more efficient for lock-in excitation than for white noise excitation. This indicated that the effectiveness of TMDs is usually overestimated in practical situations if white noise excitation is used as actual wind excitations and the building is well out of lock-in excitation range. It is believed that the locations of the peaks in the wind excitation spectra relative to the natural frequencies of

the building-TMD system and the magnitude of the spectral peaks are the two important factors which cause the difference between the theoretical and experimental results and affect the effectiveness of the tuned mass damper. The practical application procedure of the semi-analytical method has been demonstrated by means of a series of selection diagrams or contours of optimum TMD parameters. Some possible extension of this technique to other types of wind tunnel tests was also mentioned.

Chapter 6

MODE SHAPE CORRECTIONS FOR WIND TUNNEL TESTS OF TALL BUILDINGS

6.1 Introduction

Aeroelastic model tests are commonly used to provide information on the overall wind-induced mean and dynamic loads and responses of a tall building. A two-degree-of-freedom model as described in Chapter 3, which simulates the building response in its two orthogonal fundamental sway modes of vibration, is effective for tall buildings of compact cross-section where the alongwind and crosswind responses are dominant. Another aeroelastic model for pure fundamental torsion vibration, as discussed in Chapter 4, is also a convenient and efficient way to explore the anatomy of torsional excitation and predict the torsional response of wind-induced tall buildings when the coupled effects between translational and torsional vibrations of tall buildings can be ignored.

However, if the prototype fundamental mode shapes of translational vibration depart significantly from a straight line variation, some adjustments to the results obtained from aeroelastic tests of translational vibration become necessary. Similarly significant corrections are needed to adjust the fundamental torsional responses because the aeroelastic model of torsional vibration type is maintained at a constant magnitude mode shape. The same problem exists in the force balance technique although there are some differences between the two testing techniques in the principle and method of estimating building responses.

Based on the co-spectrum of the longitudinal turbulence component of the wind velocity, which can be expressed analytically (e.g. Davenport,

1961), Vickery (1971, 1972) derived expressions for estimating the errors in calculating the response of buildings in the alongwind direction. A similar correction cannot be developed for the crosswind or lift direction as there are no reliable analytical models for the wind-induced lift forces. Saunders and Melbourne (1977), Kwok (1982), Kareem (1984), Holmes (1987) and Milford (1987) examined two limiting cases of mode shape correction factors in alongwind and crosswind directions for low and high correlations of wind forces with height. However, the additional assumptions, that the spectrum of the force per unit height was invariant with the height of buildings for low correlation of wind forces and the spectrum was a constant for high correlation, may cause the results to deviate from the actual limiting values of mode shape correction factors, especially for torsional correction factors.

Referring to the force balance technique, Tschanz and Davenport (1983) suggested a method by which base-shear measurements may be used to obtain approximate torsional mode shape correction. Tallin and Ellingwood (1985) used pressure measurement data to find the generalised torsional load spectrum and, consequently, they found that the RMS modal torque for a linear mode shape should be 57% of the measured base torque and the RMS modal torque for a cantilever mode shape should be 51% of the measured torque by the force balance technique. Vickery et al. (1985) estimated corrections to both top accelerations and base moments, primarily for sway components, from both analytical and experimental aspects. Boggs and Peterka (1989) further discussed mode shape corrections in the force balance technique. They suggested two adjustment factors: one applicable to displacements and accelerations; and a second applicable to equivalent static loads.

In this Chapter, the re-estimation of mode shape corrections is based on the aeroelastic testing technique and actual generalised mass (or mass moment of inertia), but the analytical procedure can also be applied to the force balance technique and the case of nominal generalised mass (or mass moment of inertia). Sources of error is identified for the aeroelastic testing technique. Two limiting values of error, for low and high correlations of wind loads with height, are discussed, based on a reasonable assumption of

the co-spectra of alongwind, crosswind and torsional excitations. The general expressions for mode shape correction factors are suggested and compared with previous results in the literature.

6.2 Identification of Sources of Error

In the following discussion, equations are generally developed for sway modes using F as a force and m as a mass; the equations will normally apply also to torsion if these are interpreted as torque T and mass moment of inertia m_t , respectively. Some equations which appeared in Chapter 5 are repeated in this Chapter for completeness and easy reference. The coupled effects between three fundamental modes of vibration are not considered in this Chapter.

The fundamental mode of vibration of a prototype tall building is governed by the equation

$$m^* \ddot{\xi} + c^* \dot{\xi} + k^* \xi = F^*(t) \quad \dots \dots \dots (6.1)$$

where m^* , c^* , k^* , F^* and ξ are the prototype building generalised mass, damping, stiffness, load and response, respectively. They are functions of the building's mass distribution m , height h , mode shape ϕ , natural frequency n_0 , wind-induced load F and critical damping ratio ζ . These parameters take the following form:

$$\left. \begin{aligned} m^* &= \int_0^h m(z) \phi^2(z) dz \\ k^* &= (2\pi n_0)^2 m^* \\ c^* &= 2\zeta \sqrt{k^* m^*} \\ F^*(t) &= \int_0^h F(z, t) \phi(z) dz \end{aligned} \right\} \dots \dots \dots (6.2)$$

The displacement of the building, $y(z,t)$, is related to the generalised response ξ by

$$y(z, t) = \xi(t)\phi(z) \dots \dots \dots (6.3)$$

In particular, if $\phi(z)$ is normalised using $\phi(h) = 1$, the motion of the top displacement, y_1 , of the building should be

$$m^* \ddot{y}_1 + c^* \dot{y}_1 + k^* y_1 = F^*(t) \dots \dots \dots (6.4)$$

In comparison, the generalised equation of motion of the building model shown in Fig. 3.5, which has a linear mode shape, is

$$m_1^* \ddot{y}_1 + c_1^* \dot{y}_1 + k_1^* y_1 = F_1^*(t) \dots \dots \dots (6.5)$$

where

$$\left. \begin{aligned} m_1^* &= \int_0^h \tilde{m}(z) (z/h)^2 dz \\ k_1^* &= (2\pi n_0)^2 m_1^* \\ c_1^* &= 2\zeta \sqrt{k_1^* m_1^*} \\ F_1^*(t) &= \int_0^h F(z, t) (z/h) dz \end{aligned} \right\} \dots \dots \dots (6.6)$$

Comparing Eqs. 6.5 and 6.6 with Eqs. 6.4 and 6.2, and providing that the generalised mass m_1^* , natural frequency n_0 , and critical damping ratio ζ in Eqs. 6.5 and 6.6 are modelled to be actual building parameters in Eqs. 6.2 and 6.4 according to the modelling requirements, the error caused by the aeroelastic modelling technique only occurs in the generalised wind excitation.

The spectrum of the generalised wind excitation, $F^*(t)$, in Eqs. 6.2 and 6.4 can be written as

$$S_F(n) = \int_0^h \int_0^h C_0(z_1, z_2, n) \phi(z_1)\phi(z_2) dz_1 dz_2 \dots \dots \dots (6.7)$$

while the corresponding spectrum in Eqs. 6.5 and 6.6 is

$$S_{F_1}(n) = \int_0^h \int_0^h C_0(z_1, z_2, n) (z_1/h) (z_2/h) dz_1 dz_2 \dots \dots \dots (6.8)$$

in which $C_0(z_1, z_2, n)$ is co-spectrum of fluctuating alongwind, crosswind, or torsional excitation.

Clearly, the general equation to correct the generalised alongwind and crosswind excitation spectrum for a linear mode shape to that for an arbitrary mode shape is

$$\eta^2(n) = \frac{S_F(n)}{S_{F_1}(n)} = \frac{\int_0^h \int_0^h C_0(z_1, z_2, n) \Phi(z_1) \Phi(z_2) dz_1 dz_2}{\int_0^h \int_0^h C_0(z_1, z_2, n) (z_1/h) (z_2/h) dz_1 dz_2} \dots \dots \dots (6.9)$$

For the type of aeroelastic model of torsional vibration shown in Fig. 4.4, the general equation to correct the generalised torsional excitation spectrum for a constant mode shape to that for an arbitrary mode shape is

$$\eta_t^2(n) = \frac{S_T(n)}{S_{T_1}(n)} = \frac{\int_0^h \int_0^h C_0(z_1, z_2, n) \Phi(z_1) \Phi(z_2) dz_1 dz_2}{\int_0^h \int_0^h C_0(z_1, z_2, n) dz_1 dz_2} \dots \dots \dots (6.10)$$

The quantity $\eta(n)$ or $\eta_t(n)$ is referred to as the mode shape correction factor below.

6.3 Two Limits to Mode Shape Correction Factor

6.3.1 Assumption of co-spectrum

A precise estimate of the correction factor, $\eta(n)$ or $\eta_t(n)$, is difficult as it requires information on the co-spectrum of the time-varying component of the wind load per unit height at various heights along the building and the fundamental vibration modes of the building. However, two limiting cases of the mode shape correction factor for low and high correlation of

the wind loads can be examined. If the assumption for the co-spectrum of wind loads is not only reasonable but also simple, the two limiting values of the correction factor will be independent of frequency variable, n , and will be reliable enough to estimate building response errors in the aeroelastic modelling technique.

Consider the following form for the co-spectrum

$$C_0(z_1, z_2, n) = W(z_1)W(z_2)S_f(n)R(z_1 - z_2, n) \dots \dots \dots (6.11)$$

where $W(z)$ is the amplitude of the fluctuating wind force or torque at height z ; $S_f(n)$ is the unit fluctuating wind velocity spectrum related to the fluctuating wind force or torque, and $R(z_1 - z_2, n)$ is a cross-correlation function which depends on the separation distance $|z_1 - z_2|$. This type of co-spectrum can be used to describe alongwind excitation quite well. For crosswind and torsional excitations, it is only an approximate description. Amplitude dependent excitations in the crosswind direction such as lock-in and galloping are not considered here.

The amplitude of the fluctuating wind force or torque, $W(z)$, is considered to be

$$W(z) = W(h) \left(\frac{z}{h}\right)^{\alpha\nu} \dots \dots \dots (6.12)$$

in which α is the power law exponent of the mean wind velocity profile; ν is a constant referring to wind excitation types. $\nu = 1$ is probably more appropriate for alongwind turbulence excitation because of the existence of the mean wind force in this direction. For crosswind wake excitation and torsional excitation, the values of ν are not available at this stage from both field measurement and wind tunnel test. $\nu = 2$, which represents a general relationship between wind speed and wind force, is adopted in this study.

At the same time, a power law with exponent, β , is taken as the general form for actual mode shape, i.e.:

$$\Phi(z) = \left(\frac{z}{h}\right)^\beta \dots \dots \dots (6.13)$$

Now, consider two limiting cases of the correction factor for low and high correlation levels.

6.3.2 Low correlation level

For a low correlation level, the correlation of wind loads falls off rapidly with the increasing distance $|z_1 - z_2|$, i.e., assuming

$$R(z_1 - z_2, n) = \begin{cases} 1 & z_1 = z_2 \\ 0 & z_1 \neq z_2 \end{cases} \dots \dots \dots (6.14)$$

As a result, substituting Eqs. 6.11 to 6.14 into Eq. 6.9 or 6.10, one obtains a limiting value of the correction factor as follows:

for alongwind responses

$$\eta_{a_1} = \left[\frac{\int_0^h W^2(z) \Phi^2(z) dz}{\int_0^h W^2(z) (z/h)^2 dz} \right]^{\frac{1}{2}} = \left[\frac{2\alpha + 3}{2\alpha + 2\beta + 1} \right]^{\frac{1}{2}} \dots \dots \dots (6.15)$$

for crosswind responses

$$\eta_{c_1} = \left[\frac{\int_0^h W^2(z) \Phi^2(z) dz}{\int_0^h W^2(z) (z/h)^2 dz} \right]^{\frac{1}{2}} = \left[\frac{4\alpha + 3}{4\alpha + 2\beta + 1} \right]^{\frac{1}{2}} \dots \dots \dots (6.16)$$

for torsional responses

$$\eta_{t_1} = \left[\frac{\int_0^h W^2(z) \Phi^2(z) dz}{\int_0^h W^2(z) dz} \right]^{\frac{1}{2}} = \left[\frac{4\alpha + 1}{4\alpha + 2\beta + 1} \right]^{\frac{1}{2}} \dots \dots \dots (6.17)$$

6.3.3 High correlation level

Another limiting value can be achieved for the high correlation level, i.e., assuming

$$R(z_1 - z_2, n) = 1 \quad \dots \dots \dots (6.18)$$

The result for alongwind responses is

$$\eta_{a_2} = \frac{\int_0^h W(z) \Phi(z) dz}{\int_0^h W(z) (z/h) dz} = \frac{\alpha + 2}{\alpha + \beta + 1} \quad \dots \dots \dots (6.19)$$

for crosswind responses:

$$\eta_{c_2} = \frac{\int_0^h W(z) \Phi(z) dz}{\int_0^h W(z) (z/h) dz} = \frac{2\alpha + 2}{2\alpha + \beta + 1} \quad \dots \dots \dots (6.20)$$

for torsional responses:

$$\eta_{t_2} = \frac{\int_0^h W(z) \Phi(z) dz}{\int_0^h W(z) dz} = \frac{2\alpha + 1}{2\alpha + \beta + 1} \quad \dots \dots \dots (6.21)$$

6.4 Characteristics of Mode Shape Correction Factor

6.4.1 Alongwind correction factor

The alongwind mode shape correction factors η_{a_1} and η_{a_2} are plotted in Fig. 6.1 for several typical values of α and $0 < \beta < 2$. It can be seen that all curves pass through a value of unity for β equal to unity. Despite the difference in the assumption about the cross-correlation function, the corresponding two curves for the low and high correlation levels are relatively close to each other, especially in the range of practical interest from $\beta = 0.5$ to 2.0. It can also be seen that the effect of terrain

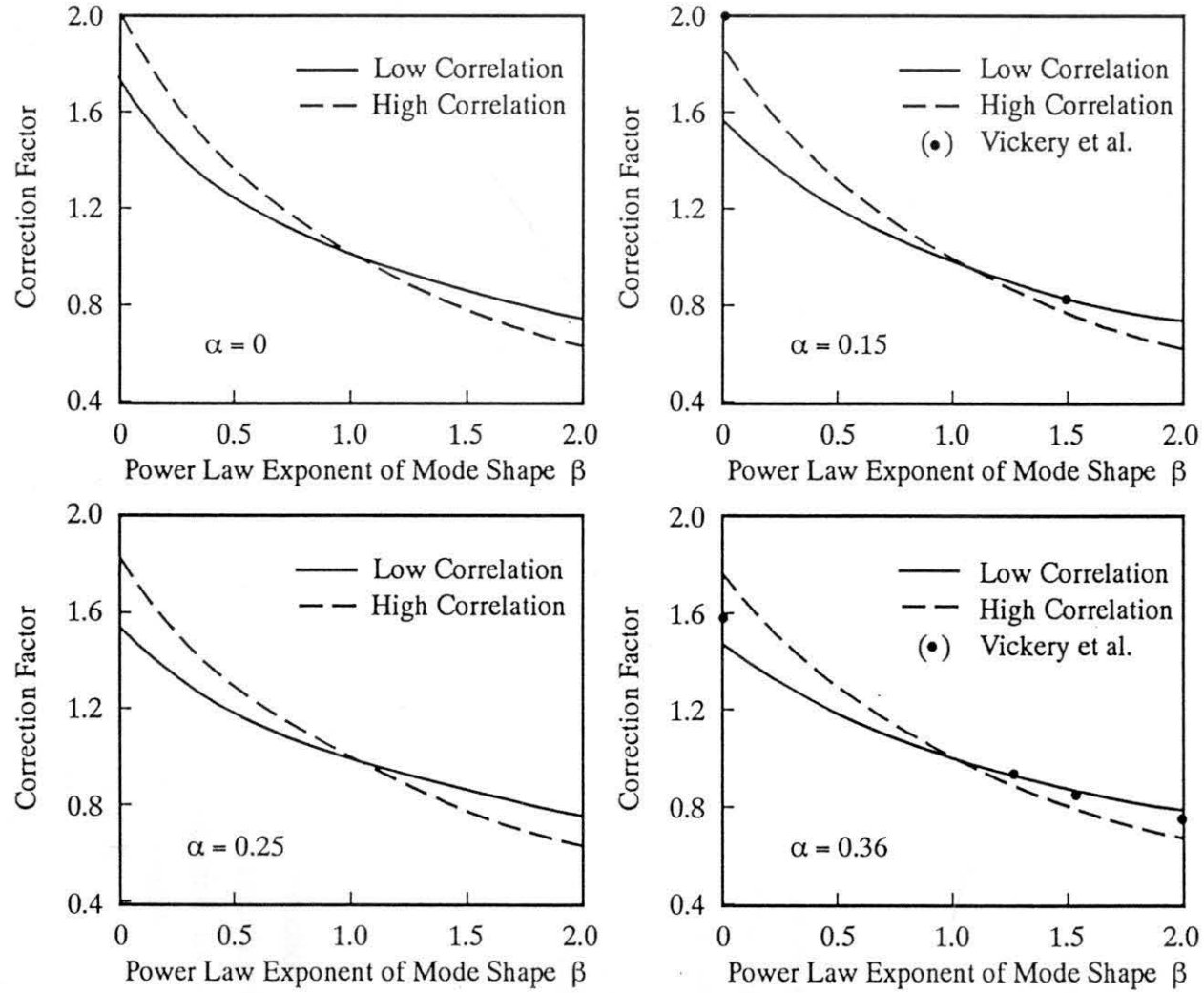


FIG.6.1 ALONG-WIND MODE SHAPE CORRECTION FACTOR

conditions on mode shape correction factors is not apparent when $\beta > 1$.

6.4.2 Crosswind correction factor

Variations of the crosswind mode shape correction factors, η_{c1} and η_{c2} , with α and β are shown in Fig. 6.2. The curves have the same characteristics as the alongwind mode shape correction factors. However, the terrain parameter α affects the crosswind correction factors more than the alongwind correction factors. With the increase of α , the curves become flatter.

6.4.3 Torsional correction factor

The torsional mode shape correction factors η_{t1} and η_{t2} are plotted in Fig. 6.3. All curves pass through a value of unity for β equal to zero and then decrease with increasing β values. With the increasing α values, the two limiting values of the correction factors increase towards a value of unity. Comparing with the translational correction factors, the torsional correction factor is sensitive to the non-uniformities of the sectional wind torque with height.

6.5 Comparison and Discussion

Firstly, it is noted that the expression of the alongwind correction factor for the high correlation level, i.e., Eq. 6.19, is the same as that implied in the approximate derivation of gust response factor for alongwind loading by Vickery (1972). The expressions of the crosswind and torsional correction factors for the high correlation level, i.e., Eqs. 6.20 and 6.21, are the same as those suggested by Boggs and Peterka (1989) for both sway modes and torsional mode, respectively. They used different approximate derivation for the force balance technique. It is also noted that, for $\alpha = 0$, the expressions of the alongwind correction factors are the same as those of the crosswind correction factors and those provided by Holmes (1987). Therefore, the present mode shape correction factors seem to be more general.

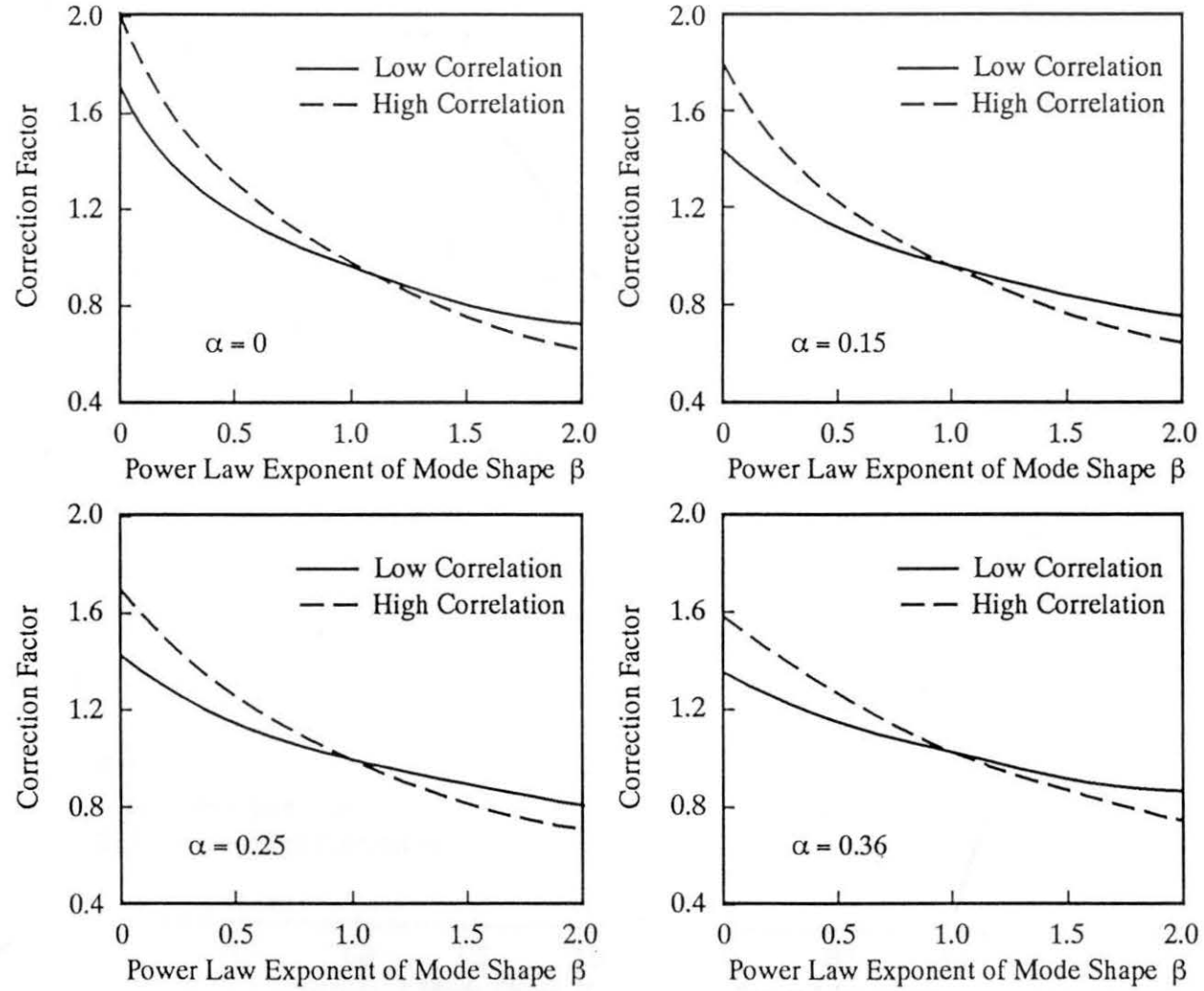


FIG.6.2 CROSS-WIND MODE SHAPE CORRECTION FACTOR

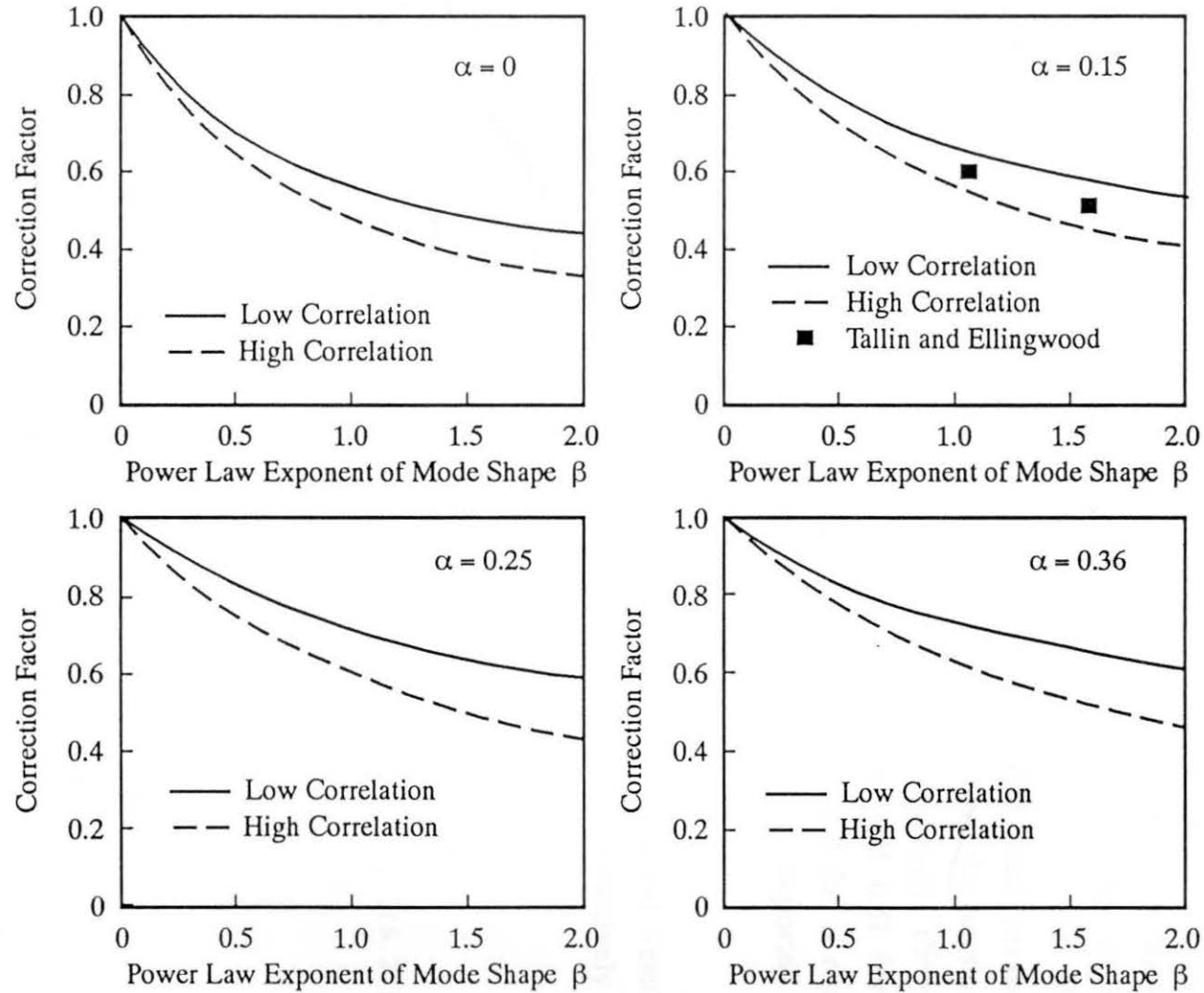


FIG.6.3 TORSIONAL MODE SHAPE CORRECTION FACTOR

Vickery et al. (1985) carried out wind tunnel measurements of the sway mode shape correction for a square-section building in two different terrain simulations. Their experimental results showed that the correction factors were not sensitive to frequency variable n in a range of reduced frequencies of practical interest for tall buildings, which supported the present assumption for the co-spectra of the wind loads. Some of their results are also plotted on Fig. 6.1, and are seen to agree well with the curves of the low correlation level, when $\beta > 1$, and with the curves of the high correlation level, when $\beta < 1$. Tallin and Ellinwood (1985) used pressure measurement data for a particular building model to analyse the torsional mode shape correction factor. They found that "generalised torque" correction factors should be 0.57 for a linear mode shape and 0.51 for a cantilever mode shape. These values are also shown in Fig. 6.3 for α equal to 0.15. Unfortunately, the velocity profile exponent was not reported in their paper.

From the above comparison, especially with the experimental results, mode shape correction factors should in practice be taken conservatively as follows:

$$\eta_a = \begin{cases} \frac{\alpha + 2}{\alpha + \beta + 1} & \beta < 1 \\ \left(\frac{2\alpha + 3}{2\alpha + 2\beta + 1} \right)^{\frac{1}{2}} & \beta > 1 \end{cases} \dots \dots \dots (6.22)$$

for alongwind response;

$$\eta_c = \begin{cases} \frac{2\alpha + 2}{2\alpha + \beta + 1} & \beta < 1 \\ \left(\frac{4\alpha + 3}{4\alpha + 2\beta + 1} \right)^{\frac{1}{2}} & \beta > 1 \end{cases} \dots \dots \dots (6.23)$$

for crosswind responses;

$$\eta_t = \left[\frac{4\alpha + 1}{4\alpha + 2\beta + 1} \right]^{\frac{1}{2}} \dots \dots \dots (6.24)$$

for torsional responses.

Referring to the comparison between the experimental data and empirical values of the dynamic base torque, which are shown in Fig. 4.11 of Chapter 4, the error can now be partly explained. For category 2, $\alpha = 0.15$, η_t ranges from 0.78 ($\beta = 0.5$) to 0.59 ($\beta = 1.5$) according to Eq. 6.24. The corresponding values in Fig. 4.11 is 0.5 on average. Therefore, the error shown in Fig. 4.11 can be adjusted by the correction factor η_t to some extent. Further comparison of the described aeroelastic model in Chapter 4 with the MDOF aeroelastic model should be based on several given building models because the mode shape parameter β and the mass moment distribution of the building are not directly reflected in the empirical formulae.

The relationships between the standard deviations of the top (twist angular) displacement and acceleration responses and the generalised excitation spectrum can be easily obtained, according to random vibration theory.

$$\sigma_{y_1} = \frac{1}{k^*} \left[\int_0^h |H(n)|^2 S_F(n) dn \right]^{\frac{1}{2}} \dots \dots \dots (6.25)$$

and

$$\sigma_{\ddot{y}_1} = \frac{1}{k^*} \left[\int_0^h (2\pi n)^4 |H(n)|^2 S_F(n) dn \right]^{\frac{1}{2}} \dots \dots \dots (6.26)$$

which are derived from Eqs. 6.2 and 6.4.

Similar expressions can be obtained from Eqs. 6.5 and 6.6 for building models in the wind tunnel. Because the two limiting values of the mode shape correction factors are not dependent on the frequency variable n , it is obvious from Eqs. 6.9, 6.10, 6.25 and 6.26 that the correction factors provide direct limiting corrections for the top (twist angular) displacement and acceleration responses in the present modelling technique. In addition, the factors also provide direct limiting corrections for dynamic base torque responses, only if the actual mass moment distribution and fundamental

mode shape are used in further calculation. Clearly, the squares of the factor represent limiting corrections for the generalised excitation spectra.

It is encouraging to note that the normalised results of parametric studies of TMDs, which are discussed in Chapter 5, do not need to be corrected for difference in mode shape. This is because the standard deviation responses of the building with a TMD were normalised by the same responses of the building without a TMD, as shown in Eqs. 5.19 and 5.21. Furthermore, the two limiting correction factors were not dependent on the frequency variable. As a result, the mode shape correction factors in both numerator and denominator of Eqs. 5.19 and 5.21 were counteracted.

6.6. Conclusions

Sources of error caused by the discrepancy between the building model and prototype mode shapes were identified for the aeroelastic modelling technique. Based on a reasonable assumption of the co-spectra of wind loads, two limiting values of error, for low and high correlations of wind loads with height, were discussed. Three mode shape correction factors, for alongwind, crosswind and torsional responses respectively, were suggested to adjust the experimental response results to the prototype values. The results obtained by the proposed expressions were in reasonable agreement with the available experimental results.

Chapter 7

ANALYSIS OF AN ACTIVE CONTROL SYSTEM BASED ON AEROELASTIC TEST TECHNIQUES

7.1 Introduction

The parametric studies of passive tuned mass dampers have shown that there is a limit to motion reduction offered by passive TMD for a given tall building. If the required motion reduction exceeds this limit, an active control system may be needed to provide additional motion reduction. As mentioned in Chapter 2, an active control basically depends on the supply of external energy to counteract the dynamic response of tall buildings. It consists of (1) sensors installed at suitable locations of the building to measure either the external excitations or the structural response quantities or both, (2) devices to process the measured information and to compute the necessary control force based on given control algorithms. There are different active control systems according to the control devices and control algorithms. Only a suboptimal active mass damper control system suggested by Roorda (1975, 1980), Yang and Giannopoulos (1978, 1979a, 1979b), Samali et al. (1985) was semi-analytically investigated in this thesis by means of the wind excitation spectra measured with the tested models described in this thesis.

A suboptimal active mass damper control system mainly consists of electrohydraulic servomechanisms which may be attached to the mass damper along the x or y directions (see Fig. 7.1). This active mass damper control system is generally installed on the top floor of the building. If the mass and elastic centers of the building are identical and the mass damper is also arranged on this center, the active mass damper only reduces alongwind or crosswind vibration of the building. If the active mass damper is

installed at the side of the top floor of the building and as a result there is an offset between the center of the mass damper and the elastic (or mass) center of the building, torsional vibration of the building can also be suppressed. Sensors are used to measure the top displacement (or velocity or acceleration) of the building. Electric voltages, which are proportional to the measured building motions, are then transmitted to servovalves. The servovalves convert the electrical voltages into hydraulic piston motions. Active control forces which are proportional to the movements of the hydraulic piston are developed by an auxiliary spring between the mass damper and the building. A flow chart of the control system is also shown in Fig. 7.1.

Compared with optimal active control systems, the suboptimal active mass damper control system has the following characteristics: (1) Once the most beneficial control parameters are determined, the suboptimal active control devices work like a passive mass damper. On-line computations and associated processing equipments are not needed. As a result, the reliability and stabilisation of this suboptimal control system are much better than those of optimal active control systems. In the optimal active control system, on-line computations for the solution of the Riccati matrix equation may cause serious time delay problem and need a series of processing equipments and discrete-time formulations of control algorithms. (2) The theoretical results presented by Yang (1982) indicate that for given control parameters, the structural response quantities and control forces are not sensitive to small variations of structural characteristics, which increases the practical advantages of this system. (3) Either from a theoretical or a practical point of view, the suboptimal active control systems represent an intermediate link from passive control to optimal active control of complex civil engineering structures.

Most investigations of the application of suboptimal active control system in reducing wind-induced vibration of tall buildings are, up to date, theoretically conducted. It is important to verify theoretical research results through experiments in laboratory before full-scale control systems are installed on real buildings. The following is a semi-analytical method, based on aeroelastic wind tunnel tests, of performing parametric studies of

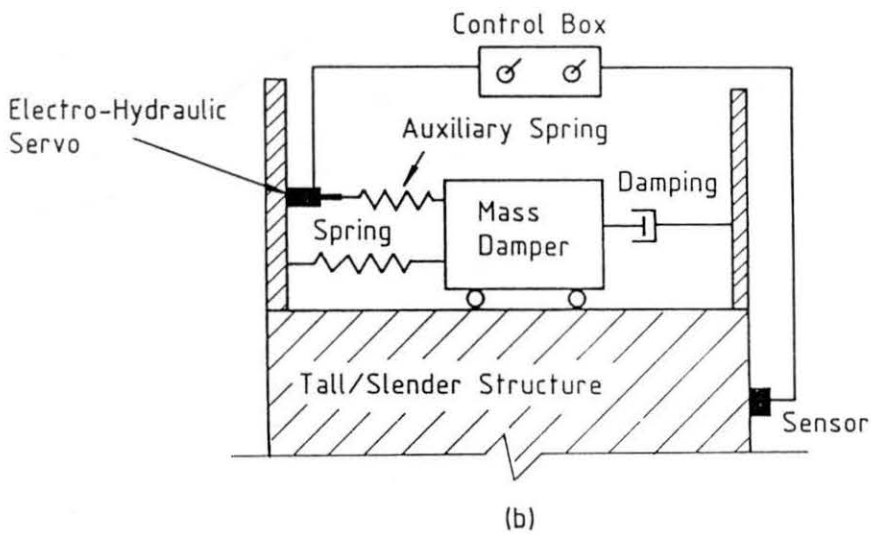
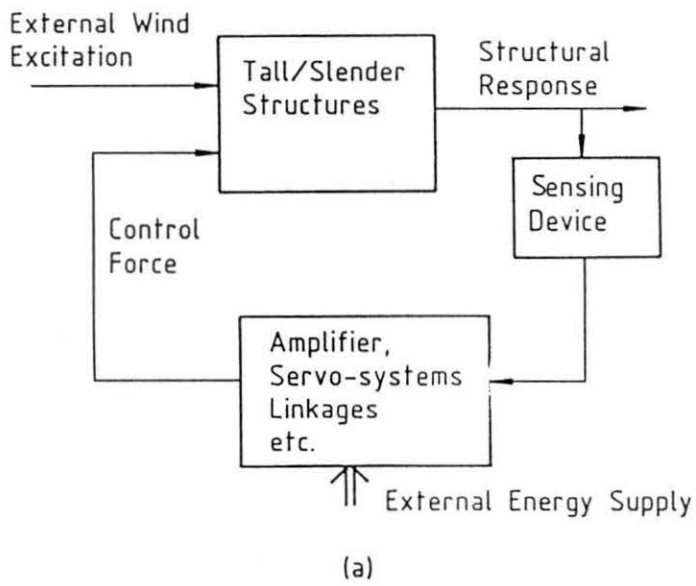


FIG.7.1 STRUCTURAL CONTROL SYSTEM:
 (a) FLOW CHART,
 (b) SUBOPTIMAL ACTIVE MASS DAMPER

the suboptimal active mass damper control system, which can be used to form a theoretical basis of future experiments.

7.2 Basic Theory

For an aeroelastic building model with an active mass damper model as shown in Fig. 7.2, the equations of motion of the system under alongwind or crosswind excitation are

$$\left. \begin{aligned} m_1^* \ddot{y}_1(t) + c_1^* \dot{y}_1(t) + k_1^* y_1(t) - c_2 \dot{z}(t) + k_2 z(t) + F_1^*(t) - P(t) \\ m_2 \ddot{z}(t) + c_2 \dot{z}(t) + k_2 z(t) = -m_2 \ddot{y}_1(t) + P(t) \end{aligned} \right\} \quad (7.1)$$

where $P(t)$ is the active control force, and the remaining notations are the same as those in Eqs. 5.6 and 5.10 of Chapter 5.

A displacement sensor is considered in this study because only a simpler calibration procedure of the aeroelastic model test is required. According to the research results presented by Roorda (1975) and Yang (1982), the relationship in frequency domain between the active force $P(t)$ and the building top displacement $y_1^a(t)$ is

$$\tilde{P}(n) = G(n) \tilde{y}_1^a(n) \quad \dots \dots \dots (7.2)$$

where

$$G(n) = \frac{K_t \tau \epsilon \lambda^2}{\epsilon^2 + \lambda^2} + i \frac{K_t \tau \epsilon^2 \lambda}{\epsilon^2 + \lambda^2}$$

$$\lambda = \frac{n}{n_0} ; \quad \epsilon = \frac{R_1}{2\pi n_0} ; \quad \tau = \frac{2\pi n_0 \kappa}{R_0}$$

in which κ is a proportional constant between the top displacement of the building model and the output voltage from the strain gauges; K_t is a proportional constant between the control force and the movement of the

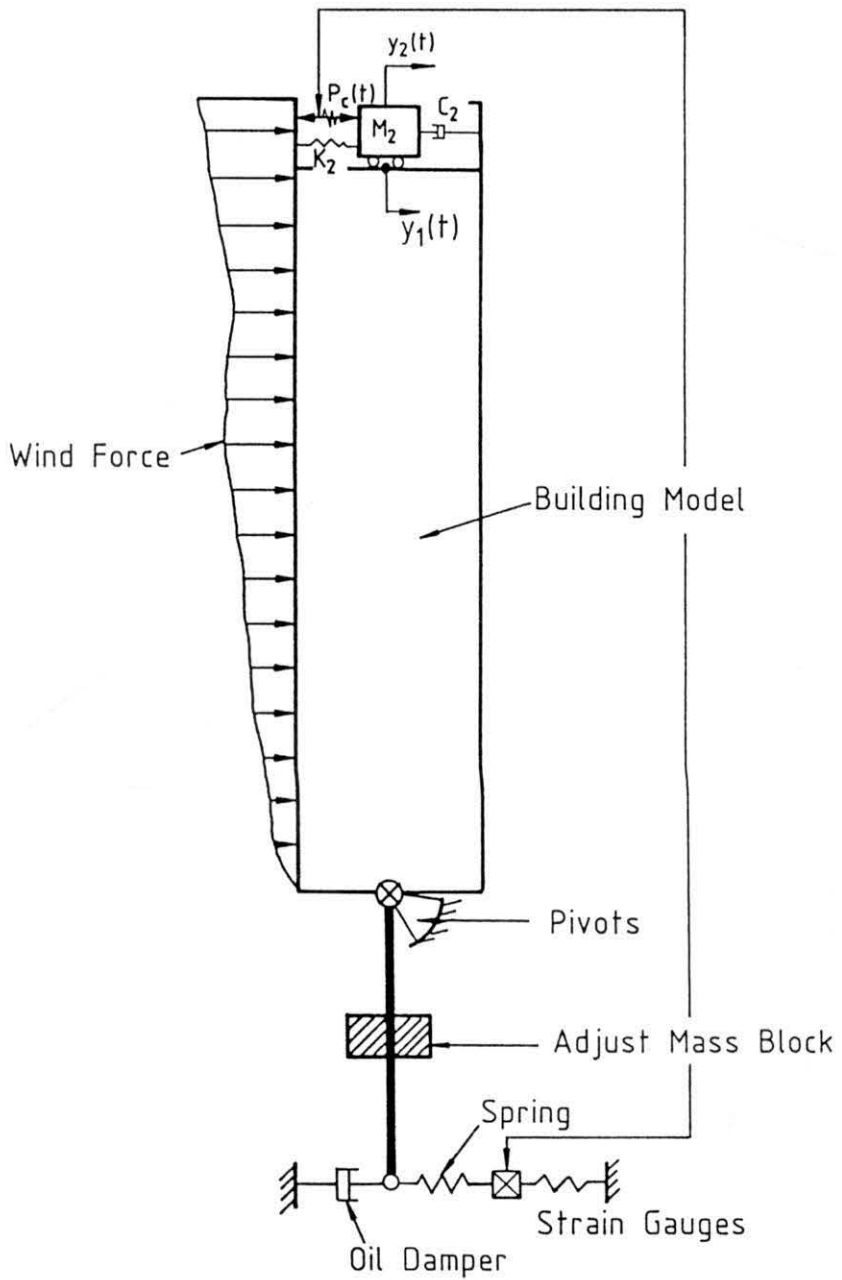


FIG.7.2 BUILDING - ACTIVE MASS DAMPER SYSTEM

hydraulic piston; R_1 is the collective loop-gain of the electrohydraulic servomechanism and $1/R_0$ is the feedback gain of the transducer in the servomechanism; ϵ and τ are the normalised loop gain and the feedback gain, respectively; \sim represents Fourier transform; $i = \sqrt{-1}$.

Taking the Fourier transforms of Eq. 7.1 and using Eq. 7.2, one obtains the power spectral density functions of the building top controlled displacement response, y_1^a , and the relative displacement response, z^a , of the damper as follows:

$$S_{y_1}^a(n) = \frac{S_{F_1}(n) |H_{y_1 F_1}^a(n)|^2}{(k_1^*)^2} \dots \dots \dots (7.3)$$

$$S_z^a(n) = \frac{S_{F_1}(n) |H_{z F_1}^a(n)|^2}{(k_1^*)^2} \dots \dots \dots (7.4)$$

where the mechanical admittance functions

$$|H_{y_1 f}^a(n)|^2 = \frac{(\chi^2 - \lambda^2)^2 + 4\lambda^2\chi^2\zeta_2^2}{a_1^2 + b_1^2} \dots \dots \dots (7.5)$$

$$|H_{z f}^a(n)|^2 = \frac{(\lambda^2 + g_1)^2 + g_2^2}{a_1^2 + b_1^2} \dots \dots \dots (7.6)$$

and in which

$$\left. \begin{aligned} a_1 &= \lambda^4 - \lambda^2(1 + \chi^2 + \mu\chi^2 + 4\chi\zeta_2^2 + g_1) - \\ &\quad 2\lambda\chi\zeta_2 g_2(1 - \mu) + \chi^2(1 + g_1 - \mu g_1) \\ b_1 &= 2\lambda[\zeta_2\chi(1 - \lambda^2 - \mu\lambda^2 + g_1 - \mu g_1) + \zeta(\chi^2 - \lambda^2)] - \\ &\quad \lambda^2 g_2 + \chi^2 g_2(1 - \mu) \\ g_1 &= \frac{K_t}{K_1} \frac{\tau\epsilon\lambda^2}{\epsilon^2 + \lambda^2} ; \quad g_2 = \frac{K_t}{K_1} \frac{\tau\epsilon^2\lambda}{\epsilon^2 + \lambda^2} \end{aligned} \right\} (7.7)$$

Substituting Eq. 5.9 into Eqs. 7.3 and 7.4, one obtains

$$S_{y_1}^a(n) = \frac{|H_{y_1 F_1}^a(n)|^2}{|H(n)|^2} S_{y_1}(n) \dots \dots \dots (7.8)$$

$$S_z^a(n) = \frac{|H_{z F_1}(n)|^2}{|H(n)|^2} S_{y_1}(n) \dots \dots \dots (7.9)$$

Note that $S_{y_1}^a(n)$ is the power spectral density of the top displacement of the building mode with an active mass damper while $S_{y_1}(n)$ is the same term without any dampers. Since $S_{y_1}(n)$ can be obtained through the aeroelastic tests of the plain model, a semi-analytical method as conducted in passive mass damper parametric studies can be used to select the most beneficial control parameters of the suboptimal active mass damper control system. This method not only provides a guideline for the corresponding active control experiments but also indicates a practical procedure for the active control system design if the semi-analytical results are in good agreement with the experimental results of the active control system.

In the same manner as the passive control system analysis, the normalised standard deviation responses of the active control system are given as follow:

$$\left. \begin{aligned} \frac{\sigma_{y_1}^a}{\sigma_{y_1}} &= \frac{[\int_0^\infty S_{y_1}^a(n) dn]^{\frac{1}{2}}}{[\int_0^\infty S_{y_1}(n) dn]^{\frac{1}{2}}} \\ \frac{\sigma_z^a}{\sigma_{y_1}} &= \frac{[\int_0^\infty S_z^a(n) dn]^{\frac{1}{2}}}{[\int_0^\infty S_{y_1}(n) dn]^{\frac{1}{2}}} \end{aligned} \right\} \dots \dots \dots (7.10)$$

In the above equations, superscript "a" is used to identify the corresponding mechanical admittance functions and power spectral densities when an active control system is utilised.

The suboptimal design of an active mass damper system depends not only on the allowable level of the structural responses, but also on the

required level of the control force. Therefore, it is necessary to estimate the magnitude of the control force. The standard deviation of the control force can be derived from Eq. 7.2.

$$\sigma_P = \left[\int_0^\infty G(n) S_{y_1}^a(n) dn \right]^{\frac{1}{2}} \dots \dots \dots (7.11)$$

The standard deviation of the mode-generalised wind force acting on the building, $F_1^*(t)$, is

$$\sigma_{F_1} = \left[\int_0^\infty S_{F_1}(n) dn \right]^{\frac{1}{2}} \dots \dots \dots (7.12)$$

in which the generalised wind force spectrum, $S_{F_1}(n)$, can be determined by using Eq. 5.9. The normalised standard deviation of the active control force is defined as the ratio of the control force standard deviation to the generalised wind force standard deviation, i.e., σ_P/σ_{F_1} .

For aeroelastic building model for pure torsion as described in Chapter 4, the suboptimal active mass damper can also provide an active control moment, $T_a(t)$, if the damper is arranged at the side of the top floor of the building model. The equations of motion of the pure torsional system with an active mass damper are the same as Eq. 7.1 if the parameters in Eq. 7.1 are properly interpreted by using the torsion notation. Therefore, the above derived equations for alongwind (crosswind) vibration can be applied to torsional vibration without any difficulties. The normalised standard deviation responses of the torsional vibration of the building-active mass damper system are

$$\left. \begin{aligned} \frac{\sigma_{\theta_1}^a}{\sigma_{\theta_1}} &= \frac{\left[\int_0^\infty S_{\theta_1}^a(n) dn \right]^{\frac{1}{2}}}{\left[\int_0^\infty S_{\theta_1}(n) dn \right]^{\frac{1}{2}}} \\ \frac{\sigma_{z\theta}^a}{\sigma_{\theta_1}} &= \frac{\left[\int_0^\infty S_z^a(n) dn \right]^{\frac{1}{2}}}{\left[\int_0^\infty S_{\theta_1}(n) dn \right]^{\frac{1}{2}}} \end{aligned} \right\} \dots \dots \dots (7.13)$$

and

$$\frac{\sigma_{T_a}}{\sigma_{T_1}} = \frac{[\int_0^\infty G_T(n) S_{\theta_1}^a(n) dn]^{\frac{1}{2}}}{[\int_0^\infty S_{T_1}(n) dn]^{\frac{1}{2}}} \dots \dots \dots (7.14)$$

7.3 Effectiveness of Active Mass Damper

7.3.1 Comparison of responses

Comparison of the top displacement responses of the building was conducted between passive and active control. The properties of the building model and three mass damper models were the same as those listed in Table 3.3 of Chapter 3. Only one crosswind top displacement response spectrum of the plain building model, for incident wind normal to the wide face of the building model and at a reduced velocity of 6, was selected as input spectrum. The parameters of the active control system are: the normalised loop gain $\epsilon = 5$; the normalised feedback gain $\tau = 15$; the normalised proportional constant $K_p/k_1^* = 0.05$. The selection of the parameters was based on the results of parametric study which is described in section 7.4. Table 7.1 shows the comparison results. It is obvious that, if electrohydraulic servomechanisms were added to the tested passive control systems, the suboptimal active control can further reduce considerably both the building top displacement and the damper relative displacement. Such a significant reduction can not be achieved by the passive mass damper with optimal parameters. It is also noted that, although the parameters of the three mass dampers were different, the top displacement response reduction levels obtained by the active control system were almost the same. This indicates that the effectiveness of the active control system was not sensitive to the variation of the mass damper parameters.

Table 7.2 shows the comparison between passive and active control for torsional vibration for the following parameters of the active control system: $\epsilon = 5$; $\tau = 15$ and $K_{t\theta}/k_1^* = 0.05$. Four different twist angular response spectra of the plain building model were selected as torsional input spectra. The properties of the building model and the mass damper model can be found in Table 4.1. It is seen that the twist angular responses of the

TABLE 7.1 COMPARISON BETWEEN PASSIVE AND ACTIVE CONTROL (TRANSLATION)

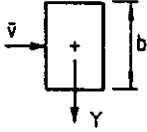
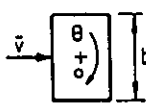
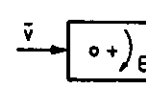
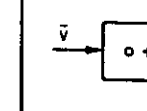
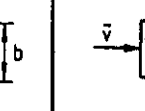
Reduced Velocity = 6 $\tau = 15; \quad \epsilon = 5$ 	TMD1		TMD2		TMD3	
	Passive	Active	Passive	Active	Passive	Active
$\sigma_{y_1}^t / \sigma_{y_1}$	0.771	0.300	0.758	0.302	0.696	0.306
$\sigma_z^t / \sigma_{y_1}$	3.553	0.854	2.769	0.756	2.499	0.745

TABLE 7.2 COMPARISON BETWEEN PASSIVE AND ACTIVE CONTROL (TORSION)

Type	Reduced Velocity = 4		Reduced Velocity = 4		Reduced Velocity = 8		Reduced Velocity = 8	
								
$\epsilon = 5$ $\tau = 15$	Passive	Active	Passive	Active	Passive	Active	Passive	Active
$\sigma_{\theta_1}^a / \sigma_{\theta_1}$	0.725	0.380	0.736	0.385	0.567	0.195	0.739	0.358
$\sigma_{z\theta}^a / \sigma_{\theta_1}$	3.951	0.830	3.889	0.812	3.712	0.732	4.061	0.841

Note: + Geometric Centre
o Elastic Centre

building were significantly reduced by the suboptimal active control system. It is also noted that the effectiveness of the active control systems depended on input spectra of torsional excitation. This phenomenon was similar to the passive mass damper control system.

7.3.2 Comparison of response spectra

The response spectrum of a building represents a distribution in the frequency domain of the energy absorbed by the building from external wind load. The angular displacement response spectra of the studied building, for wind incidence normal to the narrow face of the building and at a reduced velocity of 8, are shown in Figs. 7.3 and 7.4. For the plain building without any control, there was a sharp peak in the response spectrum which was located around the natural frequency of the building. Such spectral peak is obviously disrupted by adding a passive mass damper on the building, as shown in Fig. 7.4. There were two peaks in the response spectrum of the passive mass damper system because the mass damper–building system is a two–degree–of–freedom system. When the suboptimal active mass damper was introduced to the building, Fig. 7.3 shows that the sharp peak which happened in the plain building was completely suppressed and the response spectrum becomes a broad–band spectrum. It is interesting to note that the spectral distribution within the low frequency range ($0 < n < 3$) was almost the same for the controlled or uncontrolled systems. This indicated that the passive or active control system could not affect external wind load when the wind load was independent of the building motion. In Figs. 7.3 and 7.4, the same parameters as those in the response comparison section were used for both passive and active mass dampers.

Comparison of damper relative angular displacement spectra between passive and active control is shown in Fig. 7.5. The peaks in the passive mass damper response spectrum were significantly reduced by using the active mass damper. As a result, the standard deviation of the relative angular displacement response of the active mass damper was much smaller than that of the passive mass damper. It is seen that the spectral distribution in the low frequency range, as shown in Fig. 7.5, was different

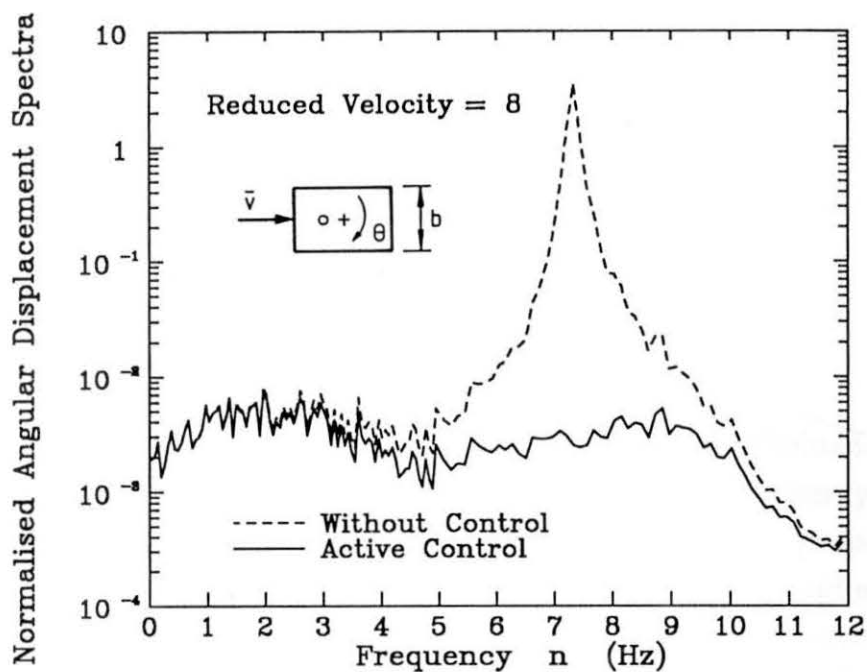


FIG. 7.3 BUILDING ANGULAR DISPLACEMENT SPECTRA WITH AND WITHOUT ACTIVE CONTROL

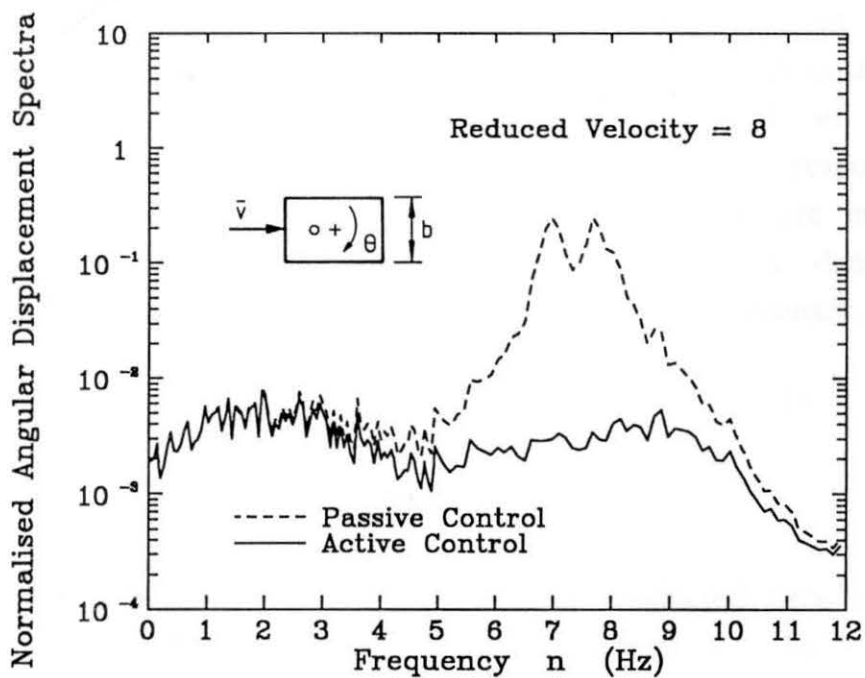


FIG. 7.4 COMPARISON OF BUILDING ANGULAR DISPLACEMENT SPECTRA BETWEEN ACTIVE AND PASSIVE CONTROL

from the response spectra of the building as shown in Figs. 7.3 and 7.4. This is because the wind load does not directly act on the dampers. It is also seen from Fig. 7.5 that the spectral amplitude of the response of the active mass damper in the low frequency range was larger than that of the passive mass damper. The exact cause of this is unknown at this stage. However, the contribution of this part of spectral amplitude to the total displacement response was quite small.

7.3.3 Comparison of frequency response functions

The frequency response functions (i.e., mechanical admittance functions) of a building reflect a capacity of transferring external energy to building itself, which is determined only by the structural internal properties of the building. The frequency response functions of the building with and without the damper are shown in Figs. 7.6 and 7.7 for torsional vibration. The same properties as before were used for both building and mass dampers. Without any dampers, there was a sharp peak in the frequency response function of the building angular displacement. This peak was located at the natural frequency of the building and the most energy absorbed by the building from wind load was attributed to this peak. With a passive mass damper, this peak was significantly reduced because the passive mass damper increased the building capacity of dissipating external energy. The active mass damper depends on the supply of the external energy to counteract the wind load so that the frequency response function was totally different from those with and without a passive mass damper. The frequency response function of the active mass damper system approached a constant of 1 and therefore there was no resonant peak in the corresponding response spectrum.

7.4 Parametric Studies of Active Mass Damper

Parametric studies of active mass damper conducted here are based on the measured wind response spectra in wind tunnel and the tested models. The properties of the building model and the mass damper are kept the same as those in Chapters 3 and 4. Therefore, only parameters related to

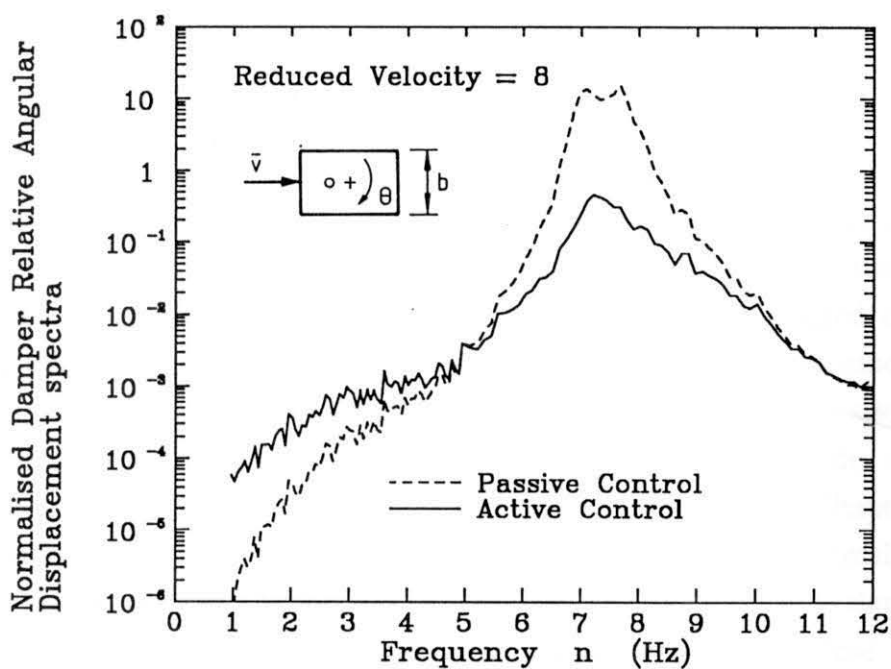


FIG. 7.5 COMPARISON OF DAMPER RELATIVE ANGULAR DISPLACEMENT SPECTRA BETWEEN ACTIVE AND PASSIVE CONTROL

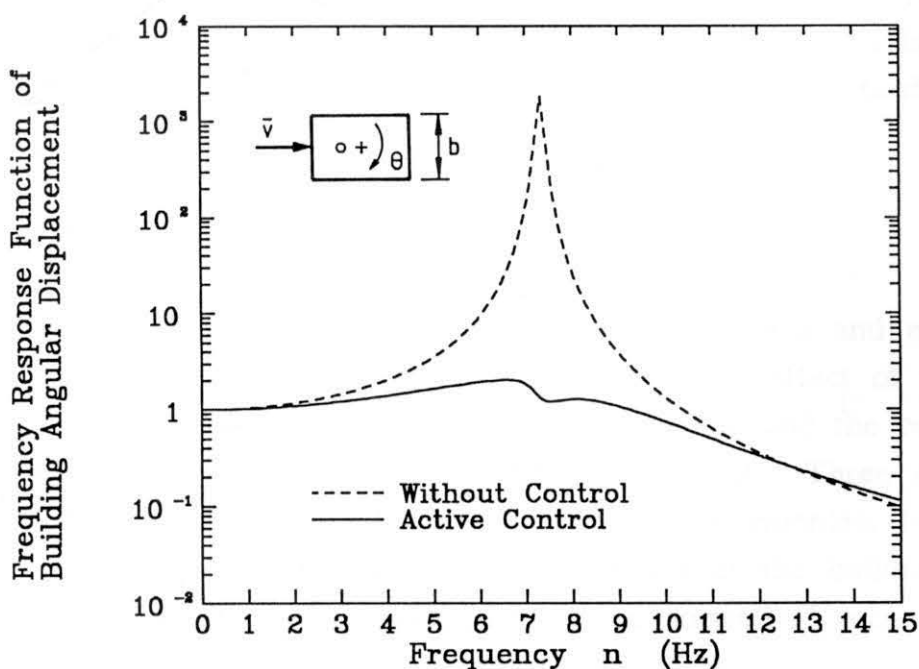


FIG. 7.6 FREQUENCY RESPONSE FUNCTIONS OF BUILDING ANGULAR DISPLACEMENT WITH AND WITHOUT ACTIVE CONTROL

the active control, i.e., K_t , ϵ and τ , are considered in conjunction with the structural response and the active control force.

7.4.1 Effect of parameters K_t and ϵ

The parameter K_t represents a proportional constant between the control force and the movement of the hydraulic piston while ϵ is the normalised loop gain. Figs. 7.8 to 7.10 show the variation of the standard deviations of the building top displacement, the damper relative displacement and the control force, respectively, with K_t and ϵ . Here input spectrum is a crosswind spectrum, for wind incidence normal to the wide face of the building and at a reduced velocity of 6 as described in Chapter 3. The mass damper is TMD 3. The standard deviations are normalised by the corresponding standard deviation of the building without any dampers. The normalised feedback gain τ equals 10. It is seen from these figures that increase of the parameter K_t reduced both building and damper responses, but the required control force increased and the increase rate of the control force was higher than the decrease rate of the building response. It is also seen that the parameter ϵ , when its value was larger than 5, did not affect the building response, the damper response and the control force. This phenomenon, at the same time, indicates that if the value of ϵ is selected to be larger than 5 the small deviation from this value in practical situation is not important.

7.4.2 Effect of parameters ϵ and τ

The same input spectrum, properties of the building and mass damper as those in the last section were used to analyse the effect of parameter ϵ and τ on the building response, the damper response and the control force. The proportional constant K_t/k_1^* of 0.05 was selected. Three contours are presented in Figs. 7.11 to 7.13, as functions of dimensionless feedback and loop gains τ and ϵ . All the standard deviations of the building response, the damper response and the control force are normalised according to Eqs. 7.10 and 7.11. Figs. 7.11 and 7.12 clearly indicated that a significant reduction in both building and damper responses can be achieved by the active mass damper control. A general trend observed from Figs. 7.11 to 7.13 was that

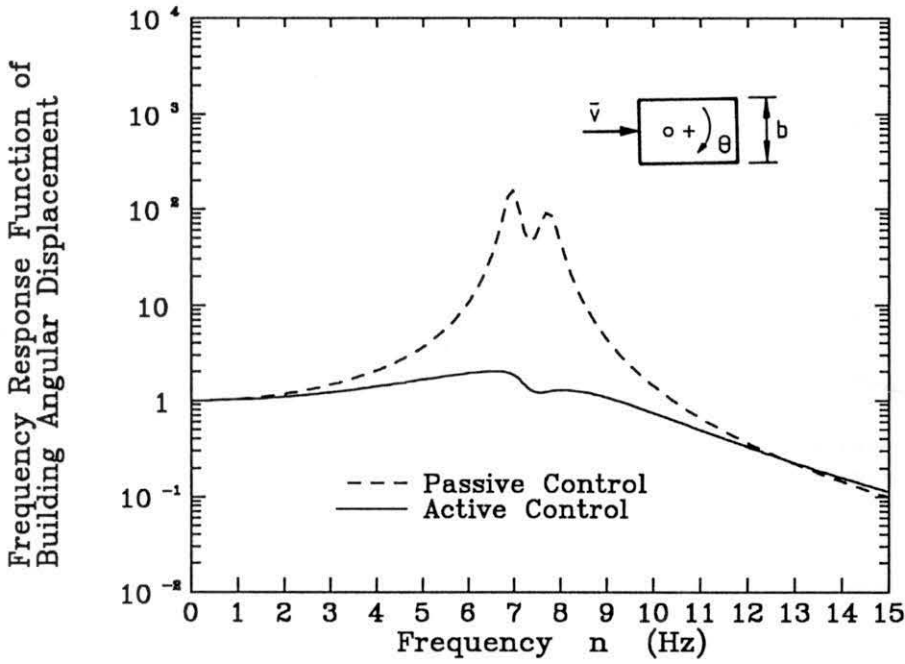


FIG. 7.7 COMPARISON OF FREQUENCY RESPONSE FUNCTIONS OF BUILDING AUGULAR DISPLACEMENT BETWEEN ACTIVE AND PASSIVE CONTROL

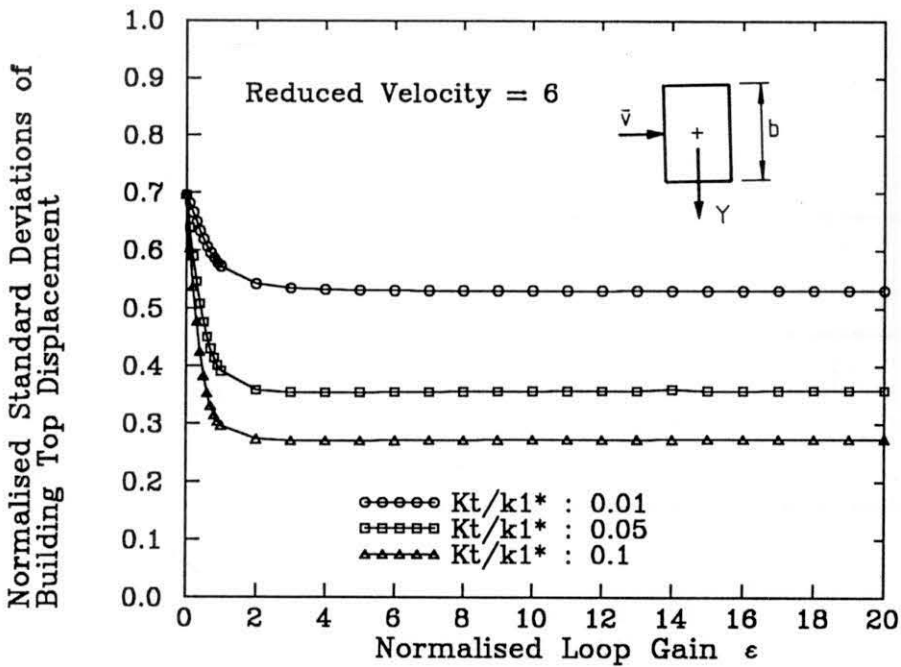


FIG. 7.8 NORMALISED STANDARD DEVIATIONS OF BUILDING TOP DISPLACEMENT IN CROSSWIND DIRECTION

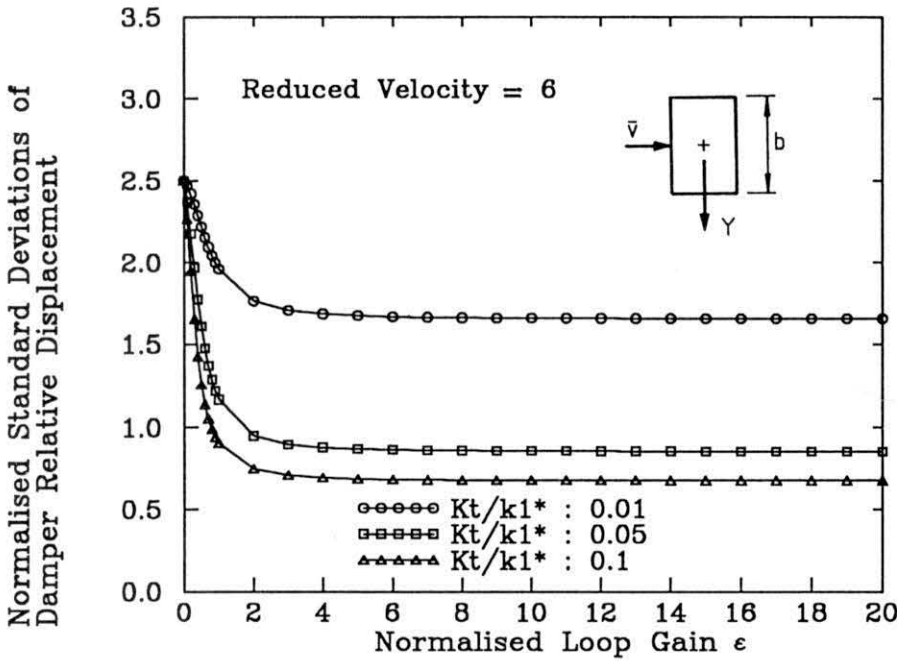


FIG. 7.9 NORMALISED STANDARD DEVIATIONS OF DAMPER RELATIVE DISPLACEMENT IN CROSSWIND DIRECTION

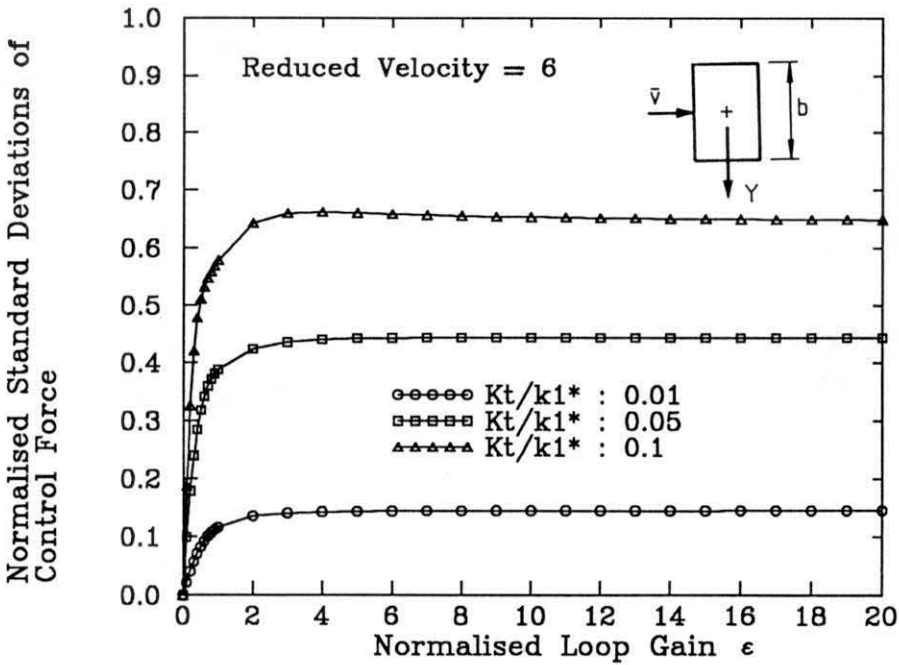


FIG. 7.10 NORMALISED STANDARD DEVIATIONS OF CONTROL FORCE FOR ACTIVE MASS DAMPER IN CROSSWIND DIRECTION

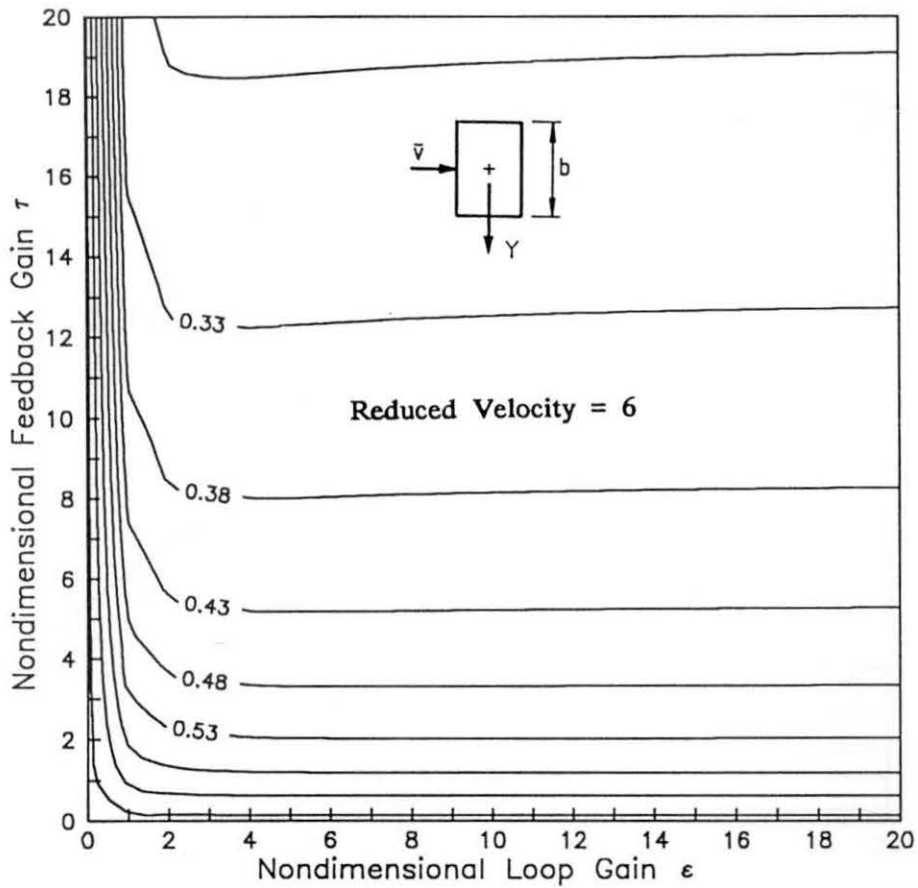


FIG. 7.11 RATIO OF TOP DISPLACEMENT STANDARD DEVIATIONS OF BUILDING WITH ACTIVE MASS DAMPER

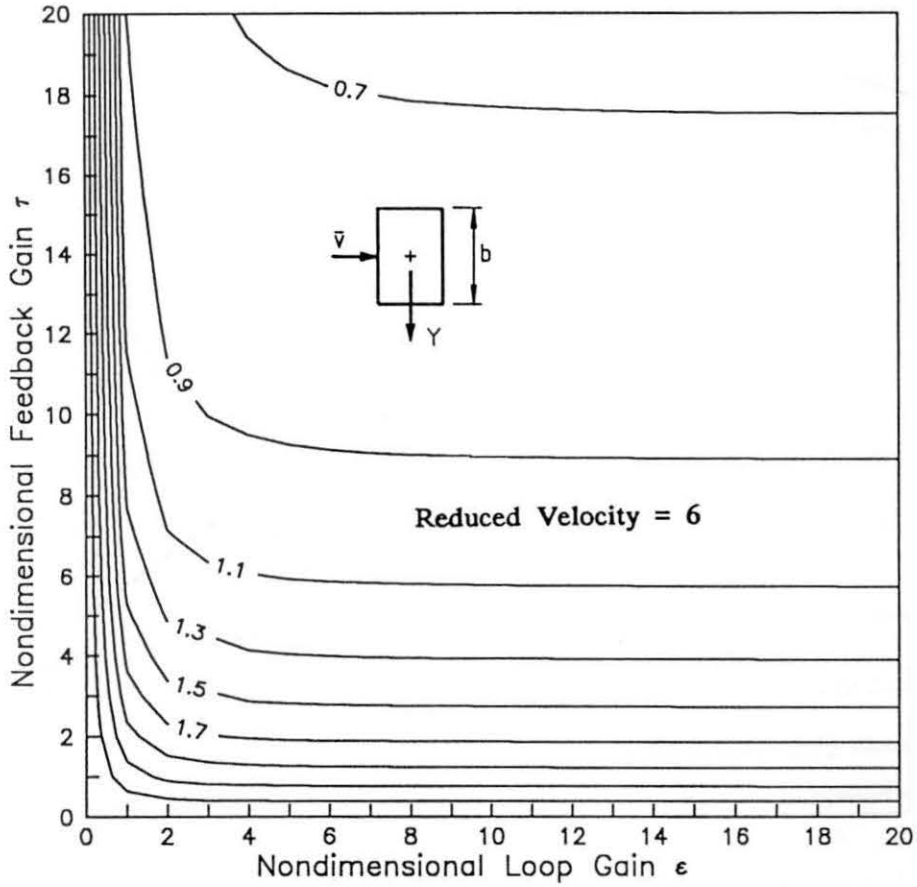


FIG. 7.12 RATIO OF RELATIVE DISPLACEMENT STANDARD DEVIATIONS OF ACTIVE MASS DAMPER

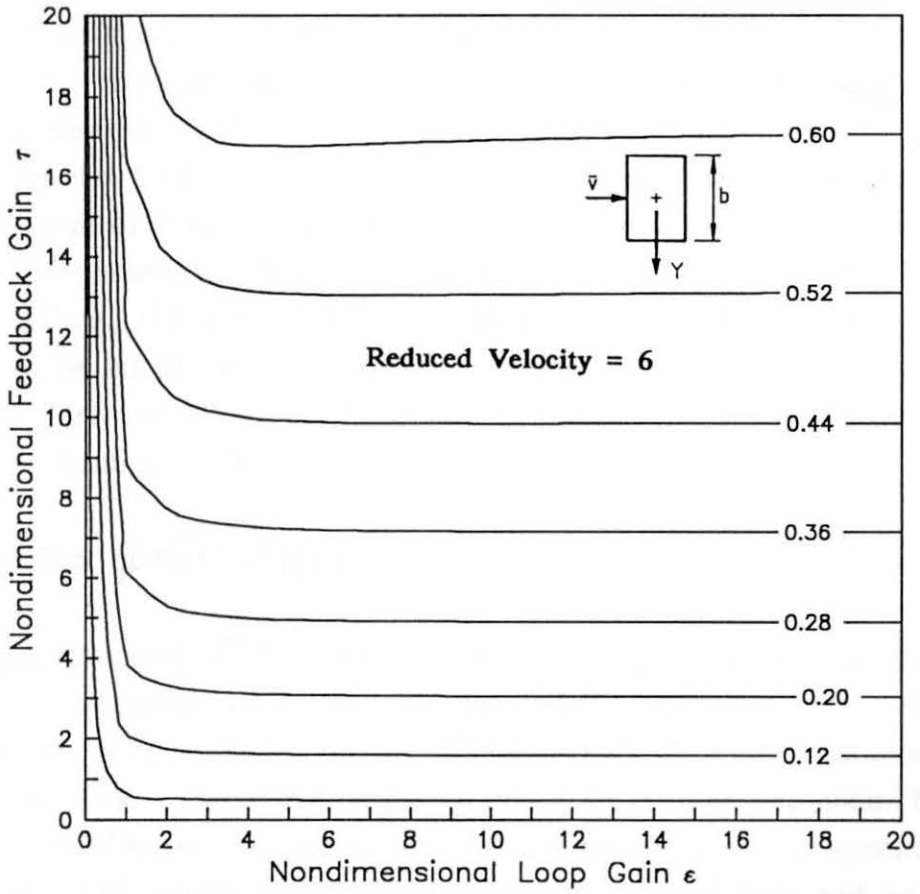


FIG. 7.13 RATIO OF STANDARD DEVIATIONS OF ACTIVE CONTROL FORCE

the responses reduced as the control force increased. It is also noted that, in the region $0 < \epsilon < 1$, all responses were very sensitive to small variation in ϵ . Therefore, this region was undesirable in practice. From the gradient of the contours, it is found that the rate of change of all responses reduced with the increase of the parameter τ . This means that there may be a limiting values for τ from a practical point of view.

Such contours can be used to determine the design parameters of the active mass damper. There are constraints on the magnitude of the control force and moment because of the limitation and the availability of the control devices. Therefore, a compromise has to be made between the reduction level of the building and damper responses and the required level of the control force. To show the magnitude of the control force in Fig. 7.13, an approximate estimate is presented. For a linear vibration mode of the building, the generalised wind force is about 1/3 of the total applied wind force on the building. By selecting $\tau = 5.5$ and $\epsilon = 5$, a normalised control force of 30%, which corresponds to the building response reduction of 58%, is about 1/10 of the total wind force.

7.4.3 Effect of wind excitations

As discussed in Chapters 3 to 5, the effectiveness of passive mass dampers depends on the external wind excitation to some extent. Therefore, it is necessary to investigate effects of wind excitation on active mass dampers. Two twist angle response spectra of the plain building, as studied in Chapter 4, were selected as torsional input spectra: one for incident wind normal to the wide face of the building and at a reduced wind velocity of 4; another for incident wind normal to the narrow face and at a reduced velocity of 8. For both input spectra, the properties of the building and mass damper models remain the same as those in Chapter 4. The normalised loop gain ϵ is equal to 5 while $K_{t\theta}/k_1^*$ is equal to 0.05. Figs. 7.14 to 7.16 show the variation of the building angular displacement, the damper relative angular displacement and the control moment with parameter τ . It is seen from these figure that, for the same value of τ , the active mass damper resulted in different motion reductions of the building for different torsional excitation spectra. However, the damper relative

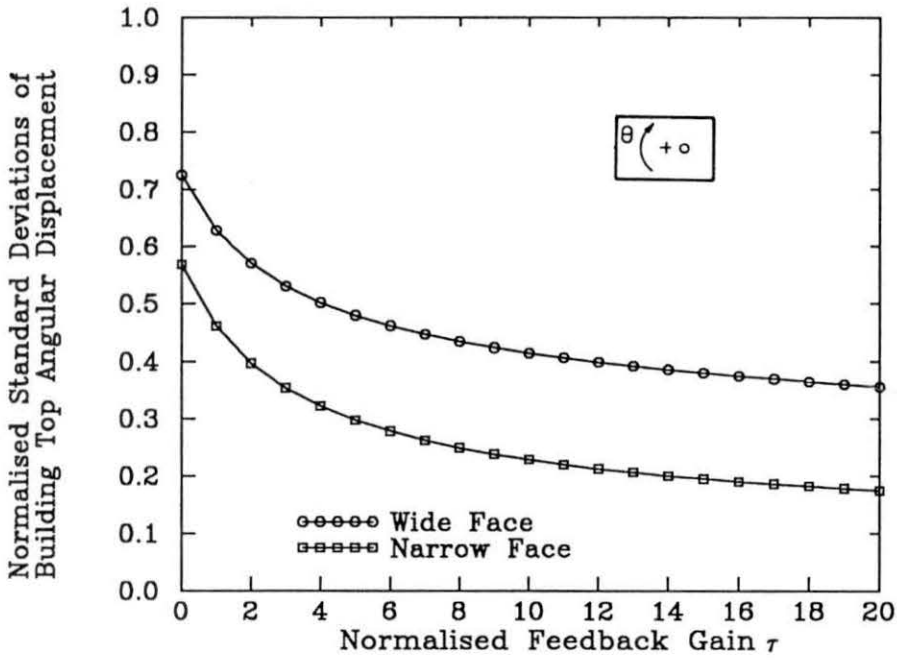


FIG. 7.14 NORMALISED STANDARD DEVIATIONS OF BUILDING TOP ANGULAR DISPLACEMENT

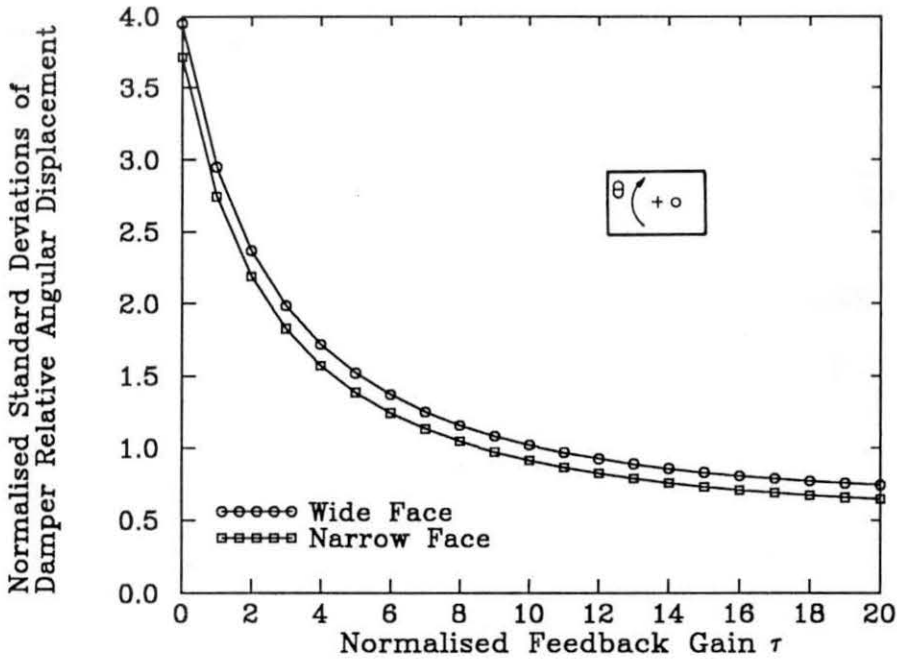


FIG. 7.15 NORMALISE STANDARD DEVIATIONS OF DAMPER RELATIVE ANGULAR DISPLACEMENT

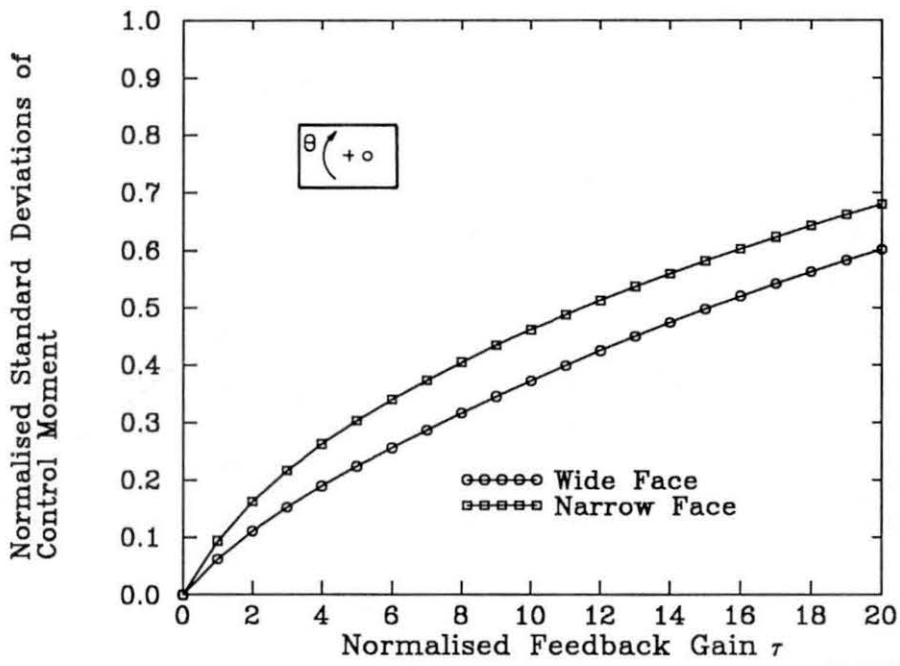


FIG. 7.16 NORMALISED STANDARD DEVIATIONS OF CONTROL MOMENT

angular displacement responses remained the same for both input spectra. This indicates that the parametric studies of an active mass damper control system should be conducted for a given wind environment. It is also seen that the building and damper responses reduced as the control moment increased. However, a reasonable value of τ should be less than 10 in the sense that a larger reduction of the building response can be achieved by a smaller control moment. Compared with the parameter ϵ , the parameter τ did not create any instability to the whole system within the range of values considered.

7.5 Conclusions

Based on the measured wind excitation or response spectra in wind tunnel for the tested aeroelastic building models, a semi-analytical method of selecting the design parameters of active mass dampers and estimating the motion reduction of both the building and the damper was proposed. This method not only provided a guideline for the experiments of the considered active control system in the future but also indicated a design procedure for the active control system by means of wind tunnel test technique. Although the present discussion was based on the simple aeroelastic models, the principle of the proposed method can be extended to the coupled translational-torsional vibration of tall buildings, in which a multi-degree-of-freedom aeroelastic model has to be used.

The results obtained by the semi-analytical method demonstrated that the active mass dampers can be used to significantly reduce the wind-induced response of tall buildings, if the control parameters were selected appropriately. The analysis of the frequency response functions also indicated that the active control system modified the structural characteristics, leading to a significant reduction of structural vibration. Under different wind excitations, the effectiveness of the active control system was different and therefore the parametric studies of the control system should be conducted for a given wind environment.

For the considered aeroelastic models, the results of parametric studies

of the active control system showed that, in general, the responses of the building and the damper decreased by increasing the control force and moment, that is, by increasing the feedback gain τ and the proportional constant K_t . However, the building, damper and control force responses were very sensitive to small variation of the normalised loop gain ϵ in the region $0 < \epsilon < 1$. Therefore this region is undesirable in practice. From the design contours, which were expressed as functions of dimensionless feedback and loop gains, the most beneficial and practical control parameters can be determined which result in a larger reduction of the building response and the damper response by using a small control force or moment.

Chapter 8

VIBRATION CONTROL OF SLENDER STRUCTURES BY TUNED LIQUID COLUMN DAMPERS

8.1 Introduction

In research fields, theory and practice depend on each other very closely. A new theory or analytical method needs to be proved through experiments or other practical activities while the proved theory can be used to explore new problems or lead to new experiments. In Chapter 3 to Chapter 7, vibration control of wind-induced tall buildings were discussed in terms of simple aeroelastic wind tunnel tests. The obtained results can be scaled up to the full scale tall buildings of which the first mode vibration is absolutely dominant. However, for slender structures such as TV towers, force and acceleration type responses usually involve more vibration modes and considering only the first mode for such response quantities may lead to non-conservative errors. Therefore, other aeroelastic modelling techniques or analytical methods have to be adopted to deal with wind-induced effects on these slender structures. In this Chapter and the next, several analytical formulations, which were derived by other scholars from the corresponding experiments for specific physical phenomenon, are combined to investigate wind-induced vibration control of complex slender structural systems.

In this Chapter an investigation is made of the possible application of tuned liquid column dampers, compared with conventional tuned mass dampers, in reducing the wind-induced response of slender structures. A tuned liquid column damper (TLCD) system is essentially a subsidiary vibration system composed of a liquid mass in a tube-like container. TLCD system suppresses the vibration of the main structures by the restoring force

due to the gravity acting upon the liquid and the damping effect due to the orifice(s) installed inside the container (Fig. 8.1). TLCD system may offer the following advantages: (1) simple equipments, arbitrary shapes and easy handling, (2) well-defined mechanism and quantitative definition of damping, (3) almost free from maintenance, (4) containers may be used as water tanks for drinking and emergency. Sakai et al. (1989) conducted a series of free vibration test and frequency sweep test of TLCD system. The experimental results were in good agreement with the analytical motion equations of TLCD system which were suggested by Saoka et al. (Sakai et al. 1989). However, studies pertaining to liquid column dampers in civil engineering applications are to date preliminary and based on greatly simplified structural and excitation models.

In present study, a slender structure is modelled as a lumped mass multi-degree-of-freedom system taking into account both bending and shear. The wind excitations are modelled as stochastic processes which are stationary in time and non-homogeneous in space. The analytical expressions for the wind excitation models were derived by Davenport (1961), Vickery and Clarke (1972) based on random vibration theory and experimental data. In order to conveniently include any desired number of vibration modes of a slender structure, a transfer matrix formulation is carried out to obtain response statistics. The methodology for periodic structures, for which identical mass and stiffness properties are used for every storey unit of the structure, is well documented in the literature (e.g., Lin and McDaniel, 1969; Yang and Lin, 1975) while the methodology and the accuracy of numerical computation for non-periodic structures are further discussed in this Chapter and Appendix C.

In addition, tuned liquid column and mass damper (TLCMD) system, which is composed of a mass damper filled with a liquid column (Fig. 8.2d), is investigated to determine the effects of liquid motion in a container on the effectiveness of such damper using water as mass. In the fundamental equations of TLCD and TLCMD, the liquid damping term is non-linear. An equivalent linearisation technique is employed to deal with this term in order to simplify the problem. Based on the derived formulation, a computer program was written by author and two numerical examples using

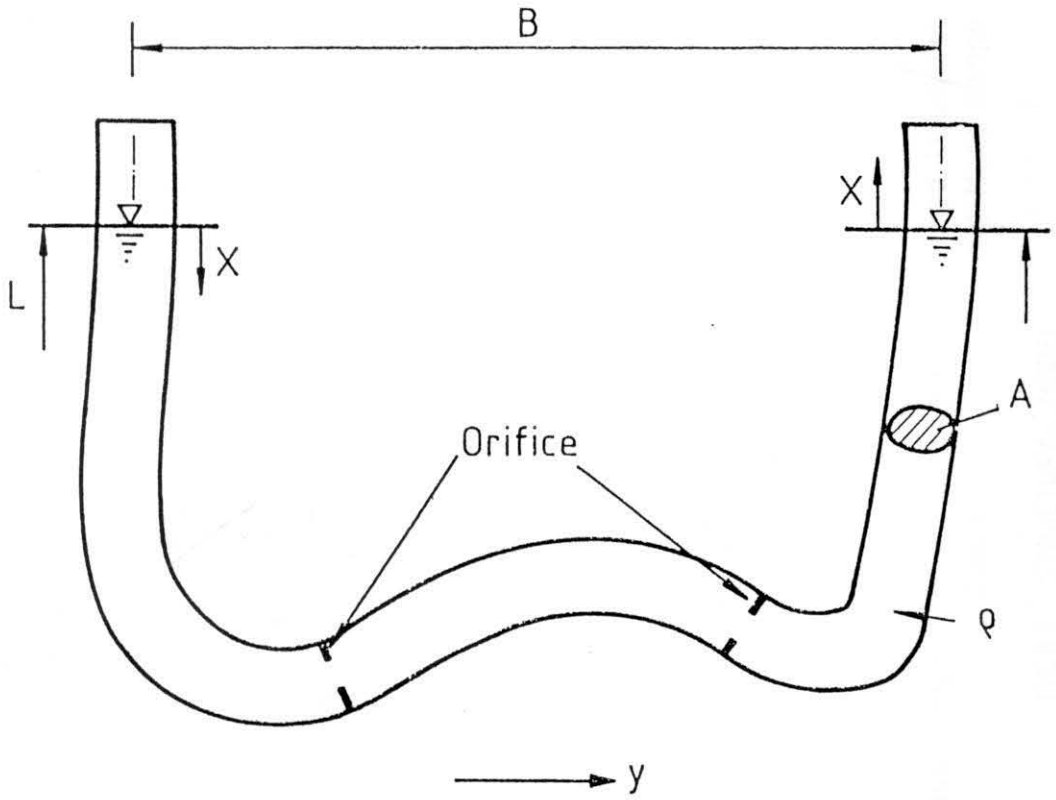


FIG. 8.1 LIQUID COLUMN TUBE

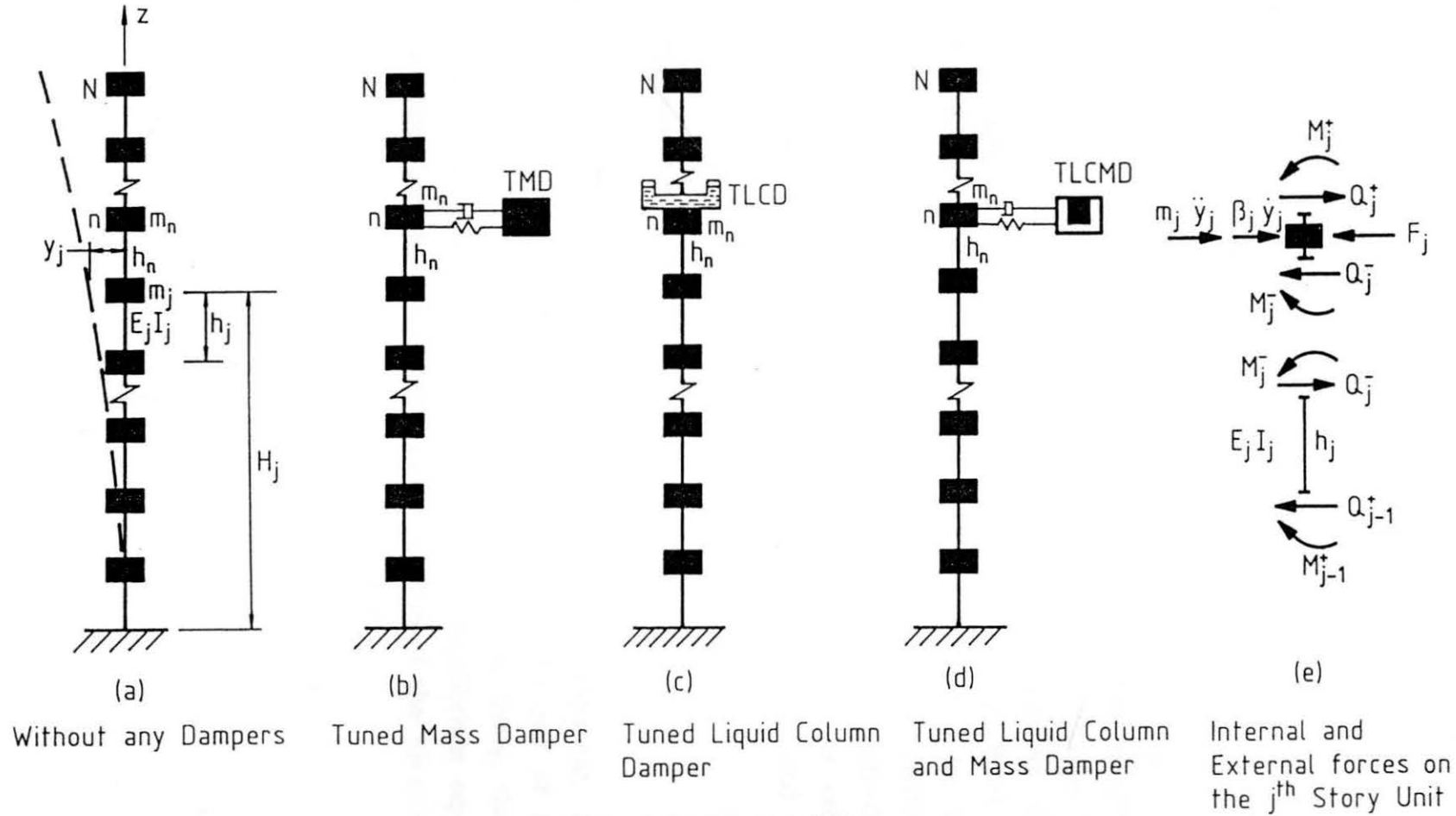


FIG.8.2 STRUCTURAL MODEL

a 76 storey, 306 m high office tower and a 370 m high TV tower are presented to demonstrate and compare the effectiveness of the abovementioned damping systems.

8.2 Formulation of the Problem

Consider an N lumped-mass multi-degree-of-freedom system as the structural model (Fig. 8.2a). Flexural rigidity between any two neighbouring lumped masses is constant. Wind excitation is applied to discrete lumped masses in the plane of the structure. Three types of passive damping devices are considered: a TMD (Fig. 8.2b), a TLCD (Fig. 8.2c) and a TLCMD (Fig. 8.2d). The damper is fixed on, or connected to, the n th mass and considered to be inside the structure so that wind excitation does not act on the damper directly. No attempt is made to use multi-dampers in this thesis. Wind excitation may be alongwind turbulence or crosswind wake excitation, which depends on the wind load spectrum used in the following formulae.

8.2.1 Transfer matrix

Let y_j^+ , φ_j^+ , M_j^+ and Q_j^+ be, respectively, the displacement, angular displacement, bending moment and shear force at the top end of the j th mass, as shown Fig. 8.2e. y_j^- , φ_j^- , M_j^- and Q_j^- are, respectively, the same quantities at the bottom end of the j th mass. The equilibrium equations, continuity equations and the force-displacement relation of the j th storey unit are given by Eq. 8.1, Eq. 8.2, and Eq. 8.3, respectively.

$$\left. \begin{aligned}
 M_j^+ &= M_j^- \\
 Q_j^- &= Q_{j-1}^+ \\
 M_j^- &= M_{j-1}^+ + Q_{j-1}^+ h_j \\
 Q_j^+ &= Q_j^- - m_j \ddot{y}_j - \beta_j \dot{y}_j + F_j
 \end{aligned} \right\} \dots \dots \dots (8.1)$$

$$\left. \begin{aligned} y_j^+ - y_j^- \\ \varphi_j^+ - \varphi_j^- \end{aligned} \right\} \dots \dots \dots (8.2)$$

$$E_j I_j y'' = M \dots \dots \dots (8.3)$$

in which m_j , β_j , h_j , E_j and I_j are, respectively, the mass, damping coefficient, height, elastic modulus and moment of inertia pertaining to storey unit j ; F_j is the wind force acting at the j th mass; a dot represents the first-order derivative with respect to time; a prime indicates the first-order derivative with respect to position coordinate.

Integrating Eq. 8.3 for the j th story unit and using the Fourier transformation, one obtains corresponding equations in frequency domain in the following matrix form:

$$\begin{bmatrix} \tilde{y}_j^+ \\ \tilde{\varphi}_j^+ \\ \tilde{M}_j^+ \\ \tilde{Q}_j^+ \end{bmatrix} = [T_j]_{4 \times 4} \begin{bmatrix} \tilde{y}_{j-1}^+ \\ \tilde{\varphi}_{j-1}^+ \\ \tilde{M}_{j-1}^+ \\ \tilde{Q}_{j-1}^+ \end{bmatrix} + \begin{bmatrix} 0 \\ 0 \\ 0 \\ \tilde{F}_j \end{bmatrix} \dots \dots \dots (8.4)$$

where "~" denotes the Fourier transform; and $[T_j]$ is known as a transfer matrix. The argument ω for the quantities in the frequency domain has been omitted for simplicity. The elements of $[T_j]$ are related to the structural parameters i.e.,

$$[T_j]_{4 \times 4} = \begin{bmatrix} 1 & h_j & \frac{h_j^2}{2E_j I_j} & \frac{h_j^3}{6E_j I_j} \\ 0 & 1 & \frac{h_j}{E_j I_j} & \frac{h_j^2}{2E_j I_j} \\ 0 & 0 & 1 & h_j \\ \bar{a}_j & h_j \bar{a}_j & \frac{h_j^2 \bar{a}_j}{2E_j I_j} & \frac{h_j^3 \bar{a}_j}{6E_j I_j} + 1 \end{bmatrix} \dots \dots (8.5)$$

where $i = \sqrt{-1}$; and $\bar{a}_j = (m_j \omega^2 - i \beta_j \omega)$.

It is clear from Eq. 8.4 that the transfer matrix $[T_j]$ represents the transfer mechanism for a storey unit. In the absence of excitation F_j , the j -1th state vector would be transferred to the j th state vector through $[T_j]$.

8.2.2 Tuned mass damper (TMD)

When a tuned mass damper is connected to the n th mass of the main structure by a dashpot and spring, its equations of motion are

$$\left. \begin{aligned} M_d \ddot{y}_d + K_d Z + C_d \dot{Z} &= 0 \\ y_d &= Z + y_n \end{aligned} \right\} \dots \dots \dots (8.6)$$

Where M_d , K_d , C_d and y_d are, respectively, the mass, spring constant, damping coefficient and absolute displacement of the damper; Z is the relative displacement of the damper with respect to the main structure; y_n is the absolute displacement of the n th mass of the main structure.

The Fourier transform of Eq. 8.6 will result in the following relationship in frequency domain:

$$\tilde{Z} = \frac{M_d \omega^2}{-M_d \omega^2 + K_d + i \omega C_d} \tilde{y}_n \dots \dots \dots (8.7)$$

For the main structure, the resultant external force, F_{nt} , applied at the n th mass is

$$F_{nt} = F_n + K_d Z + C_d \dot{Z} \dots \dots \dots (8.8)$$

Its Fourier transform is

$$\tilde{F}_{nt} = \tilde{F}_n + K_d \tilde{Z} + i \omega C_d \tilde{Z} \dots \dots \dots (8.9)$$

When \tilde{F}_{nt} is used in place of \tilde{F}_n in Eq. 8.4 for $j = n$, repeated application of Eq. 8.4 results in the following:

$$\begin{bmatrix} \tilde{y}_j^+ \\ \tilde{\varphi}_j^+ \\ \tilde{M}_j^+ \\ \tilde{Q}_j^+ \end{bmatrix} = \left(\prod_{k=1}^j [T_k] \right) \begin{bmatrix} 0 \\ 0 \\ \tilde{M}_0^+ \\ \tilde{Q}_0^+ \end{bmatrix} + \sum_{k=1}^{j-1} \left(\prod_{s=k+1}^j [T_s] \right) \begin{bmatrix} 0 \\ 0 \\ 0 \\ \tilde{F}_k \end{bmatrix} + \begin{bmatrix} 0 \\ 0 \\ 0 \\ \tilde{F}_j \end{bmatrix} \quad (8.10)$$

Note that the structure is fully fixed at the ground level and in obtaining Eq. 8.10 boundary conditions at the ground level are utilised. The top floor of the structure has a free boundary. By letting $j = N$, one can obtain a relation between the top state vector and the bottom state vector of the main structure; namely,

$$\begin{bmatrix} \tilde{y}_N^+ \\ \tilde{\varphi}_N^+ \\ 0 \\ 0 \end{bmatrix} = [A_1] \begin{bmatrix} 0 \\ 0 \\ \tilde{M}_0^+ \\ \tilde{Q}_0^+ \end{bmatrix} + \sum_{k=1}^N [A_{k+1}] \begin{bmatrix} 0 \\ 0 \\ 0 \\ \tilde{F}_k \end{bmatrix} \dots \dots \dots (8.11)$$

where

$$\left. \begin{aligned} [A_r] &= \prod_{s=r}^N [T_s] \quad (r=1, 2, \dots, N) \\ [A_{N+1}] &= [I] \end{aligned} \right\} \dots \dots \dots (8.12)$$

\prod is a chain product sign (from $k=1$ to $k=N$); $[I]$ is an identity matrix.

The third and fourth rows of Eq. 8.11 can be rearranged into

$$\begin{bmatrix} \tilde{M}_0^+ \\ \tilde{Q}_0^+ \end{bmatrix} = \begin{bmatrix} g_{11} & g_{12} & \dots & g_{1N} \\ g_{21} & g_{22} & \dots & g_{2N} \end{bmatrix} \begin{bmatrix} \tilde{F}_1 \\ \vdots \\ \tilde{F}_{nt} \\ \vdots \\ \tilde{F}_N \end{bmatrix} \dots \dots \dots (8.13)$$

where

$$\left. \begin{aligned} g_{1i} &= (a_1^{44} a_{i+1}^{34} - a_1^{34} a_{i+1}^{44}) / \Delta \\ g_{2i} &= (a_1^{33} a_{i+1}^{44} - a_1^{43} a_{i+1}^{34}) / \Delta \\ \Delta &= a_1^{43} a_1^{34} - a_1^{33} a_1^{44} \end{aligned} \right\} (i = 1, 2, \dots, N) \quad (8.14)$$

in which a_k^{ij} is the ij element of the matrix $[A_k]$.

Substituting Eq. 8.13 into the first and second rows of Eq. 8.10 and letting $j=n$, one obtains an expression for the displacement of the n th mass of the main structure.

$$\begin{bmatrix} \tilde{y}_n^+ \\ \tilde{\varphi}_n^+ \end{bmatrix} = \begin{bmatrix} s_{11} & s_{12} & \dots & s_{1N} \\ s_{21} & s_{22} & \dots & s_{2N} \end{bmatrix} \begin{bmatrix} \tilde{F}_1 \\ \vdots \\ \tilde{F}_{nt} \\ \vdots \\ \tilde{F}_N \end{bmatrix} \dots \dots \dots (8.15)$$

where

$$\left. \begin{aligned} s_{1i} &= b_1^{13} g_{1i} + b_1^{14} g_{2i} + b_{i+1}^{14} \\ s_{2i} &= b_1^{23} g_{1i} + b_1^{24} g_{2i} + b_{i+1}^{24} \end{aligned} \right\} (i = 1, 2, \dots, n-1) \quad (8.16)$$

$$\left. \begin{aligned} s_{1i} &= b_1^{13} g_{1i} + b_1^{14} g_{2i} \\ s_{2i} &= b_1^{23} g_{1i} + b_1^{24} g_{2i} \end{aligned} \right\} (i = n, n+1, \dots, N) \quad (8.17)$$

in which b_k^{ij} is the ij element of the matrix $[B_k]$, while

$$[B_k] = \prod_{s=k}^n [T_s] \quad (k = 1, 2, \dots, n) \quad \dots \dots \dots (8.18)$$

\tilde{F}_{nt} in Eq. 8.15 is a function of \tilde{y}_n^+ and \tilde{F}_n through Eq. 8.9 and Eq. 8.7.

Substituting Eq. 8.9 and Eq. 8.7, in that order, into Eq. 8.15, one obtains from the first row of Eq. 8.15:

$$\tilde{y}_n^+ = \sum_{j=1}^N \Psi_{1j} \tilde{F}_j \quad \dots \dots \dots (8.19)$$

in which

$$\Psi_{1j} = \frac{M_d \omega^2 - K_d - i\omega C_d}{M_d \omega^2 - K_d - i\omega C_d + s_{1n} M_d \omega^2 (K_d + i\omega C_d)} s_{1j} \quad \dots \dots \dots (8.20)$$

Thus the absolute displacement of the nth mass of the main structure, \tilde{y}_n , may be expressed in terms of the random wind excitation and known structural parameters. Based on Eq. 8.19, other structural response quantities which will be used to measure the effectiveness of the damper, can also be expressed in similar manner, i.e.,

$$\left. \begin{aligned} \tilde{M}_0 &= \sum_{j=1}^N \Omega_{1j} \tilde{F}_j ; & \tilde{Q}_0 &= \sum_{j=1}^N \Omega_{2j} \tilde{F}_j \\ \tilde{y}_N &= \sum_{j=1}^N \Theta_{1j} \tilde{F}_j ; & \tilde{\varphi}_N &= \sum_{j=1}^N \Theta_{2j} \tilde{F}_j \\ \tilde{Z} &= \sum_{j=1}^N \Gamma_{1j} \tilde{F}_j \end{aligned} \right\} \dots \dots \dots (8.21)$$

in which

$$\left. \begin{aligned} \Omega_{1j} &= g_{1j} - \lambda_1 s_{1j} ; & \Omega_{2j} &= g_{2j} - \lambda_2 s_{1j} \\ \Theta_{1j} &= \delta_{1j} - \eta_1 s_{1j} ; & \Theta_{2j} &= \delta_{2j} - \eta_2 s_{1j} \\ \Gamma_{1j} &= -s_{1j} M_d \omega^2 / \Delta_1 ; & \lambda_1 &= g_{1n} \Delta_2 / \Delta_1 \\ \lambda_2 &= g_{2n} \Delta_2 / \Delta_1 ; & \eta_1 &= \delta_{1n} \Delta_2 / \Delta_1 \\ \eta_2 &= \delta_{2n} \Delta_2 / \Delta_1 ; & \Delta_2 &= M_d \omega^2 (K_d + i\omega C_d) \\ \Delta_1 &= M_d \omega^2 - K_d - i\omega C_d + s_{1n} M_d \omega^2 (K_d + i\omega C_d) \\ \delta_{1j} &= a_1^{13} g_{1j} + a_1^{14} g_{2j} + a_{j+1}^{14} \\ \delta_{2j} &= a_1^{23} g_{1j} + a_1^{24} g_{2j} + a_{j+1}^{24} \end{aligned} \right\} \begin{aligned} &(j = 1, 2, \dots, N) \\ &\dots \dots (8.22) \end{aligned}$$

Eq. 8.19 and Eq. 8.21 are input-output relations in the frequency domain in which \tilde{F}_j ($j = 1, 2, \dots, N$) are the inputs and \tilde{y}_j , \tilde{M}_0 , \tilde{y}_N , \tilde{Q}_0 , $\tilde{\varphi}_N$ and \tilde{Z} are the outputs.

Finally, let

$$[A_r(m)] = \prod_{s=r}^m [T_s] \quad (r = 1, 2, \dots, m) \quad \dots \dots \dots (8.23)$$

Expressions for the state vector of the mth storey may be obtained, through Eq. 8.10 and other relevant equations as follows:

$$\left. \begin{aligned} \tilde{y}_m^+ &= \sum_{j=1}^N E_{1j} \tilde{F}_j ; & \tilde{\varphi}_m^+ &= \sum_{j=1}^N E_{2j} \tilde{F}_j \\ \tilde{M}_m^+ &= \sum_{j=1}^N E_{3j} \tilde{F}_j ; & \tilde{Q}_m^+ &= \sum_{j=1}^N E_{4j} \tilde{F}_j \end{aligned} \right\} \dots \dots \dots (8.24)$$

where

$$\left. \begin{aligned} E_{1j} &= \Lambda_{1j}(m) - \gamma_1 s_{1j} ; & E_{2j} &= \Lambda_{2j}(m) - \gamma_2 s_{1j} \\ E_{3j} &= \Lambda_{3j}(m) - \gamma_3 s_{1j} ; & E_{4j} &= \Lambda_{4j}(m) - \gamma_4 s_{1j} \end{aligned} \right\} \dots \dots \dots (8.25)$$

in which

$$\left. \begin{aligned} \Lambda_{1j}(m) &= \begin{cases} a_1^{13}(m)g_{1j} + a_1^{14}(m)g_{2j} + a_{j+1}^{14}(m) & j = 1, 2, \dots, m-1 \\ a_1^{13}(m)g_{1j} + a_1^{14}(m)g_{2j} & j = m, m+1, \dots, N \end{cases} \\ \Lambda_{2j}(m) &= \begin{cases} a_1^{23}(m)g_{1j} + a_1^{24}(m)g_{2j} + a_{j+1}^{24}(m) & j = 1, 2, \dots, m-1 \\ a_1^{23}(m)g_{1j} + a_1^{24}(m)g_{2j} & j = m, m+1, \dots, N \end{cases} \\ \Lambda_{3j}(m) &= \begin{cases} a_1^{33}(m)g_{1j} + a_1^{34}(m)g_{2j} + a_{j+1}^{34}(m) & j = 1, 2, \dots, m-1 \\ a_1^{33}(m)g_{1j} + a_1^{34}(m)g_{2j} & j = m, m+1, \dots, N \end{cases} \\ \Lambda_{4j}(m) &= \begin{cases} a_1^{43}(m)g_{1j} + a_1^{44}(m)g_{2j} + a_{j+1}^{44}(m) & j = 1, 2, \dots, m-1 \\ a_1^{43}(m)g_{1j} + a_1^{44}(m)g_{2j} + 1 & j = m \\ a_1^{43}(m)g_{1j} + a_1^{44}(m)g_{2j} & j = m+1, m+2, \dots, N \end{cases} \\ \gamma_1 &= \Lambda_{1n}(m)\Delta_2/\Delta_1 ; & \gamma_2 &= \Lambda_{2n}(m)\Delta_2/\Delta_1 \\ \gamma_3 &= \Lambda_{3n}(m)\Delta_2/\Delta_1 ; & \gamma_4 &= \Lambda_{4n}(m)\Delta_2/\Delta_1 \end{aligned} \right\} (8.26)$$

in which $a_{kj}^{(m)}$ is the ij element of the matrix $[A_k^{(m)}]$.

Note that the abovementioned formulae are also valid for the structure without a mass damper, whereby the mass of the damper in the formulae, M_d , is set equal to zero.

8.2.3 Tuned liquid column damper (TLCD)

A liquid column damper of an arbitrary shape is shown in Fig. 8.1, in which y is the displacement of the tube, x is the elevation change of the liquid and ρ , L , B , A are, respectively, the density, length of the liquid, the width, and cross-sectional area of the tube. The equation of motion of a liquid column is given by Saoka et al. and has been verified by a series of experiments (Sakai et al., 1989) as follows:

$$\rho AL\ddot{x} + \frac{1}{2}\rho A\xi|\dot{x}|\dot{x} + 2\rho Agx = -\rho AB\ddot{y} \quad \dots \dots \dots (8.27)$$

where ξ is defined as the coefficient of head loss (constant) governed by the opening ratio of the orifice(s) and g is the acceleration due to gravity. The natural angular frequency ω_1 or the natural period T_1 of the liquid column tube is given in the following equation:

$$\omega_1 = \sqrt{2g/L} \quad \text{or} \quad T_1 = 2\pi\sqrt{L/2g} \quad \dots \dots \dots (8.28)$$

It can be seen that the basic equations of a liquid column damper are similar to those of a mass damper except that there is a non-linear damping term in TLCD system. In a liquid column damper, the damper mass is represented by the mass of liquid column and the restoring force is attributed to the gravity acting upon the liquid. Therefore, it is expected that a TLCD system can be as effective as a TMD system.

When a tuned liquid column damper, as shown in Fig. 8.3, is fixed on the n th mass of the main structure, the interactive vibration equations are

$$\left. \begin{aligned}
 y_n^+ &= y_n^- \quad (= y_n) \\
 \varphi_n^+ &= \varphi_n^- \\
 M_n^+ &= M_n^- \\
 Q_n^+ &= Q_n^- - (\rho AL + m_n) \ddot{y}_n - \beta_n \dot{y}_n - \rho AB \ddot{x} + F_n \\
 \rho AL \ddot{x} + \frac{1}{2} \rho A \xi | \dot{x} | \dot{x} + 2 \rho A g x &= -\rho AB \ddot{y}_n
 \end{aligned} \right\} \dots \dots \dots (8.29)$$

For other storey units of the structure, i.e., when $j \neq n$, Eq. 8.1 is still valid.

The experimental data of the liquid column tube also showed that non-linear behaviour of the orifice damping was not high and, in terms of application to practical structures, the method of equivalent linearisation has the greatest potential (Caughey, 1963; Wen, 1980), especially for narrow-band response. Thus it is reasonable to adopt the method of equivalent linearisation to deal with the non-linear damping term rather than use Monte-Carlo method, which is very time-consuming in this case.

In this study, wind excitations are modelled as stationary Gaussian processes. The equivalent linearisation technique may be independently applied to the last equation of Eq. 8.29 (Iwan and Yang, 1972; Spanos and Iwan, 1978).

Let the equivalent linear equation be

$$\rho AL \ddot{x} + 2 \rho AC_p \dot{x} + 2 \rho A g x = -\rho AB \ddot{y}_n \dots \dots \dots (8.30)$$

The equation error will be

$$e = \frac{1}{2} \rho A \xi | \dot{x} | \dot{x} - 2 \rho AC_p \dot{x} \dots \dots \dots (8.31)$$

Obviously, the equation error, e , is also a random process.

The mean square value of the error can be minimised if

$$\frac{\partial E(e^2)}{\partial C_p} = 0 \dots \dots \dots (8.32)$$

in which $E() =$ expected value.

From Eq. 8.32, one can obtain:

$$C_p = \frac{\xi E(|\dot{x}| \dot{x}^2)}{4E(\dot{x}^2)} \dots \dots \dots (8.33)$$

By using the Gaussian probability density function,

$$E(\dot{x}^2 |\dot{x}|) = \int_{-\infty}^{\infty} \frac{|\dot{x}| \dot{x}^2}{\sqrt{2\pi} \sigma_{\dot{x}}} \exp\left(-\frac{\dot{x}^2}{2\sigma_{\dot{x}}^2}\right) d\dot{x}$$

$$= \frac{2\sqrt{2}}{\sqrt{\pi}} \sigma_{\dot{x}}^3 \dots \dots \dots (8.34)$$

Thus, one obtains

$$C_p = \frac{\sigma_{\dot{x}} \xi}{\sqrt{2\pi}} \dots \dots \dots (8.35)$$

in which $\sigma_{\dot{x}}$ is the standard deviation of the liquid elevation velocity \dot{x} . Since the equivalent damping coefficient, C_p , depends on the response, $\sigma_{\dot{x}}$, of the liquid column, an iteration solution procedure is generally required.

Using Eq. 8.30 to replace the last equation of Eq. 8.29 and then taking Fourier transforms of Eq. 8.29 yields

$$\left. \begin{aligned} \tilde{y}_n^+ &= \tilde{y}_n^- \quad (= \tilde{y}_n) \\ \tilde{\varphi}_n^+ &= \tilde{\varphi}_n^- \\ \tilde{M}_n^+ &= \tilde{M}_n^- \\ \tilde{Q}_n^+ &= \tilde{Q}_n^- + [\omega^2 \rho A L + \omega^4 \rho A B^2 / (2g - \omega^2 L + 2iC_p \omega) + \omega^2 m_n - i\omega \beta_n] \tilde{y}_n + \tilde{F}_n \end{aligned} \right\} \dots \dots \dots (8.36)$$

and

$$\tilde{x} = \frac{\omega^2 B}{2g - \omega^2 L + 2iC_p \omega} \tilde{y}_n \dots \dots \dots (8.37)$$

The term, $\omega^2 \rho A L + \omega^4 \rho A B^2 / (2g - \omega^2 L + 2iC_p \omega)$, indicates the effect of

the liquid column tube on the main structure. Since the tuned liquid column damper is not connected to other parts of the structure (i.e., $j \neq n$), Eq. 8.1 is still valid for the TLCD–structure interactive system when $j \neq n$. As a result, in similar manner to the TMD–structure system analysis, one obtains similar input–output relations in the frequency domain for the TLCD–structure system.

8.2.4 Tuned liquid column/mass damper (TLCMD)

Some existing TMDs (e.g. Sydney Centrepoint Tower) are composed of a rigid container filled with water. If the water inside the container is kept relatively still, the device is in fact a TMD. However, if the water has a relative movement with respect to the container, it will affect the motion of the container; in turn, the container as a damper will exhibit different characteristics when suppressing the vibration of the main structure. Therefore, it is necessary to study the interactions between the liquid and the container in a combined damper system. Here TLCMD system is chosen as a preliminary study of this problem.

A TLCMD is, in fact, a TLCD shown in Fig. 8.3 connected to the n th mass of the main structure by a spring and dashpot (see Fig. 8.2 d). When wind–induced vibration of the structure equipped with a TLCMD occurs, both the container and the liquid in the container oscillate. If a TLCMD is fixed on the n th mass of the main structure, it can be shown that the interactive motion equations of the system are

$$\left. \begin{aligned}
 \rho AL\ddot{x} + \frac{1}{2} \rho A\xi |\dot{x}| \dot{x} + 2\rho Agx &= -\rho AB\ddot{y}_d \\
 \rho AB\ddot{x} + (\rho AL + M_d)\ddot{y}_d + K_d Z + C_d \dot{Z} &= 0 \\
 y_d &= Z + y_n
 \end{aligned} \right\} \dots \dots \dots (8.38)$$

in which M_d is the container mass exclusive of liquid column mass; y_d is the absolute displacement of the container; other parameters are the same as before.

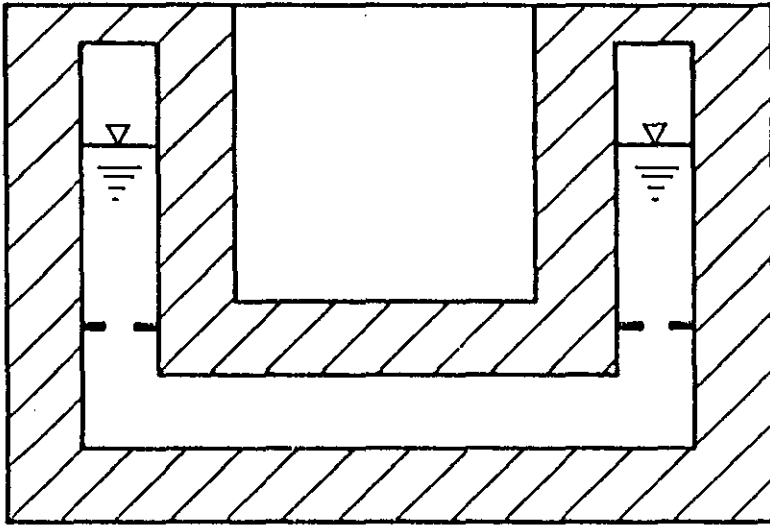


FIG. 8.3 TUNED LIQUID COLUMN DAMPER SYSTEM

From Eq. 8.38, a relation similar to Eq. 8.7 in frequency domain may be derived if the first equation of Eq. 8.38 is replaced by Eq. 8.30:

$$\tilde{Z} = \frac{\frac{\rho AB^2 \omega^4}{-\omega^2 L + 2C_p i \omega + 2g} + \omega^2 (\rho AL + M_d)}{i \omega C_d + K_d - \left[\frac{\rho AB^2 \omega^2}{-\omega^2 L + 2C_p i \omega + 2g} + \omega^2 (\rho AL + M_d) \right]} \tilde{y}_n \quad \dots (8.39)$$

Comparing Eq. 8.39 with Eq. 8.7, one finds that both equations will be identical if the density of water, ρ , equals zero or the equivalent damping coefficient, C_p , is infinite. The latter means that the total mass, $\rho AL + M_d$, should be considered when the tuned frequency is calculated in order to find the effect of the liquid motion on this combined damper in comparison with the corresponding TMD.

As before, using the same procedure as for the TMD-structure system, one obtains the input-output relations of the TLCMD-structure system.

8.2.5 Spectral relationships and system responses

Wind loads on a building are often modelled as stochastic processes which are stationary in time and nonhomogeneous in space. At the same time, the TMD-structure system is linear, and the TLCD system as well as the TLCMD system are also linearised. Thus, the input-output relations in the frequency domain, e.g., Eq. 8.21 and Eq. 8.24, can be used to construct the relationships between the cross-spectral densities of the inputs F_j ($j = 1, 2, \dots, N$) and those of the outputs, using the following definitions

$$\left. \begin{aligned} \Phi_{F_i F_j}(\omega) &= \lim_{T \rightarrow \infty} \frac{E[\tilde{F}_i \tilde{F}_j^*]}{2\pi T} \\ \Phi_{X_i X_j}(\omega) &= \lim_{T \rightarrow \infty} \frac{E[\tilde{X}_i \tilde{X}_j^*]}{2\pi T} \end{aligned} \right\} \dots (8.40)$$

in which $E[]$ = the ensemble average, and an asterisk denotes the complex

conjugate; X_i may represent any output quantity, e.g., y_n , M_0 , Q_0 , etc. T is the truncation time.

The spectral densities of the base moment, the base shear force, the top floor displacement, the top floor angular displacement, the n th mass displacement and the relative displacement of the tuned mass damper can be obtained by substituting Eq. 8.21 into Eq. 8.40:

$$\left. \begin{aligned}
 \Phi_{M_0 M_0}(\omega) &= \sum_{i=1}^N \sum_{j=1}^N \Omega_{1i} \Phi_{F_i F_j}(\omega) \Omega_{1j}^* \\
 \Phi_{Q_0 Q_0}(\omega) &= \sum_{i=1}^N \sum_{j=1}^N \Omega_{2i} \Phi_{F_i F_j}(\omega) \Omega_{2j}^* \\
 \Phi_{y_N y_N}(\omega) &= \sum_{i=1}^N \sum_{j=1}^N \Theta_{1i} \Phi_{F_i F_j}(\omega) \Theta_{1j}^* \\
 \Phi_{\varphi_N \varphi_N}(\omega) &= \sum_{i=1}^N \sum_{j=1}^N \Theta_{2i} \Phi_{F_i F_j}(\omega) \Theta_{2j}^* \\
 \Phi_{y_n y_n}(\omega) &= \sum_{i=1}^N \sum_{j=1}^N \Psi_{1i} \Phi_{F_i F_j}(\omega) \Psi_{1j}^* \\
 \Phi_{Z Z}(\omega) &= \sum_{i=1}^N \sum_{j=1}^N \Gamma_{1i} \Phi_{F_i F_j}(\omega) \Gamma_{1j}^*
 \end{aligned} \right\} \dots \dots \dots (8.41)$$

The expression for the response at other locations of the TMD-structure system can also be obtained by substituting Eq. 8.24 into Eq. 8.40. In addition, the power spectral density of the acceleration response is equal to the power spectral density of the displacement response multiplied by ω^4 . For instance, the power spectral density of the top acceleration response is given by

$$\Phi_{\ddot{y}_N \ddot{y}_N}(\omega) = \omega^4 \Phi_{y_N y_N}(\omega) \dots \dots \dots (8.42)$$

For the TLCD-structure system and the TLCMD-structure system, in the same manner one can obtain the required power spectral density of the system response. For instance, the power spectral density of the liquid elevation change in the TLCD system, can be calculated according to the following equation:

$$\Phi_{xx}(\omega) = \sum_{i=1}^N \sum_{j=1}^N \Gamma_{2i} \Phi_{F_i F_j}(\omega) \Gamma_{2j}^* \dots \dots \dots (8.43)$$

in which

$$\Gamma_{2j} = \frac{\omega^2 B}{-\omega^2 L + 2g + 2C_p i\omega} s_{1j} \quad (j = 1, 2, \dots, N)$$

In the case of a linear structure the mean wind force in the alongwind direction is responsible for the mean alongwind response of the structure alone. Since both the mean wind force and the mean structure response are static and constant, they can be computed separately. Consequently, the standard deviations of various structure response quantities can be evaluated through numerical integrations. For example, for the TMD-structure system, the standard deviations of the base moment, the base shear force, the top floor displacement, the top floor angular displacement, the nth mass displacement and the relative displacement of the tuned mass damper with respect to the nth mass of the main structure as well as the top floor acceleration are obtained from

$$\left. \begin{aligned} \sigma_{M_0} &= \left[\int_{-\infty}^{\infty} \Phi_{M_0 M_0}(\omega) d\omega \right]^{\frac{1}{2}}; & \sigma_{Q_0} &= \left[\int_{-\infty}^{\infty} \Phi_{Q_0 Q_0}(\omega) d\omega \right]^{\frac{1}{2}} \\ \sigma_{y_N} &= \left[\int_{-\infty}^{\infty} \Phi_{y_N y_N}(\omega) d\omega \right]^{\frac{1}{2}}; & \sigma_{\varphi_N} &= \left[\int_{-\infty}^{\infty} \Phi_{\varphi_N \varphi_N}(\omega) d\omega \right]^{\frac{1}{2}} \\ \sigma_{y_n} &= \left[\int_{-\infty}^{\infty} \Phi_{y_n y_n}(\omega) d\omega \right]^{\frac{1}{2}}; & \sigma_z &= \left[\int_{-\infty}^{\infty} \Phi_{zz}(\omega) d\omega \right]^{\frac{1}{2}} \\ \sigma_{\dot{y}_N} &= \left[\int_{-\infty}^{\infty} \Phi_{\dot{y}_N \dot{y}_N}(\omega) d\omega \right]^{\frac{1}{2}} \end{aligned} \right\} \dots \dots (8.44)$$

For the TLCD-structure system, the standard deviation of the liquid elevation velocity, $\sigma_{\dot{x}}$, is necessary to complete an iteration solution procedure. It can be obtained from Eq. 8.43 as follows:

$$\sigma_{\dot{x}} = \left[\int_{-\infty}^{\infty} \omega^2 \Phi_{xx}(\omega) d\omega \right]^{\frac{1}{2}} \dots \dots \dots (8.45)$$

The same may be applied to the TLCMD-structure system.

8.3 Wind Load Spectra

The aerodynamic forces acting on structures arise from the superposition of static loads due to mean wind velocity and fluctuating loads associated with atmospheric turbulence and wake excitation, as well as self-excited loads due to the oscillation of the structures themselves. The mean structure response, which is caused by the mean wind pressure, is not reduced by a damper in a linear system and, therefore, it is not included in this study. Furthermore, no reliable theoretical model up to now is developed to describe torsional excitation. Only the alongwind turbulence and the crosswind wake excitation are considered at this stage. It must be emphasised that the TLCD and the TLCMD considered in this thesis are uni-directional and thereby the alongwind turbulence and the crosswind wake excitation are applied to the structural system independently. However, it is not difficult to extend the abovementioned analysis to two or three dimensional analysis utilising bi-directional TLCD and TLCMD damper systems.

8.3.1 Alongwind turbulence spectrum

The spectrum of longitudinal turbulence proposed by Davenport (1961) is used in this thesis. For a multi-degree-of-freedom system, the one-sided cross-spectral density representation of alongwind force in frequency domain (in radians per second) is

$$\Phi_{F_i F_j}(\omega) = 24K_0 \bar{W}_{10}^2 C_a^2 (H_i H_j / 100)^{\alpha} A_i A_j R(H_i, H_j, \omega) S_f(\omega) / (2\pi) \quad (8.46)$$

where the function, $R(H_i, H_j, \omega)$, reflects the spanwise correlation of the fluctuating force and is represented by

$$R(H_i, H_j, \omega) = \exp\left[- \frac{C_1 |\omega| |H_i - H_j|}{2\pi \bar{V}_{10}} \right] \dots \dots \dots (8.47)$$

The unit fluctuating wind velocity spectrum, $S_f(\omega)$, is given by

$$S_f(\omega) = \frac{2t^2}{3n(1+t^2)^{4/3}} \dots \dots \dots (8.48)$$

in which $t = 1200n/\bar{V}_{10}$; $n = \omega/2\pi$; \bar{V}_{10} = mean wind velocity in metres per second at 10m above the ground; \bar{W}_{10} = mean wind pressure at 10m = $\frac{1}{2} \rho_a \bar{V}_{10}^2$; ρ_a = air density; K_0 = surface drag coefficient; C_a = drag coefficient; C_1 = a constant; H_i, H_j = heights of the i th and j th storey mass above the ground, respectively; α = a constant; A_i, A_j = wind areas of the i th and j th mass, respectively.

8.3.2 Crosswind wake spectrum

Vickery and Clarke (1972) proposed a Gaussian type one-sided crosswind force spectrum in the frequency domain (in radians per second) of the form shown below:

$$\Phi_{F_i F_j}(\omega) = \frac{(\rho_a C_l \bar{V}_i \bar{V}_j)^2 A_i A_j}{8\pi^{3/2} B_s f_{s_i} f_{s_j}} \cos(\alpha_1 R) \exp(-(R/\alpha_2)^2) \times \\ \times \sqrt{\exp[-(1 - \omega/2\pi f_{s_i})^2/B_s^2] \cdot \exp[-(1 - \omega/2\pi f_{s_j})^2/B_s^2]} \quad (8.49)$$

where $\cos(\alpha_1 R) \exp(-(R/\alpha_2)^2)$ is the spanwise correlation function of crosswind wake excitation; $R = 2|H_i - H_j|/(D_i + D_j)$; α_1 and α_2 are nondimensional coefficients related to the correlation length; D_i, D_j = diameters of the structure at heights H_i and H_j , respectively; \bar{V}_i, \bar{V}_j = mean wind velocities at the height H_i, H_j , respectively; $\bar{V}_i = \bar{V}_{10}(H_i/10)^\alpha$, $\bar{V}_j = \bar{V}_{10}(H_j/10)^\alpha$ in metres per second; C_l = lift coefficient; B_s = a measure of the relative width of the spectral peak; f_{s_i}, f_{s_j} = vortex shedding frequency at heights H_i and H_j , respectively, and $f_{s_i} = SV_i/D_i$, $f_{s_j} = SV_j/D_j$; S = Strouhal number.

Eq. 8.49 was first proposed by Vickery for the structures with a circular cross section, assuming $\alpha_1 = 2/3$ and $\alpha_2 = 3$. The analysis of a limited number of experimental results conducted by Reinhold has shown that Eq. 8.49 can also be applied to buildings of square cross section using values like $\alpha_1 = \frac{1}{2}$ and $\alpha_2 = 5$ (Solari, 1985). Solari further suggested $\alpha_1 = \frac{1}{2}$, $\alpha_2 = 5$ for the middle part of the building and $\alpha_1 = 0$, $\alpha_2 = 5$ for the upper

third of the building.

An improved crosswind wake excitation model which included lock-in excitation was suggested by Vickery and Basu (1983). This improved model is based on the original model but altered to include an aerodynamic damping term which depends non-linearly on response amplitude. However, the application of this model to full scale structures in terms of transfer matrix method needs further investigation.

Finally, it may be helpful to point out that the assumption on wind excitation co-spectrum in Chapter 6 is basically consistent with Eqs. 8.46 and 8.49.

8.4 Numerical Examples

Two numerical examples of different structural types and properties are considered for illustrative purposes: a 76 storey, 306m high and 44m square concrete office tower with 7.4m chamfer at the corners; a 370m high TV tower with a circular cross-section which tapers from 20m diameter to 10m diameter, and with a turret which is located at 200m high.

Many wind sensitive structures cannot be simplified to periodic structures as discussed by Lin and McDaniel (1969), and Yang and Lin (1981). Therefore, the matrix multiplication operation is unavoidable when computing the product chain of the matrices, e.g., $[A_r(m)]$. Studies in Appendix B shows that, for the non-periodic cantilever structures, the accuracy of computer results using direct matrix multiplication is guaranteed.

8.4.1 TV tower

The tower is modelled as a 9 degree-of-freedom cantilever model. The structural data used in the analysis are listed in Table 8.1. The first four natural frequencies of the structure are 0.199, 0.334, 0.821, and 1.281 Hz, respectively. Three types of damping devices, as described before, are individually fixed on, or connected to, the 4th mass of the main structure

TABLE 8.1. STRUCTURAL DATA FOR TV TOWER

Node number	Height h_j (m)	Mass m_j (tonnes)	Stiffness $E_j I_j \times 10^8$ (kN-m ²)	Damping β_j (kN/m/s)	Wind area A_j (m ²)
(1)	(2)	(3)	(4)	(5)	(6)
1	40.0	6134	1162.80	179.92	977.8
2	56.0	3853	377.80	112.89	920.6
3	56.0	2578	203.74	75.54	638.6
4	54.5	3032	59.30	88.82	947.6
5	38.5	692	33.08	20.28	249.5
6	25.0	85	8.52	2.49	150.0
7	35.5	72	2.13	2.11	98.2
8	35.5	51	0.17	1.48	47.2
9	28.5	23	0.08	0.68	20.0

where turrets are located. In order to facilitate a reasonable comparison between the three types of dampers, the mass of all dampers is kept the same and all natural frequencies are tuned to the fundamental frequency of the main structure. As for the damper damping, a sound choice is to optimise the structural responses in engineering practical limit by using different damping ratio of critical ζ in the tuned mass damper or coefficient of head loss ξ in the tuned liquid column damper. The aerodynamic data pertaining to alongwind excitation are:

- $\bar{V}_{1,0}$ = reference mean wind velocity at 10m height above ground
= 26.41 m/s;
- α = exponent for the mean wind velocity profile power law
= 0.15
- z_g = gradient height = 300m; \bar{V}_G = gradient velocity = 44 m/s;
- C_a = drag coefficient = 0.7; ρ_a = air density = 1.2 kg/m³;
- C_1 = 7.0 and K_0 = 0.007, constants in the wind spectrum.

The abovementioned aerodynamic data pertain to an open country terrain [Terrain Category 2 as described in the Australian Standard, SAA Loading Code, Part 2: Wind Loads; AS 1170.2-1989].

The aerodynamic data pertaining to wake excitation are:

- $\bar{V}_{1,0}$ = 15 m/s;
- α = 0.15;
- C_l = lift coefficient = 0.2;
- S = Strouhal number = 0.22;
- B_s = constant related to the relative width of the relative spectral peak
= 0.32.

$\bar{V}_{1,0}$ = 26.41 m/s was also used to compute the structural response under crosswind wake excitation. It is found that, when $\bar{V}_{1,0}$ = 26.41 m/s, vortex shedding resonance will develop at the second natural frequency of the tower. As a result the top displacement response of tower at the second mode of the tower is larger than that at the first mode (see Fig. 8.4). After considering that the present dampers are tuned to the first natural

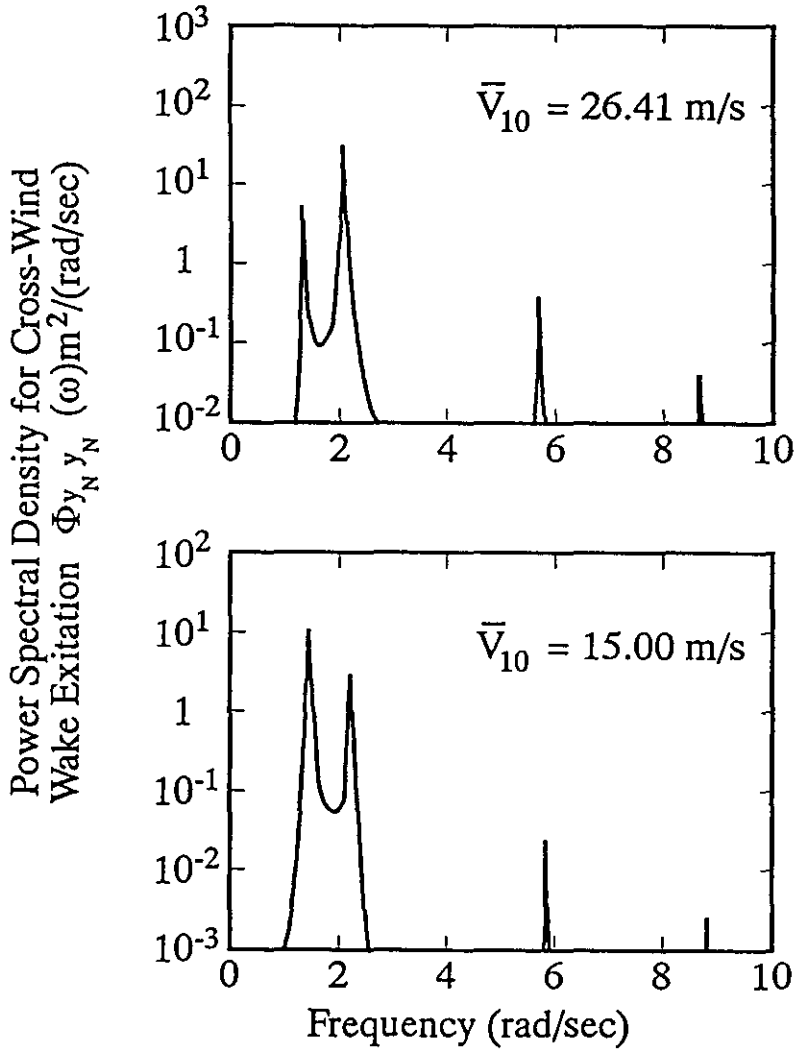


FIG. 8.4 POWER SPECTRAL DENSITY OF TOP DISPLACEMENT OF TV TOWER WITHOUT ANY DAMPERS UNDER CROSS WIND WAKE EXCITATION

frequency of the tower, mean wind velocity $\bar{V}_{1,0} = 15$ m/s is selected.

The properties of TMD, TLCD and TLCMD system are as follows:

For the TMD system: M_d = mass of the tuned mass damper = 494 tonnes; K_d = spring constant = 1061 kN/m; χ = ratio of damper frequency to structural first natural frequency = 1.0. The corresponding effective mass ratio μ of the damper for the first mode of the main structure is around 6%. The effective mass ratio μ is a ratio of the damper mass to the structural equivalent mass, as defined in Eq. 5.1.

For the TLCD system: ρ = water density = 1 tonne/m³; L = liquid length = 9.13m; M_w = mass of the liquid = 494 tonnes; g = acceleration of gravity = 9.81 m/s²; B = liquid width = 0.9L; $\chi = 1.0$.

For the TLCMD system: mass of the damper = mass of the water = 247 tonnes; $K_d = 1061$ kN/m and $L = 9.13$ m. As a result, χ = ratio of the whole damper frequency (considering the water in the container as completely still) to the first frequency of the main structure = 1.0; χ_1 = ratio of the frequency of liquid column to the whole damper frequency = 1.0.

Numerical calculations showed that, for the TMD system, the minimum response variance of the base moment was obtained when the damping ratio of the damper ζ was 17% in alongwind direction and 13% in crosswind direction (see Fig. 8.5). The base moment responses in Fig. 8.5 are normalised by the same response of the TV tower without any dampers. It is interesting to find that the trend of the responses with the damping ratio of the mass damper is similar to the semi-analytical results obtained in Chapter 5. For the TLCD system, the coefficient of head loss ξ was chosen as 30 for both directions after considering practical limits based on the experimental results (Sakai et al., 1989). A plot of the standard deviations of the base moment, which is normalised by the same response of the structure without any dampers, versus the coefficient of head loss ξ for the TLCD system is shown in Fig. 8.6. It is clear from Fig. 8.6 that increase in the coefficient ξ produces smaller response reduction when the

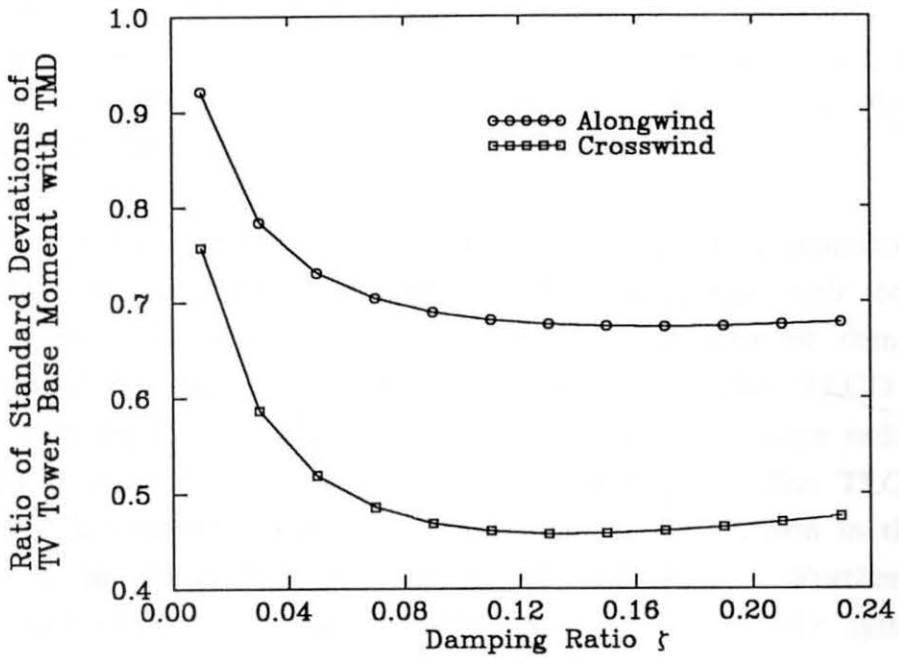


FIG. 8.5 VARIATION OF STANDARD DEVIATIONS OF TV TOWER BASE MOMENT WITH DAMPING RATIO ζ OF TMD

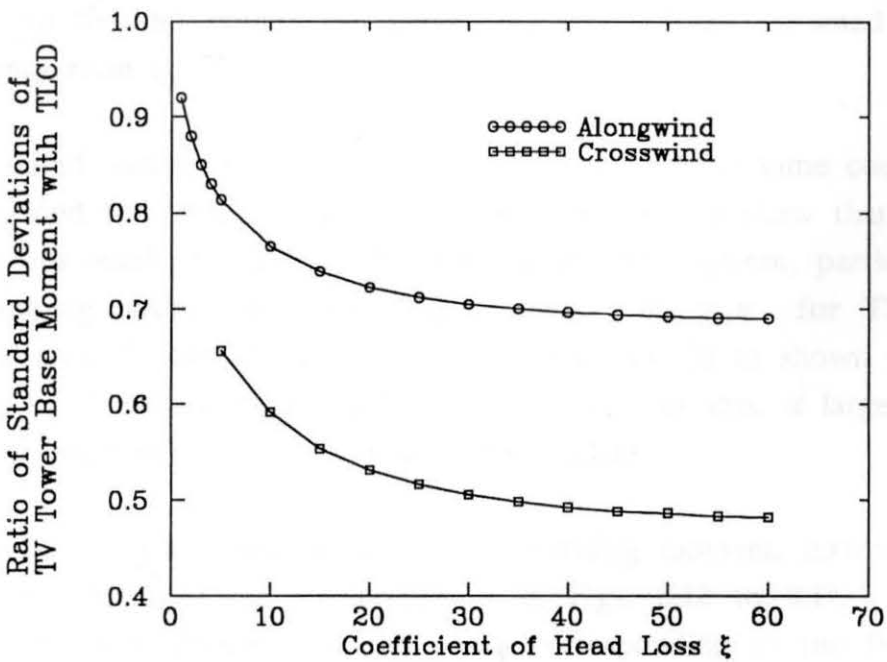


FIG. 8.6 VARIATION OF STANDARD DEVIATIONS OF TV TOWER BASE MOMENT WITH COEFFICIENT OF HEAD LOSS ξ OF TLCD

coefficient ξ is larger than 30. The trend of the responses with the coefficient of head loss is also similar to that in TMD system. Both damping ratios ($\zeta = 17\%$ in alongwind direction and 13% in crosswind direction) and the coefficient of head loss ($\xi = 30$ for both directions) are used in TLCMD system.

Table 8.2 and 8.3 present alongwind and crosswind standard deviations of eight controlling response quantities by computing their corresponding power spectral densities. It is seen that all three type of damper systems can significantly reduce the structural response. The TLCD and TMD systems are capable of achieving the same level of response reduction while the TLCD system has significant practical advantages. The TLCMD system is slightly less effective because of undesirable liquid motion in the container (referring to column 5 in Tables 8.2 and 8.3). Further numerical calculations showed that the effectiveness of the TLCMD system can be increased by setting the natural frequency of the liquid column tube higher than the frequency of the whole damper, i.e., by increasing value of χ_1 . Variation of the turret acceleration response with frequency ratio χ_1 is shown in Fig. 8.7 for both wind directions. It is seen that, the higher the frequency ratio χ_1 , the more the reduction of the structural response. The values on the last column in Tables 8.2 and 8.3 are obtained by using a frequency ratio χ_1 of 1.6.

Limited numerical calculations also showed that the same conclusions can be obtained for smaller mass ratios. Figs 8.8 to 8.9 show that the smaller mass ratios result in the less effectiveness of TMD system, particularly when the damping ratio is relatively larger. This is also true for TLCD system when the coefficient of head loss ξ is larger than 20 as shown in Figs. 8.10 and 8.11. However, for smaller coefficient of head loss, a larger mass ratio does not improve the effectiveness of the TLCD.

Power spectral densities of the base bending moment, turret acceleration and turret displacement are presented in Figs. 8.12 to 8.17. From these figures one can observe that the peaks corresponding to the first vibration mode are considerably suppressed while other peaks are nearly unaffected. For displacement type responses, the contribution of the first vibration mode

**TABLE 8.2. STANDARD DEVIATION RESPONSE OF TV TOWER
FOR ALONGWIND EXCITATION**

Response variable	WTD	TMD $\zeta = 0.17$ $\chi = 1.0$ $M_d = 494$ (tonnes)	TLCD $\xi = 30$ $\chi = 1.0$ $M_w = 494$ (tonnes)	TLCMD $\xi = 30$ $\chi = 1.0$ $\chi_1 = 1.0$ $M_d = M_w = 274$ (tonnes)	TLCMD $\xi = 30$ $\chi = 1.0$ $\chi_1 = 1.6$ $M_d = M_w = 274$ (tonnes)
(1)	(2)	(3)	(4)	(5)	(6)
M_0 (kN-m)	152,144	102,546	107,276	111,698	101,506
Q_0 (kN)	947	745	780	777	744
y_N (mm)	385	213	235	267	229
φ_N (rad)	0.0063	0.0038	0.0044	0.0046	0.0043
\ddot{y}_n (mil-g)	11.1	6.5	7.2	7.7	6.9
y_n (mm)	49	30	31	34	29
Z_d (mm)	-	43	-	30	43
X_w (mm)	-	-	62	57	21

Note: $\bar{V}_{1,0} = 26.41$ m/s; WTD: Without any Dampers;
TMD: Tuned Mass Damper; TLCD: Tuned Liquid Column Damper;
TLCMD: Tuned Liquid Column/Mass Damper

**TABLE 8.3 STANDARD DEVIATION RESPONSE OF TV TOWER
FOR CROSSWIND WAKE EXCITATION**

Response variable	WTD	TMD $\zeta = 0.13$ $\chi = 1.0$ $M_d = 494$ (tonnes)	TLCD $\xi = 30$ $\chi = 1.0$ $M_w = 494$ (tonnes)	TLCMD $\xi = 30$ $\chi = 1.0$ $\chi_1 = 1.0$ $M_d = M_w = 274$ (tonnes)	TLCMD $\xi = 30$ $\chi = 1.0$ $\chi_1 = 1.6$ $M_d = M_w = 274$ (tonnes)
(1)	(2)	(3)	(4)	(5)	(6)
M_o (kN-m)	106,810	48,839	54,012	68,128	49,563
Q_o (kN)	609	373	403	439	378
y_N (mm)	295	135	154	203	156
φ_N (rad)	0.0047	0.0026	0.0030	0.0034	0.0031
\ddot{y}_n (mil-g)	8.5	4.3	4.8	5.8	4.7
y_n (mm)	36	14	15	22	14
Z_d (mm)	—	37	—	23	36
x_w (mm)	—	—	50	47	17

Note: $\bar{V}_{10} = 15.00$ m/s; WTD: Without any Dampers;
TMD: Tuned Mass Damper; TLCD: Tuned Liquid Column Damper;
TLCMD: Tuned Liquid Column/Mass Damper

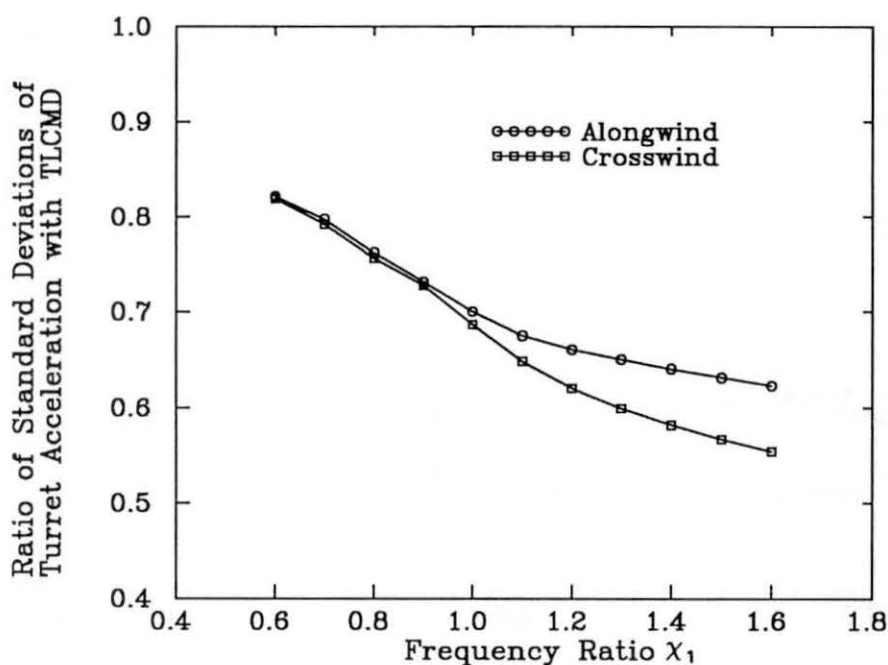


FIG. 8.7 VARIATION OF STANDARD DEVIATIONS OF TURRET ACCELERATION WITH FREQUENCY RATIO χ_1 OF TLCMD

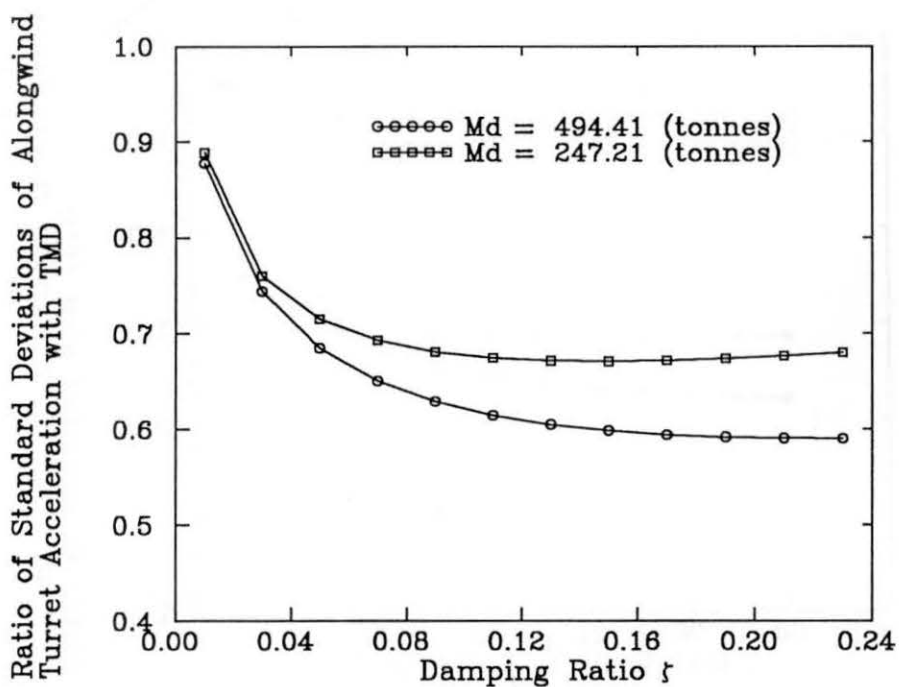


FIG. 8.8 VARIATION OF STANDARD DEVIATIONS OF ALONGWIND TURRET ACCELERATION WITH DAMPING RATIO ζ OF TMD

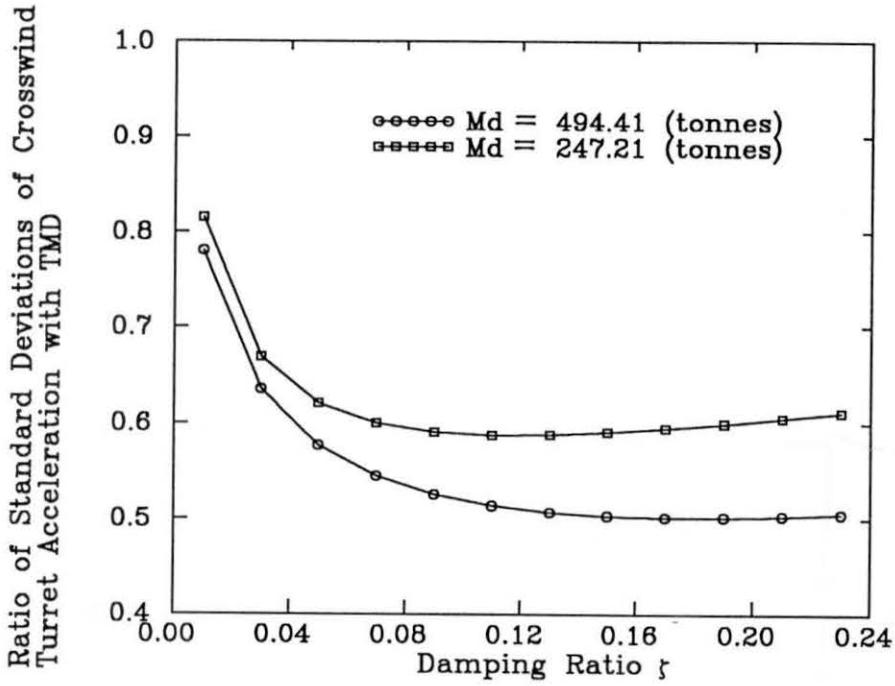


FIG. 8.9 VARIATION OF STANDARD DEVIATIONS OF CROSSWIND TURRET ACCELERATION WITH DAMPING RATIO ζ OF TMD

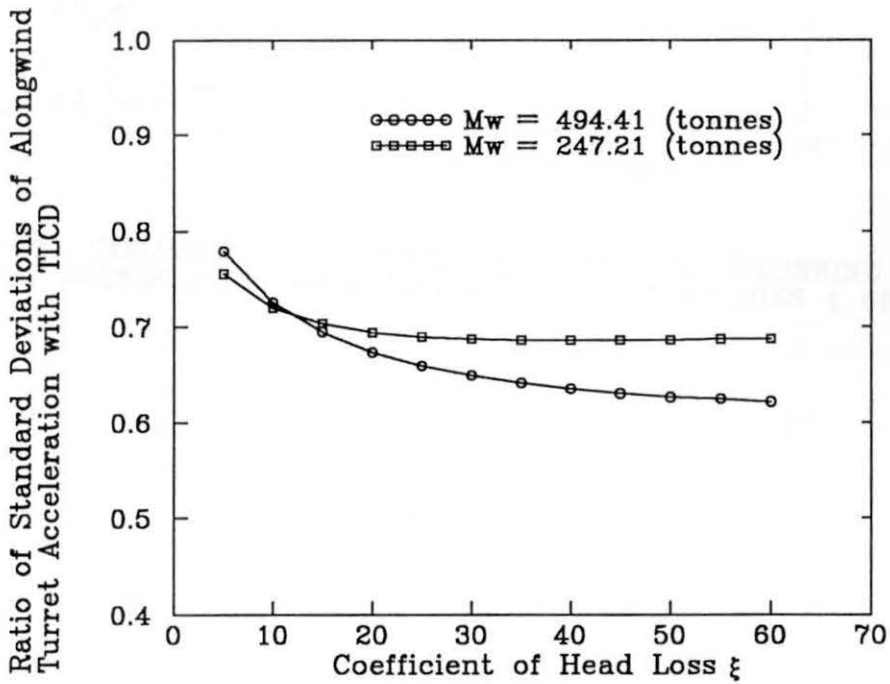


FIG. 8.10 VARIATION OF STANDARD DEVIATIONS OF ALONGWIND TURRET ACCELERATION WITH COEFFICIENT OF HEAD LOSS ξ OF TLCD

Ratio of Standard Deviations of Crosswind
Turret Acceleration with TLCD

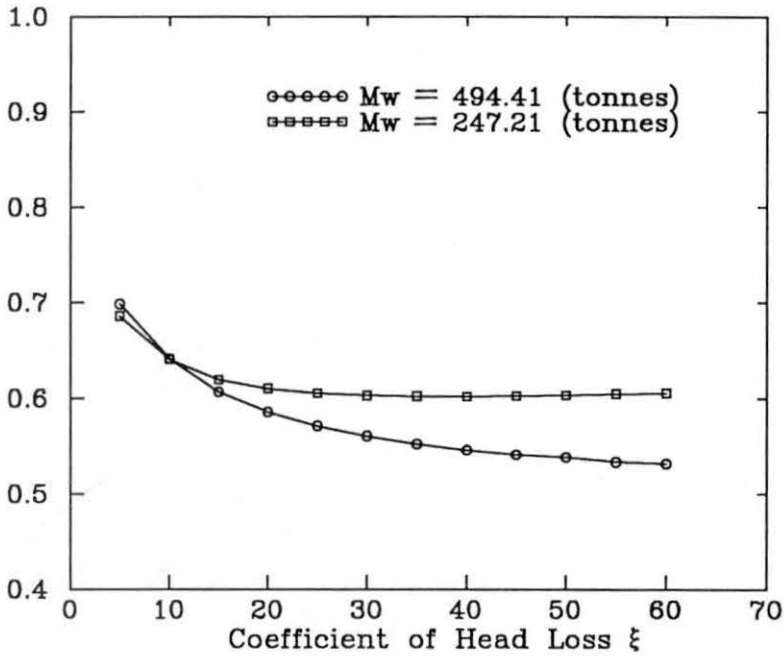


FIG. 8.11 VARIATION OF STANDARD DEVIATIONS OF CROSSWIND TURRET ACCELERATION WITH COEFFICIENT OF HEAD LOSS ξ OF TLCD

is dominant while for force and acceleration type responses, the contributions of higher modes are rather significant and considering only one mode in the analyses may lead to misleading and non-conservative results. It is particularly true for damper-structure systems tuned to the first natural frequency of the structure. In Figs. 8.12 to 8.17, the parameters of the TMD, TLCD and TLCMD are the same as those listed in columns 3, 4 and 6 in Tables 8.2 and 8.3, respectively.

8.4.2 Office tower

The office tower is modelled as a 10-degree-of-freedom cantilever model. The structural data used in the analysis are listed in Table 8.4. The first three natural frequencies of the structure are 0.175, 0.569 and 1.333 (Hz), respectively. All dampers are connected to or fixed on the top floor of the tower and have an effective mass ratio (equal to generalised mass) of 3% associated with the first mode of the main structure. The comparison of the effectiveness between the three dampers is performed in the same way as for TV tower-damper system.

The aerodynamic data pertaining to alongwind excitation are: $\bar{V}_{1,0} = 15.9$ m/s; $\alpha = 0.25$; $z_g = 400$ m; $\bar{V}_G = 40$ m/s; $C_a = 1.2$; $\rho_a = 1.2$ kg/m³; $C_1 = 7.0$ and $K_0 = 0.01$. Based on these aerodynamic data, a suburban terrain [Terrain category 3 as described in the Australian Standard, SAA Loading Code, Part 2: Wind Loads; AS 1170.2-1989] is reflected.

The aerodynamic data pertaining to wake excitation are: $\bar{V}_{1,0} = 15.9$ m/s; $\alpha = 0.25$; $C_1 = 0.40$; $S = 0.12$; $B_s = 0.26$; α_1 and $\alpha_2 = 0.5$ and 5 , respectively.

TMD, TLCD and TLCMD systems are all tuned to the first natural frequency of the building. This will lead to the following mass damper and liquid column properties: for the TMD system, $M_d = 839$ tonnes; $K_d = 1015.4$ kN/m and $\chi = 1.0$. Optimum damping ratio ζ of the TMD is found to be 15% in alongwind direction and 11% in crosswind direction (see Fig. 8.18). For the TLCD system: $\rho = 1$ tonne/m³; $L = 16.2$ m; $M_w = 839$ tonnes; $g = 9.81$ m/s²; $B = 0.9L$; $\chi = 1.0$; the coefficient of head loss $\xi = 30$. Fig. 8.19 shows the variation of standard deviations of top acceleration of office tower

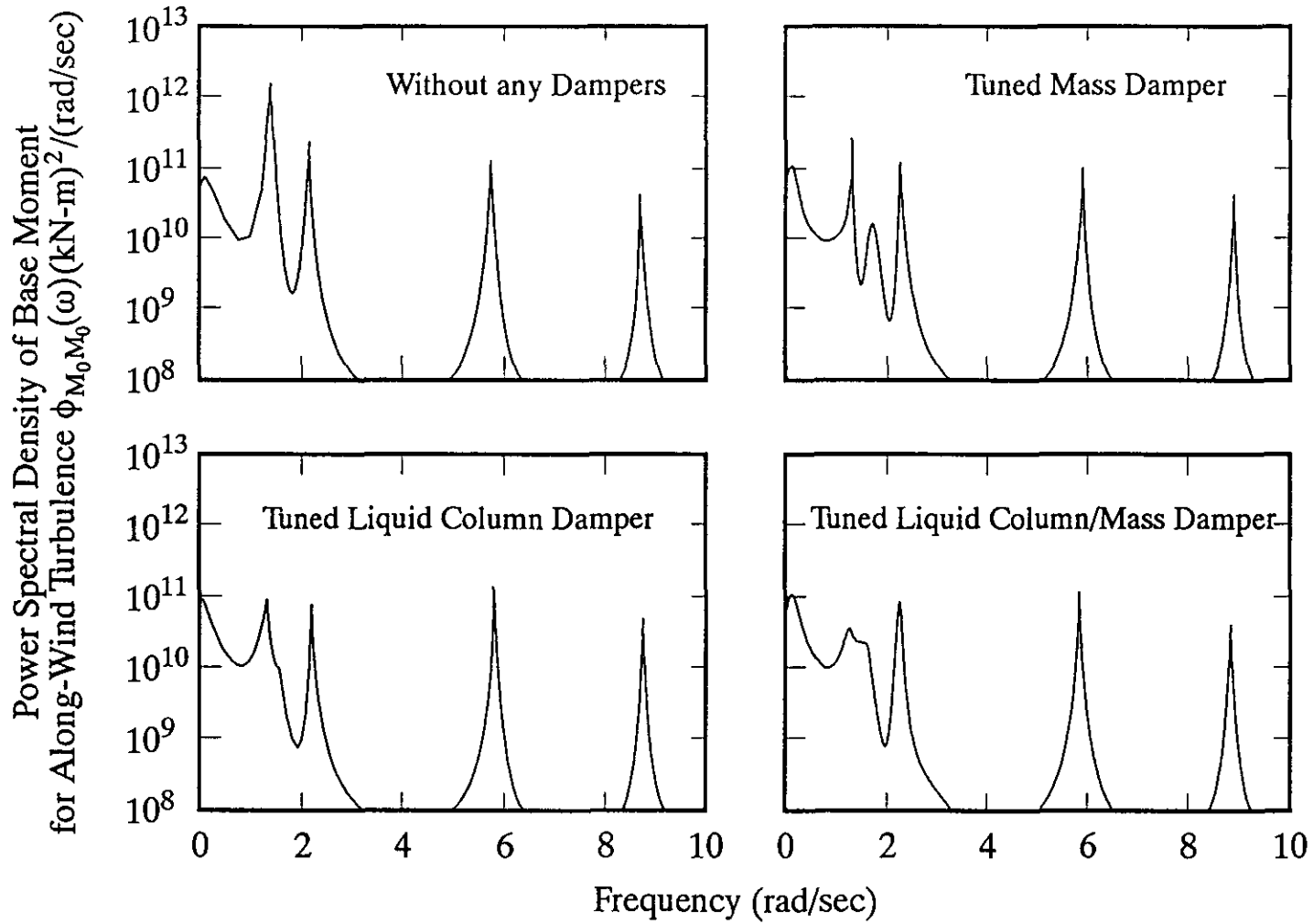


FIG.8.12 POWER SPECTRAL DENSITY OF BASE MOMENT OF TV TOWER UNDER ALONGWIND TURBULENCE

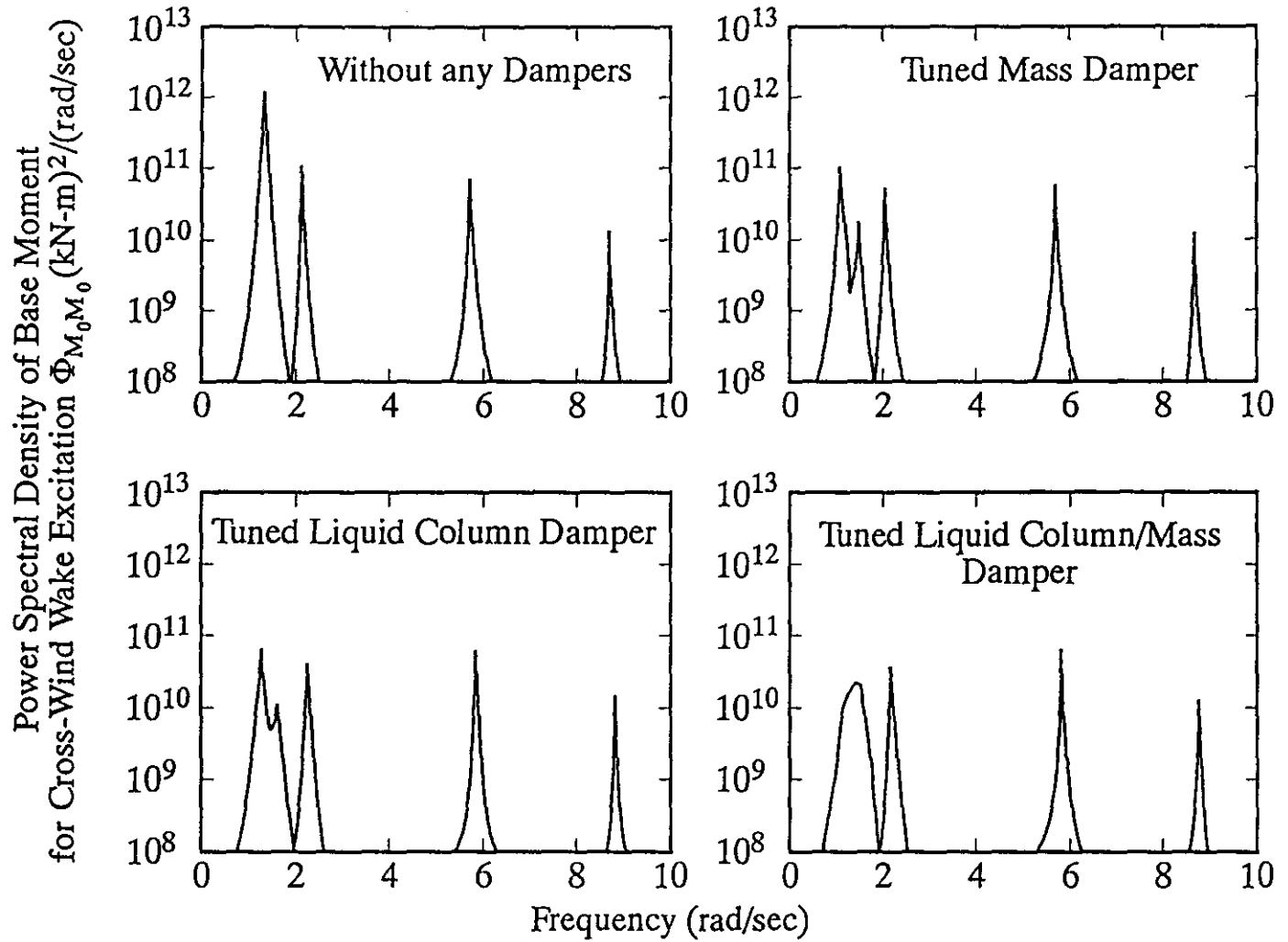


FIG. 8.13 POWER SPECTRAL DENSITY OF BASE MOMENT OF TV TOWER UNDER CROSSWIND WAKE EXCITATION

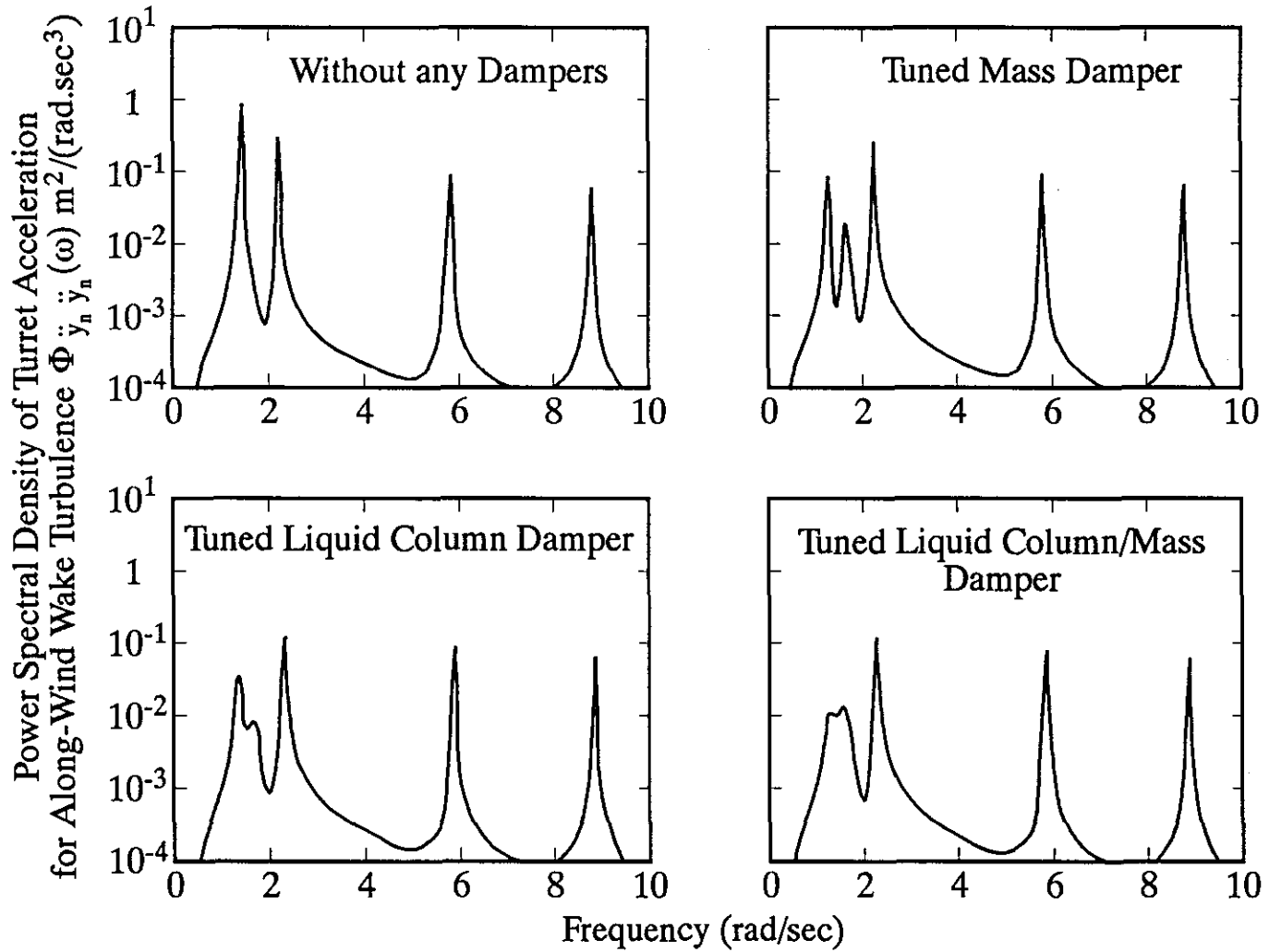


FIG.8.14 POWER SPECTRAL DENSITY OF TURRET ACCELERATION OF TV TOWER UNDER ALONGWIND TURBULENCE

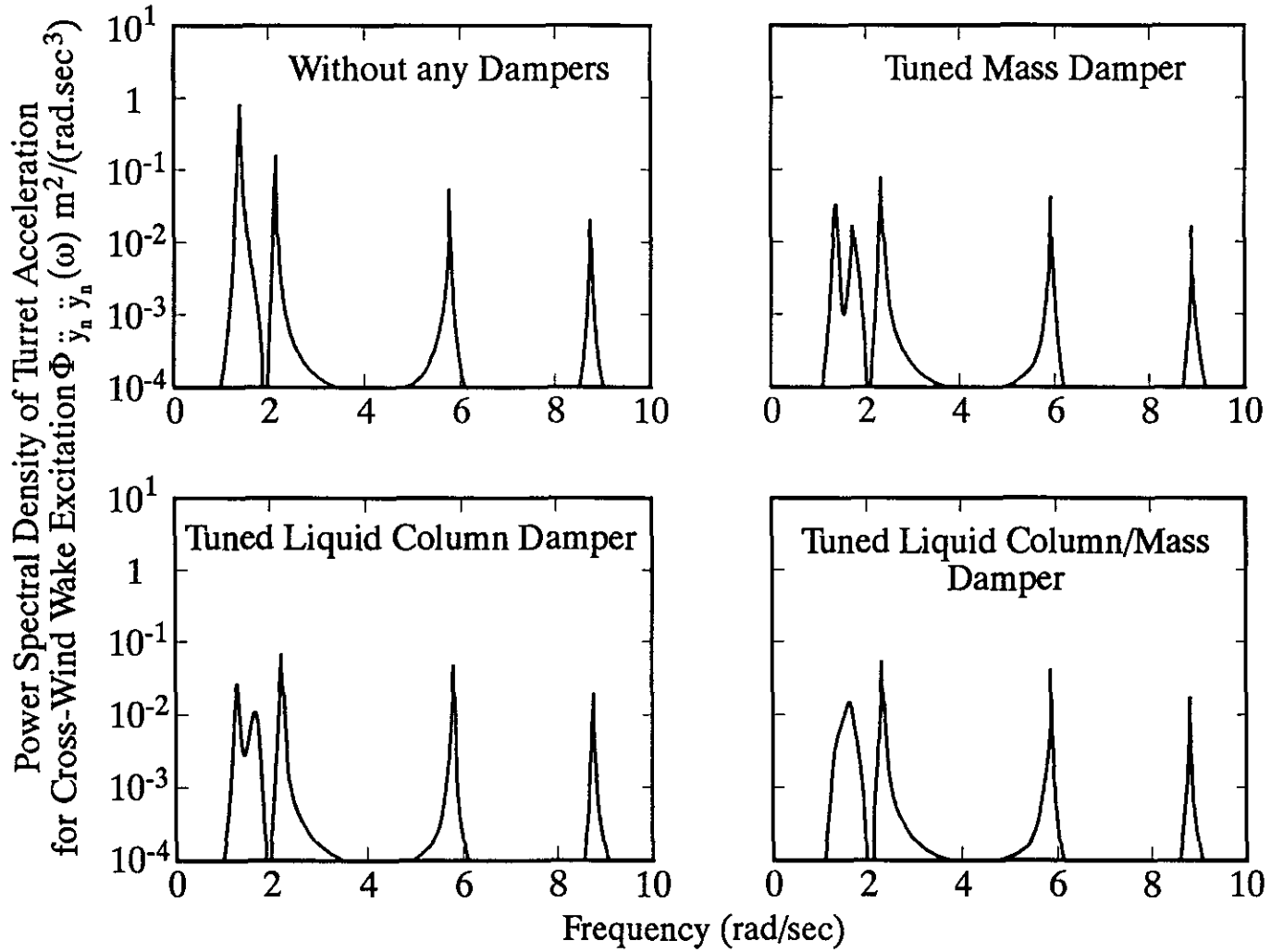


FIG.8.15 POWER SPECTRAL DENSITY OF TURRET ACCELERATION OF TV TOWER UNDER CROSSWIND WAKE EXCITATION

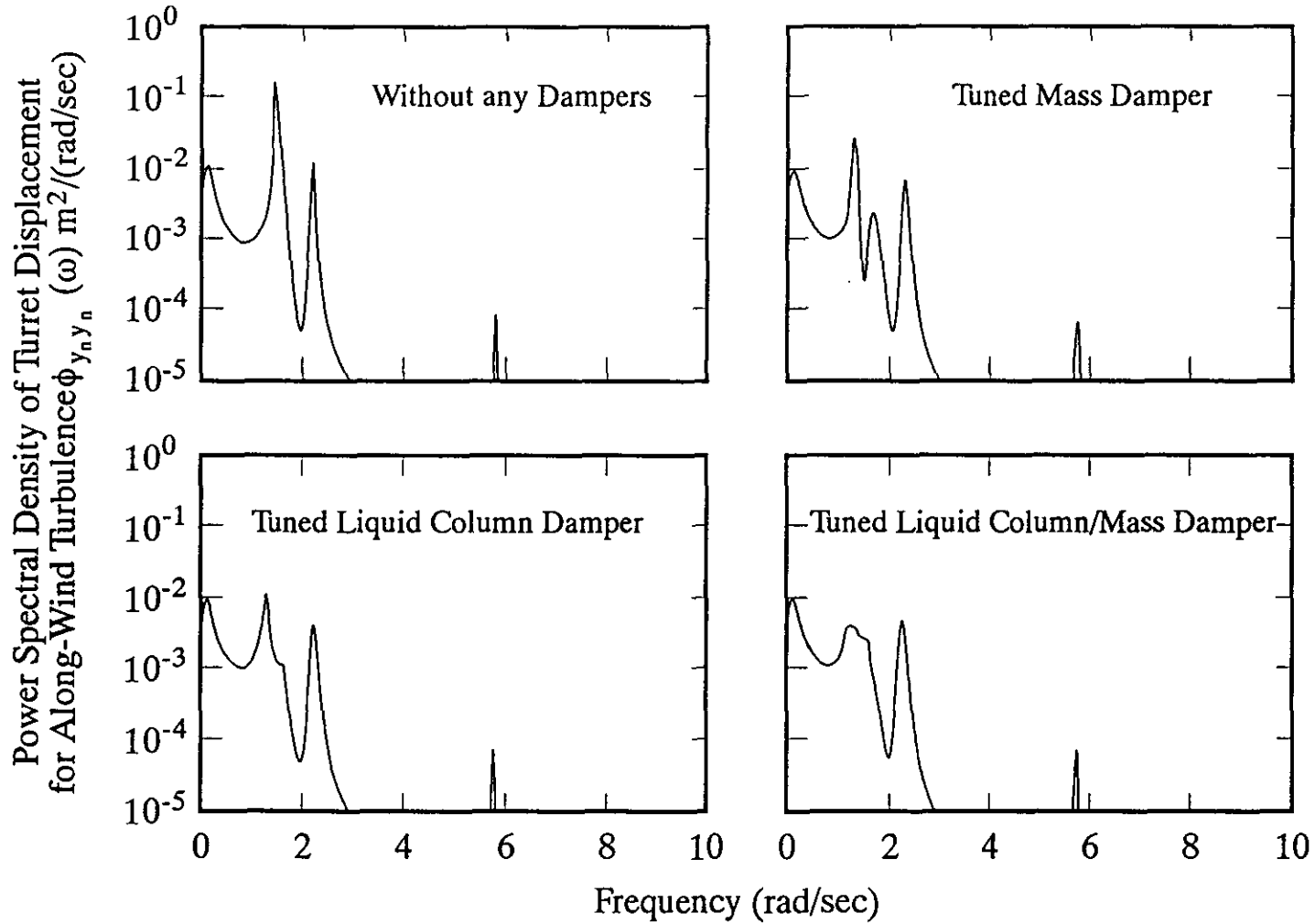


FIG.8.16 POWER SPECTRAL DENSITY OF TURRET DISPLACEMENT OF TV TOWER UNDER ALONGWIND TURBULENCE

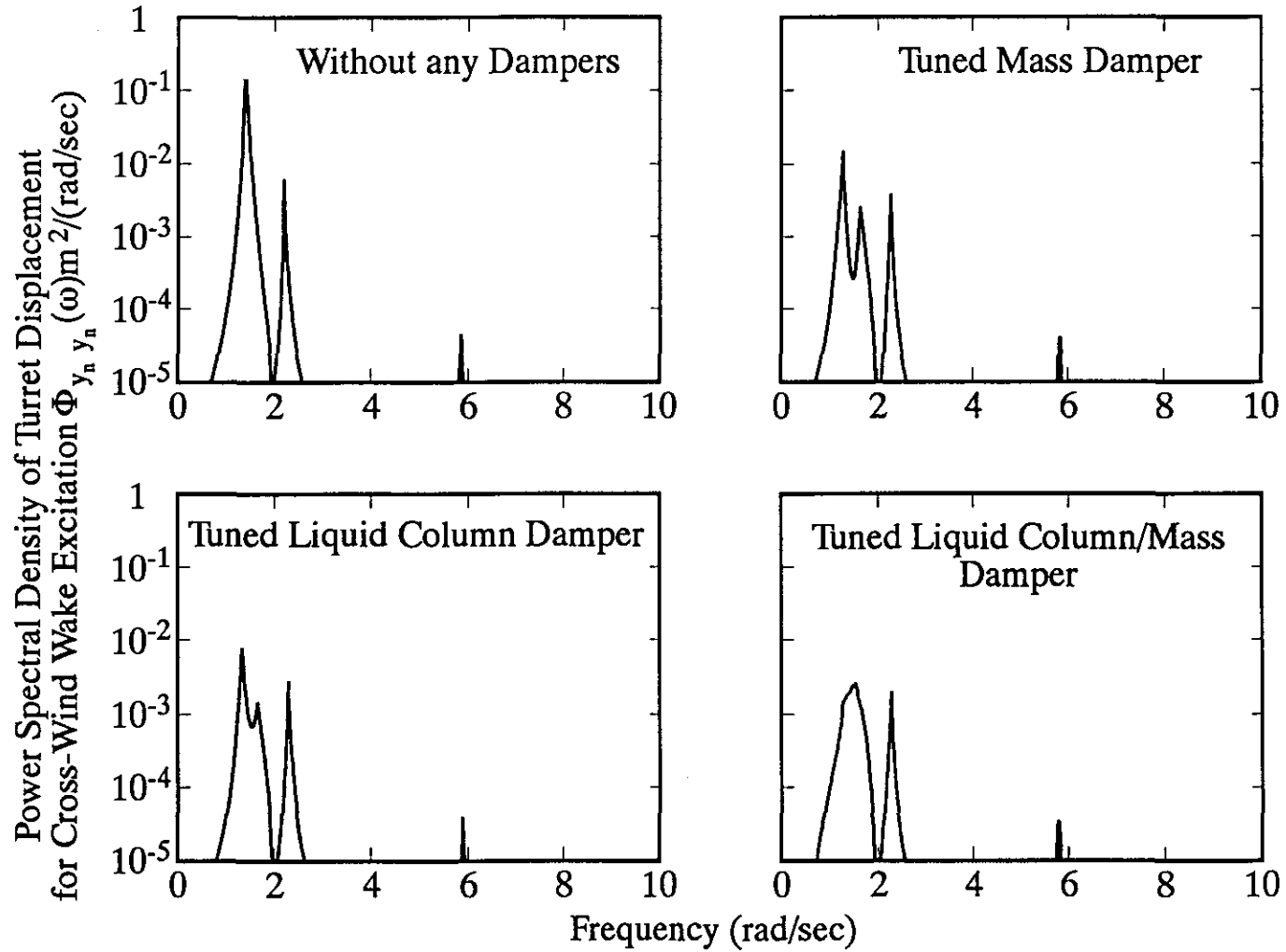


FIG.8.17 POWER SPECTRAL DENSITY OF TURRET DISPLACEMENT OF TV TOWER UNDER CROSSWIND WAKE EXCITATION

TABLE 8.4. STRUCTURAL DATA FOR OFFICE TOWER

Node number	Height h_j (m)	Mass m_j (tonnes)	Stiffness $E_j I_j \times 10^9$ (kN-m ²)	Damping β_j (kN/m/s)	Wind area A_j (m ²)
(1)	(2)	(3)	(4)	(5)	(6)
1	37.25	18774	763.0	413.0	1566.7
2	34.65	16578	450.0	364.7	1510.0
3	34.65	15657	295.0	344.5	1426.2
4	30.80	14438	188.0	317.6	1342.3
5	30.80	12864	107.0	283.0	1342.3
6	30.80	10574	55.0	232.6	1174.5
7	23.10	8010	23.0	176.2	1006.7
8	23.10	8481	14.0	186.6	1006.7
9	23.10	7686	7.5	169.1	769.2
10	24.40	7100	3.0	156.2	265.9

with coefficient of head loss ξ . It is seen that the coefficient of head loss of 30 approaches an optimum value for the crosswind vibration of the office tower. For the TLCMD system: $M_w = M_d = 419.5$ tonnes; K_d and ζ = the same as for the TMD; $\xi = 30$; $\chi = 1.0$; $\chi_1 = 1.0$ and 1.6 . For $\chi = 1.0$, it can be found from Fig. 8.20 that the effectiveness of the TLCMD system approaches that of the TMD system only when the coefficient of head loss becomes very large, i.e., the liquid in the container is kept still.

The standard deviations of office tower response quantities are given in Tables 8.5 and 8.6. Power spectral densities of top floor acceleration and base moment are presented in Figs. 8.21 to 8.24. From these tables and figures, conclusions similar to the TV tower case may be drawn. However, one can observe that only the first mode of vibration is dominant for the acceleration and force type responses in the crosswind direction. It is also interesting to note that the shape of the crosswind response spectra in Fig. 8.22 is quite similar to that in Fig. 3.11, which was obtained from the wind tunnel test. The first peak is associated with the vortex shedding in crosswind direction while the second peak is located at the first natural frequency of the office tower. It is obvious that the vortex shedding frequency of the office tower is smaller than the first natural frequency of the tower. In this case, it seems to be justified for stiffer tall buildings to assume that the experimental results obtained by simple aeroelastic wind tunnel tests are accurate enough, even though only the first vibration mode is considered in the test.

8.5 Conclusions

A transfer matrix formulation for non-periodic structures has been developed to analyse the effect of tuned mass dampers and liquid dampers on the wind-induced response of tall/slender structures. The numerical computer accuracy has also been investigated in Appendix B. The results indicated that the accuracy of the computer results using direct matrix multiplication can be guaranteed for the studied cantilever structures. The computer time, however, was 2–5 times more than that required by the analytical procedure for periodic structures.

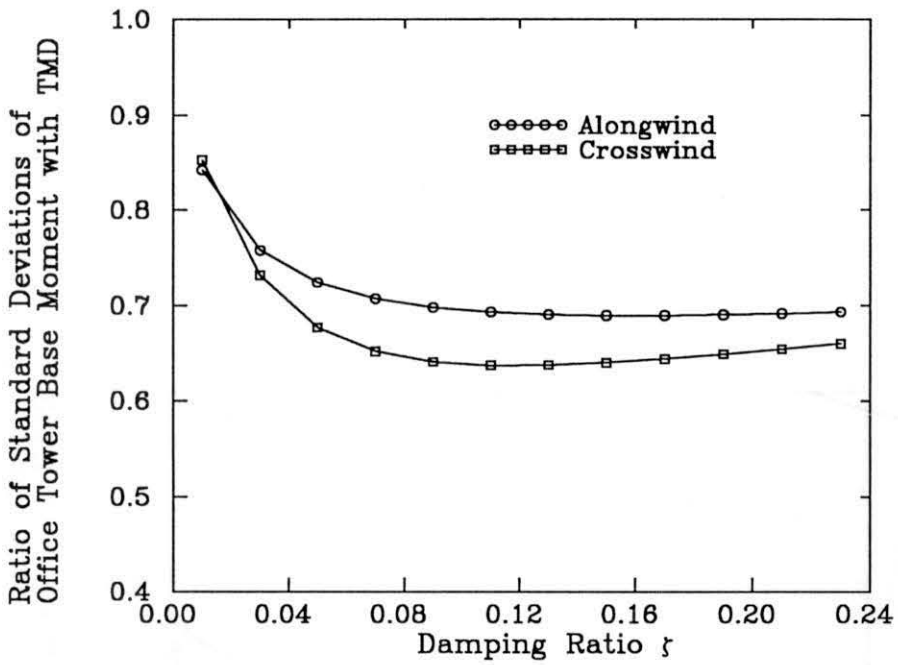


FIG. 8.18 VARIATION OF STANDARD DEVIATIONS OF OFFICE TOWER BASE MOMENT WITH DAMPING RATIO ζ OF TMD

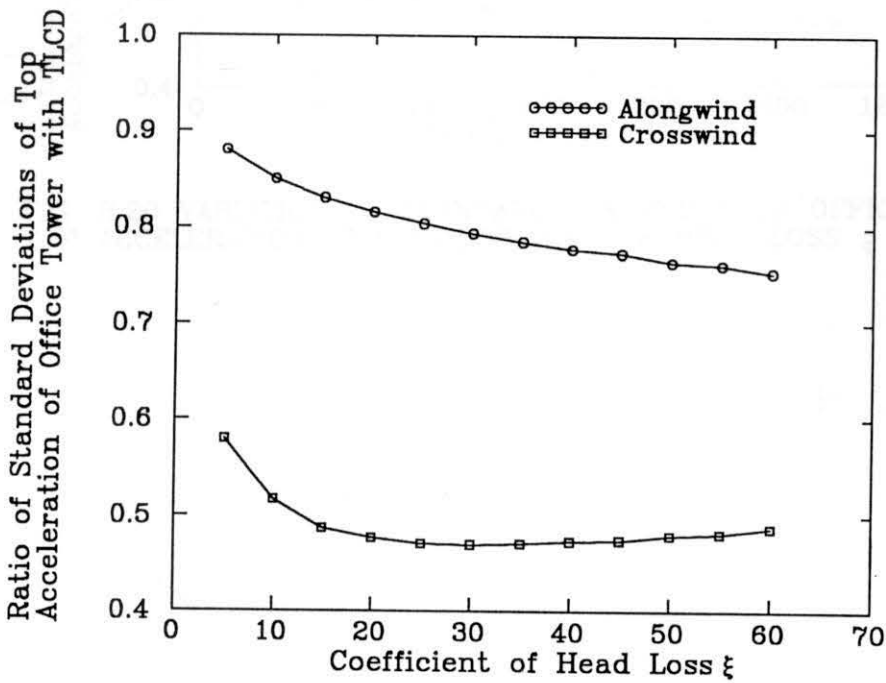


FIG. 8.19 VARIATION OF STANDARD DEVIATIONS OF OFFICE TOWER TOP ACCELERATION WITH COEFFICIENT OF HEAD LOSS ξ OF TLCD

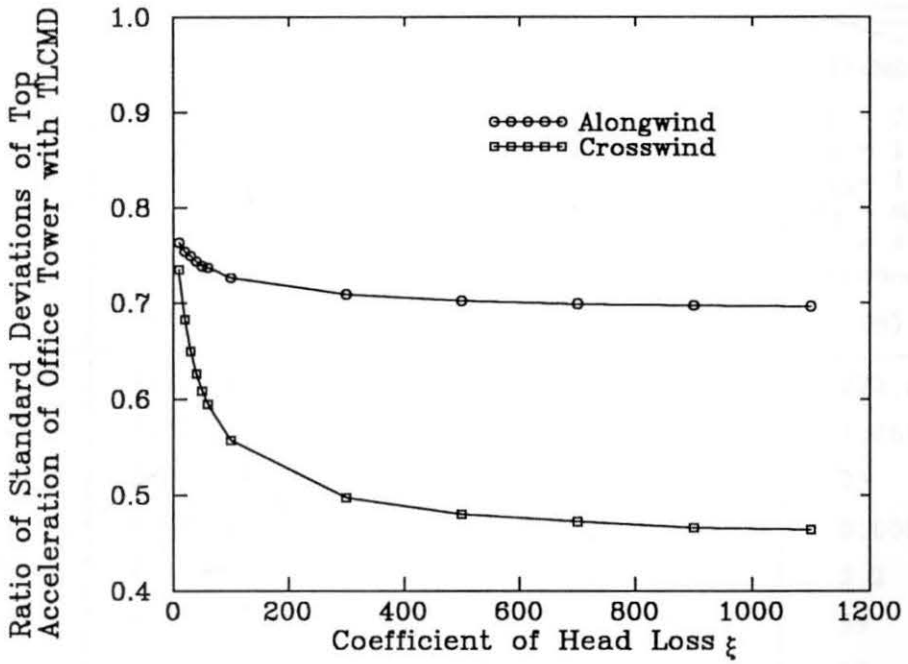


FIG. 8.20 VARIATION OF STANDARD DEVIATIONS OF OFFICE TOWER TOP ACCELERATION WITH COEFFICIENT OF HEAD LOSS ξ OF TLCMD

**TABLE 8.5. STANDARD DEVIATION RESPONSE OF OFFICE TOWER
FOR ALONGWIND EXCITATION**

Response variable	WTD	TMD $\zeta = 0.15$ $\chi = 1.0$ $M_d = 839$ (tonnes)	TLCD $\xi = 30$ $\chi = 1.0$ $M_w = 839$ (tonnes)	TLCMD $\xi = 30$ $\chi = 1.0$ $\chi_1 = 1.0$ $M_d = M_w = 419.5$ (tonnes)	TLCMD $\xi = 30$ $\chi = 1.0$ $\chi_1 = 1.6$ $M_d = M_w = 419.5$ (tonnes)
(1)	(2)	(3)	(4)	(5)	(6)
M_o (kN-m)	398,530	274,764	293,308	321,732	272,859
Q_o (kN)	2,330	1,778	1,930	1,915	1,761
y_N (mm)	38	23	24	29	23
ϕ_N (rad)	0.00036	0.00022	0.00024	0.00027	0.00021
\ddot{y}_n (mil-g)	7.7	5.3	6.1	5.8	5.2
Z_d (mm)	—	39	—	27	39
x_w (mm)	—	—	66	53	17
\dot{x}_w (mm/s)	—	—	72	57	21

Note: $\bar{V}_{10} = 15.9$ m/s; WTD: Without any Dampers;
TMD: Tuned Mass Damper; TLCD: Tuned Liquid Column Damper;
TLCMD: Tuned Liquid Column/Mass Damper

**TABLE 8.6 STANDARD DEVIATION RESPONSE OF OFFICE TOWER
FOR CROSSWIND WAKE EXCITATION**

Response variable	WTD	TMD $\zeta = 0.11$ $\chi = 1.0$ $M_d = 839$ (tonnes)	TLCD $\xi = 30$ $\chi = 1.0$ $M_w = 839$ (tonnes)	TLCMD $\xi = 30$ $\chi = 1.0$ $\chi_1 = 1.0$ $M_d = M_w = 419.5$ (tonnes)	TLCMD $\xi = 30$ $\chi = 1.0$ $\chi_1 = 1.6$ $M_d = M_w = 419.5$ (tonnes)
(1)	(2)	(3)	(4)	(5)	(6)
M_0 (kN-m)	937,392	579,598	604,392	691,795	583,968
Q_0 (kN)	4,224	2,814	2,841	3,218	2,774
y_N (mm)	102	62	63	72	59
φ_N (rad)	0.00091	0.00054	0.00055	0.00063	0.00051
\ddot{y}_N (mil-g)	11.5	5.3	5.4	7.5	5.2
Z_d (mm)	—	143	—	94	140
X_w (mm)	—	—	146	153	63
\dot{X}_w (mm/s)	—	—	150	151	65

Note: $\bar{V}_{1,0} = 15.9$ m/s; WTD: Without any Dampers;
TMD: Tuned Mass Damper; TLCD: Tuned Liquid Column Damper;
TLCMD: Tuned Liquid Column/Mass Damper

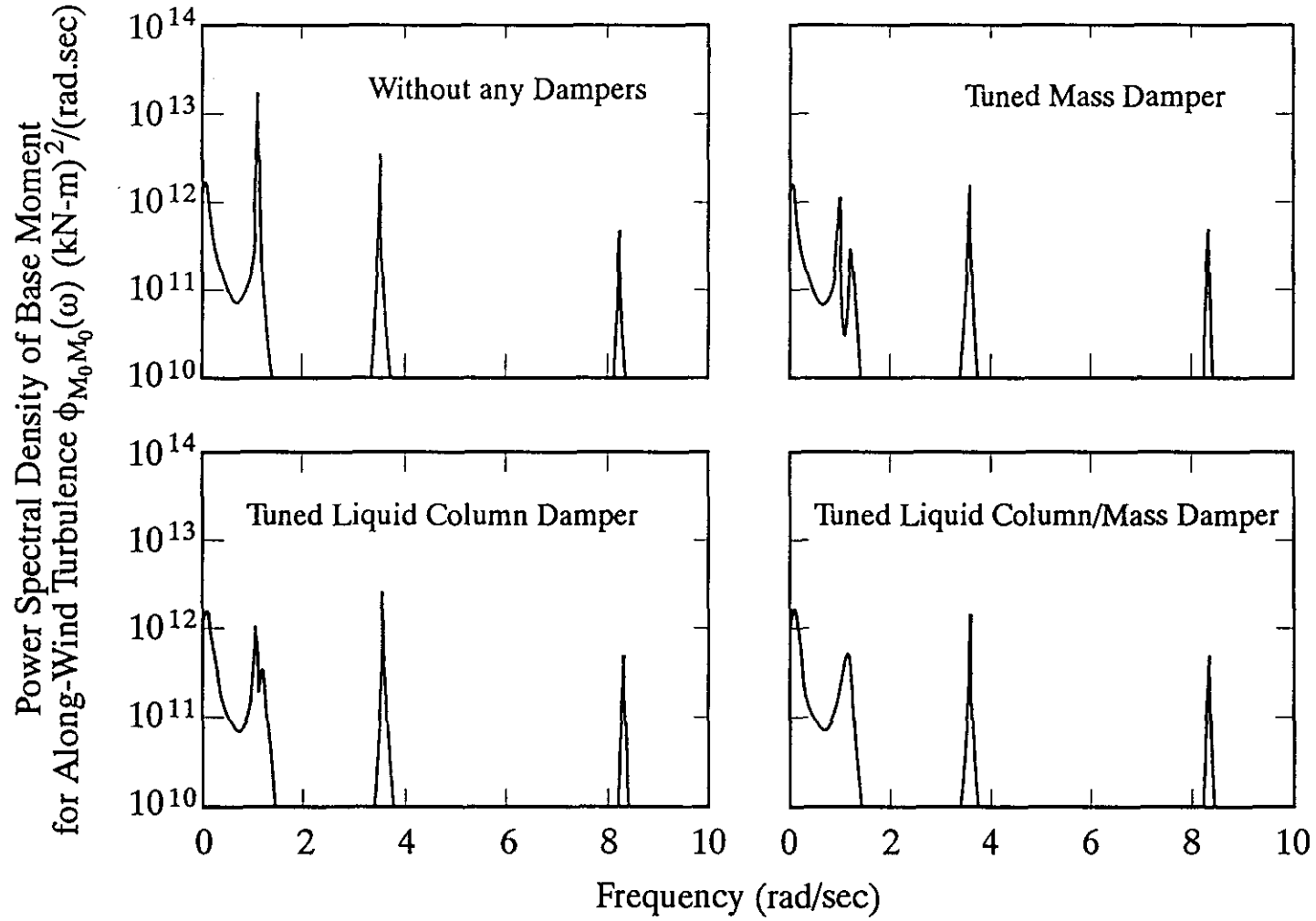


FIG.8.21 POWER SPECTRAL DENSITY OF BASE MOMENT OF OFFICE TOWER UNDER ALONGWIND TURBULENCE

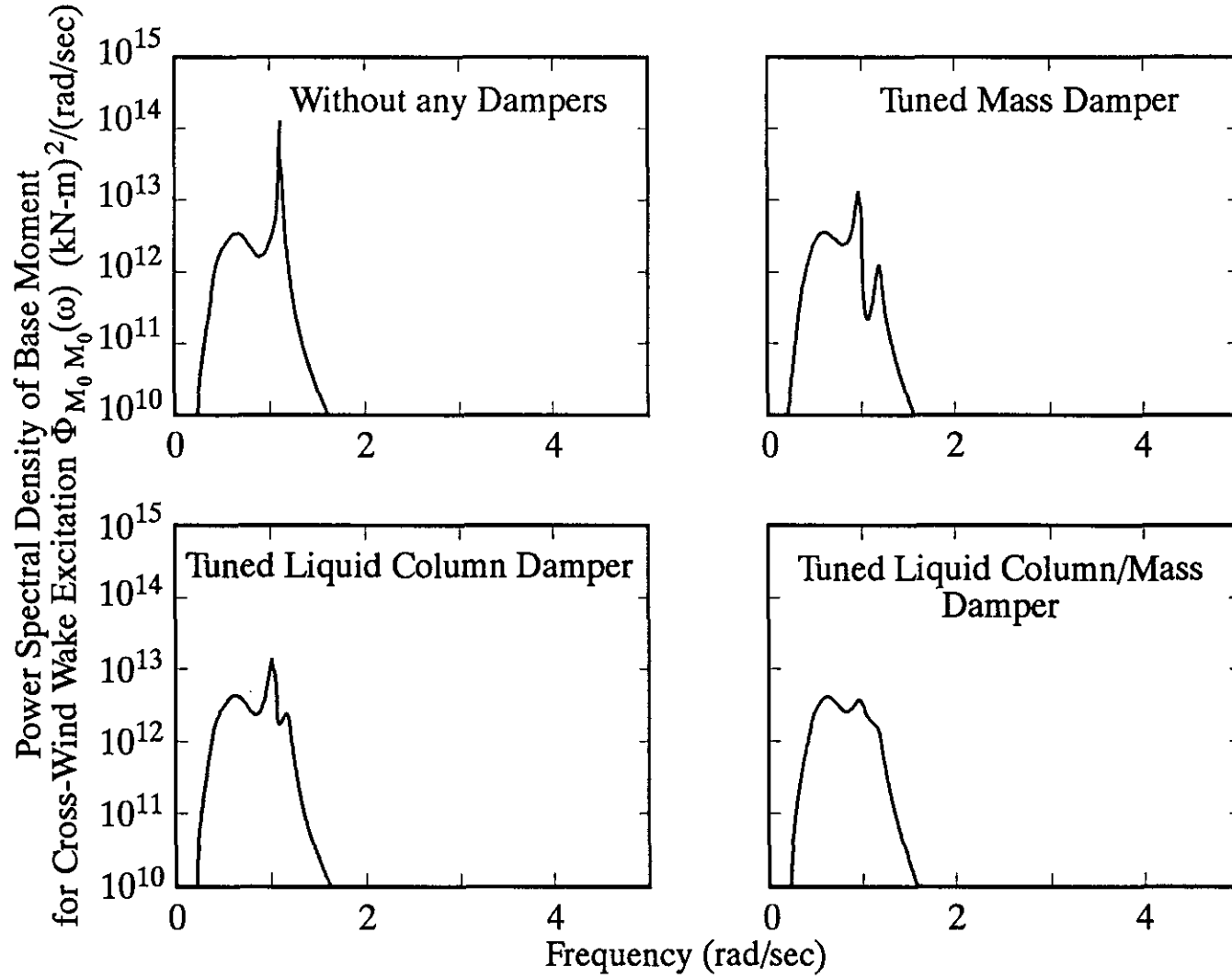


FIG.8.22 POWER SPECTRAL DENSITY OF BASE MOMENT OF OFFICE TOWER UNDER CROSSWIND WAKE EXCITATION

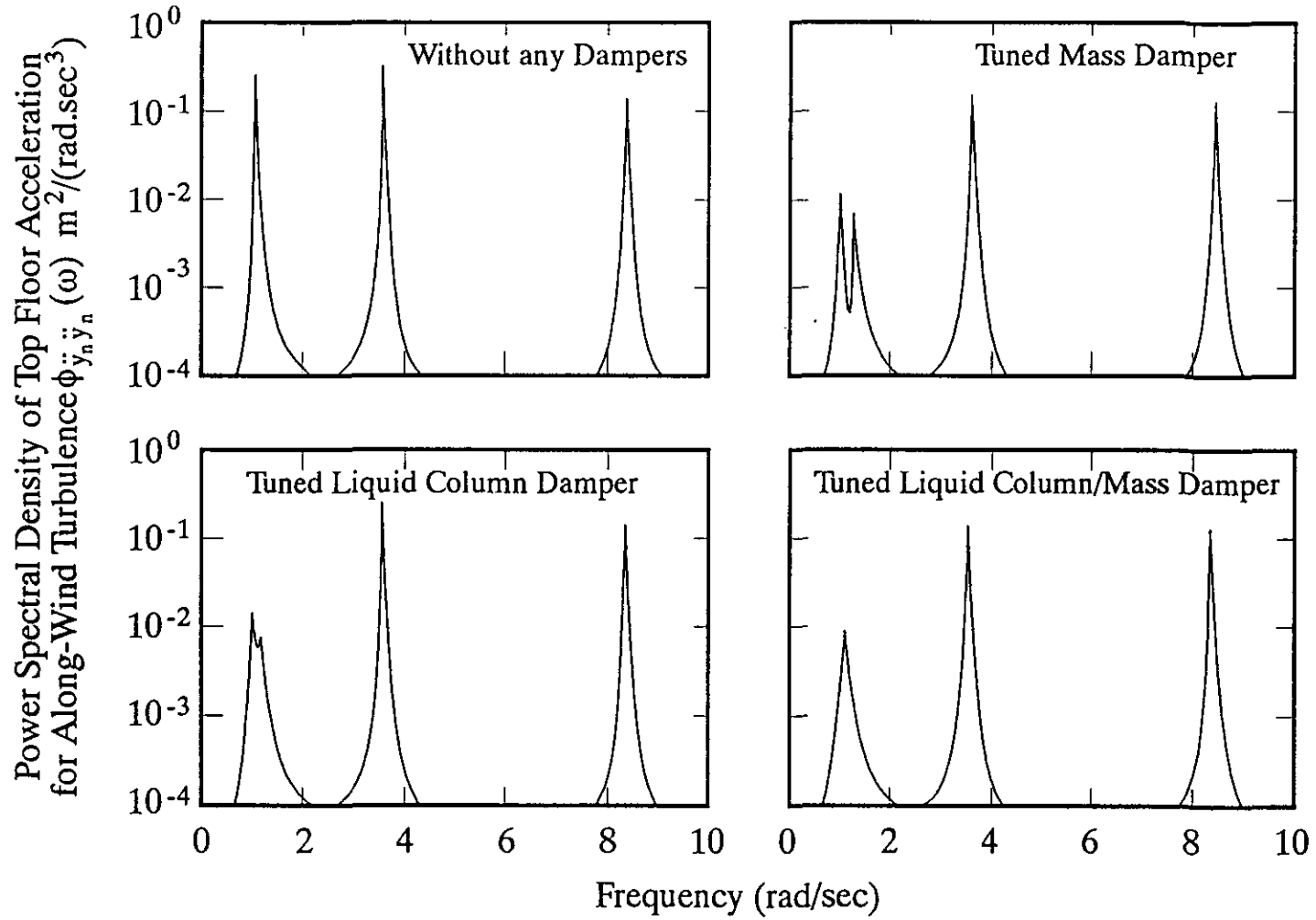


FIG.8.23 POWER SPECTRAL DENSITY OF TOP ACCELERATION OF OFFICE TOWER UNDER ALONGWIND TURBULENCE

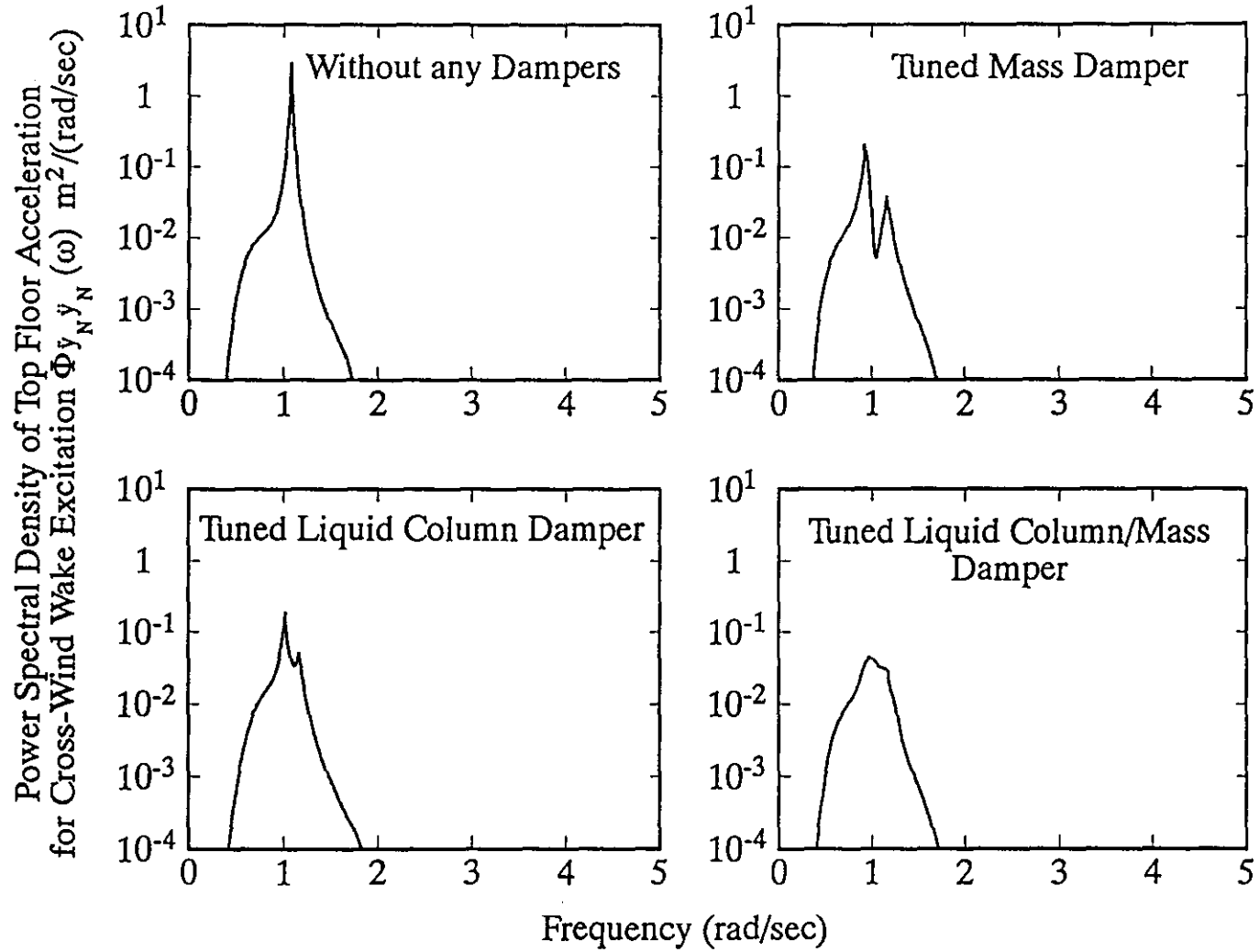


FIG. 8.24 POWER SPECTRAL DENSITY OF TOP ACCELERATION OF OFFICE TOWER UNDER CROSSWIND WAKE EXCITATION

The effectiveness of three types of dampers in reducing both the alongwind and crosswind structural responses has been illustrated. These damper systems can significantly reduce the structural response. The TLCD systems, which have significant practical advantages, can achieve the same motion reduction level as the TMD. However, when the frequency of the liquid column is the same or less than the frequency of the whole damper, the liquid motion in a TLCMD system may reduce the effectiveness of the damper. Therefore, a higher frequency ratio χ_1 should be selected for TLCMD system. .

For the slender TV tower example, wind velocity may affect the effectiveness of the dampers. For instance, vortex shedding frequency of the tower approached the second vibration mode of the tower while the damper frequency was tuned to the first vibration mode. Therefore, on some occasions, a second damper which is tuned to the second natural frequency of the structure should be considered. When a damper was tuned to the fundamental frequency of the main structure, the contribution of higher modes to force and acceleration type responses was significant. Therefore, considering only the controlled mode in the analysis may be misleading and produce non-conservative results because the responses of higher modes may become as large as or larger than the response of the controlled mode. For the office tower example, with approximate square cross section, it was found that the contribution of higher modes of vibration to force and acceleration type responses was significant only for alongwind excitation. For crosswind wake excitation, the response was dominated by the first mode of vibration only. The theoretical method described in this Chapter seems to be a way of justifying whether simple aeroelastic wind tunnel tests, in which only the first vibration mode is considered, can be used for estimating dynamic responses of some structures.

It should be emphasised that the TLCD considered here was uni-directional. For practical purposes, bi-directional tuned liquid column damper should be investigated. In addition, the analysis of the TLCMD system in this thesis is mainly for investigating the effects on the damper effectiveness of liquid motion in some TMDs in which liquid is used as mass.

Chapter 9

SOIL-STRUCTURE-MASS DAMPER INTERACTION

9.1 Introduction

The procedures developed to-date to investigate the effect of tuned mass dampers on the response of wind-sensitive structures have been based on the assumption that the structure is perfectly clamped at its base without any displacements. It should be observed that this hypothesis, although usual in wind engineering, may in some cases be detrimental to a correct analysis of the phenomenon and a reliable assessment of the effectiveness of a mass damper.

It is well known that when soil or foundation flexibility is taken into account, the natural frequencies of the soil-structure system are modified to some extent which depends on the properties of soil and structures (Novak, 1974; Solari and Stura, 1979; Ogendo, Milsted and Johns, 1983; Lin and Wu, 1984; Novak and Hifnawy, 1988). This characteristic becomes particularly important for structure-mass damper systems, where the effectiveness of a tuned mass damper greatly depends on its frequency being tuned to the natural frequency of the structure, especially for smaller mass ratios as discussed in Chapter 5. The modification of the natural frequencies of soil-structure systems causes the resonance response peaks to get closer to the dominant frequencies of the alongwind turbulence and changes the critical wind velocities related to the crosswind responses of the system. At the same time, a soft soil allows for more energy dissipation by radiation and hysteretic damping mechanism, leading to a change of the system damping. These factors will directly affect the effectiveness of tuned mass dampers and therefore it is important to present an analytical procedure for soil-structure-mass damper systems under random wind excitation.

The analysis of the wind-induced response of soil-structure-mass damper systems is more complex than that of structure-mass damper systems

or soil-structure systems. The dampers are usually confined to a few discrete locations but wind loads are distributed over the whole superstructure. Furthermore, the stiffness and damping attributed to the soil mass under the foundation are frequency-dependent and the combined soil-structure system does not possess a set of classical normal modes (Lin and Wu, 1984).

In this Chapter a theoretical framework has been developed for the dynamic analysis of soil-structure-mass damper systems excited by wind. The alongwind turbulence and the crosswind wake excitation were modelled as stochastic processes which are the same as those used in Chapter 8. The soil properties, including the footing embedment effect, were characterized by a known frequency-dependent compliant matrix (Beredugo and Novak, 1972). Only the mass damper is considered here, but the derived conclusions are believed to be applicable to the liquid damper case. The transfer matrix formulation was employed in which the frequency-dependent soil behaviour can be easily dealt with in the frequency domain and any desired number of modes may be conveniently included.

Based on the derived formulation, a computer program which is used in Chapter 8 was modified to meet present requirements. Also the two numerical examples, a 370m high TV tower and a 306m high office tower, used in last Chapter were employed in this Chapter after including the soil and footing properties. Some equations used in Chapter 8 are included here in order to make it convenient to read.

9.2 Basic Equations

As shown in Fig. 9.1, the system model used in the present study consists of an N -lumped mass multi-degree-of-freedom superstructure founded on a rigid footing which, in turn, is supported by a flexible soil mass. Only one mass damper is utilised and such damper is connected to the n th mass. The combined soil-structure-mass damper system is assumed to be linear. The rest of assumptions is same as those used in Chapter 8.

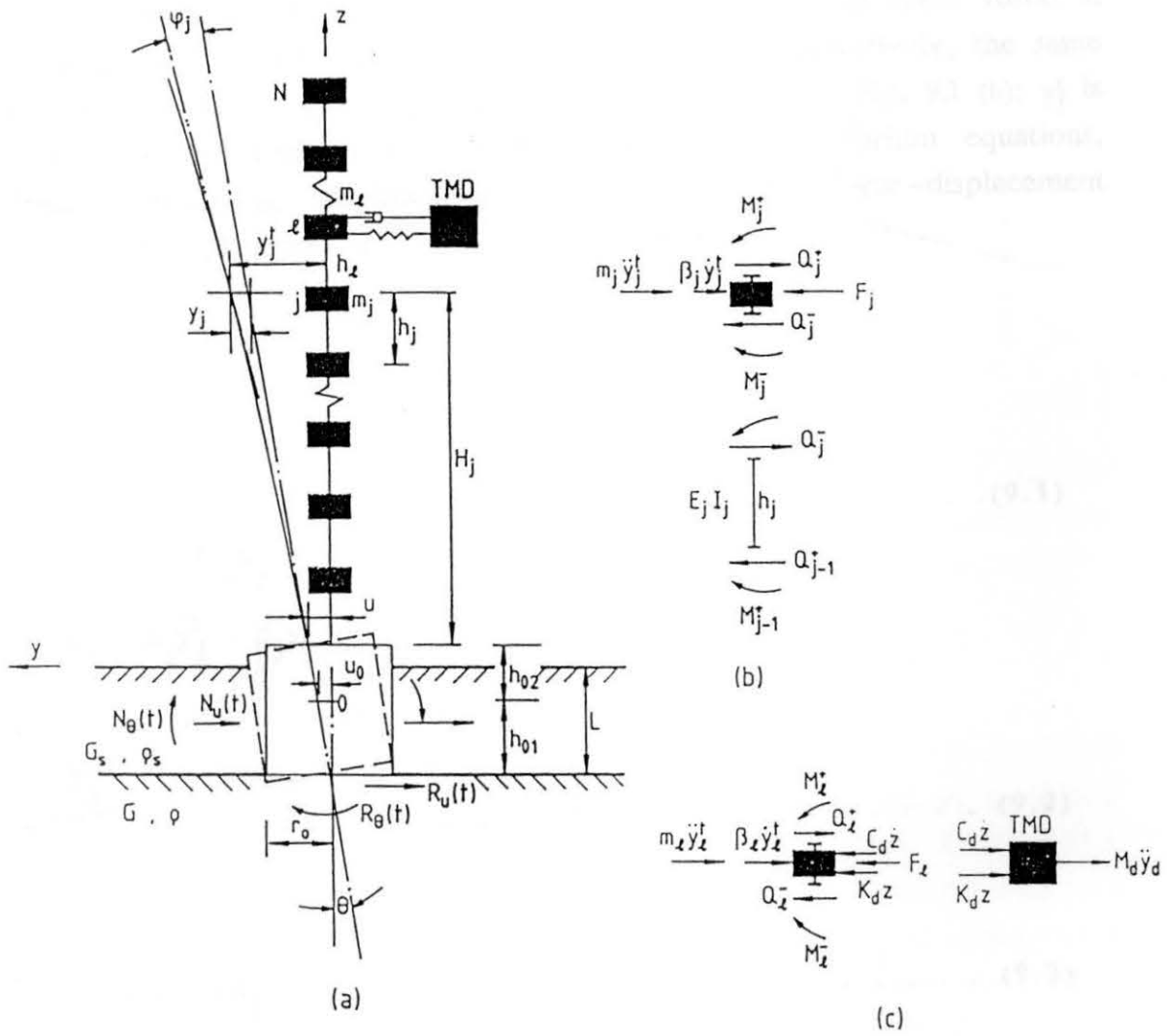


FIG.9.1 SYSTEM MODEL:

- (a) Soil-Structure-Damper System
- (b) Forces on j^{th} Story Unit
- (c) Forces on l^{th} Mass and TMD

9.2.1 Superstructure

Let u and θ be, respectively, the translation and rotation of the footing. y_j^+ , φ_j^+ , M_j^+ , and Q_j^+ are, respectively, the relative displacement to the footing, relative angular displacement, bending moment and shear force at the top end of the j th mass; y_j^- , φ_j^- , M_j^- and Q_j^- are, respectively, the same quantities at the bottom end of the j th mass, as shown in Fig. 9.1 (b); y_j^t is the absolute displacement of the j th mass. The equilibrium equations, continuity equations, displacement equation and the force-displacement relation of the j th storey unit are given as follows:

$$\left. \begin{aligned} M_j^+ &= M_j^- \\ Q_j^- &= Q_{j-1}^+ \\ M_j^- &= M_{j-1}^+ + Q_{j-1}^+ h_j \\ Q_j^+ &= Q_j^- - m_j \ddot{y}_j^t - \beta_j \dot{y}_j^t + F_j \end{aligned} \right\} \dots \dots \dots (9.1)$$

$$\left. \begin{aligned} y_j^+ &= y_j^- \\ \varphi_j^+ &= \varphi_j^- \end{aligned} \right\} \dots \dots \dots (9.2)$$

$$y_j^t = y_j + u + \theta H_j \dots \dots \dots (9.3)$$

$$E_j I_j y'' = M \dots \dots \dots (9.4)$$

In which m_j , β_j , h_j , H_j , E_j and I_j are the j th storey mass, damping, height, total height above the footing, elastic modulus and inertia moment, respectively; F_j is the wind force at the j th mass; a dot represents the first-order derivative with respect to time; a prime indicates the first-order derivative with respect to position coordinate.

The above equations are similar to those in Chapter 8. However, the effect of the footing displacement and rotation is now considered. Integrating Eq. 9.4 for the j th storey unit and using Fourier transformation, one can obtain corresponding equations in the frequency domain in the following matrix form:

$$\begin{bmatrix} \tilde{y}_j^+ \\ \tilde{\varphi}_j^+ \\ \tilde{M}_j^+ \\ \tilde{Q}_j^+ \end{bmatrix} = [T_j]_{4 \times 4} \times \begin{bmatrix} \tilde{y}_{j-1}^+ \\ \tilde{\varphi}_{j-1}^+ \\ \tilde{M}_{j-1}^+ \\ \tilde{Q}_{j-1}^+ \end{bmatrix} + \tilde{a}_j \begin{bmatrix} 0 \\ 0 \\ 0 \\ \tilde{u} + H_j \tilde{\theta} \end{bmatrix} + \begin{bmatrix} 0 \\ 0 \\ 0 \\ \tilde{F}_j \end{bmatrix} \dots \dots (9.5)$$

where "~" denotes the Fourier transform; and $[T_j]$ is known as a transfer matrix. The argument ω for the quantities in the frequency domain has been omitted for simplicity. The elements of $[T_j]$ can be found in Eq. 8.5.

9.2.2 Footing and soil

Many studies (e.g., Beredugo and Novak, 1972; Novak and Sachs, 1973) have shown that the vibrations of shallow foundations (such as mats and rafts) can be greatly affected by their partial embedment into the soil. This represents a very difficult problem to solve in a rigorous analytical way. In general, finite element technique or other discretising techniques appear very useful in solving the problem. However, it would be a loss to entirely discard the already numerous and sophisticated solutions of the surface footings because of the possible effect of embedment. Instead, it may often be quite sufficient, with all the other uncertainties, to apply an approximate correction for the effect of embedment to the solutions of surface footings.

Such an approximate analytical approach has been suggested and compared with many experimental results by Beredugo and Novak (1972), Novak and Beredugo (1972), and Novak and Sachs (1973). They discussed vertical, torsional and coupled horizontal and rocking vibration of embedded

footings. Because vertical vibration of embedded footings is not significant for wind-induced structural responses and to date there is no reliable theoretical model to describe wind-induced torsional excitation, only coupled horizontal and rocking vibration of embedded footings is considered in this thesis. This coupled vibration theory is based on the assumption that the dynamic reactions in the footing base are equal to those of an elastic half space and that the reactions acting on the footing sides are equal to those of an overlying independent elastic layer. Expressions for the coupled motion in the frequency domain are as follows, in a somewhat modified form, for $u = u_0 + \theta h_{02}$:

$$\begin{bmatrix} \tilde{\theta} \\ \tilde{u} \end{bmatrix} = \begin{bmatrix} C_{mm} & C_{mh} \\ C_{hm} & C_{hh} \end{bmatrix} \begin{bmatrix} \tilde{M}_0^+ \\ \tilde{Q}_0^+ \end{bmatrix} \dots \dots \dots (9.6)$$

where

$$C_{mm} = [(K_{uu} - \bar{m}\omega^2) + i\omega C_{uu}] / \Delta$$

$$C_{mh} = C_{hm} = -[(K_{u\theta} + \bar{m}\omega^2 h_{02} - K_{uu} h_{02}) + i\omega (C_{u\theta} - C_{uu} h_{02})] / \Delta$$

$$C_{hh} = [(K_{\theta\theta} - \bar{I}\omega^2 - 2K_{u\theta} h_{02} + K_{uu} h_{02}^2 + \bar{m}\omega^2 h_{02}^2) + i\omega (C_{\theta\theta} - 2C_{u\theta} h_{02} + C_{uu} h_{02}^2)] / \Delta$$

$$\Delta = (K_{uu} K_{\theta\theta} - \bar{I}\omega^2 K_{uu} - \bar{m}\omega^2 K_{\theta\theta} + \bar{m}\bar{I}\omega^4 - \omega^2 C_{uu} C_{\theta\theta} - 2\omega^2 C_{uu}^2 h_{02}^2 + \omega^2 C_{u\theta}^2 - K_{u\theta}^2) + i(\omega C_{\theta\theta} K_{uu} + \omega C_{uu} K_{\theta\theta} - \bar{m}\omega^3 C_{\theta\theta} - \bar{I} C_{uu} \omega^2 - 2\omega C_{u\theta} K_{u\theta})$$

in which u_0 = translation of the footing center of gravity; h_{02} = height from the footing surface to the gravity center, as shown in Fig. 9.1; \bar{m} = total mass of footing; \bar{I} = mass moment of inertia about a horizontal axis passing through the center of gravity; K_{uu} , $K_{\theta\theta}$ and $K_{u\theta}$ are the frequency dependent spring constants, and C_{uu} , $C_{\theta\theta}$ and $C_{u\theta}$ are the frequency

dependent damping coefficients. Their analytical expressions are as follows:

$$\left. \begin{aligned}
 K_{uu} &= Gr_0 \left(C_{u1} + \frac{G_s}{G} \delta S_{u1} \right) \\
 K_{\theta\theta} &= Gr_0^3 \left[C_{\theta1} + \left(\frac{h_{01}}{r_0} \right)^2 C_{u1} + \frac{G_s}{G} \delta S_{\theta1} \right. \\
 &\quad \left. + \frac{G_s}{G} \delta \left(\frac{\delta^2}{3} + \frac{h_{01}^2}{r_0^2} - \delta \frac{h_{01}}{r_0} \right) S_{u1} \right] \\
 K_{u\theta} &= -Gr_0 \left[h_{01} C_{u1} + \frac{G_s}{G} \delta \left(h_{01} - \frac{1}{2} L \right) S_{u1} \right]
 \end{aligned} \right\} \dots \dots (9.7)$$

$$\left. \begin{aligned}
 C_{uu} &= \frac{Gr_0}{\omega} \left(C_{u2} + \frac{G_s}{G} \delta S_{u2} \right) \\
 C_{\theta\theta} &= \frac{Gr_0^3}{\omega} \left[C_{\theta2} + \left(\frac{h_{01}}{r_0} \right)^2 C_{u2} + \frac{G_s}{G} \delta S_{\theta2} \right. \\
 &\quad \left. + \frac{G_s}{G} \delta \left(\frac{\delta^2}{3} + \frac{h_{01}^2}{r_0^2} - \delta \frac{h_{01}}{r_0} \right) S_{u2} \right] \\
 C_{u\theta} &= -\frac{Gr_0}{\omega} \left[h_{01} C_{u2} + \frac{G_s}{G} \delta \left(h_{01} - \frac{1}{2} L \right) S_{u2} \right]
 \end{aligned} \right\} \dots \dots (9.8)$$

In the above equations, G and G_s = the shear modulus of soil beneath the footing base and adjacent to the footing sides, respectively; r_0 = radius of the cylindrical footing or equivalent radius of a rectangular footing; δ = L/r_0 = relative embedment depth; L = embedment depth; h_{01} = height of gravity center above the footing base. Parameters C_{ij} and S_{ij} ($i = u, \theta$; $j = 1, 2$) are frequency dependent, but do not vary greatly with frequency. For practical purposes, they can often be considered approximately constant, at least over a certain frequency range of interest. Several values of such approximately constant parameters have been given by Novak (1974).

9.2.3 Mass damper

When a tuned mass damper is connected to the n th ($1 \leq n \leq N$) mass of the superstructure by a damper dashpot and spring, its equations of motion, referring to Fig. 9.1 (c), are

$$\left. \begin{aligned} M_d \ddot{y}_d + K_d Z + C_d \dot{Z} &= 0 \\ y_d &= Z + y_n^t = Z + y_n + u + \theta H_n \end{aligned} \right\} \dots \dots \dots (9.9)$$

Where M_d , K_d , C_d and y_d are, respectively, the mass, spring stiffness, damping and absolute displacement of the damper; Z is the relative displacement of the damper to the superstructure.

The Fourier transform of Eq. 9.9 results in the following relationship in the frequency domain:

$$\tilde{Z} = \frac{M_d \omega^2 (\tilde{y}_n + \tilde{u} + \tilde{\theta} H_n)}{-M_d \omega^2 + K_d + i \omega C_d} \dots \dots \dots (9.10)$$

For the main structure, the resultant external force, F_{nt} , applied at the n th mass is

$$F_{nt} = F_n + K_d Z + C_d \dot{Z} \dots \dots \dots (9.11)$$

Its Fourier transform is

$$\tilde{F}_{nt} = \tilde{F}_n + K_d \tilde{Z} + i \omega C_d \tilde{Z} \dots \dots \dots (9.12)$$

Eqs. 9.5, 9.6 and 9.10 are the basic equations of the soil-structure-mass damper system in the frequency domain. They are coupled with each other.

9.3 Frequency Response Function of the System

Frequency response functions represent a relation between the output and input of the system in the frequency domain and at a steady-state. Based on the basic equations and boundary conditions of the system, they can be derived in the following steps:

Letting \tilde{F}_{nt} replace \tilde{F}_n in Eq. 9.5, when $j = n$, one can repeatedly use Eq. 9.5 to the surface of the footing. The boundary conditions at the 0th storey (the footing surface) are $\tilde{y}_0 = \tilde{\varphi}_0 = 0$. Thus,

$$\begin{aligned}
& \begin{bmatrix} \tilde{y}_j^+ \\ \tilde{\varphi}_j^+ \\ \tilde{M}_j^+ \\ \tilde{Q}_j^+ \end{bmatrix} - \left(\prod_{k=1}^j [T_k] \right) \begin{bmatrix} 0 \\ 0 \\ \tilde{M}_0^+ \\ \tilde{Q}_0^+ \end{bmatrix} + \sum_{k=1}^{j-1} \left(\prod_{s=k+1}^j [T_s] \right) \begin{bmatrix} 0 \\ 0 \\ 0 \\ \tilde{F}_k \end{bmatrix} + \begin{bmatrix} 0 \\ 0 \\ 0 \\ \tilde{F}_j \end{bmatrix} \\
& + \left\{ \left(\sum_{k=1}^{j-1} \bar{a}_k \cdot \prod_{s=k+1}^j [T_s] \right) + \bar{a}_j [I] \right\} \begin{bmatrix} 0 \\ 0 \\ 0 \\ \tilde{u} \end{bmatrix} \\
& + \left\{ \left(\sum_{k=1}^{j-1} \bar{a}_k \cdot H_k \cdot \prod_{s=k+1}^j [T_s] \right) + \bar{a}_j \cdot H_j \cdot [I] \right\} \begin{bmatrix} 0 \\ 0 \\ 0 \\ \tilde{\theta} \end{bmatrix} \dots \dots \dots (9.13)
\end{aligned}$$

The top storey of the superstructure has a free boundary. By letting $j = N$, one can obtain a relation between the top state vector and the bottom state vector of the superstructure, namely,

$$\begin{aligned}
& \begin{bmatrix} \tilde{y}_N^+ \\ \tilde{\varphi}_N^+ \\ 0 \\ 0 \end{bmatrix} = [A_1] \begin{bmatrix} 0 \\ 0 \\ \tilde{M}_0^+ \\ \tilde{Q}_0^+ \end{bmatrix} + [B] \begin{bmatrix} 0 \\ 0 \\ 0 \\ \tilde{u} \end{bmatrix} + [C] \begin{bmatrix} 0 \\ 0 \\ 0 \\ \tilde{\theta} \end{bmatrix} + \sum_{k=1}^N [A_{k+1}] \begin{bmatrix} 0 \\ 0 \\ 0 \\ \tilde{F}_k \end{bmatrix} \\
& \dots \dots \dots (9.14)
\end{aligned}$$

where

$$\left. \begin{aligned} [A_r] &= \prod_{s=r}^N [T_s] \quad (r=1, 2, \dots, N) \\ [A_{N+1}] &= [I] \\ [B] &= \sum_{k=1}^N \bar{a}_k [A_{k+1}] \\ [C] &= \sum_{k=1}^N \bar{a}_k H_k [A_{k+1}] \end{aligned} \right\} \dots \dots \dots (9.15)$$

in which \prod is a chain product sign and the direction of the matrix multiplication is from $k = r$ to $k = N$; $[I]$ is a unit matrix; $[B]$ is an influence matrix of the footing translation while $[C]$ is an influence matrix of the footing rotation.

Substituting Eq. 9.6 into Eq. 9.14, from the third and fourth rows of Eq. 9.14, we obtain

$$\begin{bmatrix} \tilde{M}_0^+ \\ \tilde{Q}_0^+ \end{bmatrix} = \begin{bmatrix} g_{11} & g_{12} & \dots & g_{1N} \\ g_{21} & g_{22} & \dots & g_{2N} \end{bmatrix} \begin{bmatrix} \tilde{F}_1 \\ \vdots \\ \tilde{F}_{nt} \\ \vdots \\ \tilde{F}_N \end{bmatrix} \dots \dots \dots (9.16)$$

where

$$\left. \begin{aligned} g_{1i} &= (d^{22}a_{i+1}^{34} - d^{12}a_{i+1}^{44})/\Delta_1 \\ g_{2i} &= (d^{11}a_{i+1}^{44} - d^{21}a_{i+1}^{34})/\Delta_1 \\ \Delta_1 &= d^{21}d^{12} - d^{11}d^{22} \end{aligned} \right\} \dots \dots \dots (9.17)$$

$$\left. \begin{aligned} d^{11} &= a_1^{33} + b^{34}C_{hm} + c^{34}C_{mm} \\ d^{12} &= a_1^{34} + b^{34}C_{hh} + c^{34}C_{mh} \\ d^{21} &= a_1^{43} + b^{44}C_{hm} + c^{44}C_{mm} \\ d^{22} &= a_1^{44} + b^{44}C_{hh} + c^{44}C_{mh} \end{aligned} \right\} \dots \dots \dots (9.18)$$

In the above equations, a_k^{ij} is the ij element of matrix $[A_k]$; b^{ij} is the ij element of matrix $[B]$ and c^{ij} represents the ij element of matrix $[C]$.

It should be noted that the resultant external force \tilde{F}_{n_t} (transformed) in Eq. 9.16 is governed by Eq. 9.12 and Eq. 9.10. Therefore, Eq. 9.16 includes five unknown quantities, namely, \tilde{M}_0^+ , \tilde{Q}_0^+ , \tilde{y}_n , \tilde{u} and $\tilde{\theta}$. If Eq. 9.12, Eq. 9.10 and Eq. 9.6 are substituted into Eq. 9.16, two unknowns can be reduced and, after some algebra, the following equations can be derived:

$$\begin{bmatrix} \tilde{M}_0^+ \\ \tilde{Q}_0^+ \end{bmatrix} = \begin{bmatrix} k_{11} & k_{12} & \dots & k_{1N} \\ k_{21} & k_{22} & \dots & k_{2N} \end{bmatrix} \begin{bmatrix} \tilde{F}_1 \\ \vdots \\ \tilde{F}_n \\ \vdots \\ \tilde{F}_N \end{bmatrix} + \begin{bmatrix} k_{1n} \\ k_{2n} \end{bmatrix} \cdot D_1 \tilde{y}_n \dots \dots \dots (9.19)$$

where

$$\left. \begin{aligned} k_{1i} &= (e^{22}g_{1i} - e^{12}g_{2i})/\Delta_2 \\ k_{2i} &= (e^{11}g_{2i} - e^{21}g_{1i})/\Delta_2 \\ \Delta_2 &= e^{11}e^{12} - e^{21}e^{22} \end{aligned} \right\} (i = 1, 2, \dots, N) \dots \dots \dots (9.20)$$

while

$$\left. \begin{aligned} e^{11} &= 1 - D_1 g_{1n} (C_{hm} + H_n C_{mm}) \\ e^{12} &= - D_1 g_{1n} (C_{hh} + C_{mh} H_n) \\ e^{21} &= - D_1 g_{2n} (C_{hm} + C_{mm} H_n) \\ e^{22} &= 1 - D_1 g_{2n} (C_{hh} + C_{mh} H_n) \end{aligned} \right\} \dots \dots \dots (9.21)$$

and

$$D_1 = \frac{M_d \omega^2 (K_d + i\omega C_d)}{-M_d \omega^2 + K_d + i\omega C_d} \dots \dots \dots (9.22)$$

Up to now, Eq. 9.19 still cannot be solved because there are three unknowns involved in the two equations.

Let j in Eq. 9.13 = n , and let

$$\left. \begin{aligned}
 [A_r(n)] &= \prod_{s=r}^n [T_s] \quad (r=1, 2, \dots, n) \\
 [A_{n+1}(n)] &= [I] \\
 [B(n)] &= \sum_{k=1}^n \bar{a}_k [A_{k+1}(n)] \\
 [C(n)] &= \sum_{k=1}^n \bar{a}_k H_k [A_{k+1}(n)]
 \end{aligned} \right\} \dots \dots \dots (9.23)$$

Eq. 9.13 can be rewritten as follows:

$$\begin{bmatrix} \tilde{y}_n^+ \\ \tilde{\varphi}_n^+ \\ \tilde{M}_n^+ \\ \tilde{Q}_n^+ \end{bmatrix} = [A(n)] \begin{bmatrix} 0 \\ 0 \\ \tilde{M}_0^+ \\ \tilde{Q}_0^+ \end{bmatrix} + [B(n)] \begin{bmatrix} 0 \\ 0 \\ 0 \\ \tilde{u} \end{bmatrix} + [C(n)] \begin{bmatrix} 0 \\ 0 \\ 0 \\ \tilde{\theta} \end{bmatrix} \\
 + \sum_{k=1}^{n-1} [A_{k+1}(n)] \begin{bmatrix} 0 \\ 0 \\ 0 \\ \tilde{F}_k \end{bmatrix} + \begin{bmatrix} 0 \\ 0 \\ 0 \\ \tilde{F}_{nt} \end{bmatrix} \dots \dots \dots (9.24)$$

The first and second rows of Eq. 9.24 do not include the resultant force (transformed) \tilde{F}_{nt} . After substituting Eq. 9.6 into Eq. 9.24, they can be rearranged into

$$\begin{bmatrix} \tilde{y}_n^+ \\ \tilde{\varphi}_n^+ \end{bmatrix} = \begin{bmatrix} d^{11}(n) & d^{12}(n) \\ d^{21}(n) & d^{22}(n) \end{bmatrix} + \begin{bmatrix} \tilde{M}_0^+ \\ \tilde{Q}_0^+ \end{bmatrix}$$

$$+ \begin{bmatrix} a_2^{14}(n) & a_3^{14}(n) & \dots & a_n^{14}(n) \\ a_2^{24}(n) & a_3^{24}(n) & \dots & a_n^{24}(n) \end{bmatrix} \begin{bmatrix} \tilde{F}_1 \\ \tilde{F}_2 \\ \vdots \\ \tilde{F}_{n-1} \end{bmatrix} \dots \dots \dots (9.25)$$

where

$$\left. \begin{aligned} d^{11}(n) &= a_1^{13}(n) + b^{14}(n)C_{hm} + c^{14}(n)C_{mm} \\ d^{12}(n) &= a_1^{14}(n) + b^{14}(n)C_{hh} + c^{14}(n)C_{mh} \\ d^{21}(n) &= a_1^{23}(n) + b^{24}(n)C_{hm} + c^{24}(n)C_{mm} \\ d^{22}(n) &= a_1^{24}(n) + b^{24}(n)C_{hh} + c^{24}(n)C_{mh} \end{aligned} \right\} \dots \dots \dots (9.26)$$

in which $a_{kij}(n)$, $b_{ij}(n)$ and $c_{ij}(n)$ are the elements of matrices $[A_k(n)]$, $[B(n)]$ and $[C(n)]$ respectively.

Combining Eq. 9.19 and Eq. 9.25 results in

$$\begin{bmatrix} \tilde{y}_n^+ \\ \tilde{\phi}_n^+ \end{bmatrix} = \begin{bmatrix} s_{11} & s_{12} & \dots & s_{1N} \\ s_{21} & s_{22} & \dots & s_{2N} \end{bmatrix} \begin{bmatrix} \tilde{F}_1 \\ \vdots \\ \tilde{F}_n \\ \vdots \\ \tilde{F}_N \end{bmatrix} + \begin{bmatrix} s_{1n} \\ s_{2n} \end{bmatrix} D_1 \tilde{y}_n \dots \dots \dots (9.27)$$

where

$$\left. \begin{aligned} s_{1i} &= d^{11}(n)k_{1i} + d^{12}(n)k_{2i} + a_{i+1}^{14}(n) \\ s_{2i} &= d^{21}(n)k_{1i} + d^{22}(n)k_{2i} + a_{i+1}^{24}(n) \end{aligned} \right\} (i=1, 2, \dots, n-1) \\ \left. \begin{aligned} s_{1i} &= d^{11}(n)k_{1i} + d^{12}(n)k_{2i} \\ s_{2i} &= d^{21}(n)k_{1i} + d^{22}(n)k_{2i} \end{aligned} \right\} (i=n, n-1, \dots, N) \dots \dots (9.28)$$

Now, from the first row of Eq. 9.27, the relative displacement of the

nth mass of the superstructure can be, in the frequency domain, expressed as

$$\tilde{y}_n^+ = \sum_{j=1}^N \Psi_{1j} \tilde{F}_j \quad \dots \dots \dots (9.29)$$

in which

$$\Psi_{1j} = \frac{1}{1 - s_{1n} D_1} s_{1j} \quad (j = 1, 2, \dots, N) \quad \dots \dots \dots (9.30)$$

Thus the relative displacement of the nth mass of the superstructure, \tilde{y}_n^+ , is expressible in terms of the random wind excitation, known structural and soil parameters. It is of interest to note that, if the elements of the soil compliance matrix in Eq. 9.6 are equal to zero, namely, $\tilde{u} = \tilde{\theta} = 0$, Eqs. 9.28, 9.29 and 9.30 are the same as those previously obtained for the case of rigid soil in Chapter 8. This agreement provides an additional partial check for the present results.

Now, based on Eqs. 9.6, 9.10 and 9.19, the structural base shear and moment responses, the footing translation and rotation responses as well as the relative displacement response of the mass damper can also be expressed in the same manner.

$$\left. \begin{aligned} \tilde{M}_0^+ &= \sum_{j=1}^N \Omega_{1j} \tilde{F}_j ; & \tilde{Q}_0^+ &= \sum_{j=1}^N \Omega_{2j} \tilde{F}_j \\ \tilde{u} &= \sum_{j=1}^N X_{1j} \tilde{F}_j ; & \tilde{\theta} &= \sum_{j=1}^N X_{2j} \tilde{F}_j \\ \tilde{Z} &= \sum_{j=1}^N \Gamma_{1j} \tilde{F}_j \end{aligned} \right\} \dots \dots \dots (9.31)$$

in which

$$\left. \begin{aligned} \Omega_{1j} &= k_{1j} - \lambda_1 s_{1j} ; & \Omega_{2j} &= k_{2j} - \lambda_2 s_{1j} \\ X_{1j} &= C_{hm} \Omega_{1j} + C_{hh} \Omega_{2j} ; & X_{2j} &= C_{mm} \Omega_{1j} + C_{mh} \Omega_{2j} \\ \Gamma_{1j} &= D_2 (\Psi_{1j} + X_{1j} + H_n X_{2j}) ; \\ \lambda_1 &= \frac{k_{1n} D_1}{s_{1n} D_1 - 1} ; & \lambda_2 &= \frac{k_{2n} D_1}{s_{1n} D_1 - 1} \\ D_2 &= \frac{\omega^2 M_d}{-\omega^2 M_d + K_d + i\omega C_d} \quad (j = 1, 2, \dots, N) \end{aligned} \right\} \dots \dots \dots (9.32)$$

As for the top relative displacement and angular displacement of the superstructure, we can use a similar method, starting from the first and second rows of Eq. 9.14, to obtain

$$\left. \begin{aligned} \tilde{y}_N^+ &= \sum_{j=1}^N \theta_{2j} \tilde{F}_j \\ \tilde{\phi}_N^+ &= \sum_{j=1}^N \theta_{2j} \tilde{F}_j \end{aligned} \right\} \dots \dots \dots (9.33)$$

in which

$$\left. \begin{aligned} \theta_{1j} &= n_{1j} + n_{1n} D_1 (\Psi_{1j} + X_{1j} + H_n X_{2j}) \\ \theta_{2j} &= n_{2j} + n_{2n} D_1 (\Psi_{1j} + X_{1j} + H_n X_{2j}) \\ n_{1i} &= r^{11} g_{1i} + r^{12} g_{2i} + a_{i+1}^{14} \quad (i = 1, 2, \dots, N) \\ n_{2i} &= r^{21} g_{1i} + r^{22} g_{2i} + a_{i+1}^{24} \quad (j = 1, 2, \dots, N) \\ r^{11} &= a_1^{13} + b^{14} C_{hm} + c^{14} C_{mm} \\ r^{12} &= a_1^{14} + b^{14} C_{hh} + c^{14} C_{mh} \\ r^{21} &= a_1^{23} + b^{24} C_{hm} + c^{24} C_{mm} \\ r^{22} &= a_1^{24} + b^{24} C_{hh} + c^{24} C_{mh} \end{aligned} \right\} \dots \dots \dots (9.34)$$

Eqs. 9.29, 9.31 and 33 are input-output relations in the (transformed) frequency domain in which \tilde{F}_j ($j = 1, 2, \dots, N$) are the inputs and \tilde{y}_n , \tilde{M}_0 , \tilde{Q}_0 , \tilde{u} , $\tilde{\theta}$, \tilde{Z} , \tilde{y}_N and $\tilde{\phi}_N$ are the outputs. The outputs corresponding to various variables are also called the frequency response functions. In the foregoing frequency domain analysis, the common factor $e^{i\omega t}$ of all steady-state sinusoidally varying quantities has been omitted. In addition some symbols, e.g., Ω_{1j} and Ω_{2j} , which have been used in Chapter 8 are still used in this Chapter although these variables have slightly different meaning due to inclusion of footing and soil.

General expressions for the state vector of any storey, say the m th storey, can also be obtained. They are summarised as follows:

Let

$$\left. \begin{aligned}
 [A_r(m)] - \prod_{s=r}^m [T_s] \quad (r = 1, 2, \dots, m) \\
 [A_{m+1}(m)] - [I] \\
 [B(m)] - \sum_{k=1}^m \bar{a}_k [A_{k+1}(m)] \\
 [C(m)] - \sum_{k=1}^m \bar{a}_k H_k [A_{k+1}(m)]
 \end{aligned} \right\} \dots \dots \dots (9.35)$$

then

$$\left. \begin{aligned}
 \tilde{y}_m^+ - \sum_{j=1}^N E_{1j} \tilde{F}_j \quad ; \quad \tilde{\varphi}_m^+ - \sum_{j=1}^N E_{2j} \tilde{F}_j \\
 \tilde{M}_m^+ - \sum_{j=1}^N E_{3j} \tilde{F}_j \quad ; \quad \tilde{Q}_m^+ - \sum_{j=1}^N E_{4j} \tilde{F}_j
 \end{aligned} \right\} \dots \dots \dots (9.36)$$

where

$$\left. \begin{aligned}
 E_{1j} &= \Lambda_{1j}(m) + D_1 \Lambda_{1n}(m) [\Psi_{1j} + X_{1j} + H_n X_{2j}] \\
 E_{2j} &= \Lambda_{2j}(m) + D_1 \Lambda_{2n}(m) [\Psi_{1j} + X_{1j} + H_n X_{2j}] \\
 E_{3j} &= \Lambda_{3j}(m) + D_1 \Lambda_{3n}(m) [\Psi_{1j} + X_{1j} + H_n X_{2j}] \\
 E_{4j} &= \Lambda_{4j}(m) + D_1 \Lambda_{4n}(m) [\Psi_{1j} + X_{1j} + H_n X_{2j}]
 \end{aligned} \right\} (j=1, 2, \dots, N) \quad (9.37)$$

$$\left. \begin{aligned}
 \Lambda_{1j}(m) &= \begin{cases} t^{11} g_{1j} + t^{12} g_{2j} + a_{j+1}^{14}(m) & j = 1, 2, \dots, m-1 \\ t^{11} g_{1j} + t^{12} g_{2j} & j = m, m+1, \dots, N \end{cases} \\
 \Lambda_{2j}(m) &= \begin{cases} t^{21} g_{1j} + t^{22} g_{2j} + a_{j+1}^{24}(m) & j = 1, 2, \dots, m-1 \\ t^{21} g_{1j} + t^{22} g_{2j} & j = m, m+1, \dots, N \end{cases} \\
 \Lambda_{3j}(m) &= \begin{cases} t^{33} g_{1j} + t^{34} g_{2j} + a_{j+1}^{34}(m) & j = 1, 2, \dots, m-1 \\ t^{33} g_{1j} + t^{34} g_{2j} & j = m, m+1, \dots, N \end{cases} \\
 \Lambda_{4j}(m) &= \begin{cases} t^{43} g_{1j} + t^{44} g_{2j} + a_{j+1}^{44}(m) & j = 1, 2, \dots, m-1 \\ t^{43} g_{1j} + t^{44} g_{2j} & j = m, m+1, \dots, N \end{cases}
 \end{aligned} \right\} \dots \dots (9.38)$$

$$\left. \begin{aligned}
t^{11} &= a_1^{13}(m) + b^{14}(m)C_{hm} + c^{14}(m)C_{mm} \\
t^{12} &= a_1^{14}(m) + b^{14}(m)C_{hh} + c^{14}(m)C_{mh} \\
t^{21} &= a_1^{23}(m) + b^{24}(m)C_{hm} + c^{24}(m)C_{mm} \\
t^{22} &= a_1^{24}(m) + b^{24}(m)C_{hh} + c^{24}(m)C_{mh} \\
t^{33} &= a_1^{33}(m) + b^{34}(m)C_{hm} + c^{34}(m)C_{mm} \\
t^{34} &= a_1^{34}(m) + b^{34}(m)C_{hh} + c^{34}(m)C_{mh} \\
t^{43} &= a_1^{43}(m) + b^{44}(m)C_{hm} + c^{44}(m)C_{mm} \\
t^{44} &= a_1^{44}(m) + b^{44}(m)C_{hh} + c^{44}(m)C_{mh}
\end{aligned} \right\} \dots \dots \dots (9.39)$$

in which $a_k^{ij}(m)$, $b^{ij}(m)$ and $c^{ij}(m)$ are the (i,j) element of the matrix $[A_k(m)]$, $[B(m)]$ and $[C(m)]$, respectively.

Finally, the frequency response functions of the absolute displacement or angular displacement of any storey can be obtained by using

$$\left. \begin{aligned}
\tilde{y}_m^t &= \tilde{y}_m + \tilde{u} + \tilde{\theta}H_m \\
\tilde{\varphi}_m^t &= \tilde{\varphi}_m + \tilde{\theta}
\end{aligned} \right\} \dots \dots \dots (m = 1, 2, \dots, N) \quad (9.40)$$

in which y_m^t and φ_m^t represent the absolute displacement and angular displacement of the mth mass; y_m and φ_m are the corresponding relative displacement and angular displacement.

9.4 System Response

Since the system in the present study is linear, the input-output relations in the frequency domain, e.g., Eq. 9.29 and Eq. 9.31, can be used to construct the relationships between the cross-spectral densities of the inputs F_j ($j = 1, 2, \dots, N$) and those of the outputs, using the same definitions as described by Eq. 8.40. The alongwind turbulence spectrum expressed by Eq. 8.46 and the crosswind wake excitation spectrum by Eq. 8.49 are also

used in this Chapter.

As a result, the spectral densities of the bottom moment, the bottom shear force, the nth mass relative displacement and absolute displacement, the translation and rotation of the footing and the relative displacement of the tuned mass damper can be derived as follows:

$$\left. \begin{aligned}
 \Phi_{M_0 M_0}(\omega) &= \sum_{i=1}^N \sum_{j=1}^N \Omega_{1i} \Phi_{F_i F_j}(\omega) \Omega_{1j}^* \\
 \Phi_{Q_0 Q_0}(\omega) &= \sum_{i=1}^N \sum_{j=1}^N \Omega_{2i} \Phi_{F_i F_j}(\omega) \Omega_{2j}^* \\
 \Phi_{y_n y_n}(\omega) &= \sum_{i=1}^N \sum_{j=1}^N \Psi_{1i} \Phi_{F_i F_j}(\omega) \Psi_{1j}^* \\
 \Phi_{y_n^t y_n^t}(\omega) &= \sum_{i=1}^N \sum_{j=1}^N \Psi_{2i} \Phi_{F_i F_j}(\omega) \Psi_{2j}^* \\
 \Phi_{u u}(\omega) &= \sum_{i=1}^N \sum_{j=1}^N X_{1i} \Phi_{F_i F_j}(\omega) X_{1j}^* \\
 \Phi_{\theta \theta}(\omega) &= \sum_{i=1}^N \sum_{j=1}^N X_{2i} \Phi_{F_i F_j}(\omega) X_{2j}^* \\
 \Phi_{Z Z}(\omega) &= \sum_{i=1}^N \sum_{j=1}^N \Gamma_{1i} \Phi_{F_i F_j}(\omega) \Gamma_{1j}^*
 \end{aligned} \right\} \dots \dots \dots (9.41)$$

The expression for the response at other locations of the superstructure can also be obtained by using Eq. 9.36 in the same manner. In addition, the power spectral density of the nth absolute acceleration response is given by

$$\Phi_{y_n^t y_n^t}(\omega) = \omega^4 \Phi_{y_n y_n}(\omega) = \omega^2 \sum_{j=1}^N \sum_{j=1}^N \Psi_{2j} \Phi_{F_i F_j}(\omega) \Psi_{2j}^* \dots \dots \dots (9.42)$$

in which

$$\Psi_{2j} = \Psi_{1j} + X_{1j} + X_{2j} H_n$$

which is derived from Eq. 9.40.

Since the present system is still a linear systems, both the mean wind

force and the mean system response can be computed separately. Consequently, the standard deviations of various system response quantities can be evaluated through numerical integrations. For those quantities in Eq. 9.41 and Eq. 9.42, the standard deviations, namely the square-root of each variance, are given by

$$\left. \begin{aligned}
 \sigma_{M_0} &= [\int_0^\infty \phi_{M_0 M_0}(\omega) d\omega]^{\frac{1}{2}}; & \sigma_{Q_0} &= [\int_0^\infty \phi_{Q_0 Q_0}(\omega) d\omega]^{\frac{1}{2}} \\
 \sigma_{y_n} &= [\int_0^\infty \phi_{y_n y_n}(\omega) d\omega]^{\frac{1}{2}}; & \sigma_{y_n^t} &= [\int_0^\infty \phi_{y_n^t y_n^t}(\omega) d\omega]^{\frac{1}{2}} \\
 \sigma_u &= [\int_0^\infty \phi_{uu}(\omega) d\omega]^{\frac{1}{2}}; & \sigma_\theta &= [\int_0^\infty \phi_{\theta\theta}(\omega) d\omega]^{\frac{1}{2}} \\
 \sigma_z &= [\int_0^\infty \phi_{zz}(\omega) d\omega]^{\frac{1}{2}}; & \sigma_{y_n^t} &= [\int_0^\infty \phi_{y_n^t y_n^t}(\omega) d\omega]^{\frac{1}{2}}
 \end{aligned} \right\} \dots (9.43)$$

In the above equations, one-sided power spectral density functions are used.

9.5 Numerical Examples

Two numerical examples and a computer program which have been used in Chapter 8 were modified to include soil flexibility. The office tower is described first and then the TV tower because the numerical results show that the effect of soil on the wind-induced response of the structure-damper system is more important for the office tower than the TV tower.

9.5.1 Office tower

The superstructure is modelled as a 10-degree-of-freedom system taking into account both bending and shear. The structural data used in the analysis can be found in Table 8.4. For rigid soil (i.e., clamped case), the first three natural frequencies of the structure are 0.175, 0.569 and 1.333 Hz, respectively.

The square foundation is assumed to have an equivalent radius of 28.2m and an embedment ratio $L/r_0 = 0.18$. The stiffness of the soil is considered variable and is characterised by the shear wave velocity. The soil density ρ_s is considered constant and equal to 1800kg/m³. The lowest shear wave velocity is 100m/sec while the highest velocity is 600m/sec. Shear wave velocities ranging from 150 to 250m/sec correspond to sands and higher than 600m/sec correspond to bedrock. The stiffness and damping parameters in Eqs.9.7 and 9.8 are considered invariable. Variable parameters could also be considered if desired; however, for the purpose of considering the overall trends, constant parameters are adequate (Novak, 1974).

The mass of the mass damper is considered constant and equal to 839 tonnes (corresponding to the effective mass ratio of 3% for the first vibration mode of the main structure). The critical damping ratio from the dashpot is also considered constant and equal to 5%. For rigid soil, the frequency of the damper is tuned to the first natural frequency of the structure and, therefore, the damper spring constant = 1015.4 kN/m. For compliant soil, two different cases are considered: one is keeping the spring constant equal to 1015.4 kN/m within the studied range of shear wave velocities; the other is to find the first natural frequency of soil-structure system and then tune the damper frequency to this system frequency.

For the wind environment, the same data as in Chapter 8 are used. In order to make it convenient to read, however, these data are described again. The aerodynamic data pertaining to alongwind excitation are:

- $\bar{V}_{1,0}$ = reference mean wind velocity at 10m height above ground = 15.9 m/s;
- α = exponent for the mean wind velocity profile power law = 0.25;
- z_g = gradient height = 400m; \bar{V}_G = gradient velocity = 40 m/s;
- C_a = drag coefficient = 1.2; ρ_a = air density = 1.2 kg/m³;
- $C_1 = 7.0$ and $\kappa_0 = 0.01$, constants in the wind spectrum.

The aerodynamic data pertaining to wake excitation are;

$$\bar{V}_{1,0} = 15.9 \text{ m/s};$$

$\alpha = 0.25;$

$C_1 = \text{lift coefficient} = 0.4;$

$S = \text{Strouhal number} = 0.12;$

$B_s = \text{constant related to the relative width of the relative spectral peak} = 0.26;$

α_1 and $\alpha_2 = \text{nondimensional coefficients related to the correlation length} = 0.5 \text{ and } 5, \text{ respectively.}$

The first three natural frequencies are plotted vs shear wave velocity of the soil, as shown in Fig. 9.2. All the natural frequencies increase with increasing stiffness of the soil and approach the corresponding frequencies in the clamped structure. The first natural frequency of the soil-structure system, when the shear wave velocity is equal to 100 m/s, is only 54% of the fundamental frequency in the clamped structure.

Figs. 9.3, 9.4 and 9.5 present the variation of the standard deviations of the alongwind office tower base moments, top total displacements and accelerations with various shear wave velocities of the soil. All standard deviation responses are normalised by the corresponding structural responses for rigid soil and without any mass dampers. In comparison with the responses of the structure-tuned mass damper system on rigid soil, soil compliancy decreases the base moment and top total acceleration responses, but increases the top total displacement responses of the soil-structure-tuned mass damper system for alongwind turbulence excitation. When comparing these results with the responses of the soil-structure system without mass dampers, it was found that when the soil is extremely soft, the tuned mass damper is not an effective method to reduce soil-structure system responses.

Power spectral densities of alongwind base moments and top total accelerations of office tower are shown in Figs. 9.6 and 9.7. Here the shear wave velocity of the soil, v_s , is 300 m/s. It can be seen that the soil compliancy has the obvious effect of shifting the locations of resonance peaks to lower frequencies and reduces all the magnitudes of the resonance peaks. The mass damper, tuned to the system fundamental frequency, can significantly reduce the first resonance peak magnitude but cannot affect the

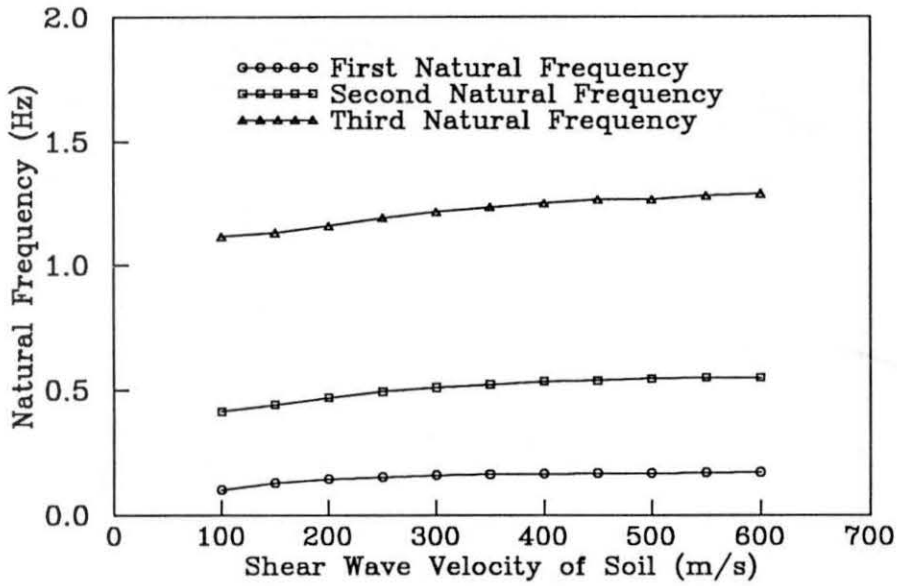


FIG. 9.2 VARIATIONS OF NATURAL FREQUENCIES OF OFFICE TOWER WITH VARIOUS SHEAR WAVE VELOCITIES OF SOIL

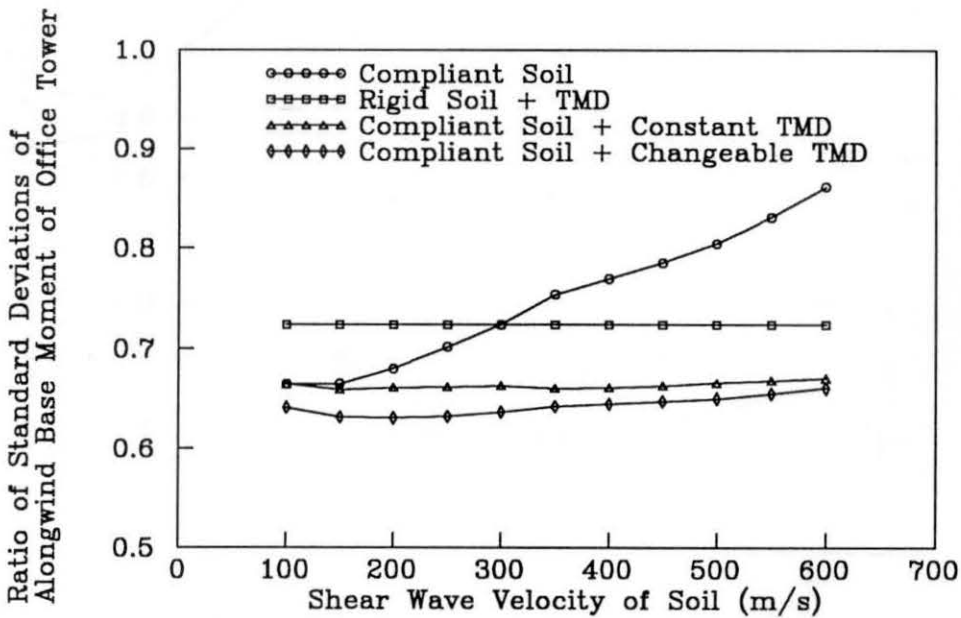


FIG. 9.3 VARIATIONS OF STANDARD DEVIATIONS OF ALONGWIND BASE MOMENTS OF OFFICE TOWER WITH VARIOUS SHEAR WAVE VELOCITIES OF SOIL

Ratio of Standard Deviations of Alongwind Displacements at Top of Office Tower

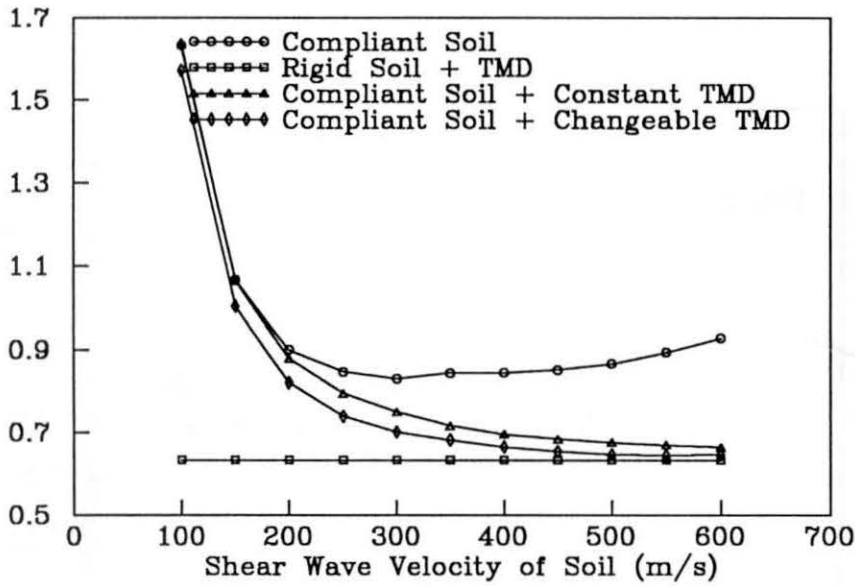


FIG. 9.4 VARIATIONS OF STANDARD DEVIATIONS OF ALONGWIND TOTAL DISPLACEMENTS AT THE TOP OF OFFICE TOWER WITH VARIOUS SHEAR WAVE VELOCITIES OF SOIL

Ratio of Standard Deviations of Alongwind Total Accelerations at Top of Office Tower

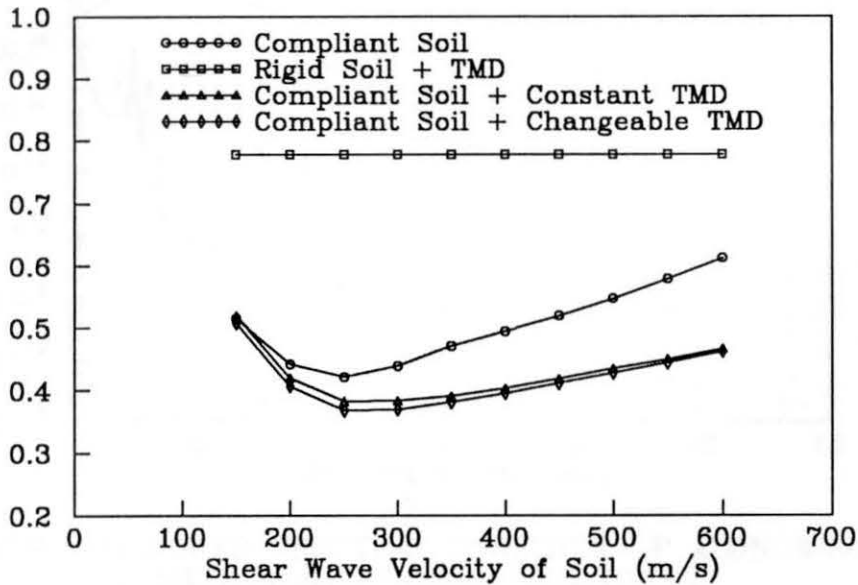


FIG. 9.5 VARIATIONS OF STANDARD DEVIATIONS OF ALONGWIND TOTAL ACCELERATIONS AT THE TOP OF OFFICE TOWER WITH VARIOUS SHEAR WAVE VELOCITIES OF SOIL

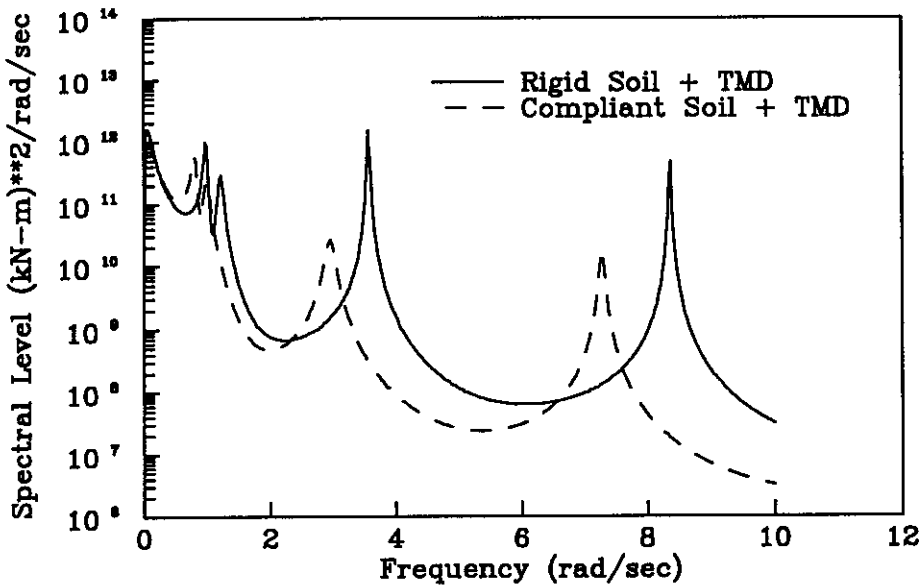
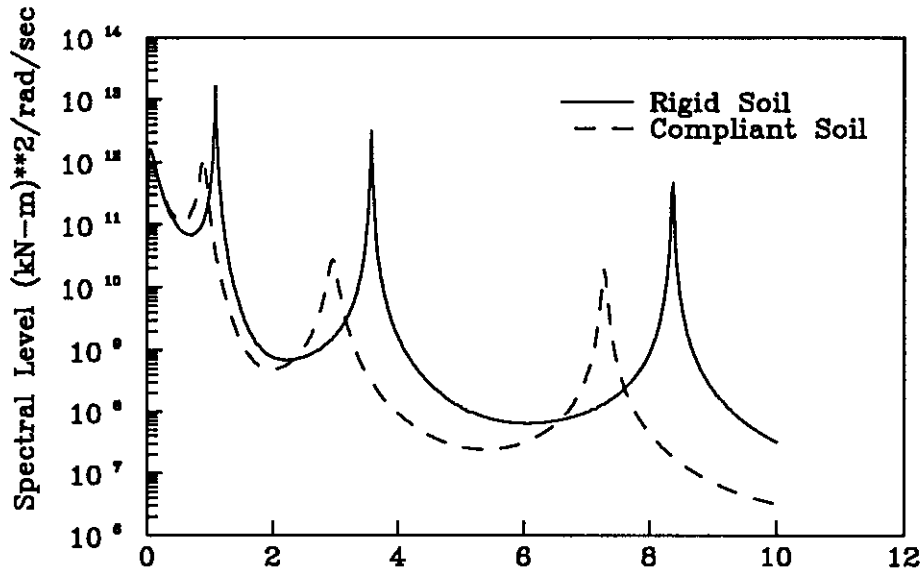


FIG. 9.6 POWER SPECTRAL DENSITIES OF ALONGWIND BASE MOMENT OF OFFICE TOWER

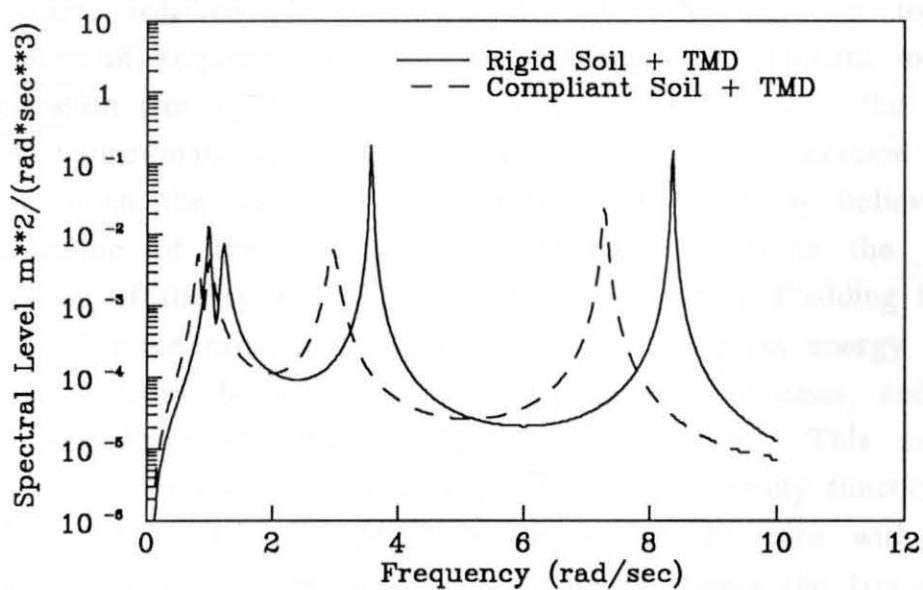
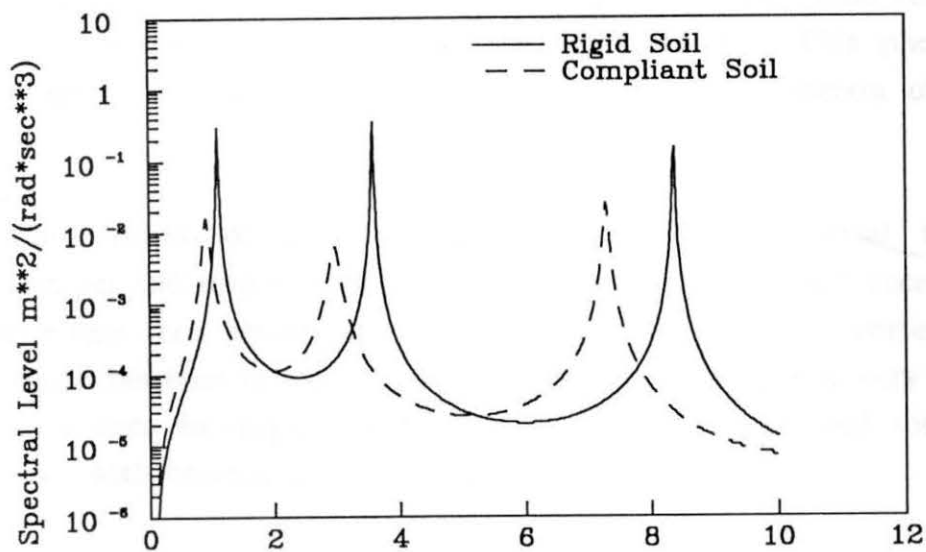


FIG. 9.7 POWER SPECTRAL DENSITIES OF ALONGWIND TOTAL ACCELERATIONS AT THE TOP OF OFFICE TOWER

higher frequency resonance peaks, regardless of whether soil compliancy is being considered or not. It can also be easily seen that the wind-induced responses of the system with a tuned mass damper should involve more vibration modes. Considering only one mode for such a combined system may lead to non-conservative errors, for the controlled mode responses may become the same as or less than the other modes. This phenomenon is particularly obvious in top total acceleration response spectra of the office tower.

Comparisons of standard deviations of the alongwind top relative acceleration and displacement of office tower with the total acceleration and displacement are shown in Figs. 9.8 and 9.9. For accelerations, the difference between relative responses and total responses is very small while the difference in displacement responses is very large and the difference increases with decreasing soil stiffness.

Figs. 9.10, 9.11 and 9.12 show the variation of the standard deviations of the crosswind tower base moments, top total displacements and accelerations with various shear wave velocities of the soil. Under crosswind wake excitation, soil compliancy increases not only the top total dynamic displacement response but also the dynamic base moment and top total acceleration (for $v_s < 250$ m/s) responses, compared with the responses of the structure-mass damper system on rigid soil. This increase will become larger when the soil becomes softer. It is believed that the modification of the system natural frequencies causes the first natural frequency of the system to get closer to the vortex shedding frequency of crosswind wake excitation. As a result, the vibration energy absorbed by the tower from the vortex shedding significantly increases, and it is more than that dissipated through damping due to soil. This explanation is strengthened by the corresponding power spectral density functions as shown in Figs. 9.13 and 9.14. In both figures for the case with tuned mass dampers, the soil compliancy ($v_s = 300$ m/s) lowers the frequency of the first resonance peak but does not reduce the magnitude of the first resonance peak.

From Figs. 9.10, 9.11 and 9.12, it is found that the mass damper should

Standard Deviations of Alongwind Accelerations at Top of Office Tower (cm/s**2)

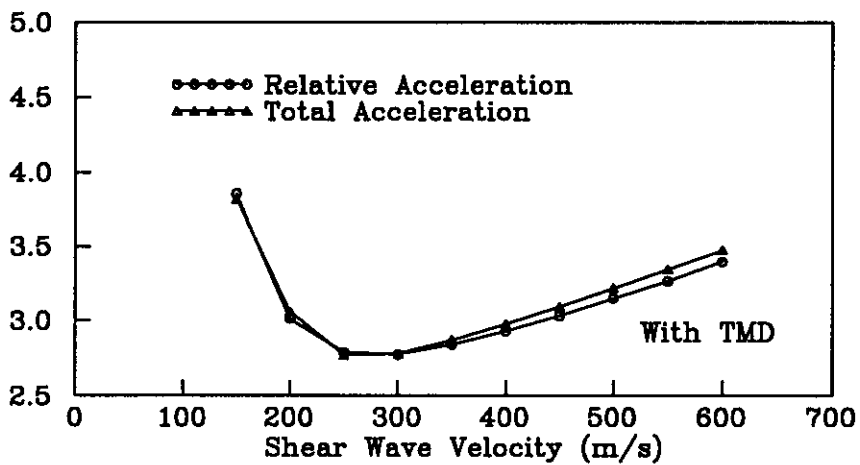
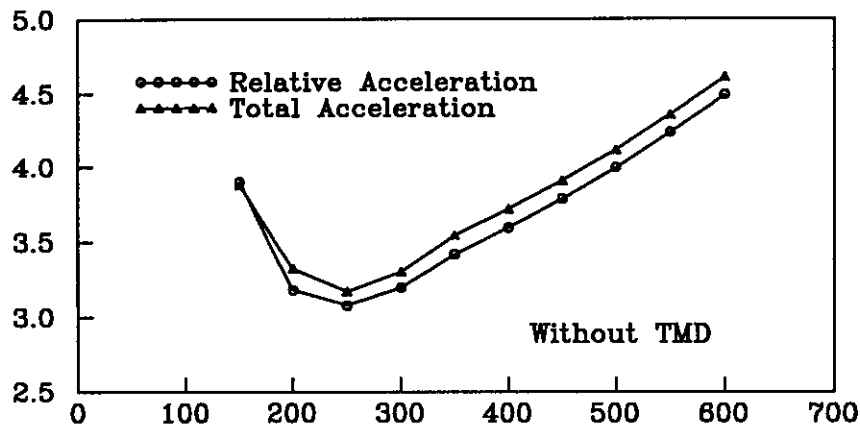


FIG. 9.8 COMPARISON OF STANDARD DEVIATIONS OF ALONGWIND ACCELERATIONS AT THE TOP OF OFFICE TOWER

Standard Deviations of Alongwind Displacements at Top of Office Tower (cm)

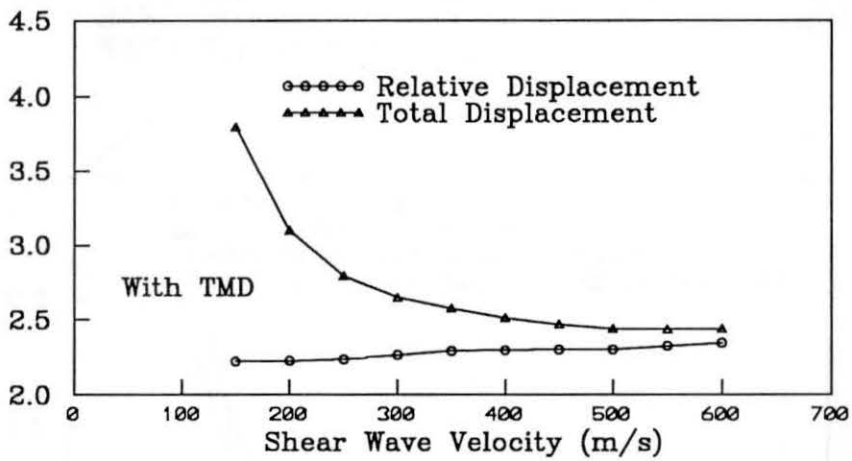
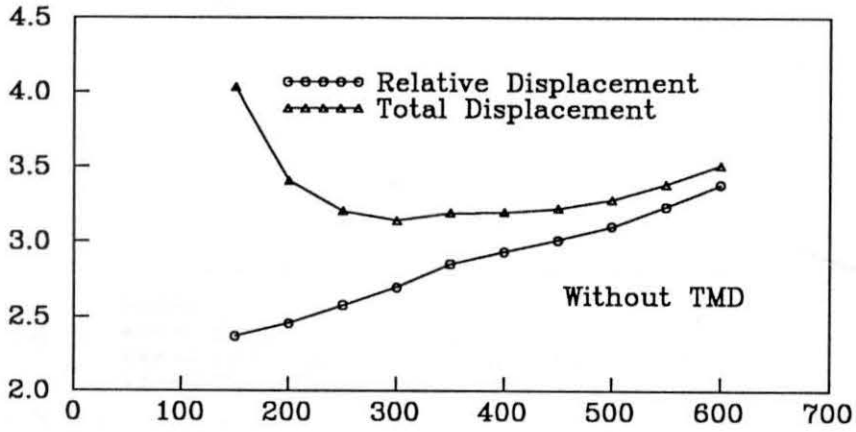


FIG. 9.9 COMPARISON OF STANDARD DEVIATIONS OF ALONGWIND DISPLACEMENTS AT THE TOP OF OFFICE TOWER

Ratio of Standard Deviations of Crosswind Base Moments of Office Tower

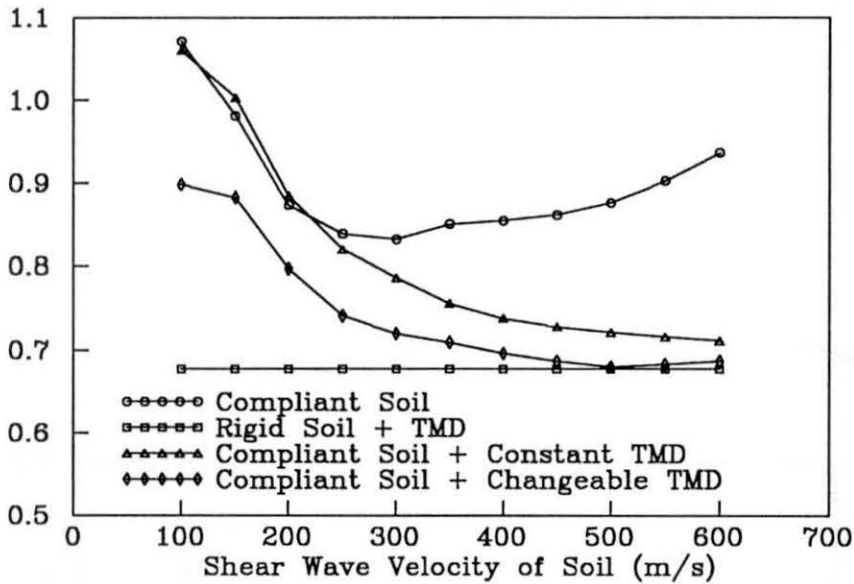


FIG. 9.10 VARIATIONS OF STANDARD DEVIATIONS OF CROSSWIND BASE MOMENT OF OFFICE TOWER WITH VARIOUS SHEAR WAVE VELOCITIES OF SOIL

Ratio of Standard Deviations of Crosswind Total Displacements at Top of Office Tower

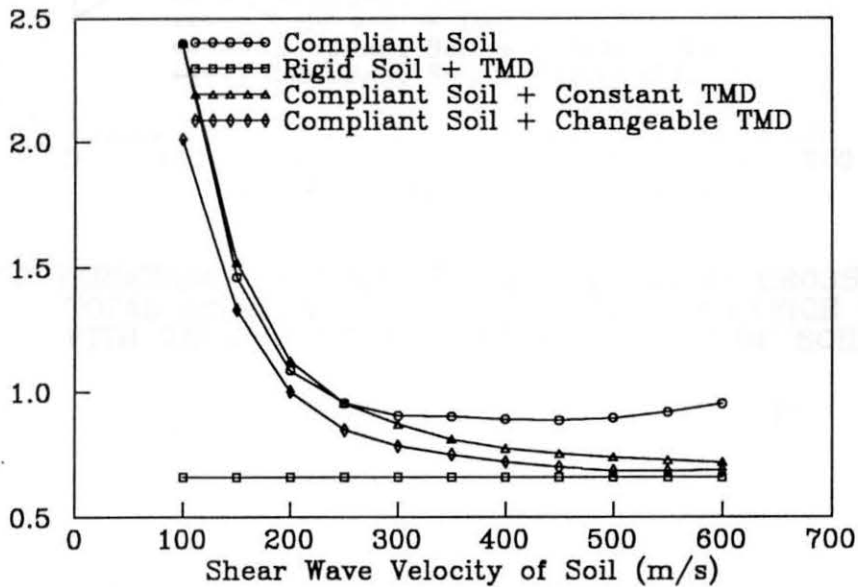


FIG. 9.11 VARIATIONS OF STANDARD DEVIATIONS OF CROSSWIND TOTAL DISPLACEMENTS AT THE TOP OF OFFICE TOWER WITH VARIOUS SHEAR WAVE VELOCITIES OF SOIL

Ratios of Standard Deviations of Crosswind Accelerations at Top of Office Tower

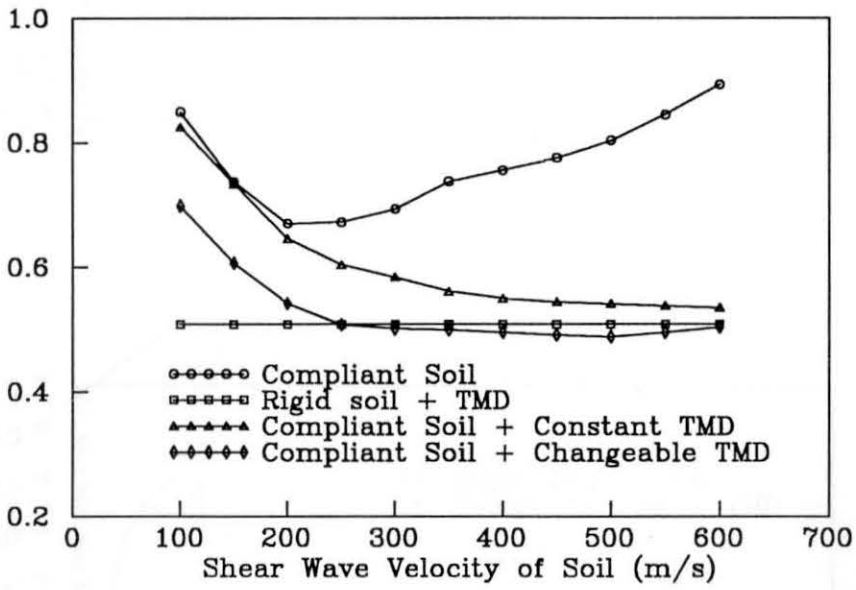


FIG. 9.12 VARIATIONS OF STANDARD DEVIATIONS OF CROSSWIND TOTAL ACCELERATIONS AT THE TOP OF OFFICE TOWER WITH VARIOUS SHEAR WAVE VELOCITIES OF SOIL

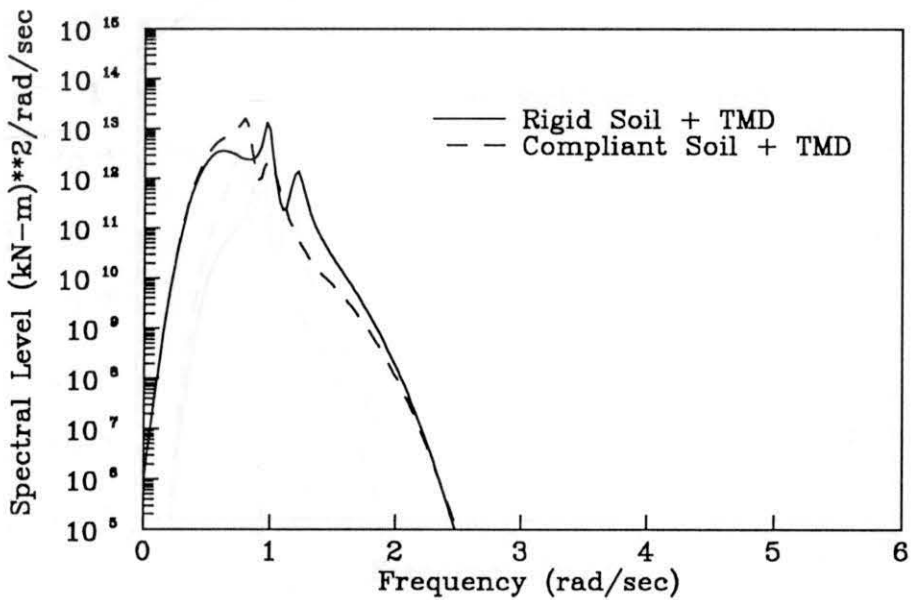
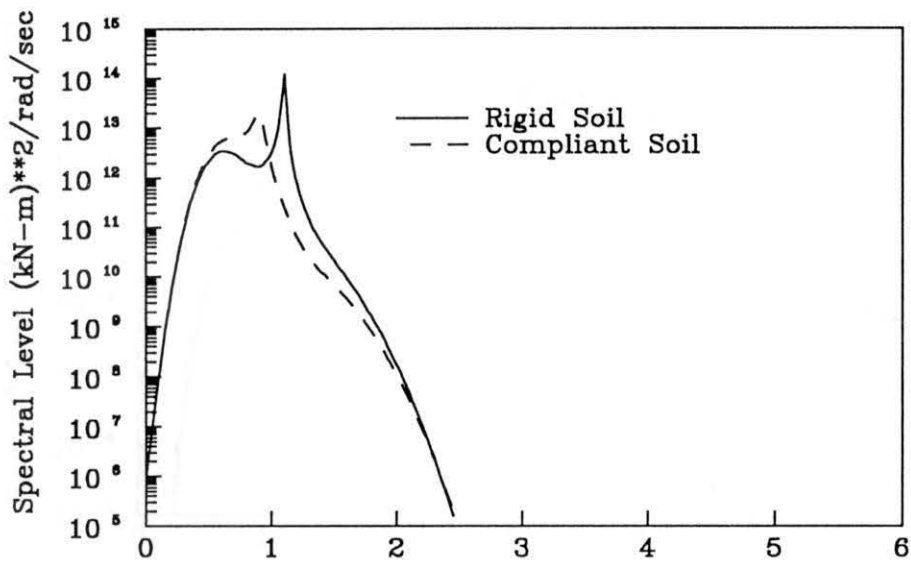


FIG. 9.13 POWER SPECTRAL DENSITIES OF CROSSWIND BASE MOMENTS OF OFFICE TOWER

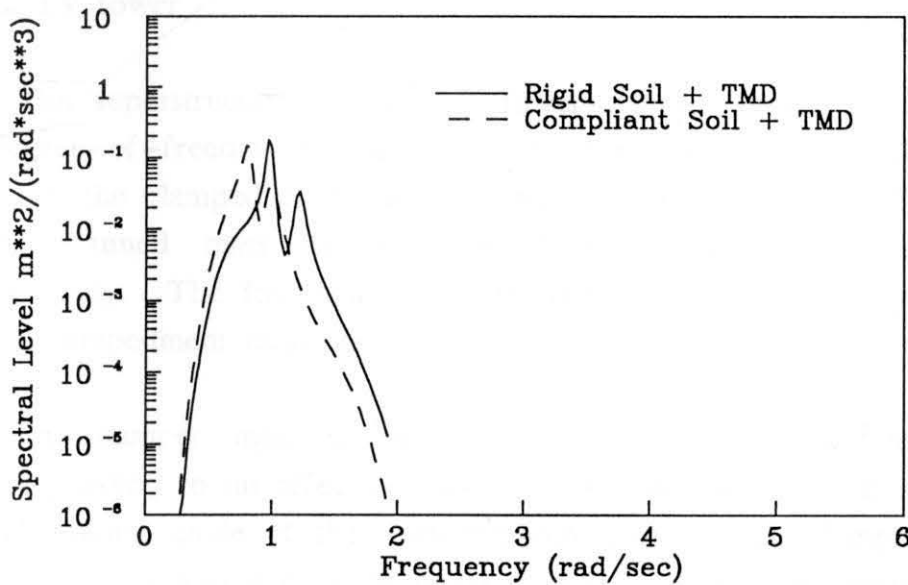
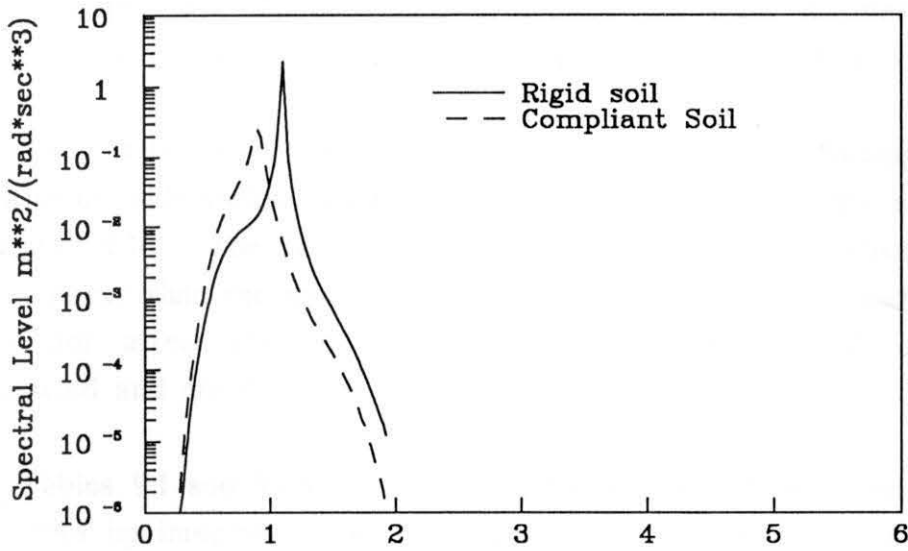


FIG. 9.14 POWER SPECTRAL DENSITIES OF CROSSWIND TOTAL ACCELERATIONS AT THE TOP OF OFFICE TOWER

be tuned to the natural frequency of the soil–structure system. If the tuning frequency of the mass damper is still tuned to the fundamental frequency of the structure with a clamped base, the effectiveness of the mass damper will decrease and eventually the mass damper will become useless or even increase the system response when the soil is very soft.

The variation of the standard deviations of the footing translational movement with various shear wave velocities of the soil are shown in Figs. 9.15 and 9.16. The footing translation under crosswind wake excitation is much larger than the alongwind footing translation. The tuned mass damper does not affect the footing translation responses at all for both the alongwind and crosswind excitations.

Tables 9.1 and 9.2 present standard deviations of ten dominant response quantities by integrating their corresponding power spectral densities for both the alongwind and crosswind excitations for rigid soil as well as for a soil with shear wave velocity of 300 m/s. It was found that the crosswind system responses were much larger than the alongwind system responses.

9.5.2 TV tower

The superstructure of the soil–tower–damper system is modelled as a 9–degree–of–freedom system. The structural data can be found in Table 8.4. In the clamped case, the first four natural frequencies of the structure without tuned mass dampers are 0.199, 0.334, 0.821, and 1.281 Hz, respectively. The foundation is a circular flat slab with a radius of 25.8m and an embedment ratio $L/r_0 = 0.25$. The same soil properties as in section 9.5.1 are used.

The damper mass is considered constant and equal to 494 tonnes (corresponding to an effective mass ratio of around 6% with respect to the first vibration mode of the main structure); the critical damping ratio from the dashpot is also a constant equal to 5%. The damper spring stiffness is treated in the same way as the office tower–damper system.

The aerodynamic data pertaining to alongwind excitation are: $\bar{V}_{1,0} = 26.41$ m/s; $z_g = 300$ m; $\bar{V}_G = 44$ m/s; $C_a = 0.7$; $\rho_a = 1.2$ Kg/m³; $C_1 = 7.0$ and

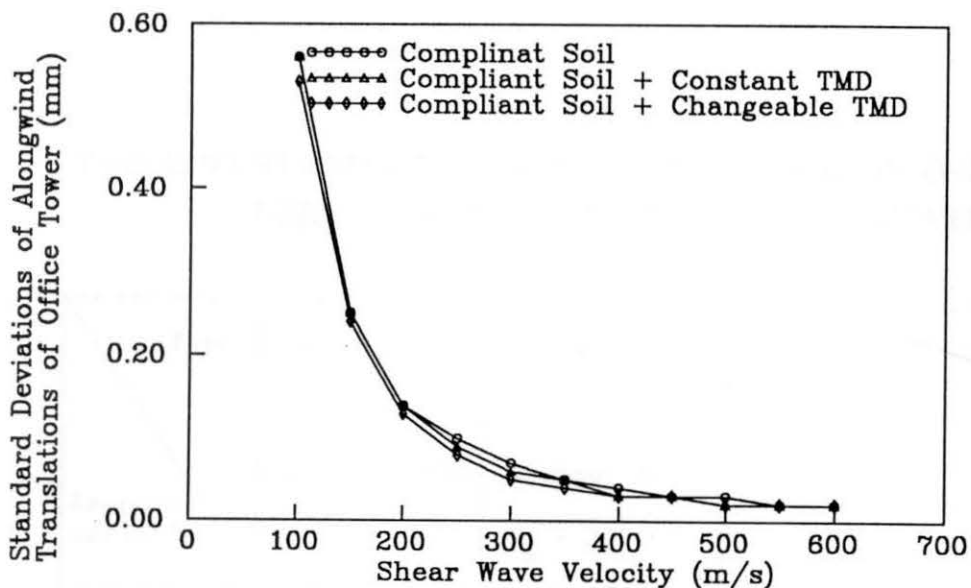


FIG. 9.15 VARIATIONS OF STANDARD DEVIATIONS OF ALONGWIND FOOTING TRANSLATIONS OF OFFICE TOWER WITH VARIOUS SHEAR WAVE VELOCITIES OF SOIL

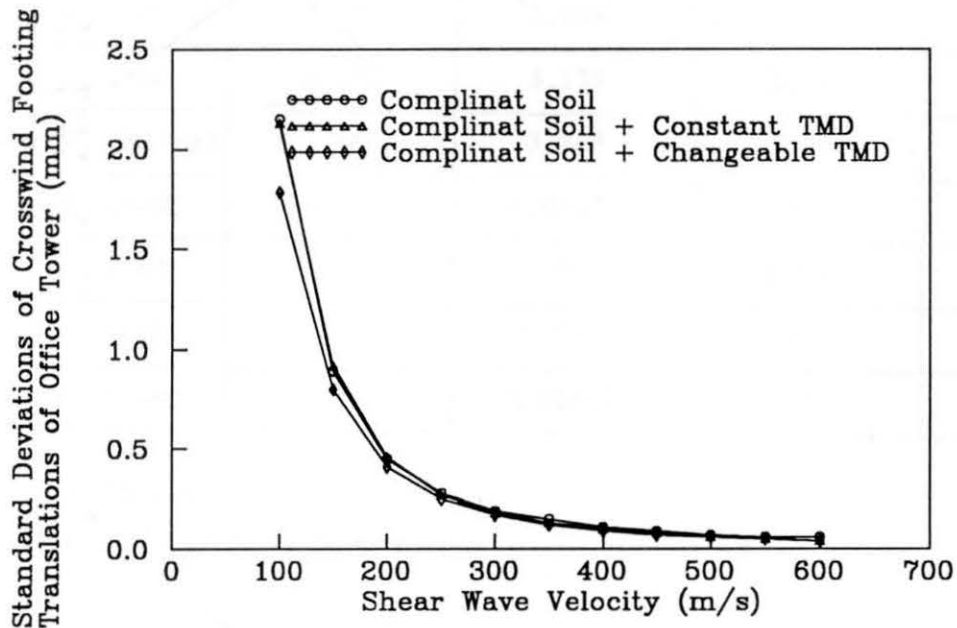


FIG. 9.16 VARIATIONS OF STANDARD DEVIATIONS OF CROSSWIND FOOTING TRANSLATIONS OF OFFICE TOWER WITH VARIOUS SHEAR WAVE VELOCITIES OF SOIL

**TABLE 9.1 STANDARD DEVIATION RESPONSE OF OFFICE TOWER
FOR ALONGWIND TURBULENCE EXCITATION**

Type Response variable	Rigid Soil	Compliant Soil	Rigid Soil	Compliant Soil
	(without TMD)	(without TMD) $V_s = 300$ m/s	(with TMD)	(with TMD) $V_s = 300$ m/s
M_0^+ (kN-m)	398,530	288,456	288,422	253,838
Q_0^+ (kN)	2,330	1,605	1,895	1,476
y_N (cm)	3.781	2.694	2.389	2.264
\ddot{y}_N (mil-g)	7.666	3.258	5.967	2.829
y_N^t (cm)	3.781	3.139	2.389	2.650
\ddot{y}_N^t (mil-g)	7.666	3.368	5.967	2.833
φ_N (rad)	0.00036	0.00023	0.00023	0.00019
Z_d (cm)	0	0	6.620	6.997
u (cm)	0	0.007	0	0.008
θ (rad)	0	0.00002	0	0.00001

$\bar{V}_{10} = 15.9$ m/s

TMD: Tuned Mass Damper

**TABLE 9.2 STANDARD DEVIATION RESPONSE OF OFFICE TOWER
FOR CROSSWIND WAKE EXCITATION**

Response Variable	Type	Rigid Soil	Compliant Soil	Rigid Soil	Compliant Soil
		(without TMD)	(without TMD) $V_s = 300$ m/s	(with TMD)	(with TMD) $V_s = 300$ m/s
M_0^+ (kN-m)		937,392	779,887	634,741	674,769
Q_0^+ (kN)		4224.0	3687.9	2953.4	3206.9
y_N (cm)		10.180	7.972	6.718	6.907
\ddot{y}_N (mil-g)		11.498	6.924	5.837	5.003
y_N^t (cm)		10.180	9.224	6.718	7.990
\ddot{y}_N^t (mil-g)		11.498	7.970	5.837	5.758
φ_N (rad)		0.00091	0.00069	0.00060	0.00061
Z_d (cm)		0	0	20.580	24.973
u (cm)		0	0.019	0	0.017
θ (rad)		0	0.00004	0	0.00004

$\bar{V}_{10} = 15.9$ m/s

TMD: Tuned Mass Damper

$K_0 = 0.007$. For crosswind wake excitation, the aerodynamic data are: $\bar{V}_{1,0} = 15$ m/s; $\alpha = 0.15$; $C_1 = 0.2$; $s = 0.22$ and $B_s = 0.32$. The above mentioned aerodynamic data are the same as those in Chapter 8.

Fig. 9.17 shows the variation of the natural frequencies of the tower with various shear wave velocities of the soil. For the TV tower-soil system, the modification of the natural frequencies of the system is much less than that for the office tower-soil system described previously. This may be attributed to the proportion of the foundation stiffness to the structure stiffness and the structural inherent properties. The first natural frequency of the soil-structure system, when the shear wave velocity is equal to 100 m/s, is about 85% of the fundamental frequency of the clamped structure. As a result, the shifting of the resonance peak locations to lower frequencies is also smaller, as shown in Figs. 9.18 to 9.21. In these figures, one can observe that the soil compliancy mainly reduce the higher resonance response peaks while the tuned mass damper can considerably suppress the first mode vibration of the system. Therefore, the combination of soil compliancy and tuned mass damper gives satisfactory results. It is also seen that the contribution of the higher modes is rather significant for both alongwind and crosswind directions.

The variation of the standard deviations of the tower base moments, turret total displacements and accelerations with various shear wave velocities of the soil are shown in Figs. 9.22 to 9.24 (for alongwind turbulence), and in Figs. 9.25 to 9.27 (for crosswind wake excitation). In comparison with the responses of the tower-tuned mass damper system on rigid soil, soil compliancy decreases the base moment and turret total acceleration responses of the soil-TV tower-tuned mass damper system not only for alongwind turbulence but also for crosswind wake excitation. The reduction of response in the crosswind direction is due to the decrease in the critical wind speed and the height at which that wind speed occurs, as well as to the increase in damping due to soil. The lowering of the critical wind speed range indicates that most severe wind load range along the tower height approaches the tower base and causes less vibration. Tables 9.3 and 9.4, in which eleven dominant response quantities are presented, also give an insight into other system responses, especially for the tuned mass damper.

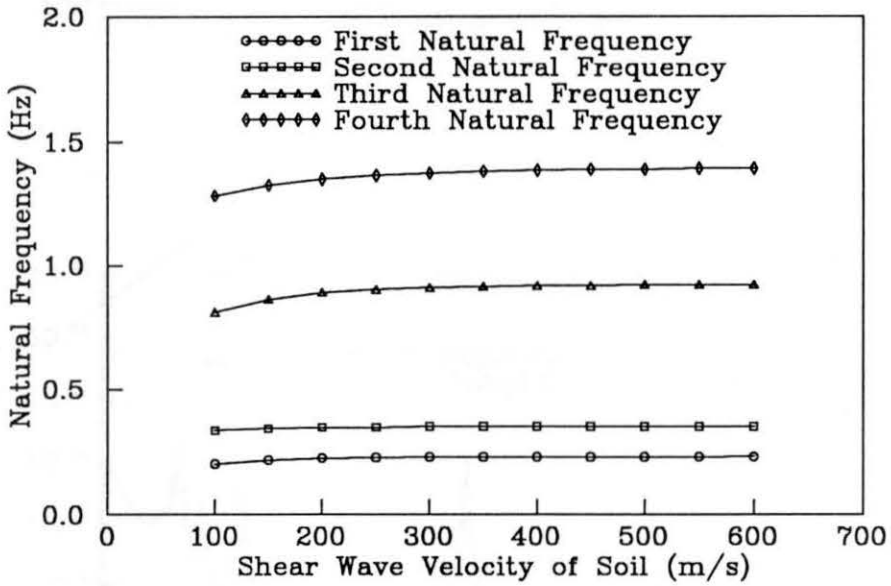


FIG. 9.17 VARIATIONS OF NATURAL FREQUENCIES OF TV TOWER WITH VARIOUS SHEAR WAVE VELOCITIES OF SOIL

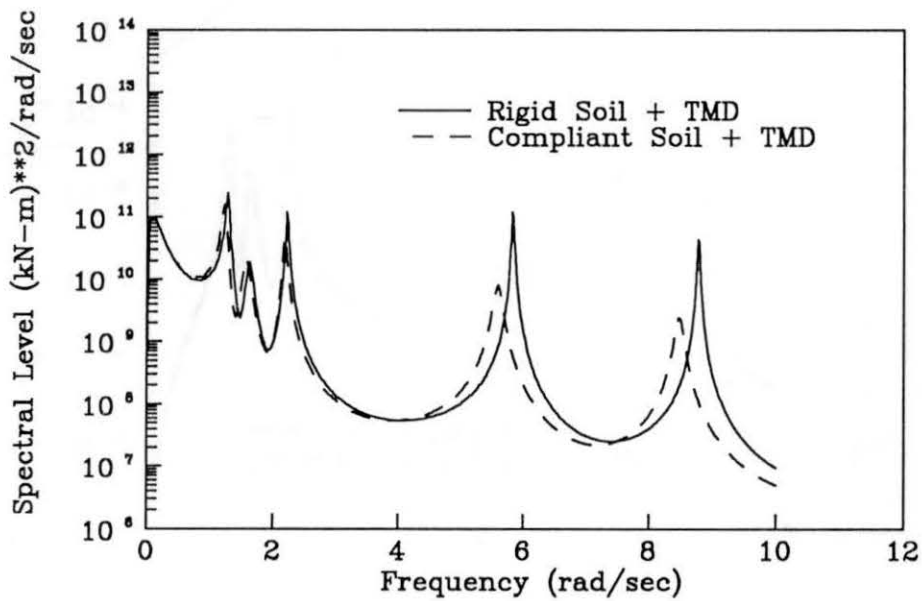
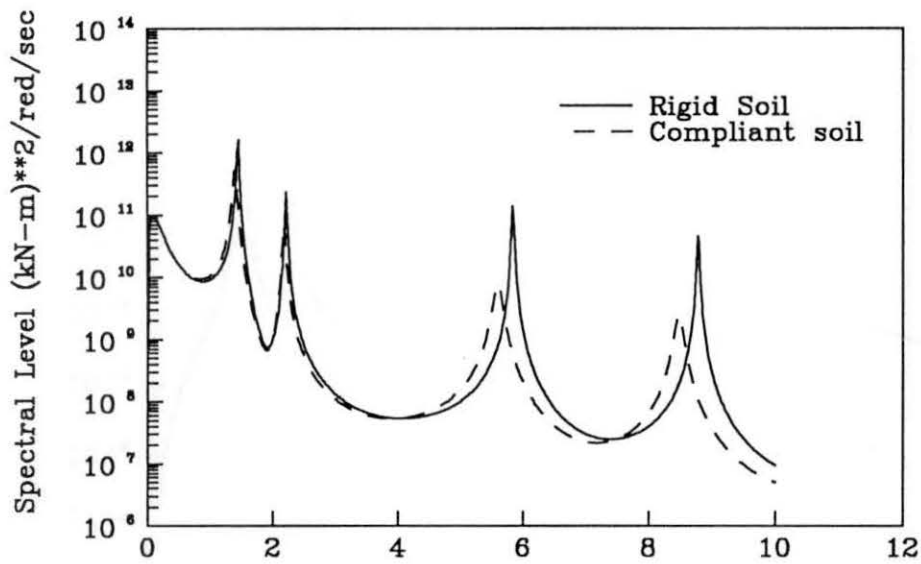


FIG. 9.18 POWER SPECTRAL DENSITIES OF ALONGWIND BASE MOMENTS OF TV TOWER

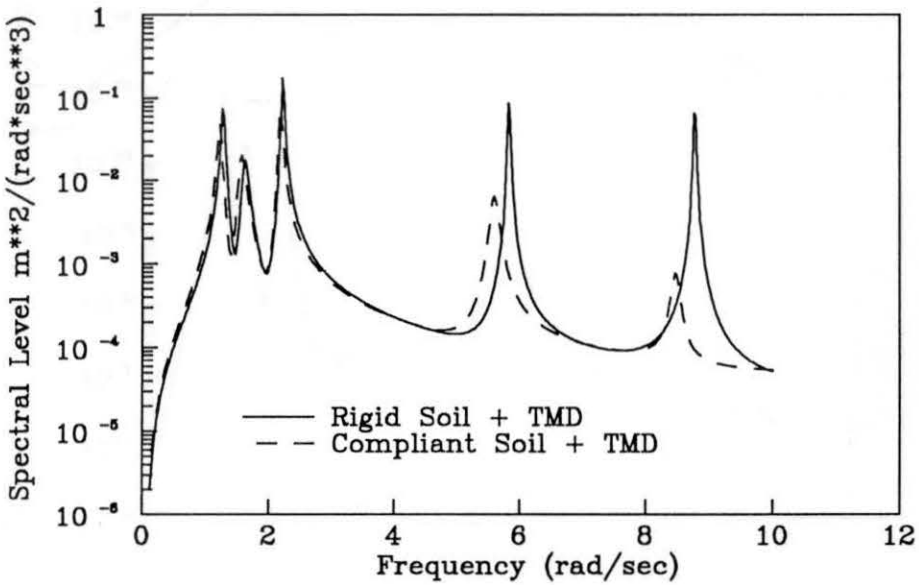
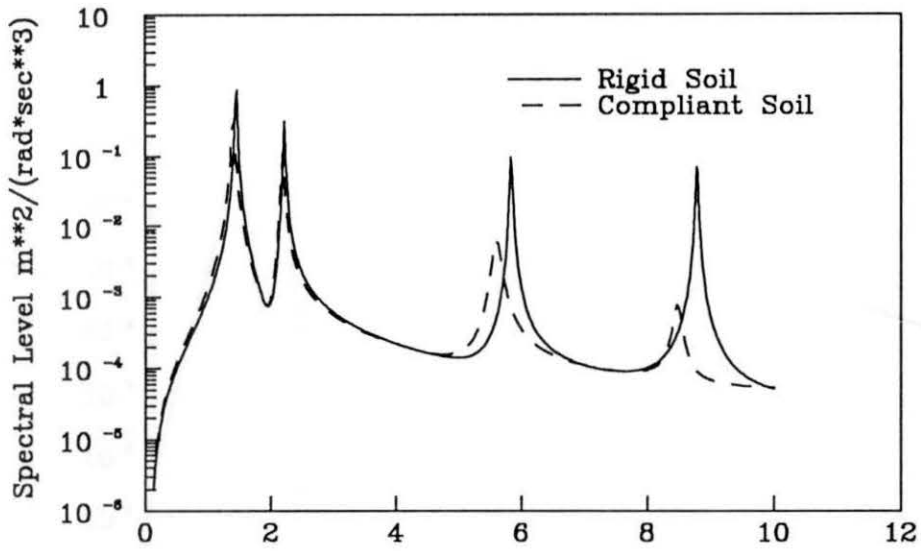


FIG. 9.19 POWER SPECTRAL DENSITIES OF ALONGWIND TURRET TOTAL ACCELERATIONS OF TV TOWER

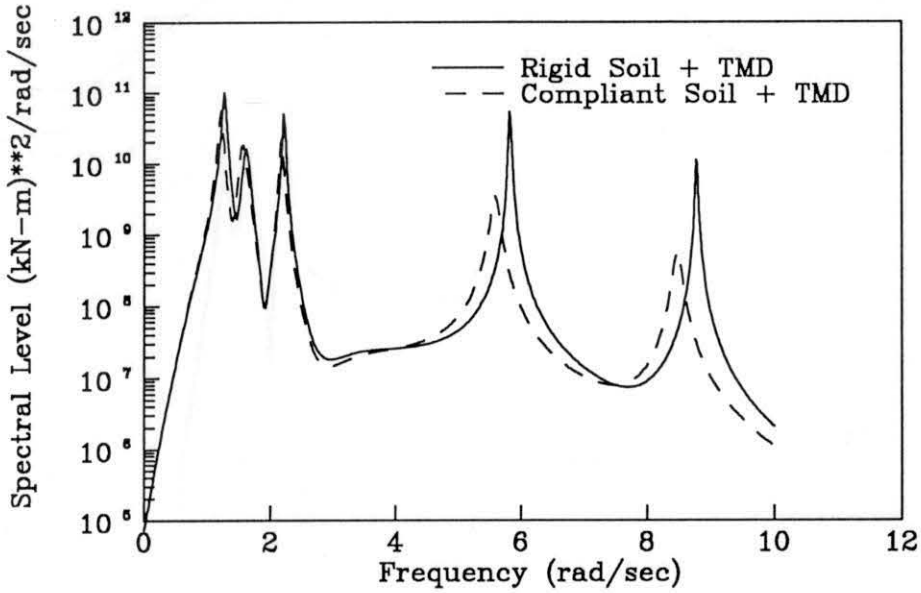
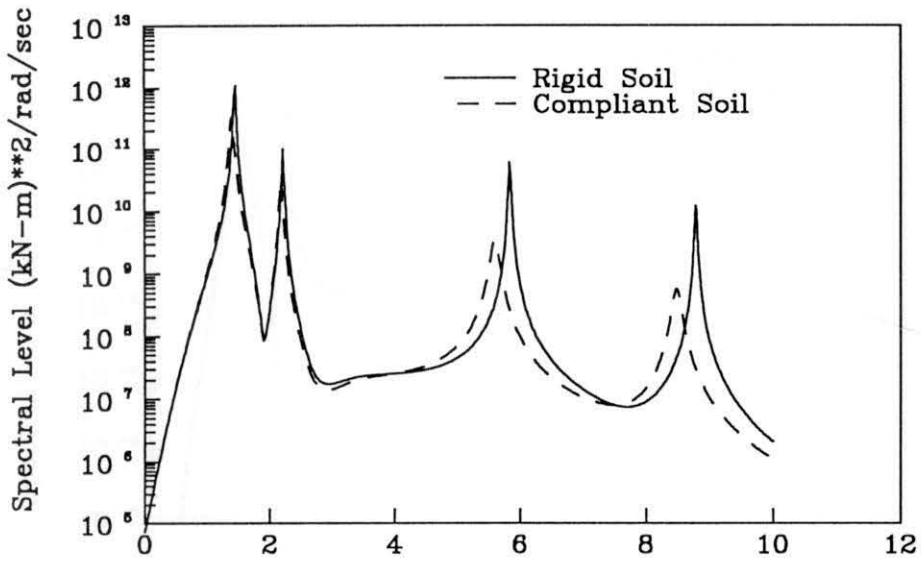


FIG. 9.20 POWER SPECTRAL DENSITIES OF CROSSWIND BASE MOMENTS OF TV TOWER

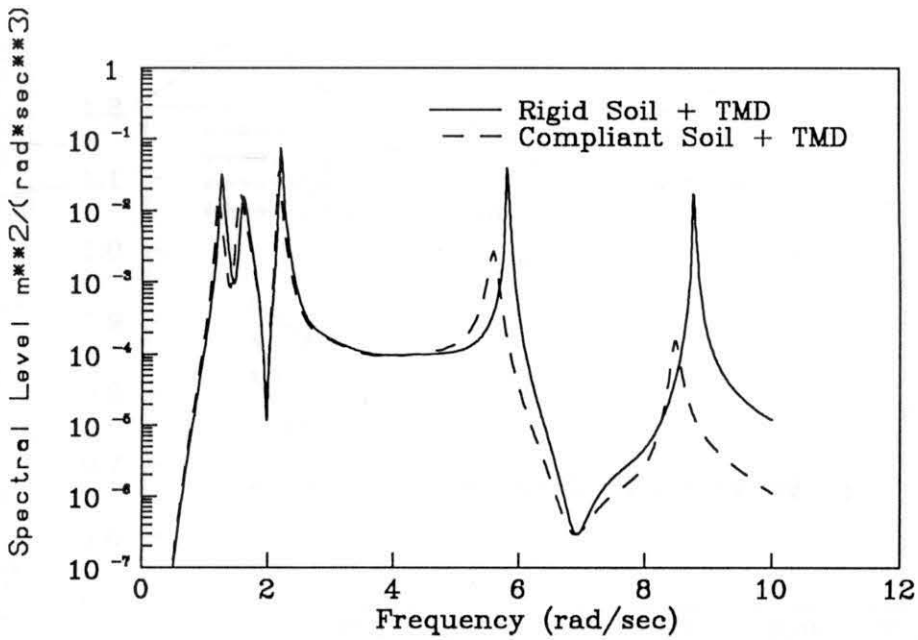
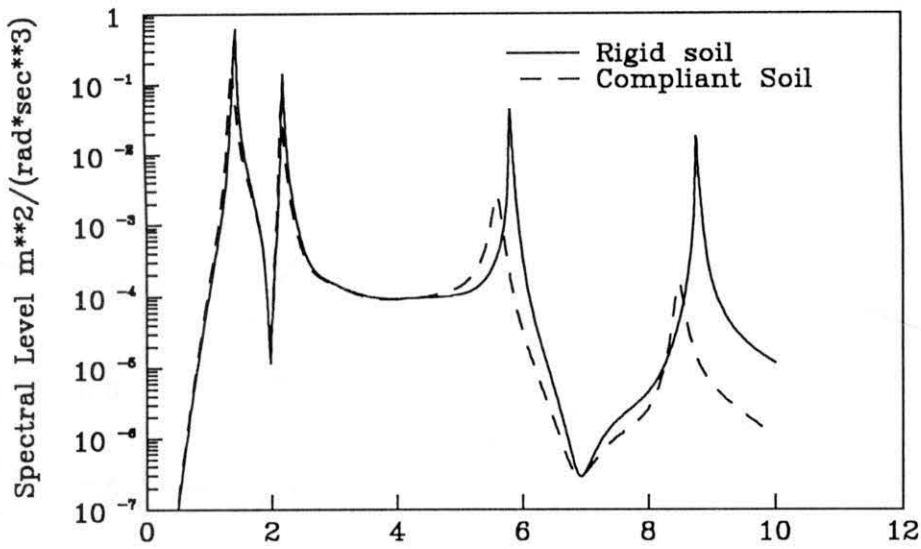


FIG. 9.21 POWER SPECTRAL DENSITIES OF CROSSWIND TURRET TOTAL ACCELERATIONS OF TV TOWER

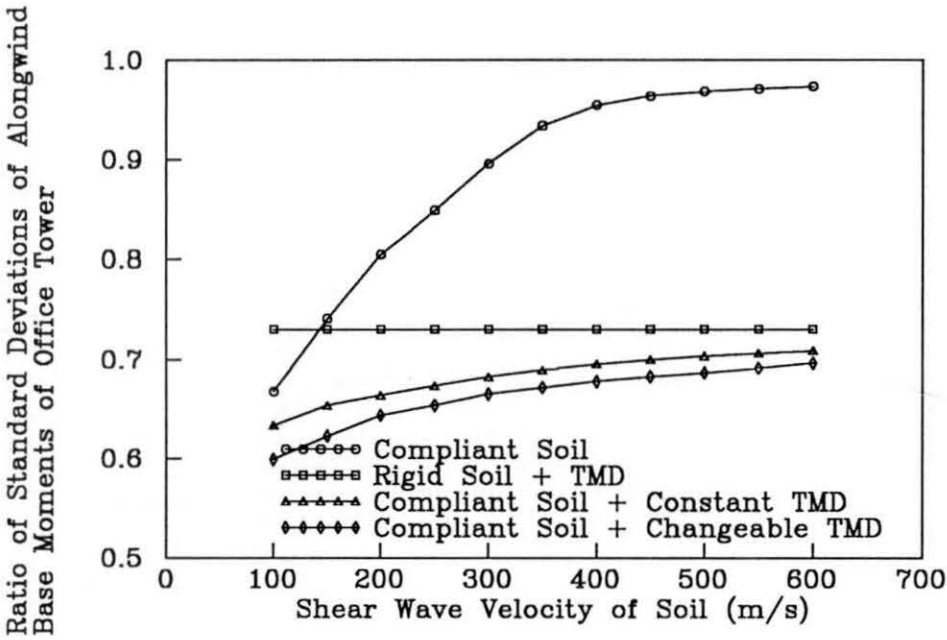


FIG. 9.22 VARIATIONS OF STANDARD DEVIATIONS OF ALONGWIND BASE MOMENTS OF TV TOWER WITH VARIOUS SHEAR WAVE VELOCITIES OF SOIL

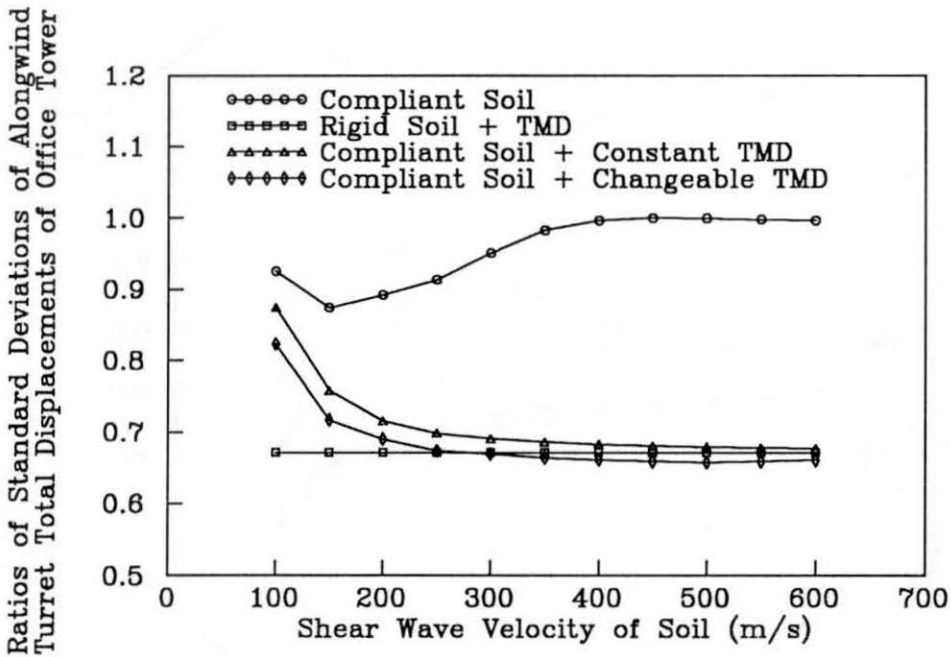


FIG. 9.23 VARIATION OF STANDARD DEVIATIONS OF ALONGWIND TURRET TOTAL DISPLACEMENTS OF TV TOWER WITH VARIOUS SHEAR WAVE VELOCITIES OF SOIL

Ratios of Standard Deviations of Alongwind Turret Total Accelerations of Office Tower

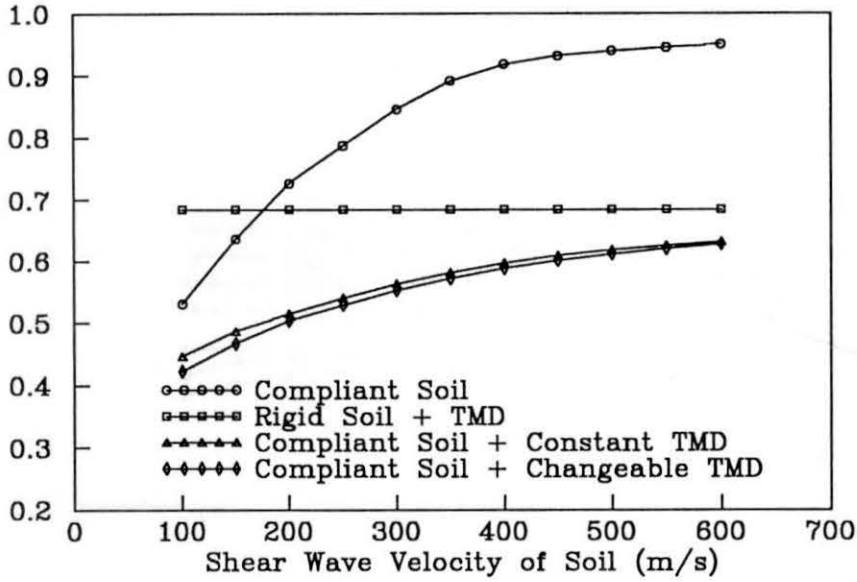


FIG. 9.24 VARIATIONS OF STANDARD DEVIATIONS OF ALONGWIND TURRET TOTAL ACCELERATIONS OF TV TOWER WITH VARIOUS SHEAR WAVE VELOCITIES OF SOIL

Ratio of Standard Deviations of Crosswind Base Moments of TV Tower

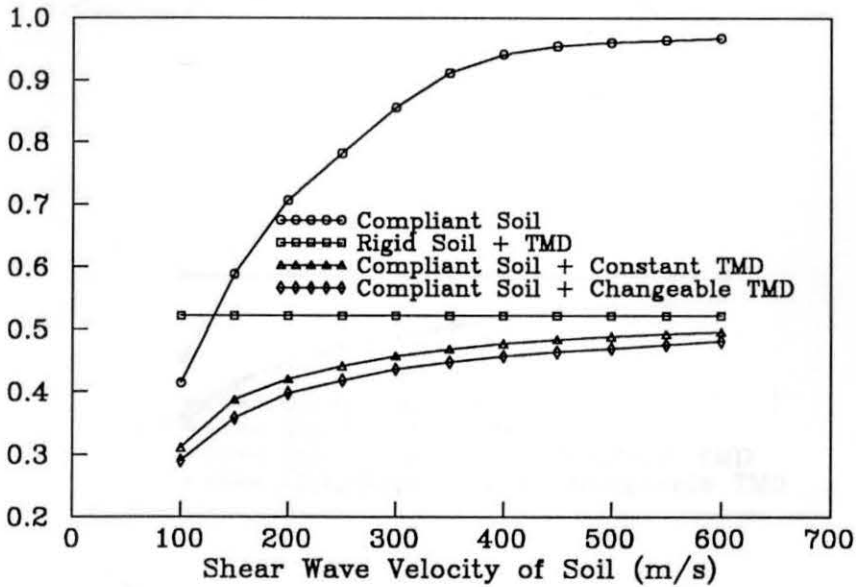


FIG. 9.25 VARIATIONS OF STANDARD DEVIATIONS OF CROSSWIND BASE MOMENTS OF TV TOWER WITH VARIOUS SHEAR WAVE VELOCITIES OF SOIL

Ratio of Standard Deviations of Crosswind
Turret Total Displacements of TV Tower

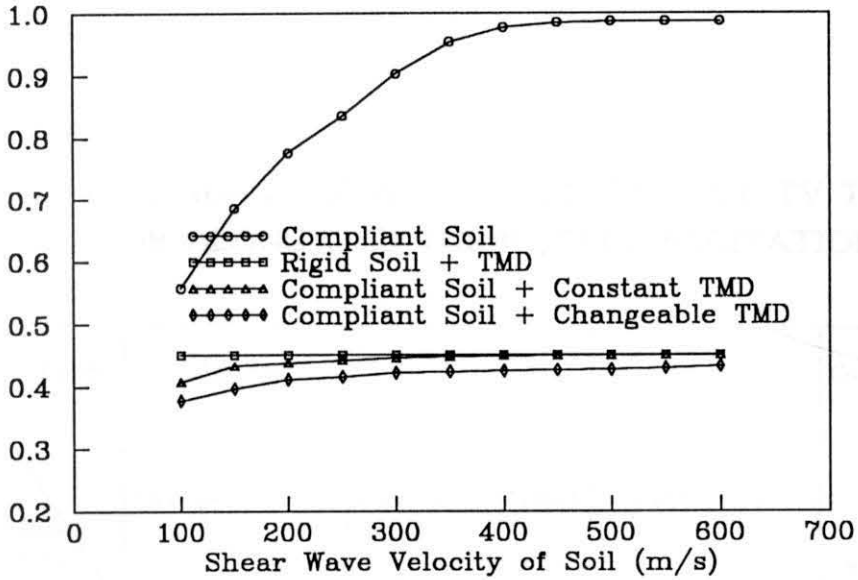


FIG. 9.26 VARIATIONS OF STANDARD DEVIATIONS OF CROSSWIND TURRET TOTAL DISPLACEMENTS OF TV TOWER WITH VARIOUS SHEAR WAVE VELOCITIES OF SOIL

Ratio of Standard Deviations of Crosswind
Turret Total Accelerations of TV Tower

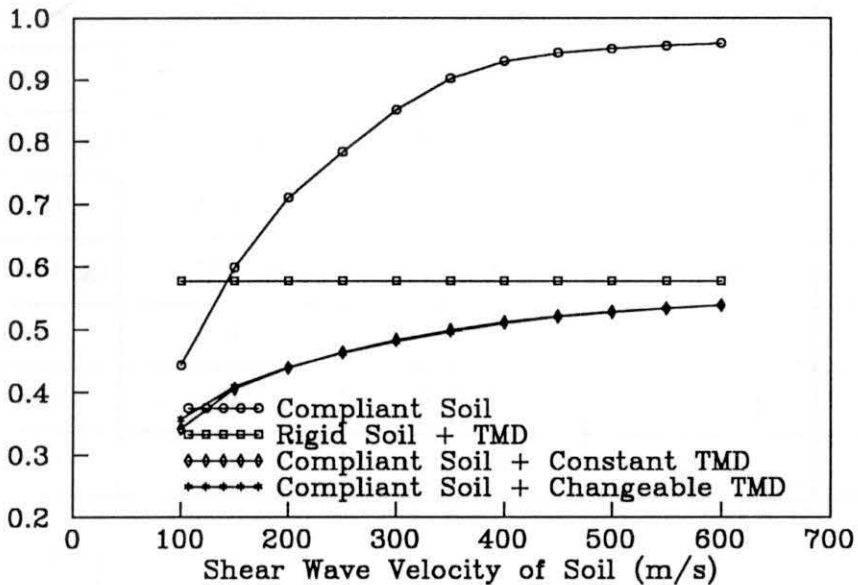


FIG. 9.27 VARIATIONS OF STANDARD DEVIATIONS OF CROSSWIND TURRET TOTAL ACCELERATIONS OF TV TOWER WITH VARIOUS SHEAR WAVE VELOCITIES OF SOIL

**TABLE 9.3 STANDARD DEVIATION RESPONSE OF TV TOWER
FOR ALONGWIND TURBULENCE EXCITATION**

Response Variable \ Type	Rigid Soil	Compliant Soil	Rigid Soil	Compliant Soil
	(without TMD)	(without TMD) $V_s = 300 \text{ m/s}$	(with TMD)	(with TMD) $V_s = 300 \text{ m/s}$
M_0^+ (kN-m)	152,144	136,310	111,106	101,179
Q_0^+ (kN)	947.3	807.6	789.4	664.1
y_N (cm)	38.502	34.304	24.773	23.334
φ_N (rad)	0.00628	0.00546	0.00460	0.0041
y_t (cm)	4.863	4.435	3.264	3.116
\ddot{y}_t (mil-g)	11.104	9.073	7.598	5.987
y_t^t (cm)	4.863	4.625	3.264	3.254
\ddot{y}_t^t (mil-g)	11.104	9.899	7.598	6.141
Z_d (cm)	0	0	7.650	7.633
u (cm)	0	0.005	0	0.004
θ (rad)	0	0.00001	0	0.00001

$\bar{V}_{10} = 26.41 \text{ m/s}$

TMD: Tuned Mass Damper

**TABLE 9.4 STANDARD DEVIATION RESPONSE OF TV TOWER
FOR CROSSWIND WAKE EXCITATION**

Response Variable \ Type	Rigid Soil	Compliant Soil	Rigid Soil	Compliant Soil
	(without TMD)	(without TMD) $V_s = 300$ m/s	(with TMD)	(with TMD) $V_s = 300$ m/s
M_0^+ (kN-m)	106,810	91,438	55,781	46,610
Q_0^+ (kN)	609.4	499.7	406.3	306.9
y_N (cm)	29.490	25.568	15.940	14.997
φ_N (rad)	0.00470	0.00402	0.0031	0.00281
y_t (cm)	3.546	3.073	1.598	1.433
\ddot{y}_t (mil-g)	8.481	6.913	4.893	3.892
y_t^t (cm)	3.546	3.202	1.598	1.496
\ddot{y}_t^t (mil-g)	8.481	7.218	4.893	4.080
Z_d (cm)	0	0	5.741	5.649
u (cm)	0	0.003	0	0.002
θ (rad)	0	0.00001	0	0.00000

$\bar{V}_{10} = 15$ m/s

TMD: Tuned Mass Damper

9.6. Conclusions

A theoretical framework has been developed to analyse the effects of both tuned mass dampers and soil compliancy on the wind-induced response of slender structures. The frequency-dependent properties of soil and the contributions of higher modes can be conveniently introduced into the analysis of the soil-structure-mass damper system in terms of a transfer matrix formulation. Non-periodic superstructures can also be considered in this theoretical framework.

For soil-structure systems, soil compliancy has the effect of shifting the locations of resonance peaks to lower frequencies. The soil-structure interaction effects depended on a number of factors including soil, footing, structure and the nature of external excitations. In most cases, the general trend of the soil-structure interaction effects was to reduce the structural response. However, the example of an office tower showed that, for soft soil, soil compliancy increased the total displacement responses in both alongwind and crosswind directions.

For damper-structure systems on rigid soil, the tuned mass dampers demonstrated effectiveness in suppressing both the alongwind and crosswind induced dynamic response of structures. In order to achieve such high effectiveness, an important condition is that the mass damper should be tuned to the natural frequency of the structure, especially for the smaller effective mass ratios.

For soil-structure-damper systems, particularly when the soil was very soft, the tuned mass damper was not an effective method to reduce soil-structure system responses. For moderately stiff soil, the mass damper should be tuned to the natural frequency of the soil-structure system rather than the natural frequency of the structure with a clamped base. The effectiveness of the mass damper decreased with decreasing stiffness of the soil.

In comparison with the responses of the damper-structure system on rigid soil, the numerical examples showed that, under alongwind turbulence

excitation, soil compliancy decreased the base moment and total acceleration responses of both the office tower and the TV tower, but increased total displacement responses. For shear wave velocities of soil $V_s < 250$ m/s and for the dynamic base moment, total top dynamic displacement and acceleration, the responses of the office tower-damper system were increased under crosswind wake excitation. It is believed that the modification of the natural frequencies of the system caused the first natural frequency of the system to get closer to the vortex shedding frequency. Consequently, the vibrational energy absorbed by the tower due to the vortex shedding process was significantly increased and exceeded that dissipated through damping due to the soil. On the other hand, soil compliancy decreased the same responses of the TV tower-damper system under crosswind wake excitation. The reduction in responses was due to the decrease in the critical wind speed and the height at which that wind speed occurred, as well as to the increase in damping due to the soil. The assumption that the structure is clamped at its base with no displacements was still satisfactory when both foundation and soil were stiff enough. Based on these results, it is important to consider the effect of soil on the wind-induced response of the structure-damper system, especially for office towers under crosswind wake excitation and when the soil is soft.

Chapter 10

GENERAL CONCLUSIONS AND RECOMMENDATIONS

The main aims of the research conducted in this thesis were given in Chapter 1 as:

- (a) To evaluate, by using aeroelastic model tests in wind tunnel, the effectiveness of passive tuned mass dampers (TMDs) in suppressing tall building vibrations induced by alongwind turbulence excitation, crosswind wake excitation, lock-in excitation and torsional excitation.
- (b) To provide, by combining experimental results with theoretical analysis, a reliable and economical method of determining optimum design parameters of passive TMDs for wind-excited tall buildings.
- (c) To perform parametric studies of a suboptimal active mass damper control system and to estimate its effectiveness in reducing wind-induced building vibration compared with passive TMDs.
- (d) To address a new approach that facilitates the mitigation of wind-induced motions of slender structures by utilising tuned liquid column dampers.
- (e) To assess the effect of soil compliancy under the footing of slender structures on the effectiveness of TMDs arranged on the slender structures.

The secondary considerations accompanying the main aims were given as: to investigate wind-induced torsional vibration of tall buildings by using aeroelastic modelling technique in wind tunnel tests; and to examine mode shape corrections which are applicable to the simple aeroelastic tests of tall buildings in wind tunnel.

The major conclusions of the research project and a number of recommendations for further research are described in the following sections.

10.1 Conclusions

10.1.1 Control of alongwind and crosswind vibrations by TMDs

The results of the aeroelastic tests demonstrated the effectiveness of TMD system in reducing the dynamic response of the building induced by wind excitations of different mechanisms. The TMD system reduced the vibration caused by alongwind turbulence excitation, partial incidence turbulence in crosswind direction and crosswind wake excitation by 20% to 40%. The TMD system was found to be more effective in reducing the vibration caused by lock-in excitation by a factor 2 or more.

TMD system usually increases the overall effective damping of building rather than change the wind loads acting on the building. However, under motion-dependent lock-in excitation, not only can the TMD absorb most of the vibrational energy which concentrates at the natural frequency of the building, it can also change both the magnitude and mechanism of the external wind excitation.

10.1.2 Torsional vibration and control by TMDs

The aeroelastic modelling technique for pure torsion vibration was found to be a convenient and efficient way to explore the mechanism of wind-induced torsional excitation and to predict the wind-induced torsional response of tall buildings. This technique allows some aeroelastic effects to be considered and the effectiveness of passive control systems can also be readily demonstrated.

From the basic rectangular building model tests, it was shown that the maximum dynamic response occurred at around 0° , i.e., with wind incidence normal to the narrow face of the rectangular building. The maximum mean torque occurred at 10° and 60° . The experimental results also showed that

the torsional responses were essentially normally distributed and the torsional aerodynamic damping was small in the reduced wind velocity range studied.

With the wind incidence normal to the wide face of the building, vortex shedding is the dominant mechanism of torsional excitation. With the wind incidence normal to the narrow face, there are two important excitation mechanisms: incident turbulence which exerts its influence mainly on the windward halves, and flow re-attachment intermittencies on the leeward halves of the two side faces of the building.

For the eccentric model with a 10% geometric eccentricity ratio, the maximum dynamic torque still occurred at around 0° and 180° , while the maximum mean torque was recorded at 120° . At a reduced wind velocity of 8, the maximum dynamic torque of the eccentric model increased by 30% and the maximum mean torque increased by a factor of 2 or more, compared with the values of the basic model.

For the eccentric model with a TMD, the results showed that there was up to a 30% reduction in response for wind incidence normal to the wide face of the building and a 45% reduction for wind incidence normal to the narrow face. The effectiveness of the TMD was also found to be dependent on the type of torsional excitation.

10.1.3 Parametric study of TMDs

A proposed semi-analytical method, combined with conventional aeroelastic test or other wind tunnel test techniques, can provide a reliable estimate of the reduction of the building motion and optimum design parameters of the TMD, without having to perform a series of wind tunnel tests of the building with different TMDs. The effects of wind intensity and direction, surrounding environment, building size, shape, mass, stiffness, and natural damping on the response reduction of the building can readily be investigated. The results obtained by this semi-analytical technique were in good agreement with the corresponding experimental results.

In contrast, the conventional parametric study method, which is based

on a white noise excitation model, usually overestimates the effectiveness of TMDs for most real situations. It is believed that the inability of the white noise excitation model to simulate the locations of the peaks in the wind excitation spectra relative to the natural frequency of the building-TMD system and the magnitudes of the spectral peaks causes the difference between the theoretical and experimental results.

10.1.4 Mode shape corrections

Sources of error caused by the discrepancy between the building model and prototype mode shapes were identified for the aeroelastic modelling technique. Two limiting values of error, for low and high correlations of wind loads with height, were discussed. Three mode shape correction factors, for alongwind, crosswind and torsional responses respectively, were suggested to adjust the experimental response results to the corresponding prototype values. The results obtained by the proposed expressions were in reasonable agreement with the available experimental results.

10.1.5 Active mass dampers

The semi-analytical method was also used to investigate the effectiveness of a suboptimal active mass damper control system. The results showed that the effectiveness of passive tuned mass dampers can be considerably enhanced by the inclusion of a suboptimal active control system. The analysis of the frequency response functions indicated that the active control system modified the structural characteristics, leading to a significant reduction of structural vibration.

The results of parametric studies of the active control system showed that, in general, the responses of the building and the damper can be decreased by increasing the control force or moment, that is, by increasing the feedback gain τ and the proportional constant K_t . However, the response of the building and the damper, and the control force were very sensitive to small variations of the normalised loop gain ϵ in the region $0 < \epsilon < 1$. Therefore, setting of the loop gain within this region is undesirable in practice. The most beneficial control parameters can be

readily determined from generalised design contours which are expressed as functions of dimensionless feedback and loop gains.

10.1.6 Tuned liquid column dampers

A transfer matrix formulation for non-periodic structures has been developed to analyse the effect of liquid column dampers (TLCD) and liquid column/mass dampers (TLCMD) on the wind-induced response of slender structures. The numerical computer accuracy of direct matrix multiplication was investigated and the results indicated that the accuracy of the computed results can be guaranteed. Two numerical examples of full-scale slender structures showed that both TLCD and TLCMD can significantly reduce the structural response. TLCD systems, which have significant practical advantages, can achieve the same motion reduction level as passive mass dampers. However, the liquid motion in a TLCMD system may reduce the effectiveness of the damper if the frequency of the liquid column is the same or less than the frequency of the whole damper. Therefore, a higher frequency ratio χ_1 should be selected for TLCMD system.

For the slender TV tower example, when a damper was tuned to the fundamental frequency of the main structure, the contribution of the higher modes of vibration to force and acceleration type responses was significant. Therefore, considering only the controlled mode in the analysis may lead to misleading and non-conservative results because the responses of the higher modes can become as large as or even larger than the response of the controlled mode. For the office tower example, it was found that the contribution of the higher modes of vibration to force and acceleration type responses was significant only for alongwind excitation. For crosswind wake excitation, the response was dominated by the first mode of vibration.

10.1.7 Soil-structure-mass damper interaction

The transfer matrix formulation for non-periodic structures was also used to analyse the effect of soil compliancy on the wind-induced response of slender structures equipped with mass dampers. The frequency-

dependent properties of soil and the contributions of higher modes of vibration can be conveniently introduced into the analysis of the soil-structure-mass damper system.

The numerical results showed that, when the soil was very soft, the mass damper was not an effective method to reduce soil-structure system responses. For moderately stiff soil, the mass damper should be tuned to the natural frequency of the soil-structure system rather than the natural frequency of the structure with a clamped base.

In comparison with the responses of the damper-structure system on rigid soil, the numerical examples showed that, under alongwind turbulence excitation, soil compliancy decreased the base moment and total acceleration responses of both the office tower and the TV tower, but increased the total displacement responses. For shear wave velocities of soil $V_s < 250$ m/s, the dynamic base moment, total top dynamic displacement and acceleration responses of the office tower-damper system were increased under crosswind wake excitation. It is believed that the modification of the natural frequencies of the system caused the first natural frequency of the system to get closer to the vortex shedding frequency. Consequently, the vibrational energy transferred to the tower due to the vortex shedding process was significantly increased and exceeded that dissipated through soil damping. On the other hand, soil compliancy decreased the same responses of the TV tower-damper system under crosswind wake excitation. The reduction in responses was due to a decrease in the critical wind speed and the height at which that wind speed occurred, as well as to the increase in soil damping.

10.2 Recommendations for further research

(a) In this thesis, the aeroelastic test of alongwind and crosswind vibration control were carried out on a 1:400 scale CAARC model in a suburban boundary layer wind model while the torsional vibration control experiment was conducted on a same scale rectangular tall building model in an open country boundary layer wind model. The structural damping ratios of both

building models were respectively assumed to be 1.0% and 1.2%. Although the experimental results have showed the effectiveness of the TMD systems in suppressing the wind-induced alongwind, crosswind and torsional vibrations within these test conditions, it is desirable to collect more data on the behaviours of passive mass dampers with sufficient variation in parameters such as building shape, building size, structural damping ratio, turbulence intensity level, mean velocity profile and surrounding wind environment.

(b) The torsional vibration experiments conducted in this thesis were preliminary and limited as the main aim of the project was vibration control of wind-induced tall/slender structures. It is possible, by using the present aeroelastic torsion test rig, to provide information on the torsional instability and the sensitivity of torsional response or excitation to changes in the structural damping, the turbulence intensity and the building configuration. Torsional interference between tall buildings is also an interesting research topic. With the accumulation of generalised torsional excitation spectra of different buildings, a generalised design procedure similar to the crosswind response prediction procedure proposed by Kwok(1982) can be developed.

(c) Some theoretical studies on coupled translational-torsional vibration of wind-induced tall buildings indicated that the offset between the center of mass, stiffness and aerodynamic force may significantly increase the structural response because of the inertial and elastic coupling effects. However, the information on the corresponding experimental study in wind tunnel is very limited. Based on current research experience and results of separate translational and torsional vibrations of wind-induced tall buildings and their control, experiments should proceed to investigate the coupled vibrations of tall buildings.

(d) Based on the measured wind excitation or response spectra in wind tunnel and the tested aeroelastic building models, a semi-analytical method of selecting the design parameters of active mass dampers and estimating the motion reduction of both building and damper was proposed in this thesis. This method has significant practical advantages. For passive TMD control system, the results obtained by this semi-analytical method were found to

be in good agreement with the experimental results. With further refinement and development to the existing experimental technique, active mass damper control system can be studied experimentally to verify the results obtained by the semi-analytical method.

(e) In the present study of liquid column damper systems, the liquid column dampers were uni-directional. For practical application, bi-directional tuned liquid column dampers should be investigated. Such investigation may be conducted after the basic motion equations of the bi-directional TLCD is obtained through the corresponding experiments.

NOTATION

The following symbols are used in the thesis. The notation for less commonly used variables is defined in the text as the quantities are introduced. Roman characters are listed first, followed by Greek characters.

- A - Cross-sectional area of the structure; Area of the structure normal to the wind
- b - Width of the structure normal to the wind
- B - Width of the liquid column
- B_s - Constant related to the spectral peak width
- c^* - Generalised damping
- C_a - Drag coefficient
- C_d - Damping coefficient of the mass damper
- C_l - Lift coefficient
- $C_o(z_1, z_2, n)$ - Co-spectrum of fluctuating wind
- C_p - Equivalent damping coefficient of the liquid column damper
- C_{ij} - Frequency dependent damping coefficients due to soil

D	- Diameter of the structure
ds	- Elemental length of the building perimeter
E	- Elastic modulus of the structure
f_s	- Vortex shedding frequency
F	- Force
g	- Acceleration due to gravity
G	- Shear modulus of soil beneath the footing base
G_s	- Shear modulus of soil adjacent to the footing sides
h	- Height of the building model
h_j	- Height of the jth storey unit
H	- Height of the structure above the ground
$H_{xy}(n)$	- Mechanical admittance function or frequency response function between x and y
I	- Moment of inertia
[I]	- Identity matrix
I_u	- Longitudinal turbulence intensity
k^*	- Generalised stiffness
K_d	- Stiffness of the mass damper
K_o	- Surface drag coefficient

K_{θ}	- Rotation stiffness of the structure
K_{ij}	- Frequency dependent spring coefficients due to soil
L	- Length; Length parameter; Footing embedment depth
L_{BL}	- Length associated with the external air flow
L_S	- Length associated with the structure
$m(z)$	- Mass per unit height of the structure
m^*	- Generalised mass
\bar{m}	- Total mass of the footing
M	- Bending moment
M_d	- Mass of the mass damper
M_w	- Liquid mass of the liquid damper
n	- Frequency
n_0	- Fundamental frequency of the structure
n_{BL}	- Frequency associated with the external air flow
P	- Air pressure; Probability; Active control force
Q	- Shear force
$ r $	- Torque arm of the element ds

- r_0 - Radius of the cylindrical footing or equivalent radius of a rectangular footing
- $R(z_1-z_2, n)$ - Cross-correlation function
- $R_x(\tau)$ - Autocorrelation function of response x
- S - Strouhal number
- S_0 - Power spectral density function of white noise excitation
- $S_{uu}(n, z)$ - Power spectral density function of the longitudinal fluctuating velocity at height z
- $S_{xx}(n)$ - Power spectral density function of the structural response x
- T - Base torque of the structure; Natural period; Truncation time
- \bar{T} - Base mean torque response of the structure
- $[T]$ - Transfer matrix
- u - Translation of the footing
- u_0 - Translation of the gravity centre of footing
- $\bar{V}(z)$ - Mean longitudinal velocity at height z
- \bar{V}_G - Mean longitudinal velocity at gradient height z_g
- V_r - Reduced velocity

$W(z)$	- Mean wind load at the height z
x, y, z	- System of rectangular Cartesian coordinates
x	- Elevation change of the liquid column
\bar{x}	- Mean alongwind response of the structure
z	- Height above ground
z_g	- Gradient height
z_r	- Reference height
Z	- Relative displacement of the damper
α	- Mean wind approach angle; Exponent for the mean wind speed profile
β	- Mode shape parameter; Damping coefficient of the structure
δ	- Relative embedment depth of the footing
ϵ	- Normalised loop gain
ζ, ζ_s	- Damping ratio
ζ_2	- Damper damping ratio
ζ_a	- Aerodynamic damping ratio
ζ_t	- Total damping ratio
η	- Mode shape correction factor

θ	- Twist angle of the structure; Rotation of the footing
$\bar{\theta}$	- Mean twist angle response of the structure
$\ell_{ux}(h)$	- Integral length scale of longitudinal turbulence at height h
$\lambda_{I\theta}$	- Mass moment scale of inertia
$\lambda_{K\theta}$	- Rotation stiffness scale
λ_L	- Geometric scale
λ_m	- Mass scale
λ_v	- Velocity scale
λ_T	- Time scale
$\lambda_{\rho s}$	- Structural density scale
μ	- Air viscosity; Mass ratio
ξ	- Building generalised response; Coefficient of head loss
ρ	- Liquid density
ρ_a	- Air density
ρ_s	- Density of the structure; Soil density
σ_T	- Standard deviation base torque response of the structure

- $\sigma_u(z)$ - Standard deviation of longitudinal fluctuating velocity at height z
- σ_x - Standard deviation alongwind response of the structure
- σ_y - Standard deviation crosswind response of the structure
- σ_z - Standard deviation relative displacement of the damper
- σ_θ - Standard deviation twist angle response of the structure
- τ - Time delay; Normalised feedback gain
- φ - Angular displacement
- $\Phi(z)$ - Modal shape
- $\Phi_{xx}(n)$ - Power spectral density function of random variable x
- χ - Frequency tuning
- ω - Angular frequency

REFERENCES

Abdel-Rohman, M., and Leipholz, H.H. (1978). Active control of flexible structures, *J. Struct. Div., ASCE*, Vol.104, pp. 1251-1266.

Alfriend, K. (1974). Partially filled viscous ring nutation damper, *J. Spacecraft*, Vol. 11, No. 7, pp. 456-462.

Amieux, J.C., and Dureigne, M. (1972). Analytical design of optimal nutation damper, *J. Spacecraft*, Vol. 9, No. 12, pp. 934-936.

Architectural Record (1971). Dampers blunt the wind's force on tall buildings, Sept., pp. 155-158.

ASCE Manuals and Reports on Engineering Practice No. 67 (1987a). *Wind tunnel model studies of buildings and structures*, prepared by the Task Committee on Manual of Practice for Wind Tunnel Testing of Buildings and Structures of the Committee on Aerodynamics of the Aerospace Division of the American Society of Civil Engineers.

ASCE a State-of-the Art Report (1987b). *Wind loading and wind-induced structural response*, prepared by the Committee on Wind Effects of the Committee on Dynamic Effects of the Structural Division of the American Society of Civil Engineers.

Australian Standards, SAA Loading Code Part 2 — *Wind Forces*, AS 1170, Part 2-1983.

Australian Standards, SAA Loading Code Part 2: *Wind Loads*, AS 1170.2-1989.

Balendra, T., and Nathan, G.K. (1987). Longitudinal, lateral and torsional

oscillations of a square section tower model in an atmospheric boundary layer, *Eng. Struct.*, Vol. 9, October, pp. 218 - 224.

Basu, R.I., and Vickery, B.J. (1983). Across-wind vibrations of structures of circular cross-section, Part II, development of a mathematical model for full-scale application, *J. Wind Eng. Ind. Aerodyn.*, 12, pp. 75-97.

Beredugo, Y.O., and Novak, M. (1972). Coupled horizontal and rocking vibration of embedded footings, *Canadian Geotechnical J.*, Vol. 9, pp. 477-497

Boggs, D.W., and Peterka, J.A. (1989). Aerodynamic model tests of tall buildings, *J. Eng. Mech., ASCE*, Vol. 115, No. 3, March, pp. 618-635.

Caughey, T.K. (1963). Equivalent linearisation techniques, *J. Acous. Soc. America*, Vol. 35, No.11, pp. 1706-1711.

Cermak, J.E. (1972). Wind effects on tall buildings - areas for research, *Proc. Int. Conf. on Planning and Design of Tall buildings*, Lehigh Univ., USA, pp. 435-440.

Cermak, J.E. (1987). Advances in physical modelling for wind engineering, *J. Eng. Mech., ASCE*, Vol. 113, No. 5, May, pp. 737-756.

Crandall, S.H., and Mark, W.D. (1963). *Random vibration in mechanical systems*, Academic Press, New York, N.Y.

Davenport, A.G. (1961). The application of statistical concepts to the wind loading of structures, *Proc. I.C.E.*, Vol. 19, pp. 449-472.

Davenport, A.G. (1962). The response of slender line like structures to a gusty wind, *Proc. I.C.E.*, Vol.23, p.389.

Davenport, A.G. (1966). The relationship of wind structure to wind loading, *Proc. Int. Conf. on Wind Effects on Buildings*, H.M.S.O., Paper No. 2.

Davenport, A.G. (1967). Gust loading factors, *J. Struct. Div., ASCE*, Vol. 93, ST2, pp. 11–34.

Davenport, A.G. (1971). the response of six building shapes to turbulent wind, *Phil. Trans. Roy. Soc. Lond., Series A*, No. 269, pp. 385–394.

Davenport, A.G. (1979). The influence of turbulence on the aeroelastic responses of tall structures to wind, *IAHR/IUTAM Symposium on Practical Experience with Flow-Induced Vibrations*, Karlsruhe, Germany, pp. 681–695.

Davenport, A.G., and Hill-Carroll, P. (1986). Damping in tall building: its variability and treatment in design, *Building Motion in Wind, ASCE*, Edited by N. Isyumov and T. Tschanz, pp. 43–57.

Deacon, E.L. (1955). Gust variation with height up to 150m, *Quart. J. Roy. Met. Soc.*, 81, No. 350, Oct., pp. 562–573.

Den Hartog, J.P. (1956). *Mechanical vibrations*, McGraw-Hill Book Co., Inc., New York, N.Y.

Durgin, F.H., and Tong, P. (1972). The effect of twist motion on the dynamic multimode response of a building, *IUTAM-IAHR Symposium on Flow-Induced Structural Vibrations*, Karlsruhe, Germany, pp. 382–400.

Engineering News Record (1971). Tower cables handle wind, water tank damps it, Dec. p. 23.

Engineering News Record (1975). Hancock Tower now to get dampers, Oct., p. 11.

Engineering News Record (1976). Lead hula-hoops stabilise antenna, Jul., p. 10.

Engineering News Record (1977). Tuned mass dampers steady sway of skyscrapers in wind, Aug., pp. 28–29.

ESDU (1974). Characteristics of atmospheric turbulence near the ground, Part II: Single point data for strong winds (neutral atmosphere), *Engineering Science Data Unit*, Item No. 74031, London.

ESDU (1978). Across-wind response due to vortex shedding: Isolated circular cylindrical structures in wind or gas flows, *Engineering Sciences Data Unit*, Item No. 78006, London.

Feld, L.S. (1971). Superstructure for 1350ft World Trade Centre, *Civ. Eng., ASCE*, Jun. pp. 66-70.

Foutch, D.A., and Safak, E. (1981a). Torsional vibration of wind-excited symmetrical structures, *J. Wind Eng. Ind. Aerodyn.*, Vol. 7, No. 2, March, pp. 191-201.

Foutch, D.A., and Safak, E. (1981b). Torsional vibration of along-wind excited structures, *J. Eng. Mech., ASCE*, Vol. 107, No. EM2, April, pp. 323-337.

Fujii, K., Tamura, Y., Sato, T., and Wakahara, T. (1990). Wind-induced vibration of tower and practical application of tuned sloshing damper, *J. Wind Eng. Ind. Aerodyn.*, 33, pp. 263-272.

Fujino, Y., Pacheco, B.M., Chaiseri, P., and Sun, L.M. (1988). Parametric studies on tuned liquid damper (TLD) using circular tanks by free-oscillation experiment, *Struct. Eng./ Earthquake Eng., JSCE*, No. 398, Oct., pp. 177-187.

Greig, G.L. (1980). Towards an estimate of wind-induced dynamic torque on tall buildings, M.E.Thesis, University of Western Ontario, Canada.

Hart, G.C., DiJulio, R.M., and Lew, M. (1975). Torsional response of high-rise buildings, *J. of Struct. Div., ASCE*, Vol. 101, No. ST2, Proc. Paper 11128, pp. 397-416.

Hayashida, H., and Iwasa, Y. (1990). Aerodynamic shape effects of tall

building for vortex induced vibration, *J. Wind Eng. Ind. Aerodyn.*, 33, pp. 237–242.

Hirsch, G. (1979). Critical comparison between active and passive control of wind induced vibrations of structures by means of mechanical devices, *Structural Control*, H.H.E. Leipholz, Ed., North Holland SM Publishing Co., pp. 313–339.

Homles, J.D. (1987). Mode shape correction factors for dynamic response to wind, *Eng. Struct.*, Vol. 9, July, pp. 210 – 212.

Homles, J.D. (1991). Private Communication.

Islam, M.S., Ellingwood, B., and Corotis, R.B. (1990). Dynamic response of tall buildings to stochastic wind load, *J. Struct. Eng., ASCE*, Vol. 116, No. 11, November, pp. 2982–3002.

Isyumov, N. (1982). The aeroelastic modelling of tall buildings, *Proc. Int. Workshop on Wind Tunnel Modelling for Civil Engineering Applications*, Gaithersburg, Maryland, USA, Cambridge Univ. Press, pp. 373–407.

Isyumov, N., Holmes, J.D., Surry, D., and davenport, A.G. (1975). A study of wind effects for the First National City Corporation project – New York, U.S.A., *Special Study Report*, BLWT–SS1–75, Univ. of Western Ontario, Canada, Apr.

Isyumov, N., and Poole, M. (1983). Wind induced torque on square and rectangular building shapes, *J. Wind Eng. Ind. Aerodyn.*, Vol. 13, pp. 183–196.

Iwan, W.D., and Yang, I.M. (1972). Application of statistical linearisation techniques to nonlinear multidegree of freedom systems, *J. applied Mech., ASME*, Vol. 39, pp. 545–550.

Jeary, A.P., Lee, B.E., and Sparks, P.R. (1979). The determination of model wind loads from full-scale building response measurements, *Proc. 5th Int.*

Conf. on Wind Engineering, Fort Collins, Colorado, Pergamon Press, pp. 577–591.

Jeary, A.P., and Winney, P.E. (1972). Determination of structural damping of a large multi-flue chimney from the response to wind excitation, *Proc. I.C.E.*, Vol. 53, Dec., Part 2, Tech. Note 65, pp. 569–577.

Kareem, A. (1982). Acrosswind response of buildings, *J. Struct. Div., ASCE*, Vol. 108, No. ST4, Apr., pp. 869–887.

Kareem, A. (1983). Mitigation of wind induced motion of tall buildings, *J. Wind Eng. Ind. Aerodyn.*, 11, pp. 273–284.

Kareem, A. (1984). Model for predicting the across-wind response of building, *Eng. Struct.*, Vol. 6 (2), pp. 136–141.

Kareem, A. (1985). Lateral-torsional motion of tall buildings to wind loads, *J. Struct. Eng., ASCE*, Vol. 111, No. 11, November, pp. 2479–2496.

Kareem, A. (1990). Reduction of wind induced motion utilising a tuned sloshing damper, *J. Wind Eng. Ind. Aerodyn.*, 36, pp. 725–737.

Keel, C.J., and Mahmoodi, P. (1986). Design of viscoelastic dampers for Columbia Centre Building, *Building Motion in Wind*, ASCE, Edited by N. Isyumov and T. Tschanz, pp. 66–81.

Kobori, T. (1990). Earthquake and wind induced vibration control technology towards the super-high-rise building, *Tall Buildings: 2000 and Beyond*, 4th. World Cong., Nov., Hong Kong, pp. 917–934.

Kwok, K.C.S. (1977). Cross wind response of structures due to displacement dependent excitations, *Ph. D. Thesis*, Dept. Mech. Eng., Monash Univ., Australia.

Kwok, K.C.S. (1982). Cross-wind response of tall buildings, *Eng. Struct.*, Vol. 4, October, pp. 256–262.

Kwok, K.C.S. (1983). Full-scale measurements of wind-induced response of Sydney Tower, *J. Wind Eng. Ind. Aerodyn.*, 14, pp. 307-318.

Kwok, K.C.S. (1987). Tuned mass damper for tall buildings and structures, Chapter 11, *Civil Engineering Practice*, Vol. 1 - Structures, Edited by P.N. Cheremisnoff, N.P. Cheremisinoff and S.L. Cheng, Tech. Publishing, USA.

Kwok, K.C.S. (1988). Effect of building shape on wind-induced response of tall building, *J. Wind Eng. Ind. Aerodyn.*, 28., pp. 381-390.

Kwok, K.C.S., and Bailey, P.A. (1987). Aerodynamic devices for tall buildings and structures, *J. Mech. Eng., ASCE*, Vol. 113, No. 3, Mar., pp. 349-365.

Kwok, K.C.S., and Macdonald, P.A. (1987). Wind-induced response of Sydney Tower, *Eng. Struct.*, Vol. 12, No. 3, Jul., pp. 153-162.

Kwok, K.C.S., and Melbourne, W.H. (1981). Wind-induced lock-in excitation of tall structures, *J. Struct. Div., ASCE*, Vol. 107, No. ST1, Jan., pp. 57-72.

Kwok, K.C.S., Wilhelm, P.A., and Wilkie, B.G. (1988). Effect of edge configuration on wind-induced response of tall buildings, *Eng. Struct.*, Vol. 10, April, pp. 135-140.

Laneville, A., and Williams, C.D. (1979). The effect of intensity and large-scale turbulence on the mean pressure and drag coefficients of 2D rectangular cylinders, *Proc. 5th Int. Conf. on Wind Engineering*, Fort Collins, Colorado, Pergamon Press, pp. 397-404.

Lin, Y.K., and McDaniel (1969). Dynamics of beam-type periodic structures, *J. Eng. Ind.*, Vol. 91, Series B, No. 4, pp. 1133-1141.

Lin, Y.K., and Wu, W.F. (1984). Along-wind motion of building on compliant soil, *J. Eng. Mech., ASCE*, Vol. 110, No.1, pp. 1-19.

- Lin, Y.K., and Wu, W.F. (1984). A closed form earthquake response analysis of multistory building on compliant soil, *J. Struct. Mech.*, 12(1), pp. 87–110.
- Luft, R.W. (1979). Optimal tuned mass dampers for buildings, *J. Struct. Div., ASCE*, Vol. 105, No. ST12, Dec. pp. 2766–2772.
- Lythe, G.R., and Surry, D. (1990). Wind-induced torsional loads on tall buildings, *J. Wind. Ind. Aerodyn.*, 36, pp. 225–234.
- Mahmoodi, P. (1969). Structural dampers, *J. Struct. Div., ASCE*, Vol. 95, No. ST8, Aug., pp.1661–1672.
- Mahmoodi, P., and Keel, C.J. (1986). Performance of viscoelastic structural dampers for the Columbia Centre Building, *Building Motion in Wind*, ASCE, Edited by N. Isyumov, and T. Tschanz, pp. 83–106.
- Mahmoodi, P., and Keel, C.J. (1989). analysis and the design of multi-layer viscoelastic dampers for tall structures, *Proc. Struct. Cong., ASCE*, May, San Francisco, USA.
- Martin, C.R., and Soong, T.T. (1976). Modal control of multistory structures, *J. Eng. Mech., ASCE*, Vol. 102, pp. 613–623.
- Masri, S.F. (1967). Effectiveness of two-particle impact dampers, *J. Acous. Soc. of America*, Vol. 41, No. 6, pp. 1553–1554.
- Mataki, Y., Ohkuma, T., Kanda, J., Kitamura, H., Kawabata, S., and Ohtake, K. (1989). full-scale measurement of wind actions on CHiba Port Tower, *Takenaka Tech. Res. Rep.*, No. 42, Nov.
- McNamara, R.J. (1977). Tuned mass dampers for buildings, *J. Struct. Div., ASCE*, Vol. 103, No. ST9, Sept., pp. 1785–1798.
- Melbourne, W.H. (1972). Modelling of structures to measure wind effects, *Proc. Models Conf., Arch. Sc., Univ. of Sydney*, pp. 1–9.

Melbourne, W.H. (1975). Cross-wind response to structures to wind action, *Proc. 4th. Int. Conf. Wind Effects on Buildings and Structures*, Sept., London, Cambridge Univ. Press., pp. 343–358.

Melbourne, W.H. (1977). Probability distributions associated with the wind loading of structures, *C.E.Trans., I.E.A*, Vol Ce19, No. 1, pp. 58–67.

Melbourne, W.H. (1991). Private Communication.

Milford, R.V. (1987). Mode shape correction factors for flexural and shear type structures, *Internal Report 87/13*, Structural and Geotechnical Engineering Division, National Building Research Institute, Council for Scientific and Industrial Research, Pretoria, South Africa, November.

Miyata, T., and Miyazaki, M. (1979). Turbulence effects on aerodynamic response of rectangular bluff cylinders, *Proc. 5th Int. Conf. on Wind Engineering*, Fort Collins, Colorado, Pergamon Press, pp. 631–642.

Modi, V.J., and Welt, F. (1988). Damping of wind induced oscillations through liquid sloshing, *J. Wind Eng. Ind. Aerodyn.*, 30, pp. 85–94.

Naudascher, E., Weske, J.R., and Fey, B. (1981). Exploratory study on damping of galling vibrations, *J. Wind Eng. Ind. Aerodyn.*, 8, pp. 211–222.

Novak, M. (1974). Effect of soil on structural response to wind and earthquake, *Earthqu. Eng. Struct. Dyn.*, Vol. 3, pp. 79–96.

Novak, M., and Beredugo, Y.O. (1972). Vertical vibration of embedded footings, *J. Soil Mech. Found. Div., ASCE*, 98, 2, pp. 1291–1310

Novak, M., and Hifnawy, L.El. (1988). Structural response to wind with soil-structure interaction, *J. Wind Eng. Ind. Aerodyn.*, Vol. 28, pp. 329–338.

Novak, M., and Sachs, K. (1973). Torsional and coupled vibrations of embedded footings, *Int. J. Earthq. Eng. Struct. Dyn.*, pp. 11–33.

Ogendo, J.E.W., Milsted, M.G., and Johns, D.J. (1983). Response of steel chimneys with added damping, *J. Wind Eng. Ind. Aerodyn.*, Vol. 14, pp. 141-152.

Ormondroyd, J., and Dan Hartog, J.P. (1928). The theory of the dynamic vibration absorber, *Trans., ASME*, APM-50-7, pp. 9-22.

Parkinson, G.V. (1971). Wind-induced instability of structures, *Phil. Trans. Roy. Soc. Lond.*, Series A, Vol. 269, pp. 395-409.

Patrickson, C.P., and Friedmann, P.P. (1979). Deterministic torsional building response to winds, *J. Struct. Div., ASCE*, Vol. 105, No. ST12, Dec., pp. 2621-2637.

Peterson, N.R. (1979). Design of large scale tuned mass dampers, *ASCE Convention and Exposition*, Boston, Mass., Apr., Preprint 3578.

Reed, W.H. (1967). Hanging-chain impact dampers: a simple method for damping tall flexible structures, *Proc. 2nd. Int. Conf. on Wind effects on Buildings and Structures*, Ottawa, Canada, Univ. of Toronto Press, Sept., Paper 36, pp. 283-321.

Reinhold, T.A., Sparks, P.R., Tieleman, H.W., and Maher, F.J. (1979). Mean and fluctuating forces and torques on a tall building model of square cross-section, *Research Report*, VPI-E-79-11, College of Engineering, Virginia Polytechnic Institute and State University, blacksburg, Virginia, USA.

Reinhold, T.A., and Sparks, P.R. (1979). The influence of wind direction on the response of a square-section tall building, *Proc. 5th Int. Conf. on Wind Engineering*, Fort Collins, Colorado, Pergamon Press, pp. 685-698.

Reinhold, T.A. (1983). Distribution and correlation of dynamic wind loads, *J. Eng. Mech., ASCE*, Vol. 109, No. 6, Dec., pp. 1419-1436.

Richart, F.E., Hall, J.R., and Woods, R.D. (1970). *Vibrations of soils and*

foundations. Prentice-Hall Inc., Englewood Cliffs, U.S.A.

Roorda, J. (1975). Tendon control in tall structures, *J. Struct. Div., ASCE*, Vol. 101, No. ST3, Mar., pp. 505-521.

Roorda, J. (1980). Experiments in feedback control of structures, *Structural Control*, H.H.E. Leipholz (ed.), North-Holland Publishing Com.& Pub.

Sakai, F., Takaeda, S., and Tamaki, T. (1989). Tuned liquid column damper - new type device for suppression of building vibration, *Int. Conf. on Highrise Building*, Vol. 2, Nanjing, China, Mar.

Samali, B., Yang, J.N., and Yeh, C.T. (1985). Control of lateral-torsional motion of wind-excited buildings, *J. Eng. Mech., ASCE*, Vol. 111, No. 6, Jun., pp. 777-796.

Saunders, J.W. (1974). Wind excitation of tall buildings with particular reference to the cross-wind motion of tall buildings of constant rectangular cross-section, *Ph. D. Thesis*, Dept. Mech. Eng., Monash Univ., Australia.

Saunders, J.W., and Melbourne, W.H. (1975). Tall rectangular building response to cross-wind excitation, *Proc. 4th. Int. Conf. Wind Effects on Buildings and Structures*, Sept., London, Cambridge Univ. Press.

Saunders, J.W., and Melbourne, W.H. (1977). Wind-excited buildings — design sway stiffness, Roy. Melbourne Inst. Technol. Dept. Mech. Prod. Eng. Rep., November.

Scruton, C., and Walshe, D.E.J. (1957). A mean of avoiding wind excited oscillations of structures of circular or near circular cross-section, *N.P.L. Report Aero*. 335.

Simiu, E. (1980). Revised procedure for estimating alongwind response, *J. Struct. Div., ASCE*, Vol. 106, No. ST 1, pp. 1-10.

Skilling, J.B., Tschanz, T., Isyumov, N., Loh, P., and Davenport, A.G.

(1986). Experimental studies, structural design and full-scale measurements for the Columbia Seafirst Centre, *Building Motion in Wind, ASCE*, Edited by N. Isyumov and T. Tschanz, pp. 1-22.

Solari, G. (1982). Alongwind response estimation: closed form solution, *J. Struct. Div., ASCE*, Vol. 108, No. ST1, pp. 225-244.

Solari, G. (1985). Mathematical model to predict 3-D wind loading on buildings, *J. Eng. Mech., ASCE*, Vol. 111, No.2, pp. 254-276.

Solari, G., and Stura, D. (1979). Dynamic along-wind response of a structural system including soil flexibility, *Proc. of the Fifth Int. Wind Eng. Conf.*, Fort Collins, Colorado, USA., pp. 735-745.

Soong, T.T. (1988). Active structural control in civil engineering, a State-of-the-Art Review, *Eng. Struct.*, Vol. 10, Apr.

Soong, T.T., and Skinner, G.T. (1981). Experimental study of active structural control, *J. Eng. Mech., ASCE*, Vol. 107, No. EM6, Dec., pp. 1057-1068.

Spanos, P.T., and Iwan, W.D. (1978). On the existence and uniqueness of solutions generated by equivalent linearisation, *Int. J. Nonlinear Mech.*, Vol. 13, No. 2, pp. 71-78.

Surry, D. (1982). Consequences of distortion in the flow including mismatching scales and intensities of turbulence, *Proc. Int. Workshop on Wind Tunnel Modelling for Civil Engineering Applications*, Cambridge University Press, pp. 137-186.

Tallin, A., and Ellingwood, B. (1985). Wind induced lateral-torsional motion of buildings, *J. Struct. Eng., ASCE*, Vol. 111, No. 10, October, pp. 2197-2213.

Tallin, A., and Ellingwood, B. (1985). Analysis of torsional moments on tall buildings, *J. Wind Eng. Ind. Aerodyn.*, Vol. 18, pp. 191-195.

Tanaka, H., and Mak, C.Y. (1983). Effect of tuned mass dampers on wind-induced response of tall buildings, *J. Wind Eng. Ind. Aerodyn.*, 14, pp. 357-368.

Thoroddsen, S.T., Peterka, J.A., and Cermak, J.E. (1988). Correlation of the components of wind-loading on tall buildings, *J. Wind Eng. Ind. Aerodyn.*, Vol. 28, pp. 351-360.

Torkamani, M.A.M., and Pramono, E. (1985). Dynamic response of tall buildings to wind excitation, *J. Struct. Eng., ASCE*, Vol. 111, No. 4, April, pp. 805-825.

Tschanz, T., and Davenport, A.G. (1983). The base balance technique for the determination of dynamic wind loads, *J. Wind Eng. Ind. Aerodyn.*, Vol. 13, pp. 429-439.

Vickery, B.J. (1966). On the assessment of wind effects on elastic structures, *C.E. Trans. I.E.A.*, Oct., pp. 183-192.

Vickery, B.J. (1971). On the reliability of gust loading factors, *C.E. Trans. I.E.A.*, Apr., pp. 1-9.

Vickery, B.J. (1972). On the aeroelastic modelling of structures in wind, *Struct. Models Conf.*, University of Sydney, Sydney, Australia.

Vickery, B.J. (1979). Wind effects on buildings and structures — critical unresolved problems, *IAHR/IUTAM Practical Experiences with Flow-Induced Vibrations Symposium*, Karlsruhe, Germany, pp. 823-828.

Vickery, B.J., and Basu, R.J. (1983). Acrosswind vibrations of structures of circular cross-section, Part I, development of a mathematical model for two-dimensional conditions, *J. Wind Eng. Ind. Aerodyn.*, 12, pp. 49-73.

Vickery, B.J., and Clark, A.W. (1972). lift or across-wind response of tapered stacks, *J. Struct. Div., ASCE*, Vol. 98, No. ST1, pp. 1-20.

Vickery, B.J., and Davenport, A.G. (1970). An investigation of the behaviour in wind of the proposed Centrepoint Tower, in Sydney, Australia, *Eng. Sci. Report*, No. BLWT-1-70, Univ. of Western Ontario, Feb.

Vickery, B.J., Isyumov, N., and Davenport, A.G. (1983). The role of damping, mass and stiffness in the reduction of wind effects on structures, *J. Wind Eng. Ind. Aerodyn.*, 11, pp. 285-294.

Vickery, P.J., Steckley, A., Isyumov, N., and Vickery, B.J. (1985). The effect of mode shape on the wind-induced response of tall buildings, *Proc. 5th U.S. National Conf. on Wind Engineering*, Texas Tech. University, 1B-41 — 1B-48.

Wargan, A. (1983). Design and construction of Sydney Tower, *The Struct. Eng.*, Vol. 61A, No. 9, Sept.

Walshe, D.E., and Wootton, L.R. (1970). Preventing wind-induced oscillations of structures of circular section, *Proc. I.C.E.*, Vol. 47, pp. 1-24.

Weisner, K.B. (1979). Tuned mass dampers to reduce building wind motion, *ASCE Convention and Exposition*, Boston, Mass., Apr., Preprint 3510.

Wen, Y.K. (1980). Equivalent linearisation for hysteretic systems under random excitation, *J. Applied Mech., ASME*, Vol. 47, pp. 150-154.

Whitbread, R.E. (1963). Model simulation of wind effects on structures, *Proc. 1st. int. Conf. on Wind Effects on Buildings and Structures*, N.P.L., Teddington, Middlesex, U.K., H.M.S.O. Lond., June, pp. 284-306.

Yang, J.N. (1975). Application of optimal control theory to civil engineering structures, *J. Eng. Mech., ASCE*, Vol. 101, No. EM6, Dec., pp. 818-838.

Yang, J.N. (1982). Control of tall buildings under earthquake excitations, *J. Eng. Mech., ASCE*, Vol. 108, No. EM5, Oct., pp. 833-849.

Yang, J.N., and Giannopoulos, F. (1978). Active tendon control of structures, *J. Eng. Mech., ASCE*, Vol. 104, No. EM3, Jun., pp. 551–568.

Yang, J.N., and Giannopoulos, F. (1979a). Active control and stability of cable–stayed bridge, *J. Eng. Mech., ASCE*, Vol. 105, No. EM4, Aug., pp. 677–694.

Yang, J.N., and Giannopoulos, F. (1979b). Active control of two–cable–stayed bridge, *J. Eng. Mech., ASCE*, Vol. 105, No. EM5, Oct., pp. 795–810.

Yang, J.N., and Lin, Y.K. (1975). Frequency response functions of a disordered periodic beam, *J. Sound Vib.*, Vol. 38, No.3, pp. 317–340.

Yang, J.N., and Lin, Y.K. (1981). Along–wind motion of multistory building, *J. Eng. Mech., ASCE*, Vol. 107, No. EM 2, Apr., pp. 295–307.

Yang, J.N., Lin, Y.K., and Samali, B. (1981). Coupled motion of wind–loaded multi–story building, *J. Eng. Mech., ASCE*, Vol. 107, No. EM6, Dec., pp. 1209–1225.

Yang, J.N., and Samali, B. (1983). Control of tall building in along–wind motion, *J. Struct. Eng., ASCE*, Vol. 109, No. 1, Janu., pp. 50–68.

Yao, J.T.P. (1972). Concept of structural control, *J. Struct. Div., ASCE*, Vol. 98, No. ST7, Jul., pp. 1567–1574.

Zdravkovich, M.M. (1981). Review and classification of various aerodynamic and hydrodynamic means for suppressing vortex shedding, *J. Wind Eng. Ind. Aerodyn.*, 7, pp. 145–189.

Zuk, W. (1968). Kinetic structures, *Civ. Eng., ASCE*, Vol. 39, No. 12, pp. 62–64.

APPENDIX A

FREE DECAY VIBRATIONS OF A TWO--DEGREE-OF-FREEDOM SYSTEM

In aeroelastic tests of a tall building with a tuned mass damper, the damper model is usually so small that it is not easy to measure directly the damper damping without non-contact laser or other displacement meters. The analysis of free decay vibration of a two-degree-of-freedom system can provide an alternative way to determine the damper damping indirectly. Furthermore, it is possible, when some particular initial conditions of the system are satisfied, to show effectiveness of TMDs by free vibration decay traces of the building with and without a TMD.

The free vibration equations of the building-mass damper system with viscous damping are

$$\left. \begin{aligned} m_1^* \ddot{y}_1 + c_1^* \dot{y}_1 + k_1^* y_1 - c_2 (\dot{y}_2 - \dot{y}_1) - k_2 (y_2 - y_1) &= 0 \\ m_2 \ddot{y}_2 + c_2 (\dot{y}_2 - \dot{y}_1) + k_2 (y_2 - y_1) &= 0 \end{aligned} \right\} \quad (\text{A.1})$$

The meaning of all parameters in this equation is the same as that in Eq. 5.10.

If the system is a lightly damped system, the solution of Eq. A.1 can be simplified to

$$\left. \begin{aligned} y_1 &= \Phi_{11} e^{-\zeta_1 \omega_1 t} (A_1 \cos \omega_1 t + A_2 \sin \omega_1 t) + \\ &\quad \Phi_{21} e^{-\zeta_2 \omega_2 t} (A_3 \cos \omega_2 t + A_4 \sin \omega_2 t) \\ y_2 &= e^{-\zeta_1 \omega_1 t} (A_1 \cos \omega_1 t + A_2 \sin \omega_1 t) + \\ &\quad e^{-\zeta_2 \omega_2 t} (A_3 \cos \omega_2 t + A_4 \sin \omega_2 t) \end{aligned} \right\} \quad (\text{A.2})$$

where ω_1 and ω_2 are the first and second undamped natural angular

frequencies of the system. They can be calculated by the following formula:

$$\omega_{1,2}^2 = \frac{m_1^* k_2 + m_2^* k_1 + k_2 m_2 \bar{\tau} \Theta}{2m_1^* m_2} \quad (\text{A.3})$$

where

$$\Theta = \sqrt{m_1^* k_2^2 + m_2^* k_1^2 + k_2^2 m_2^2 - 2m_1^* m_2 k_1^* k_2 + 2m_1^* m_2 k_2^2 + 2m_2^* k_1^* k_2}$$

Φ_{11} and Φ_{21} are the undamped amplitude ratio of the first and second mode of the system. They can be expressed as

$$\left. \begin{aligned} \Phi_{11} &= \frac{k_2}{k_1^* + k_2 - \omega_1^2 m_1^*} \\ \Phi_{21} &= \frac{k_2}{k_1^* + k_2 - \omega_2^2 m_1^*} \end{aligned} \right\} \quad (\text{A.4})$$

ζ_1 and ζ_2 are the first and second mode damping values (fraction of critical damping). They are expressed as

$$\left. \begin{aligned} \zeta_1 &= \frac{c_1 \Phi_{11}^2 + (\Phi_{11}^2 - 2\Phi_{11} + 1)c_2}{2\omega_1 (m_1^* \Phi_{11}^2 + m_2)} \\ \zeta_2 &= \frac{c_1 \Phi_{21}^2 + (\Phi_{21}^2 - 2\Phi_{21} + 1)c_2}{2\omega_2 (m_1^* \Phi_{21}^2 + m_2)} \end{aligned} \right\} \quad (\text{A.5})$$

with the assumption that the off-diagonal term, $c_1 \Phi_{21} \Phi_{11} + (\Phi_{21} \Phi_{11} - \Phi_{11} - \Phi_{21} + 1)c_2$, is small and can be neglected.

Finally, the constants A_1 to A_4 can be determined by the initial conditions y_{10} , y_{20} , \dot{y}_{10} and \dot{y}_{20} (at time $t = 0$) as follows:

$$\left. \begin{aligned} A_1 &= \frac{y_{10} - \Phi_{21} y_{20}}{\Phi_{11} - \Phi_{21}} ; & A_2 &= \frac{\dot{y}_{10} + \zeta_1 \omega_1 y_{10} - \Phi_{21} (\dot{y}_{20} + \zeta_1 \omega_1 y_{20})}{\omega_1 (\Phi_{11} - \Phi_{21})} \\ A_3 &= \frac{\Phi_{11} y_{20} - y_{10}}{\Phi_{11} - \Phi_{21}} ; & A_4 &= \frac{\Phi_{11} (\dot{y}_{20} + \zeta_2 \omega_2 y_{20}) - (\dot{y}_{10} + \zeta_2 \omega_2 y_{10})}{\omega_2 (\Phi_{11} - \Phi_{21})} \end{aligned} \right\} \quad (\text{A.6})$$

If the initial displacements exactly match the pattern of the first mode ($y_{10}/y_{20} = \phi_{11}$), while $\dot{y}_{10} = \dot{y}_{20} = 0$, then $A_3 = A_4 = 0$, $A_2 \approx 0$ and $A_1 = y_{20}$. Therefore, the response becomes

$$\left. \begin{aligned} y_1 &= y_{10} e^{-\zeta_1 \omega_1 t} \cos \omega_1 t \\ y_2 &= y_{20} e^{-\zeta_1 \omega_1 t} \cos \omega_1 t \end{aligned} \right\} \quad (\text{A.7})$$

which consists of pure first-mode response.

Based on the above formulae, the damper damping can be determined as follows: (1) to calculate ω_1 and ϕ_{11} in Eqs. A.3 and A.4; (2) to measure free vibration decay trace of the building model with the TMD according to the initial conditions, i.e., $\dot{y}_{10} = \dot{y}_{20} = 0$ and $y_{10}/y_{20} = \phi_{11}$; (3) to calculate ζ_1 by using the measured free decay trace and then c_2 through Eq. A.5. If one hopes to compare the effectiveness of TMDs by using free vibration decay traces of the building with and without the TMD, the free decay trace of the building-TMD system theoretically should be obtained by using the abovementioned initial conditions. In some cases, if the initial conditions of $\dot{y}_{10} = \dot{y}_{20} = 0$ and $y_{10} = y_{20} = \text{constant}$ are used, a phenomenon known as beating may be observed because the natural frequencies of both building and damper are very close to each other. Fig. A.1 shows an example which was obtained through the free vibration test of the torsional model in Chapter 4.

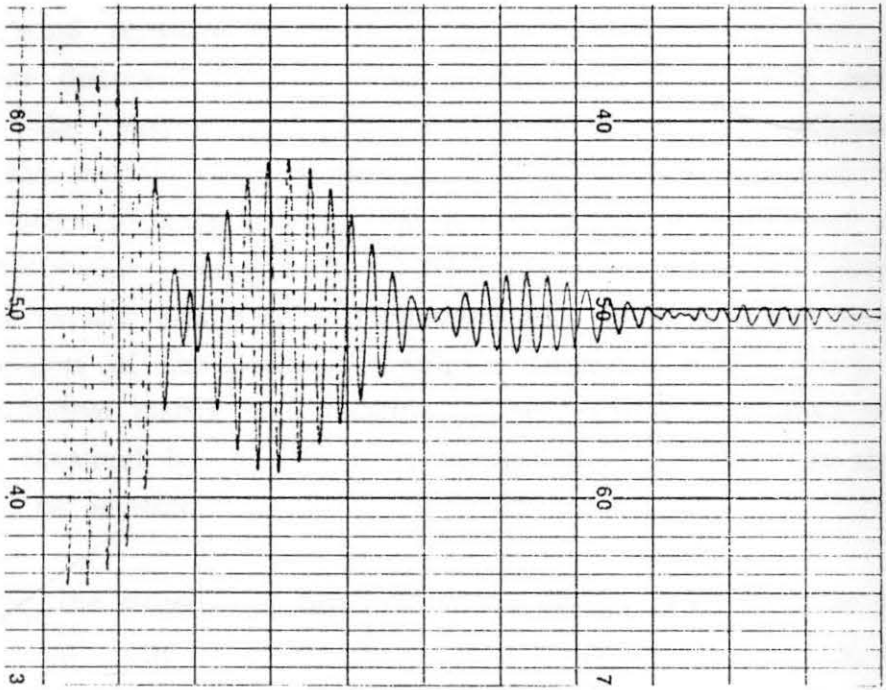


FIG. A.1 FREE VIBRATION DECAY TRACE WITH THE BEATING
IN TORSIONAL BUILDING-MASS DAMPER SYSTEM

APPENDIX B

ACCURACY OF NUMERICAL COMPUTATION FOR NON-PERIODIC STRUCTURES BY THE TRANSFER MATRIX APPROACH

Many wind sensitive structures can not be simplified into periodic structures as discussed by Lin (1969), Yang and Lin (1975, and 1980). Therefore, the matrix multiplication operation is unavoidable when computing the product chain of the matrix, e.g., $[A_r]$ in Chapters 8 and 9. When the product chain is long, the round-off error associated with the matrix multiplication operation should be investigated. For this purpose, an analytical procedure was derived (following Lin, 1969) for the computation of the elements of the periodic cantilever structure matrix $[A_r]$, without using the iterative matrix multiplication. The results were then compared with those obtained by direct matrix multiplication so that the round-off errors could be assessed.

Assuming the structural properties do not change from floor to floor, or from unit to unit, one can calculate the matrix $[T]^n$ ($n = 1, 2, \dots, N$) in place of the matrix $[A_r]$ ($r = 1, 2, \dots, N$). Because of certain properties of transfer matrixes (Lin, 1969), $[T]^n$ can be considerably simplified. In particular, the determinant of the transfer matrix, $[T]$, is equal to unity and the coefficients in the characteristic equation are symmetrically arranged. For the type of structure described in this thesis, the characteristic equation has the form

$$|T - \lambda I| = \lambda^4 - 2\mu_1 \lambda^3 + 2\mu_2 \lambda^2 - 2\mu_1 \lambda + 1 = 0 \quad \dots \dots \dots (B.1)$$

where $2\mu_1 = 4 + h^2 ab$

$$2\mu_2 = 6 - 4h^2 ab$$

$$a = m\omega^2 - i\beta\omega \quad (= \bar{a})$$

$$b = h/6EI$$

The symmetry in the characteristic equation implies that the eigenvalues

are reciprocal pairs; i.e., for every eigenvalue, λ_j , there exists another equal to λ_j^{-1} .

It is convenient to cast the eigenvalues in the form of $\lambda = e^{i\theta}$. Then, substituting $e^{i\theta}$ into Eq. B.1, one obtains a quadratic equation in terms of $\cos\theta$:

$$2\cos^2\theta - 2\mu_1\cos\theta + (\mu_2 - 1) = 0 \quad \dots \dots \dots (B.2)$$

The roots of $\cos\theta$ can be obtained analytically as follows:

$$\left. \begin{aligned} \cos\theta_1 &= \mu_1/2 + \sqrt{\mu_1^2/4 - (\mu_2 - 1)/2} = z_1 \\ \cos\theta_2 &= \mu_2/2 - \sqrt{\mu_1^2/4 - (\mu_2 - 1)/2} = z_2 \end{aligned} \right\} \dots \dots \dots (B.3)$$

Note that z_1 and z_2 are generally complex. Then to evaluate θ_1 and θ_2 we may use the formulae:

$$\theta_j = -i \ln(z_j + \sqrt{z_j^2 - 1}) \quad j = 1, 2 \quad \dots \dots \dots (B.4)$$

By use of the Cayley-Hamilton theorem, it may be shown that any analytical function of a $k \times k$ matrix can be expressed as a linear combination of any other k -independent analytic functions of the same matrix. Therefore, $[T]^n$ may be expressed as

$$[T]^n = \sum_{j=1}^k (a_j \frac{[T]^j + [T]^{-j}}{2} + b_j \frac{[T]^j - [T]^{-j}}{2}) \quad \dots \dots \dots (B.5)$$

in which a_j and b_j are evaluated by substituting different eigenvalues of $[T]$ in place of $[T]$ as follows:

$$\left. \begin{aligned} \cos(n\theta_1) &= \sum_{j=1}^k a_j \cos(j\theta_1) \\ \sin(n\theta_1) &= \sum_{j=1}^k b_j \cos(j\theta_1) \end{aligned} \right\} \dots \dots \dots (B.6)$$

Thus, if $\cos\theta_1 \neq \cos\theta_2$

$$\left. \begin{aligned} a_1 &= \frac{\cos\theta_1 \cos 2\theta_2 - \cos\theta_2 \cos 2\theta_1}{\cos\theta_1 \cos 2\theta_2 - \cos\theta_2 \cos 2\theta_1} \\ a_2 &= \frac{\cos\theta_1 \cos\theta_2 - \cos\theta_2 \cos\theta_1}{\cos\theta_1 \cos 2\theta_2 - \cos\theta_2 \cos 2\theta_1} \\ b_1 &= \frac{\sin\theta_1 \sin 2\theta_2 - \sin\theta_2 \sin 2\theta_1}{\sin\theta_1 \sin 2\theta_2 - \sin\theta_2 \sin 2\theta_1} \\ b_2 &= \frac{\sin\theta_1 \sin\theta_2 - \sin\theta_2 \sin\theta_1}{\sin\theta_1 \sin 2\theta_2 - \sin\theta_2 \sin 2\theta_1} \end{aligned} \right\} \dots \dots \dots (B.7)$$

When $\cos\theta_1 = \cos\theta_2 = \mu_1/2$, i.e., when θ_1 approaches θ_2 , these coefficients are obtained as follows:

$$\left. \begin{aligned} a_1 &= \frac{2 \cos\theta \sin 2\theta + n \sin\theta \cos 2\theta}{\sin\theta(1 + 2\cos^2\theta)} \\ a_2 &= \frac{n \cos\theta \sin\theta - \sin\theta \cos\theta}{\sin\theta(1 + 2\cos^2\theta)} \\ b_1 &= \frac{n \cos\theta \cos\theta - \sin\theta \cos 2\theta}{\sin^2\theta \sin^3\theta} \\ b_2 &= -\frac{n \cos\theta}{2\sin^2\theta} + \frac{\cos\theta \sin\theta}{2\sin^3\theta} \end{aligned} \right\} \dots \dots \dots (B.8)$$

The choice of the combinations, $[T]^j \pm [T]^{-j}$, appearing on the right hand side of Eq. B.5, results in considerable simplification, letting

$$\left. \begin{aligned} [\bar{A}] &= [T] + [T]^{-1} ; \quad [\bar{B}] = [T] - [T]^{-1} \\ [\bar{C}] &= [T]^2 + [T]^{-2} ; \quad [\bar{D}] = [T]^2 - [T]^{-2} \end{aligned} \right\} \dots \dots \dots (B.9)$$

The results may be summarised as follow:

$$[\bar{A}] = \begin{bmatrix} h^2ab + 2 & 0 & 6hb & 0 \\ -3hab & 2 & 0 & 6hb \\ ah & 0 & 2 & 0 \\ 0 & ha & 3hab & h^2ab + 2 \end{bmatrix}$$

$$[\bar{B}] = \begin{bmatrix} -h^2ab & 2h & 0 & 2h^2b \\ 3hab & 0 & 12b & 0 \\ -ah & 0 & 0 & 2h \\ 2a & ha & 3hab & h^2ab \end{bmatrix}$$

$$[\bar{C}] = \begin{bmatrix} h^4a^2b^2 + 10h^2ab + 2 & 0 \\ -3h^3a^2b^2 - 12hab & 6h^2ab + 2 \\ h^3a^2b + 4ha & 0 \\ 0 & h^3a^2b + 4ha \\ 6h^3ab^2 + 24hb & 0 \\ 0 & 6h^3ab^2 + 24hb \\ 6h^2ab + 2 & 0 \\ 3h^3a^2b^2 + 12hab & h^4a^2b^2 + 10h^2ab + 2 \end{bmatrix}$$

$$[\bar{D}] = \begin{bmatrix} -h^3a^2b^2 - 8h^2ab & 2h^3ab + 4h \\ 3h^3a^2b^2 + 18hab & 0 \\ -h^3a^2b - 2ha & 2h^2a \\ 2h^2a^2b + 4a & h^3a^2b + 2ha \\ 0 & 2h^4ab^2 + 16h^2b \\ 18h^2ab^2 + 24b & 0 \\ 0 & 2h^3ab + 4h \\ 3h^3a^2b^2 + 18hab & h^4a^2b^2 + 8h^2ab \end{bmatrix}$$

The abovementioned fomulae provide a means for the computation of the elements of $[T]^n$ from the elements of $[T]$ when n is large. It is specially efficient for periodic structures because very little additional computer time and no additional computer storage are needed if n is

increased. The typical results indicate that for a 50-storey building, the computer time using direct matrix multiplications is 2.5 times greater than the required computer time using the analytical procedure mentioned. For a 100-storey building the required time is 5 times greater. As for computational precision, it is found that the results obtained from an IBM-PC in double precision are the same, using either method, over a wide range of cantilever structure parameters and structural frequencies which included buildings between 10 to 100 storeys. The results using single precision are within one percent of the results using double precision. It is concluded therefore, that for non-periodic structures studied in this thesis (in a transfer matrix formulation) the accuracy of the computer results using direct matrix multiplication is guaranteed.

X

13 MAY 1992

UNIVERSITY OF SYDNEY LIBRARY



000000600778186

Allbook Bindery
91 Ryedale Road
West Ryde 2114
Phone: 807 6026